Multiplexed label-free electronic biosensors for clinical diagnostics

Irene Zaccari

Submitted in accordance with the requirements
for the degree of Doctor of Philosophy

University of Leeds
Institute of microwave and photonics
School of Electronics and Electrical Engineering

September 2013

The candidate confirms that the work submitted is her own and that appropriate credit has been given where reference has been made to the work of others.

Acknowledgements

I would like to take this occasion to sincerely thank my supervisor prof. Christoph Wälti for both his paternal support and professional insight throughout this research. Moreover I would like to thank prof. Giles Davies and Dr Sophie Laurenson for their valuable advice.

Thanks to Abbott Laboratories Inc. and the Engineering and Physical Sciences Research Council (EPSRC) for their funding for this research.

As per any most sincere acknowledgement, the late-night hours are the most suitable to remember all the people that have made my experience in Leeds as doctoral student most extraordinary and unforgettable. I would like to thanks my friends and companions for their support under any circumstances.

A special mention goes to Dr Steven Johnson and Dr Dave Evans for their help with my work and their company, especially in the early stages of my PhD.

To those who, working between the walls of the Bioelectronics Lab, made the everyday challenging and solitary work of a research student a joyful and engaging experience, thanks!

To Mike, Ola, Vaidas, Adam, Jay, Dean and Minde for their friendship throughout and their ability of making simple things special.

Further thanks go to those who from Italy or any other part of the globe were always close to me. With the help of Skype and Messenger, they never let the many miles from home become overwhelming.

Last, the most special thanks goes to my family, that has never wavered in their love and support. I can not describe the gratitude and love I feel for my *mamma* and *papá* that have always supported me and encouraged me in pursuing my dreams and ambitions.

To you all,
Thank you.

Abstract

The development of a highly sensitive, label-free, multiplexed biosensor platform for point-of-care diagnostics is presented. The sensor surface of a non-faradaic electrochemical impedance spectroscopy (EIS) immuno-sensor platform was developed and fully characterised.

Optimisation of the binding of monoclonal antibodies (mAb) towards the model target human chorionic gonadotropin (hCG) to the OEG self-assembled monolayers (SAMs) was carried out. Optimal conditions for immobilisation were found for buffer pH approximately one unit below the pI of the antibody. The same condition resulted in both higher antibody density on the sensor surface as well as higher response to the antigen. At the same time the surface showed good resistance to non-specific adsorption of proteins.

Based on these principles, a biosensor to detect hCG in full serum was demonstrated. By using the phase of the impedance at 100 mHz as the sensor response, a linear relationship of the phase shift vs the logarithm of hCG concentration was established between 2.6 $\times 10^{-14}$ M and 2.6 $\times 10^{-10}$ M with a sensitivity of 0.6 degree per decade, which is a significant improvement over current state-of-the-art biosensor systems.

Finally, The dielectric properties of COOH-terminated hexa(ethylene glycol)undecanethiol (OEG) and 11-mercaptoundecanol (MUD) and mixed MUD:OEG SAMs, at different ratios, were studied by means of EIS. The study demonstrates that small amounts of MUD in the mixed MUD:OEG SAMs lead to a considerable decrease of the phase of the impedance as well as a significant increase in the resistivity of the SAM at low frequencies, indicating a significant improvement of the dielectric properties. Furthermore, a considerable change in the formation of clusters of OEG molecules for mixed MUD:OEG SAMs with increasing MUD content was shown by AFM imaging.

This page would be intentionally left blank if we would not wish to inform about that.

Contents

This page would be intentionally left blank if we would not wish to inform about that.

List of Abbreviations

Acronyms

3EG-OH	Tri(ethylene glycol)undecanethiol
4EG	Tetra(ethylene glycol)carboxy-capped alkanethiol
AC	Alternating component of a waveform
AcB	Acetate buffer
AFM	Atomic force microscopy
AP	Alkaline phosphatase
APmAb-A	Alkaline phosphates conjugated mAb-A
BSA	Bovine serum albumin
CPE	Constant phase element
CV	Cyclic voltammetry
DC	Direct component or mean value of a waveform
EDC	1-Ethyl-3-[3-dimethylaminopropyl]carbodiimide
EIS	Electrochemical impedance spectroscopy
Fab	Fragment antigen binding, antibody region
Fc	Fragment crystallisable, antibody region
hCG	Human chorionic gonadotropin
IDE	Interdigitated electrodes
mAb	Monoclonal antibody
mAb-A	anti-hCG monoclonal antibody A
mAb-B	anti-hCG monoclonal antibody B
MOPS	3-(N-morpholino)propanesulfonic acid
MUD	11-mercaptoundecanol
NBT/BCIP	nitro-blue tetrazolium chloride/5-bromo-4-chloro-3'-indolyphosphate p-toluidine salt
NHS	N-hydroxysuccinimide
OCV	Open circuit voltage
OEG	Hexa(ethylene glycol)carboxy-capped alkanethiol
oligo-EG	Oligo ethilene glycol
PB	Phosphate buffer
PBS	Phosphate buffer saline
PEG	Poly ethylene glycol

SAM	Self assembled monolayer
SPR	Surface plasmon resonance
TBS	Tris buffer saline
XPS	X-ray photoelectron spectroscopy

Symbols

Symbol	Units	Meaning
$^\circ$	degrees	degree
α	-	pseudo capacitance parameter, as in $Z_Q = 1/((j\omega)^\alpha Q)$
Δ	-	ellipsometric parameter
$\Delta\varphi_{0.1}$	degrees, radians	shift of the phase angle between V and I at 0.1 Hz
ε_0	-	dielectric constant of vacuum
ε_r	-	relative dielectric constant of a material
θ	degrees, radians	SPR reflectance angle
θ_{adv}	degrees, radians	advancing contact angle
θ_{re}	degrees, radians	receding contact angle
ν		photon frequency
σ	Ω s$^{1/2}$	$(1/nFA\sqrt{2})[\beta_O/D_O^{1/2} - \beta_R/D_R^{1/2}]$
σ_{ij}	Nm$^-$1	surface tension between phase i and j
φ	degrees, radians	phase between two sinusoidal excitations
$\varphi_{0.1}$	degrees, radians	phase angle between V and I at 0.1 Hz
Ψ	-	ellipsometric parameter
ϕ_s		work function of the spectrophotometer
ω	s^{-1}	angular frequency, $2\pi f$
A	m^2	surface area
C	F	capacitance
C_{dl}	F	double layer capacitance
C_{dif}	F	diffuse layer capacitance
C_{ins}	F	coating layer capacitance
C_{tot}	F	total capacitance
-COOH		carboxylic acid group
d	m	distance
dB	-	deciBel

$\boldsymbol{E}$	NC^{-1}	Electric field
f	s^{-1}	frequency
$Fe(CN)_6^{3-/4-}$		ferri-ferrocyanide redox couple
G	J	Gibbs free energy
$\hbar$	m^2kg s$^-$1	Plank's constant, 6.62606957
H^+		hydrogen ion
I	A	current
$Im(Z)$	Ω	imaginary part of the impedance
j	-	imaginary unit $j = \sqrt{-1}$
m$^\circ$	10^{-3}degrees	millidegree
NaCl		sodium cloride
R	Ω	resistance or resistor
R_{ct}	Ω	charge transfer resistance
R_{sol}	Ω	solution resistance
R_{gas}	J mol^{-1}K	gas constant, 8.3144621
$Re(Z)$	Ω	real part of the impedance
-OH		hydroxyl group
pH	-	indicator of hydrogen ions activity
pI	-	isoelectric point
pk$_a$	-	decimal logarithm of the acid dissociation constant
q	C	electrical charge
Q	F^α	pseudo capacitance
V	V	voltage
W	$F^{1/2}$	Warburg element
z	m	cantilever displacement
Z	Ω	impedance, $Z = V/I$
Z_Q	Ω	pseudo capacitance impedance
Z_W	Ω	Warburg impedance

This page would be intentionally left blank if we would not wish to inform about that.

Chapter 1

Introduction

Since the beginning of the 17^{th} century, driven by the development of scientific methods for healthcare, medical knowledge advanced at an extraordinary pace. In a few years the circulation of blood and the functioning of the circulatory system were described, ultimately leading to the discovery of oxygen. Moreover the microscope was introduced and used to study the structure of tissues and the composition of blood.

Another area which led to significant advances in healthcare was diagnostics. Thomas Willis in 1674 published a chapter on *Pharmaceutice rationalis* on the presence of glucose in diabetic patients.[1] At around the same time, Herman Boerhaave introduced the thermometer in clinical practice for monitoring changes in body temperature of patients.[2]

Ever since, clinical scientists searched for measurable indicators of illness and therapy efficacy to help in their effort of treating patients and improving their quality of life.[3,4]

The continuous discovery of new indicators for the presence or risk of a medical condition is heavily reliant on the development of sophisticated tools for the measurement and analysis of these indicators.

A very large proportion of these indicators are biological molecules, usually found in biological fluids, that are linked to physiological events happening in the human body. These molecules are often referred to as biomarkers. The altering of the physiological events caused by a medical condition causes, in general, a change in the concentration of these biomarkers.

Tools for the detection and measurement of such biomarkers in biological fluids, e.g. high blood-levels of glucose for diabetes, have been proven to be of great use in clinical diagnostics.[5] In recent years, increasing longevity and the consequent increase of chronic and degenerative medical conditions has led to an unprecedented demand on healthcare providers for early and accurate detection of biomarkers in clinical samples.

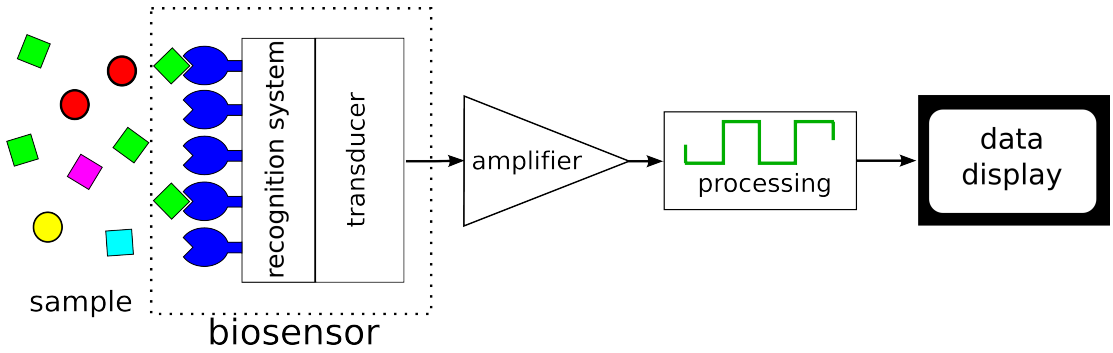

Figure 1.1: Schematic illustration of a biosensor. Typically, the transducer is coated with a recognition system. When the specific target in the sample analysed binds to the recognition system, this event changes one or more of the properties of the recognition system. The transducer transforms this change into an electrical signal which is sent to an electronic interface, which in turn records and processes the signal to produce a readable output. The processed output is then displayed for the operator's interpretation.

Arguably, one of the most promising technologies to deliver this challenge are biosensors.

1.1 Biosensors

A biosensor is an analytical device where a biological event, for example the binding of an analyte, or biomarker, is converted into a quantifiable and processable signal (figure 1.1). A biosensor is typically composed of:[6] a *recognition system*, also called bioreceptor or probe, that specifically binds to the target; an *interface architecture*, where a specific biological event takes place and gives rise to a signal which is picked up by the *transducer element*. The transducer signal is converted to an electronic signal, amplified by a detector circuit, and sent for processing to be converted to a meaningful physical parameter describing the process being investigated. Finally, the resulting quantity has to be presented through an interface to the human operator.

More recently, the demand of clinical analysis and monitoring of biological samples has been moved from clinical laboratories to less equipped locations, such as bed-side care in hospitals and non-hospital care-providing facilities, e.g. nursing homes or the patient home itself. At the same time, the tests are carried out by untrained or low-level trained users, therefore a demand for the instrumentation employed to be self-contained, portable and easy-to-use has increased considerably. Moreover, the time-to-result and sample manipulation procedure need to be reduced and simplified, respectively, and

innovative aids for the interpretation of the results have to be developed.

To meet this increasing demand of easy-to-use, accurate instrumentation, new devices enabling self-diagnosis and on demand monitoring of clinically relevant biomarkers in chronic patients' blood samples, e.g. glucose, have entered the healthcare market starting to enable self diagnosis and on demand monitoring of patients' blood levels, of such biomarkers.[4]

Furthermore, a demand for devices that can assist with routine check-up procedures and can perform screening for a multitude of risk-factor indicators for common diseases, such as for cardiovascular conditions or cancer indicators, is continuously increasing, as demands for early diagnosis of degenerative pathologies keep rising.

In response to this challenge an upward trend in research efforts has been seen in the past 30 years, and as a result the number of publications in the biosensors field has steadily increased.

Biosensor research aims to deliver devices that can detect analytes or biomarkers from clinical samples, such as blood and urine samples, considered to be indicative of a clinical condition. Biosensor devices have to be easy-to-use but also highly sensitive and accurate. Ideally, they should be portable and the waiting time for the output should be on the timescale of minutes. Moreover, they should ideally have the potential of multiplexing, i.e. performing analysis of multiple biomarkers simultaneously, and from a small sample volume.

In summary, a biosensor should fulfil a series of characteristics to be used as a diagnosis aid:[7]

- The biosensor should be specific, i.e. it should respond to the target and only the target.
- It should be able to recognise selectively the target from a complex solution, like urine or blood samples.
- It should not respond to other independent quantities like temperature, or ambient noise. If the sensor is susceptible to such quantities they should be controlled.
- The sensor response should be an invertible function, i.e. for one concentration there should be only one output value of the response, and each output value should map to only one concentration.
- The dynamic range, i.e. the concentration range at which the sensor response is unique, should be as wide as possible and should include the clinically relevant values. Sensor responses linear in concentration of the biomarker over two orders of magnitude or more are usually considered to have a wide sensor response.[7]

- The lowest detectable concentration, above measurement noise, should be less than the lowest clinically relevant concentration. This concentration is often called limit of detection and it is usually determined as three times the standard deviation of the baseline fluctuations.

- The sensor output should be reproducible, i.e. for a certain target concentration the sensor should have a predictable response.

The biological component that act as detection probe in a biosensor might be one of many biological molecules. Some examples are proteins: such as enzymes[8,9] (specific biological catalysts that accelerate biological reactions upon binding of a certain molecule), receptors (cell surface proteins that mediate the communication of the cell with the surrounding medium by binding to molecules in the extracellular space and inducing or repressing certain activity in the cell) and antibodies[10,11] (initiator of the immune response, used by the immune system for the recognition of foreign objects and molecules).

Other molecules, such as nucleic acids[12,13] (DNA and RNA sequences) or smaller molecules such as cofactors (small non-protein molecule necessary for the functioning/activation of a protein), inhibitors (a molecule that usually binds to a protein to decrease its activity), or antigens (protein or non-protein molecules that are the target of an antibody), can also be used as probes.

More recently, artificial recognition elements have been developed for sensor applications. For example molecular imprinted polymers,[11] i.e. synthetic polymers that have been engineered to have a pocket that selectively binds to a desired target, and aptamers,[14,15] short DNA, RNA sequences or small proteins, that bind a target molecule by binding a region of the target.

One of the key events in a biosensor is the binding of the target to a bioreceptor on the recognition element. The formation of the target–probe complex leads to a change in one or more of its chemo-physical properties, such as mass, heat or optical (e.g. refractive index, photon emission) and electrical (e.g. impedance, conductivity, generation of an electron flow, charge state) properties.

These changes can be detected by a wide range of transducers. Biosensors are often classified by the transducer used, for example: mass sensitive[16] (bulk or superficial acoustic wave sensor), optical[17] (measuring change in fluorescence, luminescence or refractive index) or electrochemical[18–20] (amperometric, potentiometric, impedimetric, field-effect).

Biosensors can detect the target either directly (label-free[21]) or indirectly (by means

of a label).[22] The label is a second probe that is activated only upon the binding of the target to the recognition element or in a successive step. Labelled biosensors require either a pre-labelling of the sample or multiple binding steps to generate the signal measured from the biosensor itself.

A well known example of labelled biosensors are sandwich-assays,[22,23] where an antigen, the target, binds to an antibody immobilised on a surface, the primary antibody. The signal is then generated through the binding of a second labelled antibody, the secondary antibody, to the immobilised target.

A great advantage of labelled biosensors is the possibility of amplification of the signal measured by the transducer that can lead to highly sensitive biosensors.[24] The amplification mechanism relies on the labelled probe to keep generating the biochemical signal detected by the transducer once bound to the target.

This double recognition system, other than enabling amplification of small signals, is very resistant to unwanted non-specific response, i.e. sensor signals arising from the interaction of the sensor surface with other molecules. Since the target molecule has to be bound by two probes, the chance of detecting a different molecule is reduced. Moreover, non-specific adsorption of the second probe can be reduced by pre-adsorption of an inert protein, commonly serum albumin, to the surface.[25] This protein is adsorbed non-specifically to the surface before exposure of the surface to the sample to be analysed and the secondary antibody, so that the proteins present in the sample and the secondary antibody are less likely to bind non-specifically to the surface itself.[25]

However, this type of sensor is expensive, as it requires two recognition systems and the labelling of the probes, time-consuming and makes real-time measurements a significant challenge, in fact it requires multiple washing steps and trained technicians for the analysis and interpretation of the results.

On the contrary, label-free biosensors offer the possibility of direct analyte detection from a sample with no, or very little, sample preparation and real-time measurements.[26] However, the biosensor does not have an amplification method and it relies on both a high affinity, how tightly the analyte binds to the probe of the recognition element to the target, and a very sensitive transducer. Therefore, highly sensitive biosensors and a low limit of detection are potentially more difficult to achieve with label-free sensor systems.

The first biosensor was developed for monitoring of blood-glucose levels in surgical patients.[8,25] The device coupled an enzyme that oxidises glucose to an amperometric sensor sensitive to the blood concentration of oxygen. The concentration of glucose in the blood stream could then be determined by measuring a drop in P_{O_2}[a] when the

[a] P_{O_2} is the partial pressure of oxygen (O_2) in the blood stream.

sensor surface was exposed to the sample, as explained in the next section.

Following this example, other enzymes were coupled to amperometric sensors and a variety of clinically relevant molecules were detected using the same principle,[25] essentially starting the field of electrochemical biosensors.

The home-use and over-the-counter biosensor devices market, currently in excess of US$ 13 billion, is dominated by electrochemical biosensors based on enzyme systems.[4] On the other hand, optical systems and other electrochemical techniques that are more difficult to use and require specialised user knowledge, are mostly used in laboratory environment and for research purposes.

1.1.1 Amperometric biosensors

Electrochemical sensors are sensors where an electrochemical reaction occurring at the interface of an electrode and a solution is used to detect the presence of an analyte in the solution. Electrochemical refers to chemical reactions that take place at the interface between an electron conductor (a metal electrode) and an ionic conductor (charged species dissolved in solution). Electrochemical electrodes are ideal candidates for biological detection, as these electrodes operate at the interface of electronics and solutions and most biological samples are naturally in a solution.

An electrochemical biosensor is defined as a "biosensor where the biological recognition element (biochemical receptor) is retained in direct spatial contact with an electrochemical transduction element".[27]

Most electrochemical biosensors are constructed around a three electrode arrangement.[6] The so called working electrode is the transducer and is usually functionalised by a bioreceptor. An auxiliary electrode, or counter electrode, is used to apply voltage or pass current through the working electrode. A third, reference, electrode establishes a fixed potential against which all potentials are measured. For further details refer to section 2.1.1.

Electrochemical biosensors can be classified according to the quantity measured:[6] *amperometric*,[28,29] when a generated current is measured; *potentiometric*,[30] where there is a measurable potential or charge accumulation; *impedimetric*,[31,32] which measures impedance (both resistance and capacitance), and *field-effect*,[20] which uses transistor technology to measure current as a result of a potentiometric effect at a gate electrode.

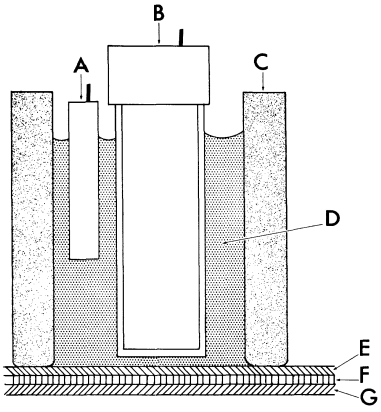

Figure 1.2: On the left, schematic of the electrode cell as proposed by Clark et al.[8] The electrochemical cell consists of a reference electrode (A) and a sensing electrode (B) held in a cylinder (C), the end of which is covered with a multiple membrane. The cell is filled with a suitable electrolyte, which may contain an enzyme. The membranes (E) and (G) have a layer of concentrated enzyme (F) between them. The product of the reaction occurring at (F) is oxygen, the inner membrane (E) is made of ion impermeable plastic so that the electrodes are electrically and ionically isolated from the system being analysed. The sensing, P_{O_2}, electrode, is pressed tightly against the membrane transducer. Adapted from Clark et al.[8]

1.1.1.1 Enzyme based biosensors

As mentioned, the first example of an electrochemical biosensor is an amperometric sensor for the monitoring of glucose in blood samples proposed by Clark et al. in 1962.[8] An amperometric sensor usually consists of an electrode that can measure a current change due to a chemical reaction occurring in solution when a fixed potential is maintained at the electrode.

In Clark's sensor glucose oxidase (GOx – an enzyme that oxidises glucose) was dissolved in a solution entrapped between a membrane and an amperometric sensor (figure 1.2). A sample of blood is extracted from the patient blood stream and passed through the membrane, the glucose in the blood sample is oxidised according to:[25]

$$\text{glucose} + O_2 + H_2O \xrightarrow{\text{GOx}} \text{gluconic acid} + H_2O_2. \tag{1.1}$$

Oxygen is consumed in the reaction and the rate of decrease of P_{O_2}, monitored by the electrode, is a function of the glucose concentration (figure 1.3 A). By polarising the P_{O_2} electrode so that it is positive in respect to the reference electrode, for platinum electrodes, this typically requires positive biases of +0.7 V or higher vs Ag/AgCl

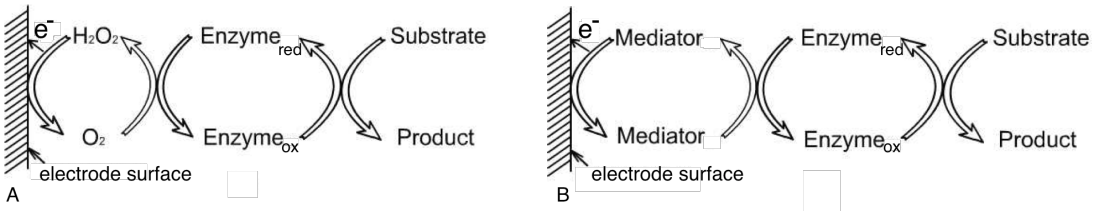

Figure 1.3: Schematic principle of electrochemical reactions of first generation (A) and second generation (B) amperometric biosensor. Adapted from Wang et al.[33]

reference electrode,[25] H_2O_2 is oxidised according to:

$$H_2O_2 \longrightarrow H^+ + O_2 + 2\,e^-. \tag{1.2}$$

The current produced is proportional to the concentration of glucose in solution. However the process, and therefore the measurement, is dependent on the presence of oxygen in the sample to support the reaction catalysed by the enzyme and produces a linear relationship between the response and glucose concentration for the relevant ranges especially above 5 mg/ml.[25]

One of the approaches used to overcome this problem is the introduction of mediators, such as ferroncene and its derivatives[34] or benzoquinone,[35] employed as electron acceptors. The reaction principle is illustrated in figure 1.3 B. An example of second-generation glucose-sensor uses a small diffusing redox mediator, 1,4-diaminoanthraquinone,[36] to facilitate the electron transfer between the gold electrode and enzyme as below:

$$\text{glucose} + \text{GOx}_{\text{ox}} \longrightarrow \text{GOx}_{\text{red}} + \text{glucolactone}; \tag{1.3}$$

$$2\,\text{Mediator}_{\text{ox}} + \text{GOx}_{\text{red}} \longrightarrow \text{Mediator}_{\text{red}} + \text{GOx}_{\text{ox}} + 2\,H^+. \tag{1.4}$$

The introduction of such mediators also reduces the operating potential of the working electrode (+ 0.2 V or lower)[25] with respect to the potential used for the oxidation of H_2O_2. Furthermore the mediators can be retained at the electrode surface by a discrete membrane, mixed with the enzyme in a carbon paste or entrapped in an electrogenerated film.[37–39] Alternatively, the mediator can be covalently attached to a polymer incorporating an enzyme[40] or to the immobilised enzyme itself.[41]

In the third generation of amperometric sensor the reaction itself causes the response and no product or mediator diffusion is directly involved. The enzyme is usually trapped in close proximity with the electrode and it is electrically connected to the electrode surface – for example by entrapping the enzyme on a conducting polymer, such as

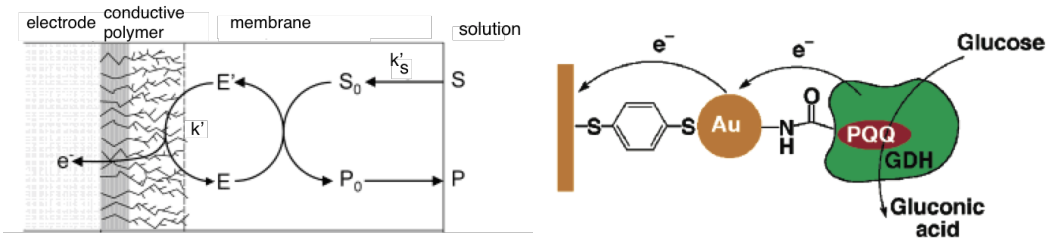

Figure 1.4: Left, schematic representation of processes involved in a third generation enzyme electrode. S and P are the substrate and product, respectively. E and E' are the oxidised and reduced form of the enzyme, respectively. k' is the heterogeneous rate constant for enzyme reoxidation and k'$_s$ is the mass-transfer rate constant through the membrane of the substrate. Right, example of non mediated electrical contacting of the enzyme with the electrode. The nanoparticle is associated with the gold electrode and the enzyme. The enzyme (GDH) is bound to the nanoparticle through the cofactor (PQQ). Adapted from Palmisano et al.[43] and Zayats et al.[44]

polypyrrole,[42,43] or by binding the enzyme to gold nanoparticles by means of a cofactor[44] (figure 1.4). The working principle for both a conductive polymer and gold nanoparticle enzyme sensor is illustrated in figure 1.4. This glucose sensor works according to the principle of direct electron transfer from the redox enzyme to the conducting medium.[45]

Oxidase and reductase enzymes, i.e. enzymes that catalyse the oxidation (loss of electrons) or reduction (gain of electrons) of a substrate, are ideal for electrochemical applications because they are specific to the target and generate a known number of electrons per catalysis reaction. The resulting current can be directly detected by the electrode. Unfortunately, such enzymes are not available for most of the targets of interest in clinical applications. However, antibodies can be used, at least as recognition molecules, as they offer highly selective binding affinity to a wide range of molecules. Thus, a large number of sensors that use an antibody as part of the recognition element have been developed.[11]

Even if the antibodies do not act as an enzyme, many electrochemical techniques allow the detection of analytes by responding directly to the binding between the antibody and its antigen.[26] Biosensors that use antibodies or antibody fragments as recognition element are called immuno-sensors. The antibody transfers its selectivity and sensitivity for the analyte to the biosensor by binding the analyte with high affinity and bringing it in close proximity to the sensor surface, even in the presence of other substances. Therefore, the antibody is usually immobilised in proximity to, or directly on the transducer.[46,47]

Other molecules in solution might still bind to the surface and generate a non specific

response. Many publications focus on this aspect. Later in this chapter, we will discuss some of the approaches used in biosensor technology to avoid non-specific binding of molecules to the sensor surface.

To appreciate the influence of the glucose sensor on biosensor research we point out that even after so many years from the launch of the first biosensor, the market of home-use electrochemical biosensors is still dominated by electrochemical enzyme-coupled biosensors.[4,7] In fact the first hit of a google search of the keyword 'biosensor' is an electrochemical biosensor promoted as an alternative method to the enzyme-coupled glucose sensor.[46]

This particular biosensor uses ion channels linked to antibody fragments – the sub-units of the antibody which contains the recognition site, that are utilised instead of whole antibodies. The ion channels are proteins, usually crossing the cell membrane, that allow ions to cross the cell membrane upon certain conditions. In this sensor, ion channels are immersed in a lipid membrane that is attached to the electrode surface. The ion channels cross the lipid membrane allowing transfer of ions between the solution and the electrode surface.

When the antibodies bind the antigens, the ion channels are closed and thus interrupting the flow of ions through the membrane. The authors state that sub-pico-molar concentration of the analyte can be detected, and that by using an appropriate antibody fragment for a specific target of interest, a wide range of molecules can be detected.[46]

1.1.2 Impedance biosensors

We have already seen examples of amperometric biosensors. A second very often used electrochemical technique measures the change of impedance at the electrode-solution interface. Usually a probe is bound to the surface and upon binding of the antigen a change in impedance across the electrode-solution interface is detected.[48] The impedance is usually evaluated by applying a potential perturbation, such as a voltage step or a sinusoidal wave, and measuring the current response.[49] The impedance, Z, is then obtained as a ratio between the voltage and the measured current as $Z = V/I$, according to Ohm's law.

To obtain reliable impedimetric biosensors, certain characteristics are required. The system response should be dependent only on the detection of the target, and not on other variables, e.g. temperature. The system should be stable in time and the perturbation applied to the electrodes during the measurement should not influence the binding event and the measurement itself.[7]

When an electrode is immersed in solution the species dissolved in the solution (ions, polar molecules, solvent molecules, and any other molecule) approach the electrode and

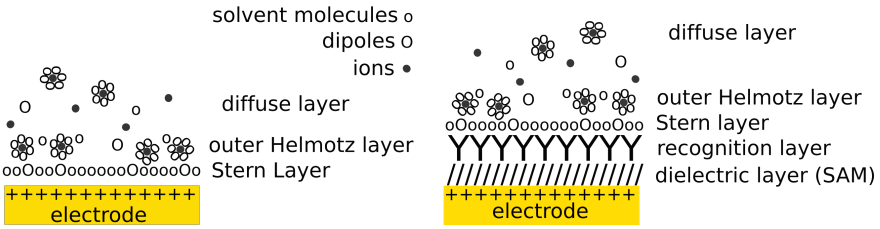

Figure 1.5: Depiction of electrochemical double layer formation at a bare (left) and functionalised (right) electrode. Adapted from Bard and Faulkner.[49]

according to their charge, they arrange themselves at a certain distance from the electrode surface (figure 1.5), creating the so called electrochemical double layer, as detailed in section 2.1.3.[49–51] Briefly, at a given potential, the electrode surface possesses a certain charge, and the opposite charged species in solution will act to compensate this surface charge by accumulating at the electrode. The first layer from the electrode, referred to as Stern layer, is constituted by charged species and dipoles strongly adsorbed at the electrode–solution interface and bound by van der Waals interactions. The second layer, instead, consists of solvated ions that approach the electrode only up to a certain distance.[49] In first approximation, the electrode and the double layer form a capacitor referred to as the double layer capacitance C_{dl}.

The double layer capacitance depends on the species dissolved in solution and on the properties of the electrode surface. Detection of analytes in solution using this electrochemical technique has been demonstrated for a variety of targets.[52–54] Usually the electrode is modified by immobilising a bioreceptor (e.g. an antibody) to bind a target in solution.[48,55,56] The detection takes place when the binding of the target to the probe immobilised on the electrode changes the impedance of the system by changing the dielectric properties or thickness of the recognition layer.[7,21,52]

1.1.2.1 Capacitive biosensors

Capacitive biosensors are impedimetric biosensors that measure the change in capacitance of the recognition element upon binding of the target. When building a capacitive biosensor, the electrode is usually coated by an insulating layer that blocks most of the electron exchange taking place between the electrode and ions or other molecules in solution.[48,57] This is most desirable as a good blocking layer significantly increases the sensitivity.[21]

In a sensor with a coating layer and a recognition element immobilised on top of it, the total capacitance of the electrode can be modelled as a series of three capacitors[48,52,57]

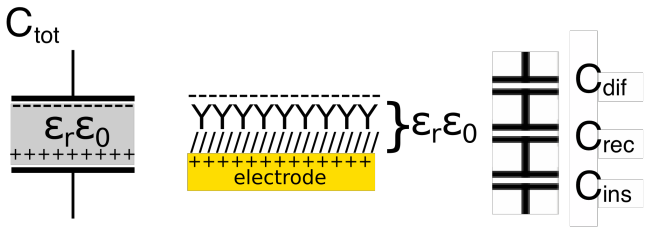

Figure 1.6: Depiction of model used for capacitve biosensors.

(figure 1.6), one associated with the coating layer, C_{ins}, one with the recognition element and the Stern layer, C_{rec}, and one with the diffuse layer and the bulk solution, C_{dif}, therefore:

$$1/C_{tot} = 1/C_{ins} + 1/C_{rec} + 1/C_{dif}. \tag{1.5}$$

The binding of the analyte to the bioreceptor will change the capacitance of the recognition layer by a change in the dielectric constant and/or the thickness of the layer.[24] The change in capacitance in the recognition layer, resulting from the binding of the target, is easier to measure if the smallest capacitor is C_{rec}, because the smallest capacitance dominates the total capacitance.

This model is valid if the permeability of electrons between the electrode and the solution, of both the insulating and recognition layers, can be neglected. Therefore, the choice of the constituents of the insulating and the biorecognition layers is critical.[21] Using this method, biosensors for clinical diagnostic were developed by Berggren et al. demonstrating highly sensitive detection of hCG for concentration ranging between 15×10^{-15}M and 10^{-9}M,[48] and interleukine-6 was detected between 5 $\times 10^{-16}$ M and 5 $\times 10^{-9}$ M.[32] The detection limits obtained are lower than clinical applications demand.

Following their work, other targets useful for food contamination monitoring were detected in a similar way, including cholera citotoxin in the concentration range from 10^{-13} to 10^{-10} M,[53] and staphylococcal enterotoxin B in a linear range between 10^{-16} M and 10^{-14} M (2.8 pg/ml - 2.8 ng/ml).[54] It is worth noting that for food monitoring highly sensitive techniques are required because in general the relevant toxins are incapacitating already at very low concentrations in food, in fact the assumption of a dose of 0.4 ng/kg of enterotoxin B is already debilitating.[54]

Interdigital electrodes. A different approach to build a capacitive biosensor is to have the recognition element immobilised between two electrodes, typically interdigitated electrodes (IDE)[58] as shown in figure 1.7 A. IDEs are constituted by a two electrodes in the shape of a comb disposed as in the schematic of figure 1.7 B.

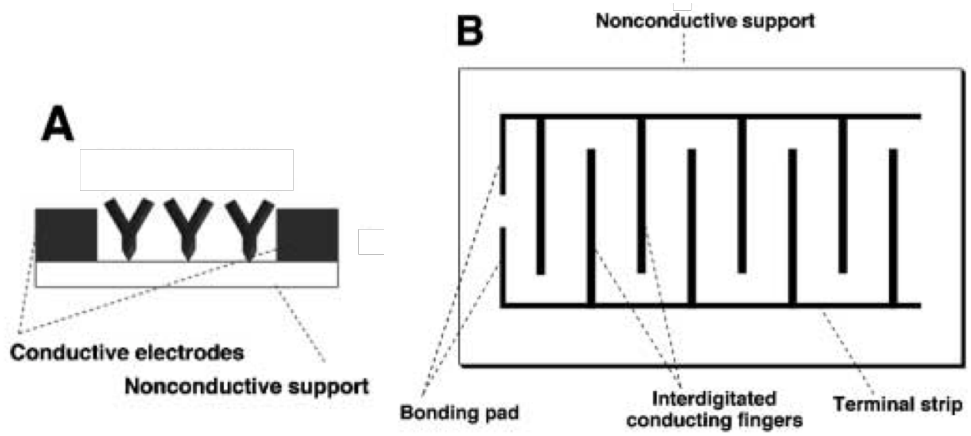

Figure 1.7: A) Depiction of interdigitated electrode functionalisation with antibodies between conducting electrodes. B) Sketch of the geometry of interdigitated electrodes. Adapted from Katz et al.[59]

For this kind of electrode the change of the dielectric properties of the medium in the gaps between the two electrodes, resulting from the binding with the analyte, is measured. The capacitance of the electrodes can be described as $C = \varepsilon_r \varepsilon_0 A/d$, where ε_r is the dielectric constant of the medium, ε_0 is the permittivity of free space, A is the electrode surface area of the lateral walls of the electrodes and d is the distance between the digits of the electrodes. When the binding between the bioreceptor and the analyte occurs the dielectric constant will change because the water molecules are replaced by the analyte, which has a significantly different ε_r.[58]

The cardiovascular disease biomarker C-reactive protein (CRP) was detected with an interdigitated electrochemical biosensor. The risks for cardiovascular diseases are defined low for a CRP concentration below 1.0 μg/ml, moderate for a CRP level from 1.0 to 3.0 μg/ml, and high for concentrations over 3.0 μg/ml. It was demonstrated that the sensor response was dependent on both concentration of the target between 25 and 800 ng/ml, as well as the frequency used to excite the sensor between 50 and 350 MHz, enabling tuning the sensor to different detection ranges.[58,60] The impedance of the sensor depended both on concentration and on the frequency of the potential perturbation applied. This was used to shift the concentration at which the linear range starts so to shift the sensor response linear range to include the clinically relevant range.[58]

1.1.2.2 Electrochemical impedance spectroscopy

The study and characterisation of the impedance as function of frequency is usually performed by electrochemical impedance spectroscopy (EIS). This method consists of

applying a small sinusoidal voltage (V) and changing the frequency of the voltage over a certain range. The current response at each frequency (I) is then measured, and the complex impedance is calculated as:

$$Z(\omega) = V(\omega)/I(\omega), \tag{1.6}$$

where ω is the angular frequency, i.e. if f is the frequency of the voltage applied, in Hertz, then $\omega = 1/(2\pi f)$; $j = \sqrt{-1}$ is the imaginary unit.

In general, the impedance is a complex number and it can be represented by either its real, $Re(Z)$, and imaginary, $Im(Z)$, parts as $Z = Re(Z) + jIm(Z)$, or by its magnitude, $|Z| = \sqrt{Re(Z)^2 + Im(Z)^2}$, and phase, $\varphi(Z) = \text{arctg}(Im(Z)/Re(Z))$. The term impedance spectroscopy comes from the fact that the impedance is measured across multiple frequencies thus giving a spectrum of the impedance.

Often EIS is used as a tool for the characterisation of the electrode properties in addition to its sensing applications. In fact in many biosensor publications the change of impedance at the working electrode is often reported also as means of characterisation of the electrode properties at each state of the sensor development and not only as means of detection.[7,61]

Two kinds of EIS measurements are usually distinguished, faradaic and non-faradaic. Faradaic refers to the presence of a current generated by electron transfer between the working electrode and species in solution which either oxidise or reduce. Therefore, when EIS is performed in the presence of species that favour the transfer of electrons, called redox probes, then the measurement method itself is called faradaic EIS. On the other hand, when EIS measurements are carried out with no redox species in solution they are generally referred to as non-faradaic measurements.

Starting with non-faradaic measurements, IDEs were used to detect the binding of an antigen to an antibody immobilised between the side walls of the electrodes.[59] The binding of the antigen alters the properties of the gap between the electrodes thus changing both the real and imaginary parts of the impedance. In first approximation, a change in conductivity changes $Re(Z)$ and a change in capacitance changes $Im(Z)$. The binding of the antibody between the gaps was reported to change the capacitance of the electrode, while the binding of the antigen to the immobilised antibody mostly changed the conductivity.[59]

On the other hand, for planar electrodes, the impedance at the electrode solution interface is monitored. The formation of the antibody-antigen complex was observed using a differential impedance amplifier on polymer modified electrodes. The difference of the real part of the impedance between an electrode with immobilised antibodies as

recognition elements, and one only modified with the polymer was measured.[61] The use of a differential technique, where an electrode modified with a probe is compared to an electrode without the probe, means the sensor response coming from the target and a non-specific response can be easily distinguished.

This is a good example to underline the potential of electrochemical biosensors to use very reliable and available technology, such as differential amplifiers or lock-in amplifiers, to create instrumentation suited for biological detection.

Often the electrode-solution interface of planar electrodes is modelled with an equivalent circuit. An equivalent circuit is an electrical circuit composed of a series of electrical components that has the same impedance, across a large frequency range, as the sensor under study.[6,62–64] Usually the variation of one of the elements of such an equivalent circuit is monitored and used as the sensor output. To find the values of each component of the equivalent circuit, least squares minimisation fitting procedures of the impedance spectra are performed.

For non-faradaic EIS, similar to capacitive biosensors, the simplest equivalent circuit available for modelling the electrode-solution interface is an RC circuit (see figure 1.8 A). In this case, the change in capacitance can be seen in a change of the imaginary part of the impedance, in fact for such a circuit $Im(Z) = -1/(\omega C)$, where C is the capacitance. The capacitance of the electrode can be measured at multiple potential biases. Since antigens and antibodies are usually charged proteins, the charge state of the electrode can affect the binding affinity between them. The binding of an antibody to its antigen, in particular a peptide of a foot-and-mouth virus, was detected and monitored in real time by EIS.[65] The peptide was immobilised as the capture molecule on a planar electrode, and the antibody upon binding to the peptide changes the capacitance of the electrode. For monitoring of the kinetics of the binding in real time, measurements at a single frequency were carried out.[65]

Similar to above, for planar electrodes, to ensure specificity of the signal, the measurement can be taken as a differential between the signal coming from an electrode with the probe and one without the probe.[66] This method was used for the detection of rabbit IgG[b] by their respective antibody, anti-rabbit IgG antibodies, coupling the latter to a self-assembled cystamine monolayer on a gold electrode. The detection of rabbit IgG was based on the analysis of capacitance changes by non-faradaic EIS. The sensor showed a dynamic range between 0.5 to 8.5 ng/ml.[66]

A different approach was proposed by Lillie et al.[67] Instead of looking at the capacitance of the electrode the phase of the impedance, φ, was monitored at low frequency,

[b]IgG is an abbreviation used for immunoglobulines G, IgG are a class of antibody.

were the sensor shows sensitivity to molecular binding. Antibodies were immobilised on a conductive polymer on gold IDEs and the change in the phase of the impedance at low frequency was used for the detection of luteinising hormone in the clinically relevant range. However the sensor showed some problems with unspecific binding.[67]

As mentioned, the phase of the impedance is given by $\varphi = \text{arctg}(Im(Z)/Re(Z))$. This quantity is directly measurable, i.e. it does not need fitting of the impedance spectrum, but is rarely used for biosensor applications. However it can be measured by lock-in amplifiers that are very reliable and accurate electronic instrumentation, and can be very sensitive to binding of analytes to the sensor surface, especially in the low frequency range.

Moreover, the phase of the impedance depends on the ratio between the real an imaginary part and does not change with the size of the electrode, while the both $Re(Z)$ and $Im(Z)$ do. This is of great advantage with a view towards miniaturisation of electrodes and creation of electrodes arrays. In fact the signal of a sensor based on the phase of the impedance does not scale with the size of the electrode.

Non-faradaic EIS can also be used to characterise properties of tissue samples. It was used to characterise the tissue resistance in patients with lesion of the carotid artery. The electrochemical behaviour of the tissue was modelled with an appropriate equivalent circuit and this method was sensitive enough to detect different kinds of lesions of the artery walls. In fact, the impedance of the tissue would vary with the thickness of the artery wall and the fat content of the tissue.[68]

Alternatively, instead of the capacitance, the conductivity of the recognition layer can be measured in the presence of a redox probes, i.e. a molecule or a pair of molecules that oxidise and reduce at certain potentials by exchanging electrons with the electrode. Usually EIS is carried out by biasing the electrode with a voltage equal to the equilibrium potential of the redox couple. Since there is a current of electrons flowing from the electrode to solution and vice versa this kind of measurement is usually called faradaic EIS.

The addition of redox probes to the sample analysed adds a small complication to the sample handling procedure, especially in the context of point-of-care applications, however it can also amplify the output of the sensor, therefore it is often chosen in laboratory environments.

For faradaic impedance systems the conductivity change of the recognition layer varies with the binding of the target. In particular, the target blocks the access of the redox probes to the surface and the conductivity of the recognition layer decreases. This

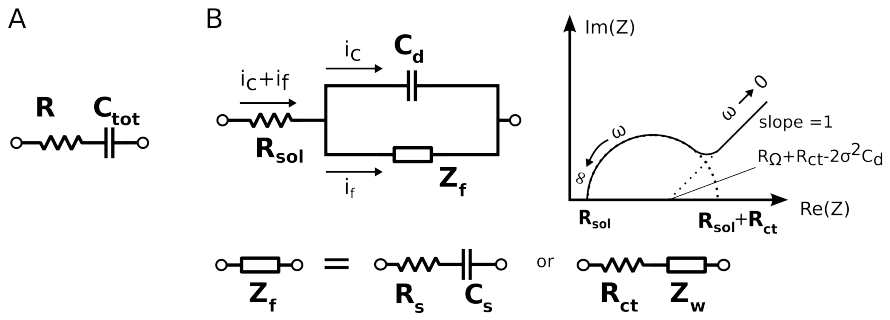

Figure 1.8: Equivalent circuit proposed to model the electrode-solution interface. A) RC model, B) Randles equivalent circuit and Nyquist plot of the impedance. Redrawn from Bard and Faulkner.[49]

process is usually studied by means of the so called *Randles equivalent circuit* (figure 1.8B) where the total current through the electrode-solution interface is considered as the sum of the current from the faradaic processes, i_f, and from the double-layer charging current, i_c. The double-layer capacitance is represented by the capacitor C_d whereas the faradaic process is considered as a generic impedance, Z_f. Both currents, of course, pass through the solution resistance, R_{sol}.

The impedance Z_f can be described as a *series resistance*, R_s, and a pseudo-capacitance – the pseudo-capacitance originates from the accumulation of charges at the electron solution interface induced by faradaic reactions, i.e. due to passage of current, rather than electrostatic, non-faradaic, accumulation of charge typical of a standard capacitor), C_s, or as the so called *charge-transfer resistance*, R_{ct}, and the *Warburg impedance*, Z_w (figure 1.8B)[49].

The parameters of the circuits can be evaluated from the *Nyquist plot* of the total impedance (figure 1.8 B). The Nyquist plot of a quantity is the plot of the imaginary part against the real part of said quantity. At low frequencies ($\omega \to 0$) the curve $Im(Z)$ vs $Re(Z)$ is linear with a unity slope. At such frequencies the time scales of the measurement are comparable with diffusion processes occurring at the electrode-solution interface which hence become dominant. These processes are represented in the equivalent circuit by the Warburg impedance. As the frequency rises, this process becomes less relevant because the time scale of the measurement is too fast. At high frequency R_{ct} and the double-layer capacitance, C_d, are the elements that dominate the impedance.

At high-frequencies ($\omega \to \infty$) the Warburg element becomes negligible with respect to R_{ct} and the frequency dependence of the system is only due to the double layer capacitance. In fact the Nyquist plot, in this frequency limit, is a circumference centred on $R_\Omega + R_{ct}/2$ with a diameter equal to R_{ct} (figure 1.8). For sensors based on faradaic EIS

measurements, R_{ct} is usually extracted from the Nyquist plot and used as the sensor output.

The main sensing mechanism for faradaic EIS techniques is to detect the variation of the amount of redox probes that can access the electrode, depending on the amount of binding of the target to the recognition element, thus varying the electron current generated by the exchange of electrons between the electrode and the redox couple.

A common methodology is to immobilise the probe on or in close proximity to the electrode surface and then expose the sensor to the analyte solution in the presence of a redox couple. In general, the binding of the target to the surface impedes the access of the redox couple to the sensor electrode, and therefore R_{ct} increases.

For example, the interactions between the recombinant dust mite allergen Der f2 and its antibody were monitored by faradaic EIS, with the use of $[Fe(CN)_6]^{3-/4-}$ as redox couple.[69] The interactions between the antigen and the antibody altered the interfacial electron transfer resistance, R_{ct}, by preventing the redox species to approach the electrode. The results showed that R_{ct} increased from 220 Ω to 780 Ω with increasing concentration of the allergen from 2 μg/ml to 300 μg/ml.[69]

A different approach can be to control the access of the redox probes in solution to the surface by changing the surface charge of the electrode. A negatively charged aptamer, i.e. a short engineered peptide, was immobilised on the sensor surface and, since the redox couple $Fe(CN)_6^{3-/4-}$ was negatively charged, the charge of the aptamer suppressed the access of the redox couple to the surface. However, when the positively charged target bound to the aptamer, the total charge of the surface became more positive allowing easier access to the redox probes, thus increasing the conductivity of the layer. The concentration of lysozyme was detected from a buffer solution for concentrations between 3 and 17.5 $\times 10^{-12}$ M, and the electron transfer resistance decreased from 3.33 to 2.34 kΩ as the lysozyme concentration increase.[15]

Electrochemical biosensors for direct, label free, detection of various analytes by means of EIS are a very attractive because of their fast execution and the relatively low-cost of the instrumentation, in respect with other sensing techniques.[7] In fact the number of publications using EIS for the development of biosensors has been increasing steadily.[7]

In many publications it was demonstrated that EIS has the capabilities of yielding very sensitive biosensor readouts. Impedance spectroscopy can also be used to gain detailed information on the resistance and capacitance properties of the sensor in multiple measurement conditions, e.g. the voltage bias of the input and its frequency, which may be useful for further tuning and improvement of the sensor itself.

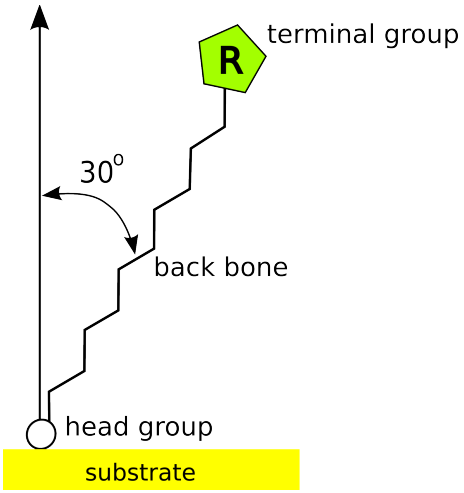

Figure 1.9: Schematic illustration of a decanethiol molecule tethered to a gold surface.

1.2 Electrode modification

So far we focused on electrochemical measurement techniques, however another key factor when creating a successful biosensor is the engineering of the surface of the sensor transducer. Depending on the kind of technique employed, different properties of the transducer have to be optimised. As discussed above, for capacitive biosensors, it is desirable to block any access to current flowing from the solution to the electrode. On the contrary, for faradaic measurements we want to have the highest possible change in conductivity upon the binding of the target.

Moreover the probe has to be attached to, or be located in close proximity of, the electrode surface but at the same time it is desirable to avoid non-specific binding of molecules in solution to the surface itself. The latter property is of particular concern for the analysis of real clinical samples, as urine and blood samples are rich in protein and salt content.

Self-assembled mononlayers (SAMs) are a powerful tool for the engineering of electrode surfaces owing to their reliability and relative ease of forming ordered and predictable monolayers by exploiting gold-thiol chemistry.

A SAM is a layer, one molecule thick, of molecules that adsorb spontaneously onto a solid surface from solution or vapour phase. Each SAM molecule comprises three parts (figure 1.9): the head group, which attaches the molecule to the surface usually by a covalent bond and governs the self-assembly process; the back bone, which stabilise the SAM through secondary binding forces; and finally the terminal or functional group,

which can have different properties and usually giving the SAM its chemical and physical properties.[70]

The modification of the electrodes by means of SAMs can confer various desired properties to the electrode by changing the functional group. For example, the capability of immobilisation of bioreceptors or the resistance to unwanted non-specific interactions between other molecules present in solution and the electrode. The modification of electrodes with SAMs can in fact not only be used for impedimetric biosensors but for a great variety of sensors, e.g. amperometric,[28] mass[71] and optical[17] biosensors.

The terminal group dominates the properties of the interface between the surface and the above solution.[70] For example -CH_3 and -CF_3 terminal groups make the SAM surface hydrophobic, metallophobic and highly anti-adherent, while -COOH, -NH_2 or -OH groups yield hydrophilic surfaces with good metal ion binding properties.[70] Both -COOH and -NH_2 terminal groups can be chemically modified for the attachment of proteins.

For example the carboxylic acid can be modified by means of ethyl(dimethylaminopropyl) carbodiimide (EDC) and N-hydroxysuccinimide (NHS) activation to attach proteins on the molecule via covalent bonds. The NHS-EDC chemistry allows the modification of carboxylic acids to NHS ester, which mediates the creation of an amide bond between an amine group (NH_2), usually present on proteins, and the acid itself, in this case on the SAM.

In a SAM the molecules arrange in such a way that the total free energy of the system is minimised, creating a complex structure in which the intermolecular forces reduce the number of degrees of freedom, e.g. they can not freely rotate.[70,72] SAMs can be formed not only on planar surfaces but on surfaces of all shapes and sizes, and also on a range of nanostructures.[73]

Among SAMs, the most widely used are those of alkanethiols[74] on noble metals and for a minor part on semiconductors. On a gold substrate, the alkyl chains are highly packed, with few macroscopic defects, and tilted at approximately 30°, in respect to the surface normal.

It was shown by electron diffraction[75,76] and scanning tunnelling microscopy[77,78] (STM) that monolayer of alkanethiols on Au(111) surfaces show hexagonal symmetry for sulphur atoms with spacing of ≈5 Å, as shown in figure 1.10, and a calculated area per molecule of 21.4 $Å^2$.[79]

The tilted arrangement of the alkyl chains arises as a result of less than ideal spacing of binding sites in the (111) orientated Au (5 Å), an ideal scenario for lowest free energy of intermolecular van der Waals interaction would result from a spacing of approximately

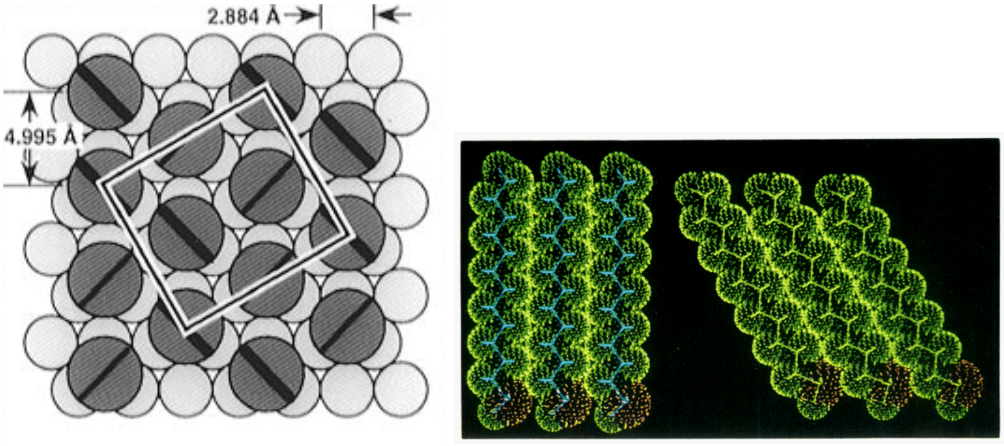

Figure 1.10: Left, model of alkanethiol monolayer (large circles) on Au(111) surface (small circles). Diagonal slash in large circles represents azimuthal orientation of plane defined by all-trans hydrocarbon chain. Right, 1×3 assembly at 4.24 Å spacing (left) and at 4.97 Å (right) of decanethiol. Reprinted from Poirier[79] and Ulman et al.[80]

4.6 Å. Thus the alkyl chains tilt so that the distance between the chains is ≈4.6 Å (figure 1.10).[72]

In the same way functional groups that have a cross section bigger than 21.4 Å do not allow optimal packing, leading to less ordered monolayers, due to the steric hindrance of the functional group. For example the hexagonal packing of decanethiol and mercapto-undecanoic acid (MUA) was compared by STM.[81] The SAM formed from MUA and decanthiol have a similar structure. However, while decanethiol SAM presents large uniform areas with the same hexagonal arrangement, MUA forms a compact monolayer with a mixture of diverse morphologies and less ordered domains, which shows a difference between acid- and methyl-terminated alkanethiols.[81]

The capabilities of surface modification and functionalisation provided by SAMs make them a powerful tool in the hands of biochemists and bioengineers in biosensor design. SAMs have been used to immobilise enzymes, antibodies, engineered proteins, DNA, membranes and whole cells onto the sensors surface. Being able to modify noble metals allows the functionalisation of electrodes and therefore the use of SAMs as building blocks for electrochemical biosensors. Moreover, as discussed later, the possibility of creating mixed SAMs, i.e. adsorption of SAMs with different terminal groups onto the same surface, further extends their applications.

1.2.1 SAM formation and stability

It is commonly recognised that the first self-assembled monolayer (SAM) was observed by Bigelow et al in 1946,[82] when they generated a molecular film on a clean glass surface

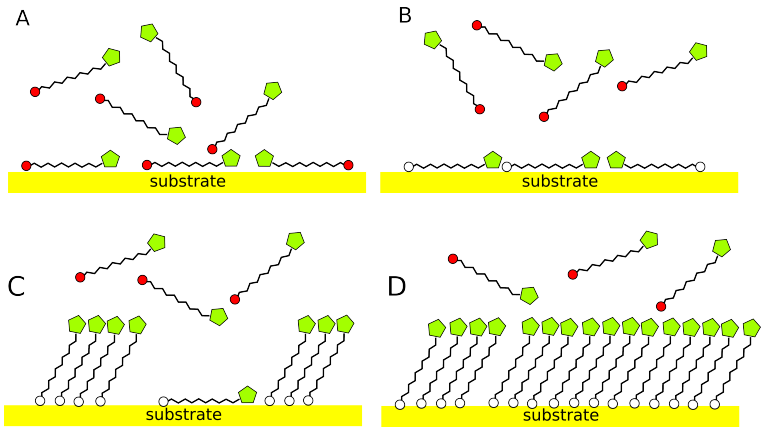

Figure 1.11: Schematic illustration of the different steps taking place during the self-assembly of alkanethiols on gold: (A) physisorption, (B) formation of S-Au bonds, (C,D) surface crystallisation process.

by the spontaneous adsorption of long chain alcohols in dilute solutions. However, this SAM was unstable and easily removed. Instead, the first types of strongly bound chemisorbed monolayers were achieved using siloxane chemistry, etching a silicon surface and coating the surface with active silanol (Si-OH) groups.[83]

However, nowadays, the most widely used SAMs are obtained by adsorption of organo-sulphur compounds onto gold.[72,74,84] Although sulphur compounds are known to react with wide range of materials like gold, silver, copper, platinum, mercury, iron, nanosize γ-Fe_2O_3 particles, colloidal gold particles, GaAs and InP surfaces, gold is the most commonly used.[72] One reason for this preference lies in the gold-sulphur interaction nature. This interaction is stronger than the one between gold and many other chemical groups such as acids, amines, etc.[85] hence allowing favourable monolayer assembly.

Kinetic studies of alkanethiol adsorption onto gold surfaces have shown three adsorption kinetic steps (figure 1.11): the first step is considered a precursor step, which consists of the physisorption of the alkanethiols; followed by a second step, which takes few minutes, where the thiol molecules are chemisorbed onto the gold surface; and a slower step, which lasts several hours, where ordered domains are formed.[70,86]

The initial step is difficult to observe owing to the very short time scales over which the precess occurs. However for short physisorbed molecules, which have slower kinetics, this initial step was successively observed by STM at a temperature of 5 K, and for longer alkanethiols indirect evidence of this process has been reported.[77,87]

The second step, consisting of a rapid reaction between the -SH group and a gold atom with the formation of a sulphur-gold bond, was described by diffusion-controlled

Langmuir adsorptions, and was found to depend strongly on the thiol concentration.[86] The kinetics of this step is governed by the surface/head-group reaction, and the activation energy generally depends on the electron density of the adsorbing sulphur.

The final step can be described as a surface crystallisation process,[86] where electrostatic interactions and van der Waals forces between the alkyl chains lead to the formation of a well ordered monolayer. The word 'crystallisation' is used to underline that a high degree of order in the SAM is achieved. The kinetics of this step are related to chain disorder (gauche defects), the different components of chain-to-chain interactions (van der Waals, dipole-dipole, etc.), and the surface mobility of chains.[86] The alkyl side chains then assemble together to maximise the interactions between them. It was found that the kinetics is faster for longer alkyl chains, probably due to the increased van der Waals interactions.[86]

Moreover, the thiols have the ability to move along the gold surface. This mechanism plays an important role in the formation of the final equilibrium structure of the monolayer: migration of the alkanethiols between neighbouring sites is essential for healing of defects.[72]

In conclusion, longer alkyl chains lead to more ordered SAMs with fewer defects. However, if the chain contains a bulky terminal group, the two chemisorption steps are coupled, and the kinetics is greatly impeded by the chain disorder.[88]

The choice of the alkanethiols chain length is related to the needs of the particular application in use. If the access of species from the solution to the gold surface has to be prevented, then a chain of 10 or more carbons is required.[89] Electron transfer through a densely packed monolayer depends exponentially with the separation between the donor and the acceptor of electrons and thus with the length of the monolayer.[90,91] At the same time, as the integrity of the monolayer decreases (due to presence of pin holes, grain boundaries or trapped solvent) the current of electron transfer increases.[89]

A mechanism involving diffusion to sparsely populated surface regions, where electron tunnelling is more probable than for the vast majority of the surface, was observed.[89] Therefore the length of the monolayer concurs in two ways, it increases the distance between the gold surface and the species in solution and it increases the packing of the monolayer due to higher chain-chain interactions.

In contrast, for some sensing application using electrochemical techniques, the underlying metal requires to be partially accessible and shorter alkanethiols are preferred. In this respect, a new generation of dithiolated scaffolds have been studied.[28,92] For example molecules containing two identical alkylthiols attached to a phenyl ring provides two binding points to the gold surface. The dithiols are expected to yielding both, more stable SAMs and higher permeability to electron transfer.

1.2.2 Functionalisation of surfaces

As discussed above, different terminal groups of the SAM molecules confer different properties to the surface. Therefore it is possible to design the chemical and physical characteristics of the modified surface by changing the functional group of the SAM. Moreover, it is possible to functionalise the same surface with different functional groups at the same time.

Several studies comparing the properties of surfaces functionalised with different ratios of different SAMs have been performed. The effect of surface wettability and charge on protein adsorption and cell adhesion, in serum, have been studied by Arima et al.[93] Mixing 1-dodecanethiols (-CH_3) with -NH_2, -OH, and -COOH capped thiols in different ratios they obtained surfaces with contact angles from 22° (100% 11-mercaptoundecanoic acid) to 109° (100% 1-dodecanethiols).

Briefly, the contact angle is the angle that a droplet placed on a surface forms with the surface itself (see section 2.2). This angle will be the result of the equilibrium of three tensions: the tension between the surface and the liquid, the liquid and the surrounding medium, often air, and the latter and the surface. In general, if the contact angle is low the surface is hydrophilic, i.e. the liquid drop spreads on the surface. In contrast, if the droplet has a high contact angle the surface is considered hydrophobic and the droplet does not spread on the surface.

It was observed that the cosine of the contact angle decreases with increasing fraction of hydrophilic groups on the surface. In contrast, both cell and protein adhesion to such surfaces go through a maximum rather than a static increase but are generally higher on hydrophilic than on hydrophobic surfaces.[93]

This, together with the fact that for surfaces with the same contact angle but different terminal groups the amount of adherent cells is different, suggests that the wettability affects the adhesion properties of the surface, but the adhesion is also determined by the chemistry of the functional groups on the surface.[93]

SAMs are often used to control protein immobilisation on surfaces, which has great potential in biosensor design because it allows to bind a protein to the transducer surface while maintaining its functionalities. It appears that initial interactions between proteins and surfaces are predominantly non-specific, electrostatic, hydrophilic, and reversible.[94,95] Over time, the protein may unfold and trigger more hydrophobic interactions and, ultimately, irreversibly adsorb to the surface[96] thereby loosing its biological activity.

The designed chemisorption of proteins on surfaces introduces more control of recog-

nition efficacy, but also the potential for increased molecular stability.[95] As mentioned above, carboxylic acid SAMs together with NHS-EDC chemistry is a very popular protocol to bind antibodies or others proteins covalently to functionalised surfaces, although it does not offer the possibility of controlling the orientation of the protein on the surface.

Usually, in biosensor applications, proteins immobilised on the surface are probes for the recognition of a target. If the probe is adsorbed to the surface in such a way that the binding region faces the surface rather than the solution it might lose the ability of binding the target, hence the orientation of the immobilised protein might be very important. However, even randomly oriented probes on surfaces have been shown to maintain the capability of binding the target.[97]

A charge dependent orientation of physically adsorbed antibodies on modified gold has been suggested. For amine-terminated monolayers the antibodies are oriented in a way that provides better orientation, i.e. the antibody recognition regions are exposed to solution, than when using monolayers terminated with -CH_3 and -COOH groups.

Moreover, the physical adsorption of the antibodies can be optimised by the use of a buffer with low ionic strength and pH lower than the antibodies' isoelectric point, pI, on both positively and negatively charged surfaces.[98]

Another way to control the orientation of the probe is to modify the probe itself. For example, the probe can be modified by adding a thiol on the terminal-group of the probe. In this case it is possible to either bind the protein directly onto the gold substrate or use a SAM with an appropriate functional group, e.g. COOH, to bind the modified probe to.

A different aspect is the density of the adsorbed probe on the surface. It was reported that when the probes adsorbed to a surface are densely packed, the ability of binding the target might decrease.[92]

To avoid that closely packed probes interfere with the binding of the target, attempts at controlling the spacing of the probes have been made. Mixing carboxylic acid terminated molecules with hydroxyl terminated molecules for the formation of a SAM is a widely used method to space the carboxylic acids, and thus the attached probes, and enhance the binding of the target molecule if this binding is limited by steric or electrostatic conditions.[95]

1.2.2.1 Inhibition of non-specific adsorption

For many applications, such as biosensors, surface coating of surgical implants, or hemodialysis membranes, the non-specific adsorption of proteins onto surfaces exposed to the samples containing various degrees of proteins, is a significant challenge. Therefore,

such non-specific adsorption must be controlled. Surfaces which inhibit non-specific adsorption are often called *non-fouling* surfaces.

The average total protein concentration in blood serum samples is between 60 and 80 mg/ml,[99] therefore high resistance to protein adsorption is desirable. Otherwise the signal coming from the binding of the antigen would be very low, with respect to the signal coming from non-specific binding, and would therefore become difficult to measure.

Before discussing how it is possible to introduce such characteristics on a surface, two distinctions have to be made: the first between protein adsorption from solutions containing only few proteins such as buffers spiked with small concentrations of proteins, and highly complex solutions, such as blood or plasma, containing large amounts of different proteins; the second between in vivo and in vitro conditions.

In fact, *non-fouling* surfaces highly resistant against adsorption of proteins from solutions with only few proteins may not be as efficient when exposed to blood, for example because the coagulation process is mediated and regulated by a long chain of factors and cofactors that ensure a controlled and selective adhesion of proteins, especially fibrinogen, and platelets. Fibrinogen and serum albumin are two proteins highly concentrated in blood and blood serum samples, namely 1.5 - 3 mg/ml and 35 - 50 mg/ml respectively.[99]

Most biosensor techniques are not selective per se, therefore the surface which mediate the biological interaction has to be functionalised in such a way that blocks non-specific adsorptions but allows the specific binding of the target, otherwise the non-specific response could mask the response of the sensor to the target, that is often in the range of pg-μg/ml as discussed previously. SAMs can be used in this respect and several types of alkanethiols have been investigated with good results in single protein solutions but with limited success with regard to blood compatibility.[73]

Oligo(ethylene glycol), poly(ethylene glycol) (PEG) and mixed positively-negatively charged SAMs have shown a good resistance to fibrinogen and serum albumin adsorption.[73,100–102] The resistance to adsorption of these proteins makes these SAMs suitable for use in biosensors aiming to minimise non-specific adsorption of proteins from blood samples.[103]

There are several reasons why molecules tend to absorb non-specifically at solid/water interfaces: the underlying solid substrate of the biosensor can be hydrophobic, hydrophilic or ionic. When a hydrophobic surface is immersed in water it forms a high energy interface, most biomolecules have hydrophobic areas usually buried away inside its structure. When proteins come into contact with hydrophobic surfaces in water, they tend to unfold to align their hydrophobic areas with the surface, leading to an overall decrease in free energy. While at the same time only leading to a less significant

increase in enthalpy.

PEG coating has been used to prevent protein adsorption from biological media. Each PEG ether group is H-bound to two water molecules.[104] This discovery was used to explain the capacity of PEG surfaces to resist protein and cell adhesion.

The protein adsorption resistance is attributed to two components, namely osmotic and elastic. The latter is caused by compression and restriction of the ethylene oxide chain/segments upon binding of a protein to the surface. The osmotic component is attributed to the loss of "water of hydration" that would take place when a large molecule attempts to be adsorbed onto the surface. The coils of the PEG chains are compressed and the water associated with the PEG chains is released into the bulk solution. This would lead to a significant increase in enthalpy which leads to a lowering of the free energy.

The osmotic pressure created by the steric repulsion inside the coil, the driving force for diluting the polymer concentration draws water back into the coil to minimise the free energy of the system and thus repels the approaching molecule. As the van der Waals contribution to the attractive force is smaller than the hydrophobic interaction between the protein and the hydrophobic surface, only the hydrophobic interaction is thought to compete with the steric repulsion.[105]

Shorter ethylene glycol (oligo-EG) terminated alkanethiol SAMs formed from ($HS(CH_2)_{11}(OCH_2CH_2)_nOH$, where n=2-17) have also been used to inhibit protein adsorption in many biosensors.[100] In these more densely packed, shorter SAMs, the non-fouling mechanism is different. In fact the short oligo-EG segment have less conformational freedom to lose upon protein adsorption than longer PEG chains. Consequently their capacity to resist protein and cell adsorption is generally attributed to the osmotic component of the steric repulsion model, the resistance of oligo-EG SAMs to the adsorption of protein is mainly due to the difficulty in dehydrating both ethylene glycol chains and the protein, and the amount of hydrogen bonds (or the mobility of oligo-EG chains).

It was shown that methoxy-terminated oligo-EG SAM with just 3 EG groups (3EG) on Au are resistant to adsorption of fibrinogen.[104,106] On the other end, the same SAM on Ag adsorbs up to 60% of a monolayer of fibrinogen.[106] The different behaviour was attributed to the difference in the conformation of the EG chains (figure 1.12). In fact, for 3EG on Au the spacing of sulfur on Au allows the EG chain to arrange in a helical conformation that can adsorb water molecules, while the smaller ($\approx$ 4.6 Å) spacing of sulphur on Ag, leads to an *all trans* conformation of the EG chain which is sterically prohibitive for the water molecule to bind to the EG groups.[104,106] Hence it was concluded that the hydration of the EG groups is essential to the non-fouling properties of the SAM.[94,106]

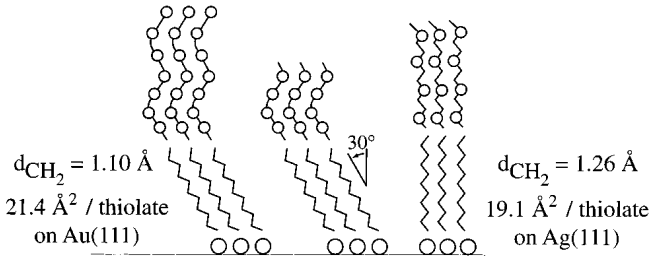

Figure 1.12: From the left, schematic depiction of oligo-EG monolayer with 6 EG groups on Au (OH terminated) and the 3EG SAM with a 30° tilt of the alkyl chain and a perpendicular orientation of the helix axis. Methoxy terminated 3EG on Ag with a perpendicular orientation of the alkyl chain and a planar zigzag conformation of the 3 EG units. Adapted from Harder et al.[106]

1.2.2.2 Mixed SAMs

Mixed monolayers have been used to functionalise the surface with different functional groups, to obtain multiple properties at the same time, and to control the spacing of a particular functional group on the surface.[107]

Mixed and reasonably homogeneous monolayers are achieved by immersing the substrate in a mixed solution of the chosen alkanethiols. It is possible to obtain different molar concentration of the grafted SAM just by varying the molarities of the SAM solution mixture.[108] The ratio between the molecules of the SAM on the surface is determined by the ratio of the molecules in solution, but is not necessarily the same.

In biosensor designs controlling the spacing of the functional group is often used to optimise the spacing of large molecules, such as antibodies, engineered proteins, DNA, cells, etc. grafted on top of the alkanethiol SAM[109] to avoid interference in the activity of one molecule with the molecules next to it.

For example, SAMs formed from a mixture of hydroxyl-terminated tri(ethylene glycol) and carboxy-terminated hexa(ethylene glycol) are often used to bind large molecules to the SAM and favour the probe target interaction by avoiding steric hindrance due to probes located close to each other on the surface.[110,111]

1.3 Thesis aim and outline

To meet the increasing demand of easy-to-use, portable, sensitive biosensors for point-of-care detection of multiple targets, the aim of this work is to develop a multiplexed label-free electrochemical biosensor platform. This thesis presents the development and characterisation of an electrochemical label-free immuno-sensor against the model target human chorionic gonadotropin (hCG), using a monoclonal antibody as bioreceptor,

suitable for highly sensitive detection in serum.

hCG belongs to the glycoprotein hormone family together with LH (luteinizing hormone), FSH (follicle-stimulating hormone) and TSH (thyroid-stimulating hormone). All members are dimers consisting of an α subunit, common to all four mentioned glycoproteins, while the β subunit is specific to the hormone and determines its biological activity. The molecular mass of hCG is about 37.5 kDa, that of the β-subunit (hCGβ) is 23.5 kDa and hCGα, the α-subunit, is 14 kDa.[112,113]

In addition to being a model system for this project, hCG is of clinical relevance as a biomarker. During pregnancy, in the first 7–10 weeks, the serum concentration increases, from the normal value of 8.6×10^{-12} M, by doubling the concentration every 1.5-2 days, up to a value between 6×10^{-8} M and 3×10^{-7} M.[114] Intact hCG, free subunits and degraded forms of hCG are sensitive biomarkers for monitoring of pregnancy, pregnancy-related disorders and several types of cancers. For example, trophoblastic tumours almost always express hCG.[114] Moreover, serum of patients with non-trophoblastic tumours present hCG immunoreactivity due to the presence of free hCGβ.[114]

Owing to its importance, several biosensors have been designed to detect hCG, and a few significant examples are discussed below. An amperometric biosensor has been designed as a sandwich assay using an anti-hCGβ antibody conjugated to a catalytic enzyme, horseradish peroxidase, as label. hCGβ was detected in horse serum with a detection limit of 7.5×10^{-12} M and an upper limit, i.e. where saturation occurs, of 2.9×10^{-10} M,[115] covering the lower end of the clinically relevant concentration range.

Briefly, a first anti-hCG antibody was immobilised on a gold electrode, subsequently the surface was exposed to the target, hCG, dissolved in horse serum. The sensor was then rinsed and exposed to the enzyme-labelled anti-hCG antibody. Finally upon exposure of the sensor to a H_2O_2 rich buffer, the horseradish peroxidase would catalyse the H_2O_2/H_2O redox reaction and a current would be recorded at the working electrode.

Although showing good sensitivity in horse serum, as any labeled biosensor, this sensor requires multiple rinsing steps and exposures to different solutions. To avoid excessive processing time from the operator, label-free biosensors for hCG have been developed.

A real-time capacitive immuno-sensor to measure hCG operating in a range of 1.6×10^{-13} M and a detection limit of 1.5×10^{-14} M in phosphate buffer has been proposed by Berggren et al.[48] In this case, anti-hCG antibodies are immobilised on a gold electrode, and the change in capacitance due to the binding of hCG to the antibody is monitored by applying a voltage step and measuring the time-dependent current response. The capacitance is calculated by least squares minimum fitting procedure of the current response, assuming that the electrode-solution interface impedance behaves

like a planar capacitor.[48] To maximise the sensitivity of the sensor, as discussed above, the working electrode was coated with a SAM and a low molarity buffer was used, thus increasing the C_{ins} and C_{dif} respectively. For further details please see section 2.1.4.4.

Although highly sensitive measurements were obtained in buffer solution, the situation looks rather different for measurements in real clinical samples. Real clinical samples are very different from low molarity buffers, in fact they contain high concentration of salts and other proteins.

A different solution for a label free hCG biosensor was proposed by Zhang et al.[116] by developing a bulk acoustic wave immuno-sensor. Detection of hCG in urine and serum in the range from 7.1×10^{-12} M to 1.4×10^{-9} M was shown.[116] In this case, an antibody is immobilised on a gold electrode on a quartz crystal transducer. When the sensor is exposed to a hCG spiked sample the antigen binds to the antibody and a change in mass is detected by a shift in the resonance frequency of the crystal.

The main advantage of the last two biosensors is the simpler execution of the measurement compared to any labeled biosensor. Despite the lack of signal amplification coming from labelling techniques, low detection limits and wide linear ranges were achieved.

An alternative electrochemical biosensor to detect hCG in serum is presented in this study. To achieve good sensitivity and selectivity, all parts of a biosensor which contribute to the final output require optimisation.

In general it is desirable to achieve good sensitivity, i.e. both low limit of detection and low noise to output ratio, and a linear output to concentration dependence over a wide concentration range, ideally covering the clinical relevant concentration range. Moreover, it is important that the sensor response is proportional to the concentration of the antigen in the sample and does not respond to other factors, such as the presence of other molecules in the sample.

To achieve this goals the interface between the transducer and the analyte is of utmost importance. In fact, thousands of publications have been dedicated to the modification of biosensor surfaces.

Therefore, the immobilisation of antibodies on the OEG SAM under different immobilisation conditions is analysed. The dependance of the amount of antibody binding on the surface and the pH is outlined. Binding of antibodies is highly increased for pHs lower than 5.5.

A relation between the amount of antibody binding and the surface response to the antigen is studied by means of surface plasmon resonance (SPR). It was found that the higher the amount of the antibodies on the surface the higher was the hCG response.

Moreover, we investigate the non-specific binding of other molecules to the modified surface.

Then the sensor surface is characterised by means of electrochemical techniques and a method for the sensing of the antigen binding to the electrode is proposed. The sensor output is generated by monitoring the phase of the impedance at low frequency and its variation with increasing concentrations of hCG. In particular, with the prospect of shortening measurement and post processing time in mind, we chose a single frequency at which the response to noise ratio was minimised and we used this quantity as output of the biosensor.

Moreover the sensor response was characterised in horse serum to show the selectivity of the sensor and to demonstrate the possibility to use this method for the analysis of real clinical samples.

The biosensor developed in this work consists of a gold electrode functionalised with an OEG monolayer, and mAb B immobilised onto the SAM by means of NHS-EDC chemistry. Measuring the phase shift of the electrode impedance as a result of the binding of intact hCG by means of non-faradaic EIS, a very high sensitivity was achieved. The detection limit in phosphate buffer was found to be lower than 2.6×10^{-17} M and a linear relationship between the phase shift and the logarithm of the concentration was found up to 2.6×10^{-13} M. In serum, the sensor can detect hCG from concentrations as low as 2.6×10^{-14} M and a has a linear response over five decades covering the clinically relevant concentration range in blood samples.

To further improve the sensitivity and repeatability of the sensors we focused our attention on the electrical characterisation of the interface between the transducer, the electrode, and the recognition element, the antibody.

The dielectric properties of acid-capped 6-(ethylene glycol)undecanethiol (OEG) SAMs and mixed mercaptoundecanol (MUD) and OEG monolayers were studied. The conductivity of the SAM decreased signficantly with the addition of small concentration of MUD in the SAM solution, especially in the range of 1 to 5 % MUD in OEG.

Thesis outline. The thesis is divided in seven chapters. In the introduction the aims of this study were outlined and the concept and important characteristics of biosensor were discussed. Moreover an overview of electrochemical label-free biosensors was given and the mechanism of detection and methods used for electrochemical biosensors were discussed.

In the second chapter the methods and techniques used in the experiments described

in the remaining chapters and their fundamental working mechanisms are explained. While chapter three instead describes the protocols and procedures followed in the experiments.

Chapter four, five and six treat the experimental work and the analysis of the data obtained.

In particular chapter four focuses on the binding and immobilisation of antibodies on OEG monolayer. The dependance of the binding of the antibody to the surface and its response to the antigen in relation to the immobilisation conditions is discussed.

In chapter five, the development of an electrochemical biosensor platform for label-free detection of the model target hCG is presented. The detection of hCG is demonstrated in buffer and in serum by means of electrochemical impedance spectroscopy. High sensitivity is achieved and a discussion of the detection mechanism and the influence of the binding of the antigen to the antibody over the impedance of the electrode is given.

Chapter six focuses on the assembly of monolayers on gold surfaces and their dielectric properties. It proposes a method for increasing the impedance of the OEG monolayer by the addition of small percentage of MUD.

In chapter seven conclusions of the whole study are presented and future perspective of the research are outlined.

Chapter 2

Methods and Techniques

In the following chapter the general concepts and the physical principles of the characterisation techniques used in this study will be discussed. The focus will be centred around the particular applications of the techniques and how they were used in this work to investigate individual stages of biosensor development. In particular, to study self-assembled monolayer (SAM) coated electrodes, the binding of recognition molecules to said electrodes, and the use of these systems as a biosensor for clinical diagnostics.

2.1 Electrochemistry

Electrochemistry studies the interactions between media containing electrons, i.e. electrodes, and media containing ions,[50] i.e. electrolytes. In particular it is concerned with the relationship between chemical and electrical effects[49] that happen at the interface between them. In electrochemical systems we focus on the transport of charges across the electrode/electrolyte interface and the factors that affect it.

Although usually only one particular electrode/electrolyte boundary is the subject of interest, this interface cannot be studied experimentally in absolution and on its own, and needs to be studied as part of a combination of boundaries. The total set of interfaces is called an *electrochemical cell*.

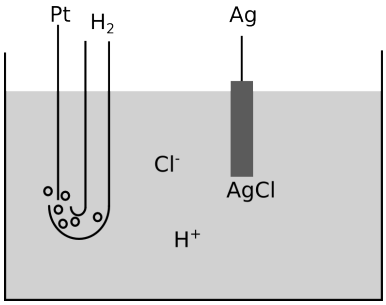

Figure 2.1: A schematic diagram depicting a typical electrochemical cell: Pt wire in a stream of H_2 and a Ag wire coated in AgCl in HCl solution. Re-drawn from Bard and Faulkner[49]

A typical electrochemical cell is shown in figure 2.1. The cell can be described as $Pt/H_2/H^+$, $Cl^-/AgCl/Ag$, where each slash represents a boundary between two media, and a comma separates two components in the same media (e.g. solution).

In general, we are interested only in one of the interfaces, the so called *working electrode*. Upon application of a voltage, between the two interfaces, we can drive the potential of the working electrode at either a more positive or more negative potential. If driving the working electrode to a more negative potential the electrons will acquire energy. A flow of electrons from the electrode to the electrolyte is induced when the energy acquired by the electrons is high enough to escape the electrode and occupy the vacant electronic states of the ions in solution. This is called a *reduction current*. In the same way, when an opposite voltage is applied, an inverse flow of electrons is induced creating an *oxidation current*.

In general the reactions that can be described as a transfer of electrons between the electrode and the solution is called a *faradaic* reaction. These follow Faraday's law, which states: the amount of chemical reaction caused by the flow of current is proportional to the amount of electricity passed.[49] In contrast if no electrons can cross the electrode/solution interface a charge accumulates at the interface, polarising the electrode. Such processes occurring at the electrode/solution interface are called *non-faradaic* processes.

2.1.1 Electrochemical potential

The *Galvani potential*, p, at a certain point, P, is defined as the work needed to bring a charge from infinity to point, P. The *Galvani potential difference*, Δp, between two media, or phases, i.e. the electrode and the electrolyte solution, instead is defined as:

$$\Delta p = [p(electrode) - p(solution)] = [\mu(electrode) - \mu(solution)]/F \tag{2.1}$$

where μ is the chemical potential of the phase and F is the Faraday constant. However neither the Galvani potential nor the Galvani potential difference are measurable. What is measurable is the difference of the Δp of two different interfaces; which is why an electrochemical cell is made of at least two half-cells, each one being an electrode/solution interface with its own Δp.

The difference between the Galvani potential differences of two interfaces, $\Delta p_1 - \Delta p_2$, is a *voltage*. Sometimes, depending on the context and the background of the authors, the terms voltage and potentials are used interchangeably.

In an electrochemical cell we measure the voltage difference between the cathode and the anode (figure 2.2). This is the summation of the Galvani potential differ-

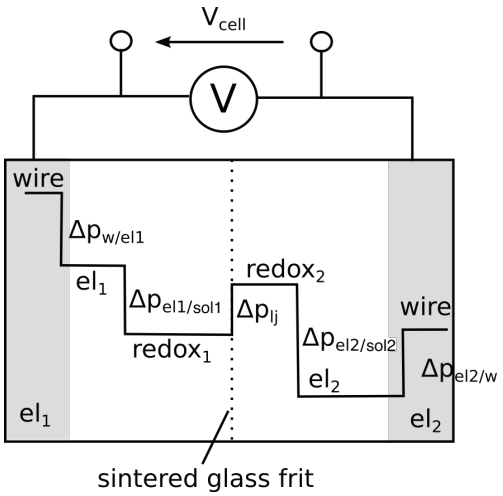

Figure 2.2: Schematic of an electrochemical cell. The measured voltage is the result of all the potential drops at each junction, metal/metal ($\Delta p_{w,el}$), metal/solution ($\Delta p_{el,sol}$), solution/solution (Δp_{lj}).

ences at each interface: metal/metal, metal/solution and solution/solution. Usually the solution/solution interface is represented by its liquid junction potential, Δp_{lj}, which is reduced as much as possible. Furthermore, the electrical connections (metal/metal) are equal and opposite so they cancel each other out, see figure 2.2. Therefore, the measured voltage is the difference between the Galvani potential differences at each electrode/solution interface:

$$\Delta V = \Delta p(el_2, sol_2) - \Delta p(el_1, sol_1) \tag{2.2}$$

where $\Delta p(el, sol)$ is the so called *electrode potential*, which is the potential drop at the electrode/solution interface.

If we consider Faraday's Law the current passing through an electrode is proportional to the rate of the reaction and the numbers of electrons involved, n, according to $I = nF \cdot rate$. Dynamic electrochemistry studies the kinetics of electron transfer reactions at the electrode/electrolyte interface, e.g. faradaic currents coming in and out of an electrode. In this case it is not the absolute voltage that matters but its relative value to another half cell at equilibrium, i.e. the potential difference of the two electrodes when no current is driven. This quantity is called *overpotential*, $\eta = \Delta p - \Delta p_{eq}$, where Δp_{eq} is the equilibrium potential.

If the electrode is polarised at a potential greater than the equilibrium potential, Δp_{eq}, then $\eta > 0$ and oxidation of the working electrode takes place, i.e. electrons flow from ions in solution to the electrode. Vice versa for $\eta < 0$ a reduction of the working electrode takes place.

The overpotential can be measured as follows: the potential of an electrode against

an electrode of a half cell with known potential, Δp_o, can be measured with the current flowing, V(I), and not flowing, V(I=0), these quantities are now given by:

$$V(I) = \Delta p - \Delta p_o,$$
$$V(I = 0) = \Delta p_{eq} - \Delta p_o,$$

therefore, $\eta = \Delta p - \Delta p_{eq} = V(I) - V(I = 0)$. The actual determination of V(I=0) can be difficult, therefore what is measured is the voltage of the electrode when no current is driven. This voltage is called open-circuit voltage (OCV).

2.1.1.1 Three-electrode cells

We have seen how it is possible to measure the overpotential using a potential of a second half cell as a reference. However what is really relevant for electrochemical studies is what is happening at one of the electrodes. When the overpotential is measured between two electrodes we cannot untangle the contribution from each electrode.

To circumvent this problem, a third electrode is introduced in the system and the voltage is measured against the third electrode. This electrode is called a *reference electrode* (RE), and it is not involved in the exchange of current between the other two electrodes.

In this configuration, the electrode of interest known as a *working electrode* (WE), the other electrode through which the current passes is called the *counter electrode* (CE).

The voltage at the working electrode, with respect to the reference electrode, can be measured, and at equilibrium is given by:

$$V_{WE-RE,eq} = \Delta p_{WE,eq} - \Delta p_{RE,eq}. \tag{2.3}$$

Instead, when current flows between working and counter electrodes, the measured voltage now also contains the overpotential at the working electrode, η_{WE}, and the potential drop across the solution between the working and reference electrode owing to the current flow from the working to the reference electrode, $I_{WE-RE}R_{WE-RE}$:

$$V_{WE-RE} = \Delta p_{WE,eq} - \Delta p_{RE,eq} + \eta_{WE} + I_{WE-RE}R_{WE-RE}. \tag{2.4}$$

A direct measurement of the overpotential occurring at the working electrode can now be obtained from the difference between equations 2.3 and 2.4, which can be expressed:

$$\eta_{WE} = V_{WE-RE} - I_{WE-RE}R_{WE-RE}, \tag{2.5}$$

once we minimise or account for the resistance drop, IR_{WE-RE}.

In general reference electrodes can be designed to have an infinite input impedance and hence the term $I_{WE-RE}R_{WE-RE} \approx 0$, and the overpotential can be approximated by:

$$\eta_{WE} = V_{WE-RE}. \tag{2.6}$$

The internationally accepted primary reference potential is the standard hydrogen electrode[49] (SHE) with all components at unit activity, i.e. $Pt/H_2(a=1)/H^+(a=1$, aqueous). Another common reference electrode also used in this study, is the silver-silver chloride electrode, i.e. Ag/AgCl/KCl (saturated in water) which has a potential of 0.197 V against SHE at 25 °C.

Usually, in an electrochemical biosensor the working electrode of the electrochemical cell acts as a transducer, it is usually functionalised by a bioreceptor and it is the electrode at which the measurement is taken. The counter electrode is used to pass a current through the working electrode, and usually no biological molecules are attached to this electrode. Last, the reference electrode is used to establish the fixed potential against which all other potentials are measured. The potential of the reference electrode does not vary with the biological and chemical processes taking place in the rest of the system. The three electrodes and the solution in which they are immersed constitute the electrochemical cell.[49–51]

2.1.2 Cyclic voltammetry

During a cyclic voltammetry (CV) procedure the voltage of the working electrode is ramped up and down between two set limit potentials, see figure 2.3. The current at the working electrode is measured and usually plotted against the voltage applied. This representation, I vs V_{WE}, is commonly called a voltammogram.

If the voltage range applied is such that some molecules in solution, or in fact on the solid, can be reduced or oxidised, the scan will produce a current peak for each reaction. Molecules that can be reduced and oxidised electrochemically within the applied potential are usually referred to as redox probes.

Consider the reversible redox, reduction $\longleftrightarrow$ oxidation, reaction:

$$A + e^- \longleftrightarrow A^-, \tag{2.7}$$

where A/A^- is a reversible redox probe in solution. When the voltage increases and approaches the reduction potential of the redox probe electrons from the working electrode leave the surface of the electrode and associate with the redox probe. Hence,

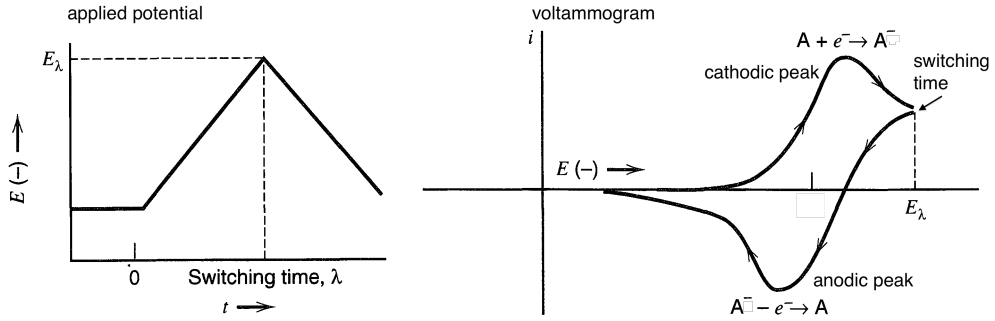

Figure 2.3: The typical scheme of a cyclic voltammetry procedure. On the left the applied potential is plotted vs time while on the right the current response is plotted vs the applied potential. Adapted from Bard and Faulkner [49]

this gains an electron, e^-, and is reduced, $A + e^- \longrightarrow A^-$. The flow of electrons from the electrode to solution results in a cathodic current. As the applied potential at the electrode continues to increase the current increases and the concentration of A next to the surface decreases until it reaches zero (cathodic peak potential). At the same time, diffusion of A from the surrounding solution increases and the mass transfer of A reaches a maximum rate and then declines as depletion occurs. Thus, the cathodic current reaches a maximum and a peak in the voltammogram is observed (figure 2.3).

At this point the potential is reversed, next to the surface there is an excess of A^-, so when the applied potential reaches the oxidation potential the electrons leave the redox probe, A^-, which loses electrons and it is oxidised, $A^- - e^- \longrightarrow A$. The electrons flow into the electrode, generating the anodic peak. The concentration of A^- decreases and the concentration of A increases until the potential reaches the anodic peak potential and the concentration of A^- approaches zero. For the same diffusion limitation as before the current has a similar shape (figure 2.3).

For example a reversible redox system often used as redox probes is ferro-ferricyanide $Fe(CN)_6^{4-/3-}$. If the redox couple is present in solution the two molecules oxidise and reduce when the voltage applied reaches the appropriate oxidation and reduction potential, exchanging current with the electrode.

The redox probes in solution are oxidised and reduced upon application of a voltage only if they can exchange electrons with the working electrode. If the electron exchange is hindered, due to slower electron transfer between the electrode and the redox probe in solution, the cathodic and anodic peak potential will occur at more negative and positive potentials, respectively.

When the transfer of electrons is blocked the peaks will disappear from the voltam-

mogram. An electrode can be blocked from exchanging electrons with the solution by introducing a coating layer, i.e. a layer of material which blocks the transfer of electrons in and out of the electrode surface.

As we will see in section 2.1.4.4 and 5.2 blocking electron transfer can be desirable. Often this condition is achieved by coating the working electrode with a compact self assembled monolayer (SAM). However defects or impurities in the electrode can lead to holes in the layer and hence the layer may only partially block the transfer of electrons.

In this situation small and broad redox peaks in the voltammogram are often observed. In general, electron transfer can occur through penetration of electrons into the layer, through tunnelling across the layer and through defects in the coating layer.[117]

2.1.3 Electrode capacitance and electrical double-layer

When a potential is applied to an electrode and the electrons cannot cross the electrode/solution interface a charge will accumulate at the electrode surface and an equal and opposite charge will be induced in the solution (see figure 2.4). This is analogous to the way in which a parallel-plates capacitor induces charge on the plates.[49] In this case the arrangement of charged molecules and dipoles in solution forms an electrical double layer. Even if it is very different from two metal plates at a given potential the electrode/solution interface is generally characterised by a capacitance, the so called *double-layer capacitance*.[49]

The term *electrical double layer* refers to the arrangement of ions and dissolved molecules in solution in proximity to an electrode that approaches the electrode to compensate for its charge with or without the application of a potential at the same electrode.[49–51]

The first theory of the formation of the double layer, formulated by von Helmholtz, consisted of a model where all the charges attracted to the electrode are located in a fixed layer situated on a plane (*outer Helmholtz plane*, OHP) and the potential drops linearly within this space (figure 2.4 A).[50,118] According to this model the potential difference, E, across two opposite charge densities equal in magnitude (q and $-q$), corresponding to the electrons at the electrode and ions at the OHP, at a distance d is:

$$E = qd/\varepsilon_0\varepsilon_r, \tag{2.8}$$

where ε_r is the relative dielectric constant of the medium between the planes. The capacitance of this charge distribution in given by:

$$C = q/E - \varepsilon_0\varepsilon_r/d. \tag{2.9}$$

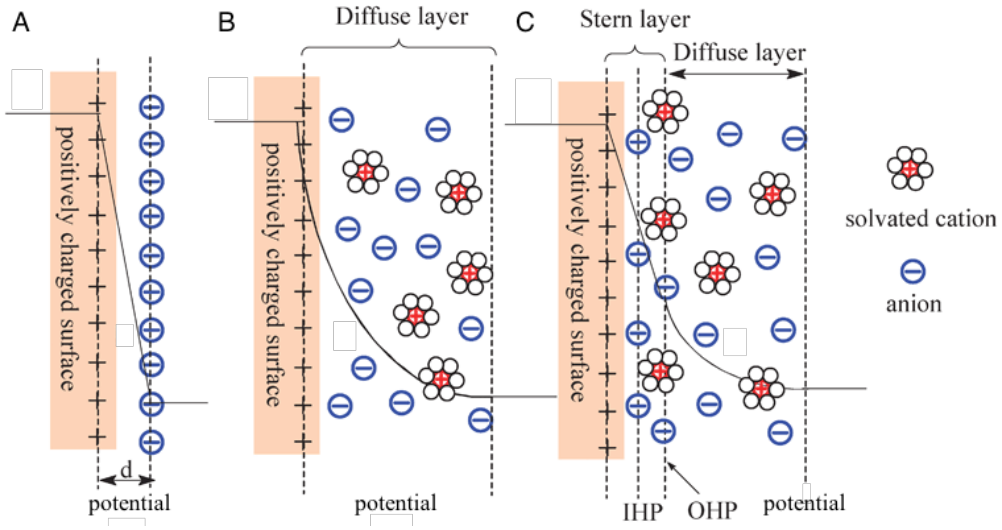

Figure 2.4: Depiction of the arrangement of charges and potential distribution at the electrode/solution interface according to the Helmholtz (A), Gouy-Chapman (B) and Stern (C) theory showing the inner Helmholtz plane (IHP) and outer Helmholtz plane (OHP). The IHP refers to the distance of closest approach of specifically adsorbed ions (generally anions) and OHP refers to that of the non-specifically adsorbed ions. The OHP is also the plane where the diffuse layer begins. d is the double layer distance described by the Helmholtz model. Redrawn from Zhang et al.[118]

Subsequently, Gouy and Chapman proposed a model based on a continuous distribution of electrolyte ions (both cations and anions) in a diffuse layer adjacent to the surface in the electrolyte solution driven by thermal motion. The charged species in solution approach the surface so that the charge of the solution in the diffuse layer is equal in magnitude and opposite in sign to the charge of the electrode. Contrary to the Helmholtz model, the potential distribution in the solution decays with the distance from the electrode as shown in figure 2.4 B. This layer was then referred to as diffuse layer.[50,118]

The Stern theory combines both theories proposing a model where the potential varies linearly from the electrode to the OHP after which it decays according to Gouy-Chapman model (figure 2.4 C). The capacitance is given by a direct summation of the Helmholtz and Gouy-Chapman respectively:[50]

$$1/C = 1/C_{HP} + 1/C_{GC} \tag{2.10}$$

As the concentration of ions in the electrolyte increases, C_{GC} increases, thus its reciprocal decreases and the electrode capacitance approaches that of the fixed layer C_{HP}.

According to the Stern theory, upon immersion of a substrate (the electrode) in a

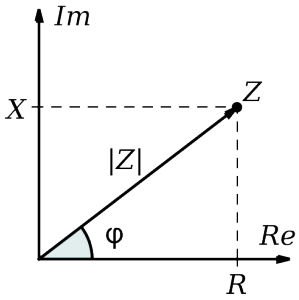

Figure 2.5: Representation of the impedance, Z, in the complex plane as imaginary, $\mathrm{Im}(Z)$, and real, $\mathrm{Re}(Z)$ parts and the polar representation where the magnitude, $|Z|$, which is the length of the vector going from the origin of the complex plane to Z and the phase, φ, which is the angle between the vector and the real axis.

solvent (the electrolyte) will wet and adsorb to the surface of the substrate. The ions and dissolved molecules in solution will adsorb at the surface in two ways. The so called *"specifically adsorbed"* molecules adsorb to the electrode by chemical or van der Waals forces, and in so doing they change the charge of the substrate surface (figure 2.4 C).[51]

These molecules, mostly anions or neutral organic molecules, lose the hydration shell that surrounded them in solution, acquire one associated with the electrode.[50] The plane that passes through the centre of these ions creates the *inner Helmholtz plane* (IHP).[49–51]

Secondly, electrostatically attracted ions, cations, approach the substrate as close as possible, whilst remaining further away from it, with respect to the specifically adsorbed molecules (see figure 2.4). These are known as *non-specifically* adsorbed molecules and maintain the solvation sheath around them forming the *outer Helmholtz plane*.

The molecules on the outer Helmholtz plane will not be sufficient to compensate for the overall charge of the substrate surface,[51] so more molecules will adsorb further away from it forming the *diffuse layer*. These molecules are more loosely bound to the surface and are consequently less ordered.

2.1.4 Electrochemical impedance spectroscopy

Electrochemical impedance spectroscopy (EIS) refers to an electrochemical technique that measures the impedance of the working electrode as a function of frequency. The measurement takes place by applying a potential perturbation at each frequency of interest and measuring the resultant current at the working electrode. The electrochemical impedance, $Z(\omega)$, is therefore estimated according to Ohm's law:

$$Z(\omega) = \frac{V(\omega)}{I(\omega)}, \tag{2.11}$$

where $V(\omega)$ and $I(\omega)$ are the applied potential and measured current respectively, in their complex representation, expressed against the angular frequency ω.
The applied voltage usually consists of a small sinusoidal perturbation (AC) typically

below 10 mV in amplitude, around a constant (DC) bias.[24] $Z(\omega)$, $V(\omega)$ and $I(\omega)$ are continuous functions in frequency, however the data acquired are discrete points in the frequency domain acquired by applying AC voltages at appropriate frequencies.

Usually the aim of EIS is to apply the smallest possible perturbation to the system so it can be studied without altering the state of the electrode.[24] Applying a DC bias alters the charge of the electrode and of any molecule attached to it. As a consequence this will have an effect on the electrical double layer surrounding the electrode. Although non-zero DC biases are usually avoided, this might be desirable in some situations.

In the case of study of redox processes at the electrode/solution interface the AC perturbation should be applied halfway between the reduction and oxidation potentials, and in this case a biased DC voltage has to be used. Other reasons that might motivate the use of a DC bias include the study of defects in coated electrodes,[119] or changing the polarisation state of the electrode to favour a certain reaction.[24]

In general the measured impedance is a complex number and can therefore be represented by either the real, Re(Z), and imaginary, Im(Z), parts or in its polar form (fig 2.5), i.e. magnitude, $|Z|$, and phase, φ, respectively. These are defined by:

$$|Z| = \sqrt{\mathrm{Re}^2(Z) + \mathrm{Im}^2(Z)};$$
$$\varphi = \mathrm{arctg}\frac{\mathrm{Im}(Z)}{\mathrm{Re}(Z)}.$$

EIS is often used to characterise the properties of the working electrode, by interrogating the electrode over a spectrum of frequencies and measuring any response to the perturbation.

If we consider the electrode impedance as representative of the system, then the complexity of the electrode/solution interface and the reactions that happen across it can be seen as a "black-box". An equivalent circuit model may be found to represent the same impedance as the system under study.

2.1.4.1 The system as a Black-box

In general any physical system can be treated as a "black-box" and can be studied by an interrogation/response method. A perturbation is introduced in the system (input) and the response of the system is recorded (output). The aim is to find a mathematical expression that describes the system (figure 2.6).

Usually the system is studied by making a mathematical transformation of the input

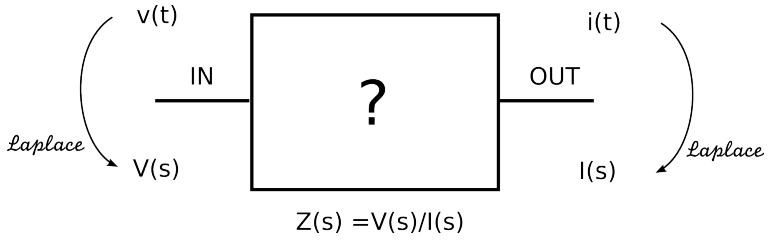

Figure 2.6: Block diagram of an unknown system. The input, v(t), and output, i(t) in time are transformed by a Laplace transformation to find the transfer function, Z(s)=V(s)/I(s) in the Laplace domain.

and output, by means of a Laplace transformation, $\mathcal{L}\{f(t)\}(s)$, according to:

$$F(s) = \mathcal{L}\{f(t)\}(s) = \int_0^\infty e^{-st} f(t)\, dt \tag{2.12}$$

In the Laplace domain, the function that models the system, the (*transfer function*), is simply obtained as a ratio between the input and output. After the determination of the transfer function the output of the system can be predicted for any given input.

The transfer function can be an abstract model of the system and is not necessarily a direct physical representation of the actual physical processes occurring in that system. For example, mechanical problems are often solved with electrical circuits made of circuit elements such as inductors, capacitors and generators to represent a mass, spring and load respectively.

This is possible because the differential equations, in the time domain, that describe the system inside the black box and the one used to describe the abstract model, e.g. an equivalent circuit, are similar. What changes are generally the coefficients of the equations. Therefore once the equations that model the system in the box are understood, by finding the coefficients that approximate the output for any given input, an equivalent model of the system is created.

The transfer function has also other interesting properties. It is independent of the input, while in the time domain the function that describes the output changes with the input. Different transfer functions can be added and multiplied when different systems interact.

After the transfer function is found, if some knowledge of the physics of the system is available, then the parameter of the equivalent model can be associated with a physical characteristic of the system.

In general the idea is that the equivalent circuit is physically representative of the system and its elements represent a specific characteristic of the system, so that the

value of the parameters will vary in accordance with the change of this characteristic.

For systems that can be interrogated by applying a voltage, like an electrode, studying the system in the frequency domain is almost equivalent to transforming the input and output by a Laplace transformation. In fact the Laplace transform of V, I and Z can be obtained by replacing $j\omega$ with the independent variable of the Laplace domain, s. $Z(j\omega)$ has therefore all the properties of a transfer function.

2.1.4.2 Equivalent circuits

Several equivalent circuits have been proposed[21,49,120,121] to approximate the impedance of a working electrode. They generally form a network of four types of circuit elements: resistors (R), capacitors (C), and non-physical elements such as a constant-phase element (CPE) or a Warburg element (W). The impedances of these elements are defined as follows:

$$Z_R = R; \tag{2.13}$$

$$Z_C = 1/(j\omega C); \tag{2.14}$$

$$Z_{\mathrm{CPE}} = 1/((j\omega)^{\alpha}Q), \quad \alpha \leqslant 1; \tag{2.15}$$

$$Z_W = 1/((j\omega)^{1/2}W). \tag{2.16}$$

We note that the Warburg element and the capacitor are special cases of the CPE where α is equal to 0.5 and 1, respectively.

A number of equivalent circuit elements are arranged into an equivalent circuit such that the impedance of the equivalent circuit matches the impedance of the system. For example if the measured impedance shows the characteristics of a resistive system then a resistor would be added. In the same way if the behaviour of the system is similar to a capacitor then the system can be modelled as such.

However the processes at the electrode/solution interface are complex, and the experimentally determined impedance cannot always be modelled by standard circuit elements, such as resistors and capacitors. To model the acquired data two elements have been introduced, namely the CPE and the Warburg element.[49]

The CPE is an element which is similar to a capacitor but instead of having a phase of -90° it has a constant phase generally smaller than -90°. When the parameter α is equal to 1 the CPE corresponds to a capacitor. The CPE has been introduced because the behaviour of a solid electrode usually deviates from that a capacitor. Generally the deviation is attributed to microscopic surface roughness[122] and chemical inhomogeneities of the surface and of the adsorbed ions.[123] Introducing a CPE improves the model by improving the data fitting for solid electrodes.

When faradaic processes come into play, the oxidation or reduction currents can be limited by the availability of the redox molecules in the solution next to the surface. To account for this, the behaviour of electrodes has been modelled by the introduction of the Warburg element.[124] This can be thought of as representing a "resistance" to mass transport.[49] This behaviour becomes dominant at low frequencies when the time scale of the voltage applied is comparable with the diffusion process of the redox species in solution. In this case the system is called a diffusion-controlled system. In contrast, at high frequencies the voltage at the working electrode changes so fast that the solvents have no time to diffuse towards or from the electrode surface, therefore the Warburg element can be neglected.

2.1.4.3 Randles circuit

As discussed previously, molecules and ions present in solution adsorb at the interface between the electrode and the solution, forming the electrochemical double layer. In first approximation, this layer exhibits a capacitive behaviour.

When redox probes are present in solution, upon application of an appropriate voltage oxidation and reduction currents between the electrode and the redox probes are expected to appear. These currents can be modelled by the introduction of a resistive component in parallel to the double layer capacitance.

Moreover, since the impedance is measured by applying a voltage between the working and counter electrodes, the solution resistance between the two electrodes passing the current should also be taken into account.

An equivalent circuit used very often to model EIS measurements in the presence of redox probes is the so called *"Randles equivalent circuit"* (figure 1.8 B). Following closely Bard and Faulkner,[49] we describe below the physical interpretation usually attributed to the circuit elements in the Randles equivalent circuit. The total current through the electrode/solution interface is considered as the sum of the current from faradaic processes, i_f, and from the double-layer charging, i_c. The double-layer capacitance is represented by the capacitor C_{dl} whereas the faradaic process are considered as a generic impedance, Z_f. Of course, both currents pass through the solution resistance, R_{sol}.

The impedance Z_f can be either described as a *series resistance*, R_s, in series with and a pseudo-capacitance, C_s or as the so called *charge-transfer resistance*, R_{ct}, and the *Warburg impedance*,[49,50] Z_w, see figure 1.8.

The pseudo-capacitance C_s originates at the electrode/solution interface when a faradaic current induces accumulation of charge at the electrode. The charge transfer in the faradaic reaction is limited by a lack of either available surface or reactive molecules

in solution. This capacitance is separated from the double layer capacitance and relies on faradaic processes, in contrast a standard capacitor accumulates charge electrostatically, which is a non-faradaic process.

The resistance R_s is a dynamic resistance, i.e. its value changes with the frequency of the voltage applied, and is related to the charge transfer resistance and the pseudo-capacitance by:[49]

$$R_s = R_{ct} - \frac{1}{\omega C_s} = R_{ct} + \frac{\sigma}{\omega^{1/2}}, \tag{2.17}$$

where σ is the slope of the linear relationship obtained when C_s and R_s are plotted against $\omega^{1/2}$. This coefficient, called *Warburg coefficient* can be predicted from the parameters of the experiment, that is:[49]

$$\sigma = RT/(F^2 A\sqrt{2})[1/(\sqrt{D_O}c_O) + 1/(\sqrt{D_R}c_R)], \tag{2.18}$$

where D_O and D_R are the diffusion coefficient of oxidised and reduced molecules, respectively, and c_O and c_R are the concentrations of oxidised and reduce molecules in solution.

The charge-transfer resistance is a pure resistive element which represent how readily the charge, the electrons, transfer at the electrode solution interface for redox processes. As described in section 2.1.1 at the equilibrium potential no net current is exchanged at the electrode. However we can consider the total net current as sum of the *exchange current* at the electrode, I_0. The latter is equal in magnitude to either the reduction or oxidation current at equilibrium. Therefore, for a one electron process, R_{ct} is defined as:[49]

$$R_{ct} = RT/FI_0. \tag{2.19}$$

When the charge transfer is very agile R_{ct} approaches zero. This implies that in this condition $R_s \to \sigma/\omega^{1/2}$.

Instead, the Warburg impedance represents the effect of mass transfer due to diffusion effects, in fact it is relevant only for low frequencies when the time scale of diffusion of the molecules are similar to the time scales of the measurement. The magnitude of the Warburg impedance is given by:[49]

$$Z_f = \left(\frac{2}{\omega}\right)^{1/2} \sigma. \tag{2.20}$$

The values of the circuit elements of the equivalent circuit can be evaluated from the *Nyquist plot*, i.e. the plot of Im(Z) vs Re(Z), of the total impedance (figure 1.8).

At low frequencies ($\omega \to 0$) the Nyquist plot of Z is linear and has a unit slope, the intercept with the real axis is equal to: $R_{sol} + R_{ct} - 2\sigma^2 C_{dl}$.

At low frequencies the system is characterised by a diffusion-controlled process. In fact, the frequency dependence comes only from the Warburg impedance. As the frequency rises R_{ct} and the double-layer capacitance, C_{dl}, becomes dominant. At high-frequencies ($\omega \to \infty$) the Warburg element becomes redundant with respect to R_{ct} then the frequency dependence is due to the double layer capacitance and R_{ct}. In this case the Nyquist plot is a circumference centred on $R_{sol} + R_{ct}/2$ with a diameter equal to R_{ct} (figure 1.8).

2.1.4.4 Coated electrode

As it is the particular interest to this study, we now discuss the typical impedance of a SAM coated electrode and some of the various equivalent circuit models used to describe such a system.

Densely packed SAMs have very good dielectric properties[125] and hinder electrons and ionic transfer from solution to the working electrode. Therefore their behaviour has been modelled by different equivalent circuits in respect to the Randles circuit.[125–127]

Due to the blocking properties of the SAM the faradaic processes become less important and therefore the impedance of the working electrode is often measured in the absence of the redox probes.[21,48,126] Thus the Randles circuit (figure 1.8 B) is no longer representative of the system.[49,128]

When the electrode is coated by a SAM the Stern layer is pushed away and the capacitance associated with the electrode changes (figures 1.5). This change in capacitance arises from the increased distance between the Stern layer and the electrode and the dielectric properties of the SAM. When using the electrode as a biosensor, which is the ultimate goal of this study, usually an additional layer, the recognition layer, is attached to the SAM[24,48] thereby leading to a further capacitive contribution to the overall impedance (figure 1.5).

There are different approaches to the modelling of the impedance of this system.

Time domain. First the total capacitance of the coated electrode, at the electrode/solution interface, can be described by a series of three capacitors.[49] The first capacitance is the one associated with the coating layer, C_{SAM}. The second is associated with the probe and its Stern layer. This capacitance includes the Stern layer, any molecule bound to the coating (such as the probe) and solvent molecules adsorbed to them, C_{rec}, e.g. water. The third capacitance takes into account the molecules associated with the diffuse layer extending into the bulk solution, C_{dif}.[48] The total capacitance can

therefore be expresses as:

$$\frac{1}{C_{tot}} = \frac{1}{C_{SAM}} + \frac{1}{C_{rec}} + \frac{1}{C_{dif}}. \tag{2.21}$$

The total capacitance, C_{tot}, can be evaluated by measuring the transient current, $i(t)$, at the working electrode that occurs as a consequence of a potentiostatic step, $u(t)$.[32,48] The impedance of the electrode/solution interface can be modelled as a resistor, R_s and a total capacitor, C_{tot}, in series. To estimate the capacitance the recorded current is then fitted to an exponential decay curve, typical of such circuits, according to:

$$i(t) = u(t)/R_s e^{-t/(R_s C_{tot})}, \tag{2.22}$$

where R_s is the dynamic resistance of the monolayer.

This method is valid only if no electrons are exchanged between the surface of the electrode and the molecules in solution. In fact, all the current measured from the system is a capacitive current. This is only the case if the coating of the working electrode has a very good blocking properties.

When a molecule binds to an immobilised probe the capacitance of the recognition layer, C_{rec}, changes. If the latter is not the smallest capacitor the change would be difficult to detect, as the smallest capacitor is found to dominate the total capacitance.[32,48] This is an important consideration for the sensitivity of the system.

In general the capacitance, C, of a parallel plates capacitor is defined by:

$$C = \varepsilon_0 \varepsilon_r A/d, \tag{2.23}$$

where ε_0 and ε_r are the absolute and relative permittivity constants, respectively. A is the surface area of the electrode and d is the distance between the two plates of the capacitor. The total capacitance, C_{tot}, can be thought of as a parallel plates capacitor where one plate is constituted by the electrode and the second plate by the outer Helmholtz plane of electrical double layer.

The change in capacitance is most commonly attributed[32,48] to a change in the distance, d, between the two plates of the capacitor, caused by the binding of the analyte to the electrode. When binding takes place the molecules in solution associated with the probe are displaced by the binding molecules, this "pushes" the electrochemical double layer further away from the electrode.

If the target has very different properties with respect to the immobilised probe (e.g. it is substantially bigger) has different dielectric constant, ε_r, or is in a different charged state, then the binding of this molecule can influence the system and lead to

the change in impedance as well.[21,24] Moreover the binding of the target displaces water molecules and the change in permittivity (ε_r is between 2 to 5 for biomolecules and 80 for water),[24] might change the dielectric properties of the final layer.

The binding event may increase the thickness of the recognition layer or decrease ε_r, thus decreasing the total capacitance, C_{tot}. To detect more easily a change in the recognition capacitance, the capacitance of the SAM and diffuse-layer should be as big as possible.

On the other hand, imperfections in the SAM can influence and in fact even dominate the sensor behaviour. These defects can be modelled by a leakage resistor added in parallel to the SAM capacitance. If the presence of defects is high enough, i.e. the resistance is low enough, the layer behaviour is dominated by the resistive behaviour which can become dominant. Thus, the introductions of such defects makes the change in C_{rec} more difficult to detect. However, for different biosensors, the changes in this resistor can also be used as sensor output.[129,130]

Frequency domain. An alternative method is to evaluate the impedance of the electrode/solution interface as function of frequency (see figure 2.7).[126] Accounting for the solution resistance between the working and counter electrode, the equivalent circuit of the system is constituted by a capacitor (CPE, with $\alpha = 1$) representing the electrode/solution interface total capacitance, and a resistor representing the solution resistance. The impedance of this circuit (figure 2.7 A) has a phase asymptotically approaching -90° for $\omega \to 0$ and 0° for $\omega \to \infty$, while the magnitude approaches the solution resistance for $\omega \to \infty$ and increases for $\omega \to 0$.

However, to account for non-ideal behaviour of the electrode,[120,121] such as surface defects, like chemical inhomogeneities or surface roughness;[120,123] surface reactions with different rate constants; or non-ideal behaviour of the coating layer[126] observed on the surface of coated electrodes; the ideal capacitor ($\alpha = 1$) associated with the SAM can be substituted by a CPE ($\alpha \leqslant 1$). This leads to a constant phase of the circuit, higher than -90°, for $\omega \to 0$ and 0° for $\omega \to \infty$. The magnitude of the impedance approaches the solution resistance for $\omega \to \infty$ and increases for $\omega \to 0$ but with slower rates as α decreases.

When the SAM has defects such as pin-holes, ions from solution can access the surface and electrons can tunnel through the monolayer more easily. Therefore the behaviour of the coating layer changes and a current can leak through the pin-holes. In such circumstances neither an ideal capacitor nor a CPE can model the leaking current. However, the current can be modelled by a resistive component and therefore the capacitance associated with the SAM is substituted by a capacitor in parallel to a

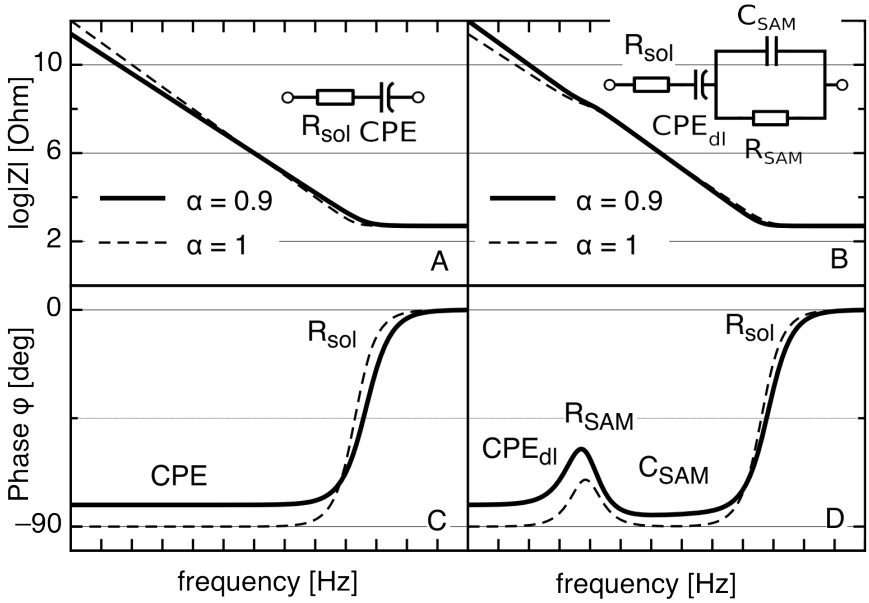

Figure 2.7: A, Magnitude and, C, phase of the impedance for the equivalent circuit shown in the inset of figure A. B, Magnitude and, D, phase of the impedance for the equivalent circuit in the inset in figure B. Two values of the α parameter of the CPE are shown, namely $\alpha = 1$ (dashed line), ideal capacitance, or $\alpha = 0.9$ (solid line), i.e. non-ideal capacitance. Next to the phase plots the circuit elements that influence the phase behaviour most significantly at the provided frequency range are indicated.

resistor, often called a leaky-capacitor.

Considering a system where the electrode is coated by a poor blocking SAM, the electrode/solution interface can be modelled by a leaky capacitance representing the leaky-SAM in series with a CPE. This represents the non-ideality of the Stern layer and a resistor representing the solution resistance as proposed in figure 2.7 B.

In this case the phase approaches 0° for $\omega \to \infty$ and drops for smaller frequencies approaching a phase $> -90^\circ$ for $\alpha < 1$. This subsequently increases again, due to the leaking current trough the SAM and will eventually drop once more approaching a constant value for $\omega \to 0$ (see figure 2.7 D). The introduction of a resistor component associated with the imperfection of the SAM layer introduces a second time constant that results in a peak in the phase of the impedance at low frequencies.

The value of the solution resistance influences the position of the first drop in phase at higher frequencies. For highly resistive SAMs (i.e. more blocking SAMs) the peak will be smaller and shifted to lower frequencies. The capacitance of the SAM and the double layer CPE instead influence mostly the height and the width of the peak (figure 2.7).

Keeping these considerations in mind a qualitative analysis of the phase spectrum of

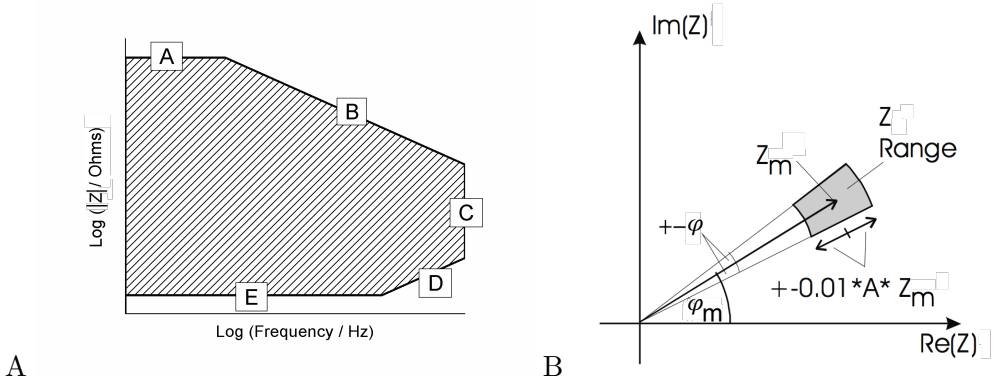

A B

Figure 2.8: A) Generic accuracy contour plot. The graph is a log-log plot, fashioned as a Bode plot. The magnitude, $|Z|$, of the impedance is plotted versus frequency. The hatched area indicates the region in which EIS measurements can be done in a specific accuracy. The labels A to E are described in the text. B) Schematic representation of the accuracy of the measured impedance Z_m defined by a percentage factor A with respect to $|Z_m|$, and a phase deviation φ with respect to φ_m. The grey area represents the region where the actual impedance Z is. Redrawn from Gamry application notes (A) and Novocontrol specification manual (B).[a]

the impedance can provide valuable information when developing an equivalent circuit model for such a system.[119]

2.1.5 Instrument accuracy and precision

The EIS measurement represents the cell but also the instrument and the connecting cables. The instrument used to perform EIS measurements was a VSP potentiostat (BioLogic, France). The instrumentation has limitations and is not always able to measure the cell correctly, in particular at extreme frequencies and impedances. The accuracy contour plot (ACP), shown in figure 2.8 A, describes a region in which the potentiostat has at least a certain accuracy (figure 2.8 B), and hence the hatched area represents the region in which the measurements can be done with a specified accuracy.

The limit A and E (figure 2.8 A) represent the maximum and minimum impedance that can be measured with a certain accuracy. The limit A is of particular interest for this study since coated electrodes can produce high impedance systems. The magnitude of the impedance is limited by drift in the current response, drift in the current in the instrument's circuits or internal resistance of the instrument. The drift can lead to a non predictable phase response while the internal resistance causes the phase to shift toward zero .

[a] www.gamry.com/application-notes/accuracy-contour-plots-measurement-and-discussion, Jan 2014, www.novocontrol.de/pdf_s/POTGAL_spec.pdf, Jan 2014

The cell current in this region is very small. For a typical EIS an AC signal of 10 mV is applied, if the cell has an impedance $|Z|$ of 1 GΩ the passing current is just 10 pA. The accuracy at this limit can be increased by increasing the amplitude of the excitation. However, at large excitations the accuracy is limited by the internal resistance of the instrument.

Analogous to limit A, at limit E the potentiostat is limited by its ability to measure high currents.

Limit B represents the accuracy limit of the potentiostat for the measurement of low capacitances. The value of this capacitive limit is a concern when studying dielectrics, or organic coatings with good blocking properties. The position of limit B is usually specified by giving the value of the capacitor whose impedance corresponds to this line, according to equation 2.15.

One way of increasing the current measured at the working electrode, as well as increasing its capacitance, is to increase the area of the working electrode so that both the current and the capacitance fall in the region of the potentiostat where accurate measurements can be performed.

Limit C represents the maximum measurable frequency. Although, in this region the instrument has the highest accuracy, the cell can produce experimental artefacts due to slow response of the reference electrode. Moreover the frequency response of the potentiostat's components and the slew rate, i.e. how fast a component's output change for a change at the input, of the potentiostat's amplifiers can affect the measurements.

Limit D is important for high frequency studies at low impedance, such as for the study of fuel cells and batteries. The main reason for artefacts to appear in this region is the inductance due to the formation of coils between the connection cables between the cell and the instrument or the movement of the cables or the cell in the coil.

The system under study is a high impedance system, and as seen in the following chapters, the main focus is on the low frequency range. Therefore limit A is the biggest concern. The ACP plot of a VSP potentiostat (BioLogic, France) fitted with low current option, as used in this study, is reported in figure 2.9. Moreover the maximum current resolution of the potentiostat is 76 fA.

As it will be shown in chapters 5 and 6, the EIS were performed between 100 kHz and 50 mHz. However the phase at 100 mHz was taken as representative value of the system. The maximum measured impedance at this frequency was obtained for mercaptoundecanol SAM on template stripped gold (see section 6.1.1) which led to $|Z|_{0.1} \approx 13$ MΩ. $|Z|_{0.1}$ is inside the ACP.

Moreover we can calculate the current passing though the working electrode for an AC excitation of 10 mV, I_{WE} is approximately 80 nA which is few orders of magnitudes

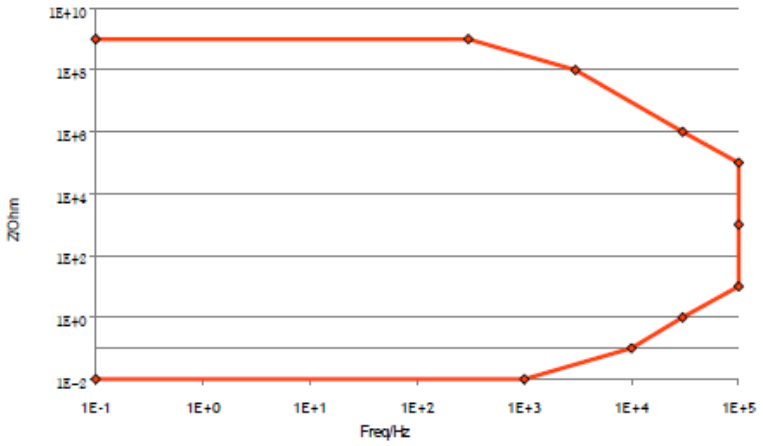

Figure 2.9: Accuracy contour plot for a VSP potentiostat fitted with low current option used in this work, the area inside the contour represents an accuracy better than 1% for the impedance's magnitude and better than 1° for the impedance's phase. Obtained from VSP potentiostat manual.[b]

higher than the current resolution.

Considering that in this work the phase *variation* of the system at a single frequency is often considered, the precision of the instrument can be more important than its accuracy. Since the precision of the instrument is not available from the manufacturer a dummy-cell has been built so that its impedance would be comparable to or higher than the system under study (figure 2.10). As a measure of precision, the standard deviation of the measured phase in the lower frequency range is reported in figure 2.11. As trade off between the size of the signal, the precision of the instrument and the time necessary to acquire a measurement, 0.1 Hz was chosen to be the single frequency to be monitored. For 0.1 Hz the standard deviation is 0.11° in both dummy-cells.

2.2 Contact angle

The wetting of a solid is the process of bringing a liquid into contact with the solid surface. Every wetting system is characterised by a contact angle between the liquid and the solid which is the result of the equilibrium between three phases: the liquid, the solid and the fluid in which they are immersed. The latter is typically a gas, e.g room air.[131] The contact angle is defined as the angle between the tangent to the liquid-fluid interface and the tangent to the solid surface at the contact line between the three phases[131] (figure 2.12). This is the result of the equilibrium between the surface tensions

[b] www.bio-logic.info/files/ec-lab/VMP3-based-installation-and-configuration-manual.pdf, Jan 2014

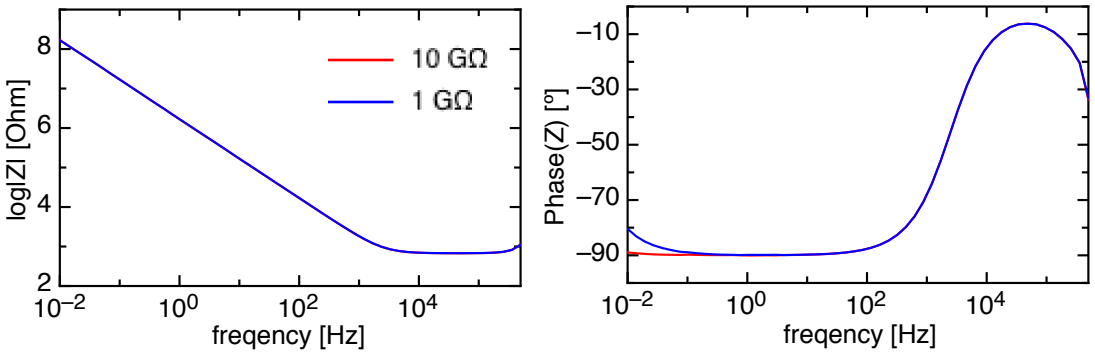

Figure 2.10: Bode plot of the measured impedance for the dummy cell where C_{ref} = 10 pF, R_{ref} = 2 kΩ, R_1 = 675 Ω, C_1 = 100 nF and R_2 is either 1 or 10 GΩ.

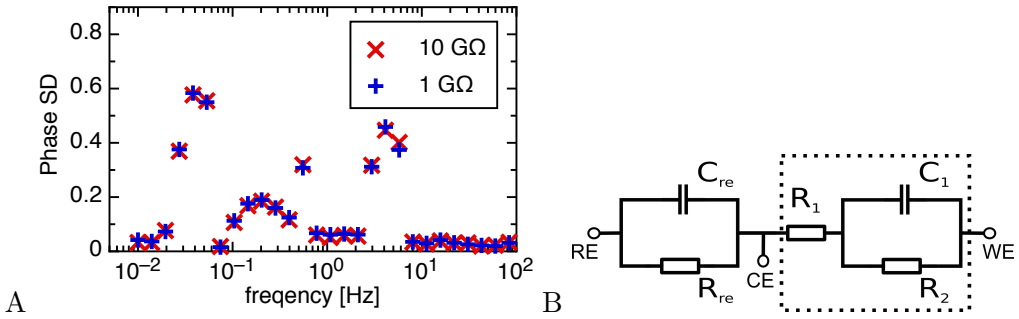

Figure 2.11: Plot of the standard deviation of the phase of the impedance (A) measured by means of EIS with a VSP potentiostat for the dummy cell (B) over 100 measurements across the space of 5 hours. The resistor R_2 in the dummy cell was varied from 1 GΩ to 10 GΩ.

of the three phases, as detailed below. In general, the lower the contact angle the more hydrophilic the solid surface is considered.

There are multiple possible solid/liquid/fluid systems but we will always refer to the one used in this study (as is found to be the most practical in a laboratory setting) which is a water drop on top of a solid surface (sessile drop) in ambient air.

Due to the complexity of the system and of the additional difficulty of real experimental conditions, as explained later on, contact angle measurements are challenging to interpret and to extract physical meaning.[131–134] However, they are relatively inexpensive and easy to undertake within a laboratory setting. Therefore, they are often used for the evaluation of hydrophobicity of a surface and are a rapid means of estimating physical and chemical homogeneity of surfaces.

The equilibrium of any system is reached when the Gibbs free energy, G, is minimal.

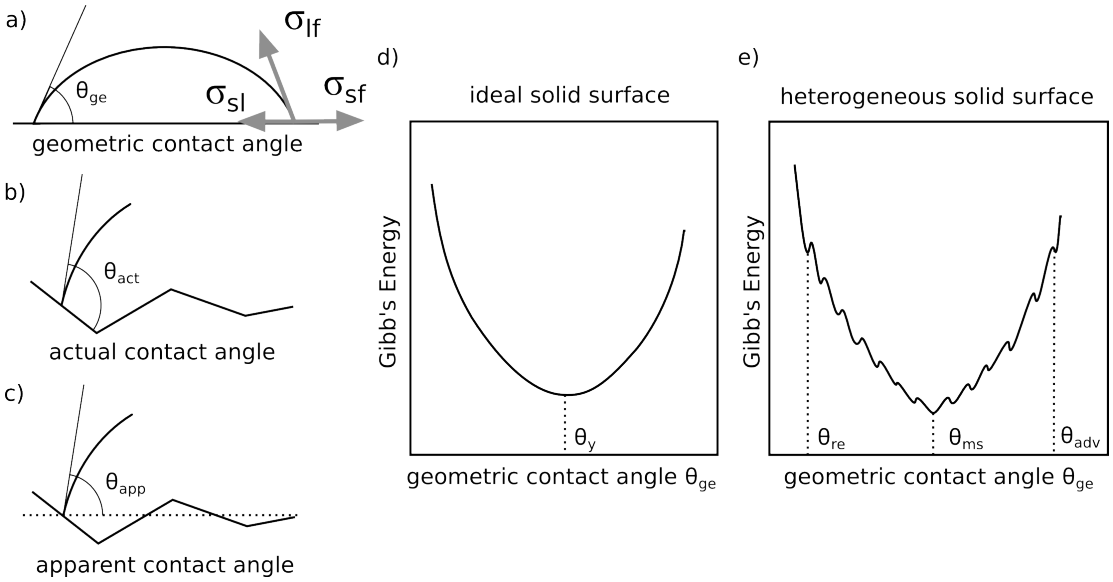

Figure 2.12: Drawing depicting of geometric contact angle (a), actual contact angle (b) and apparent contact angle (c). Relation between Gibbs free energy and Young's contact angle for an ideal surface (d) and most stable, receding and advancing contact angle, for a heterogeneous solid surface (e). Adapted from A Marmur.[131]

The Gibbs free energy for a wetting system is given by:

$$G = \sigma_{lf} A_{lf} + \sigma_{sl} A_{sl} + \sigma_{sf} A_{sf}, \tag{2.24}$$

where σ is the interfacial tension, A is the interfacial surface area and the subscripts lf, sl and sf indicate the respective liquid/fluid, solid/liquid and solid/fluid interfaces.

On an ideal surface, smooth and chemically homogeneous, the Gibbs free energy as a function of the geometric contact angle, θ_{ge}, has a single minimum called the ideal contact angle, θ_{id} (figure 2.12). If the interfacial tensions, σ, are constant over their respective interfaces then the ideal contact angle is equal to the Young's contact angle,[135] θ_Y, defined as:

$$\cos\,\theta_Y = \frac{\sigma_{sf} - \sigma_{sl}}{\sigma_{lf}}. \tag{2.25}$$

However, real surfaces are generally rough and non-homogeneous, thus the actual contact angle, θ_{act}, varies along the contact line and in general is not measurable. What is measurable instead is the apparent contact angle, θ_{app}. Therefore a relationship between θ_{app} and θ_Y would be desirable. This relationship depends on the characteristics of the solid surface under measure. In an ideal case, the apparent and ideal contact angles are

the same. If the surface is chemically heterogeneous but smooth then it would be in principle possible to measure multiple local apparent contact angles.

On a real solid surface the Gibbs free energy versus geometric contact angle function (G vs θ_{ge}) presents a discrete number of minima, each associated with a possible metastable state, see figure 2.12. The absolute minimum is the so called most stable contact angle. The extremes of the metastable states are the receding contact angle, θ_{re}, lower boundary, and the advancing contact angle, θ_{adv}, higher boundary.

Note that the receding and advancing contact angles are, respectively, the smallest and highest possible apparent contact angles measured at equilibrium, macroscopically, between the tangent of the liquid-fluid interface and the apparent solid surface. They are measured by decreasing, θ_{re}, or increasing, θ_{adv}, the volume of the drop on the surface until the contact line indeed recedes or advances.

The range of all possible metastable states, limited between θ_{re} and θ_{adv}, is called hysteresis. Because of the presence of disturbances (e.g. vibrations) in a real laboratory environment the measured hysteresis is higher than the theoretical one.[132]

The hysteresis can be used as an empirical measure of the chemical heterogeneity of the surface and as a means of estimation for the most stable contact angle. Two empirical relationships have been proposed:

$$\cos\theta_{ms} = \frac{\cos\theta_{adv} + \cos\theta_{re}}{2};$$
$$\theta_{ms} = \frac{\theta_{adv} + \theta_{re}}{2}.$$

However, neither of these relations, although widely used, has a solid theoretical foundation.[131,132]

The physical interpretation of the hysteresis is usually related to the surface roughness and chemical heterogeneity of the surface; a higher hysteresis is considered to be characteristic of higher heterogeneity and/or roughness.[133,134]

A further metastable state is often measured by placing a drop on the surface and measuring the apparent contact angle as presented. The latter is typically referred to as the static contact angle. The static contact angle is measured by simply depositing a droplet of the liquid upon the sample surface from a fixed height and leaving the drop to spread. The contact angle is therefore determined by the dynamic process that happens when the drop lands on the surface and the oscillations that follow. Therefore this state is intrinsically ill-determined and difficult to interpret.[131,132]

To ensure that the data collected experimentally are significant, one must ensure that the drop has rotational symmetry and its size is two or three orders of magnitude larger than both the surface roughness and chemical heterogeneity.[131] To meet these

conditions, for example, a camera can be used to take a picture of the drop from above to insure rotational symmetry. Moreover, many pictures per sample can be taken in different spots so to have a good understanding of the experimental error.

In this work this technique was used as a preliminary investigation to asses the chemical heterogeneity and roughness of mixed self assembled monolayers and investigate the formation of islands in the layer. It was expected that an increase in the number of islands would increase the heterogeneity of the surface thus giving rise to a higher hysteresis.

2.3 Surface plasmon resonance

Surface plasmon resonance (SPR) is a widely used technique for the characterisation of a solid/liquid interface from a physical, chemical and biological point of view. The generation of a surface plasmon is possible if free electrons are present at the interface. In practice this means that one of the two materials is usually a metal with free electrons able to conduct the plasmon. As described by Kooyman,[136] the surface plasmon can be seen as an electron density wave that propagates at the interface between the metal and dielectric.

2.3.1 Surface plasmon

Lets first approach the problem from a simple interface between two materials with different refractive indices, n_1 and n_2. The electromagnetic plane wave propagating in a medium with refractive index n can be described by an electric field $\boldsymbol{E}$ and its vector can be expressed as:

$$\boldsymbol{E} = E_0 e^{j\omega t - j\boldsymbol{k}\cdot\boldsymbol{r}}; \tag{2.26}$$

where E_0 is the amplitude of the electric field, ω is the angular frequency, $\boldsymbol{k} = (k_x, k_y, k_z)$ is the wave vector parallel to $\boldsymbol{E}$, $\boldsymbol{r} = (x, y, z)$ is the position vector and j is the imaginary unit.
Without loss of generality, we can assume a two dimensional case (figure 2.13), and define the electric field as:

$$\boldsymbol{E} = E_0 e^{j\omega t - jk_x x - jk_y y}; \tag{2.27}$$

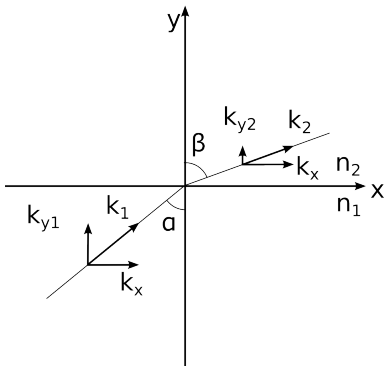

Figure 2.13: Representation of the wave vector, $\boldsymbol{k}$, and its components in a two dimensional system refracting between two materials with different refractive indices, namely n_1 and n_2. From Snell's law $n_1 \sin\alpha = n_2 \sin\beta$ therefore $k_{x1} = k_{x2} = k_x$ and $k_{y2}^2 = n_1^2(2\pi/\lambda)^2(n_2^2/n_1^2 - \sin^2\alpha)$

where the module of the wave vector is:

$$\boldsymbol{k} = \sqrt{k_x^2 + k_y^2} = n\frac{\omega}{c} = n\frac{2\pi}{\lambda}, \tag{2.28}$$

where λ and c are the wavelength and propagation velocity in vacuum, respectively, and n_1 and n_2 are the refractive index of medium 1 and 2, respectively.

When E propagates between the two media the wave vector of E will change. For particular incident angles ($\sin\alpha > n_2/n_1$) the component of the electric field normal to the incidence plane, in the second material, E_{y2}, decays exponentially with the distance from the same plane (i.e. k_{y2} is purely imaginary). This field is therefore called the *evanescent field*.

From Snell's law ($n_1 \sin\alpha = n_2 \sin\beta$) the two components of $\boldsymbol{k_2}$ will result in:

$$k_{x2} = k_{x1} = k_x, \qquad k_{y2}^2 = n_1^2 \left(\frac{2\pi}{\lambda}\right)^2 \left(\frac{n_2^2}{n_1^2} - \sin^2\alpha\right), \tag{2.29}$$

where k_y is perpendicular to the interface.

When $\sin\alpha > n_2/n_1$ k_{y_2} is purely imaginary then from equations 2.27 - 2.29 the refracted electric field will result in;

$$\boldsymbol{E}_2 = E_0 e^{-k_{y2}y} e^{j\omega t - jk_x x}. \tag{2.30}$$

$\boldsymbol{E}_2$ propagates along the x direction but decays exponentially in the y direction with a characteristic distance equal to $1/jk_{y2}$. E_2 is therefore called the *evanescent field* in the y direction.

In the case of p-polarised[c] incident light, the electric field reflection coefficient r_p,

[c] p-polarised light is the component of the light where electric field is perpendicular to the surface, essential for the excitation of the surface plasmon wave.

as described by Fresnel's equations is defined as:[136]

$$r_p = \frac{E_{in}}{E_{ref}} = |r_p|e^{j\theta} = n_1^2 \left|\frac{\tan(\alpha-\beta)}{\tan(\alpha+\beta)}\right| e^{j\theta}, \tag{2.31}$$

where θ is the phase change of the reflected field, E_{ref}, relative to the incident field, E_{in}.

The reflectance $R_p = |r_p|^2$ is defined as the ratio of the reflected intensities. In the special *resonant* case (i.e. $\alpha - \beta = \pi/2$) E_{ref} is finite for a very small E_{in}. In this case $\tan\alpha = k_{1x}/k_{1y} = -n_2/n_1$ and $\boldsymbol{k} = (k_x, k_y)$ becomes:

$$k_x^2 = k_1^2 - k_{y1}^2 = k_1^2 - k_x^2\frac{\varepsilon_1}{\varepsilon_2}; \tag{2.32}$$

$$k_x = \frac{\omega}{c}\sqrt{\frac{\varepsilon_1\varepsilon_2}{\varepsilon_1+\varepsilon_2}}; \tag{2.33}$$

$$k_{yi} = \frac{\omega}{c}\sqrt{\frac{\varepsilon_i^2}{\varepsilon_1+\varepsilon_2}}; \tag{2.34}$$

where ε_1 and ε_2 are the dielectric constants for material 1 and 2 and i is 1 or 2; in general $\varepsilon_i = n_i^2$. Equations 2.33 and 2.34 are the so called SPR dispersion equations for two half infinite media.

In the case that material 2 is a metal, then the high number of free electrons in the metal implies that for all frequencies, ω, smaller than the plasma frequency, ω_p, the dielectric constant of the metal, ε_2, will be negative and equal to:[136]

$$\varepsilon_2(\omega) = 1 - \frac{\omega_p^2}{\omega^2}, \qquad \text{for } \omega_p = \sqrt{4\pi n_e e^2/m_e} \tag{2.35}$$

where n_e is the free electron density and m_e and e are the electron mass and charge, respectively.

Thus for $\omega < \omega_p$ no electromagnetic field can propagate in the metal. However for $\varepsilon_2 > -\varepsilon_1$ it will results that k_{y1} and k_{y2} are imaginary and $k_{x1} = k_{x2}$ are real. Therefore the electromagnetic wave can propagate but only at the interface between the two materials, with evanescent components along the y direction in both materials.

For example if we consider the interface between gold and water with an incident light of $\lambda = 700$ nm, then the penetration depth in water is $1/k_{y,water} = 238$ nm and $1/k_{y,gold} = 26$ nm making the SPR sensitive only to the change in refractive index happening in the ≈240 nm closest to the gold surface.

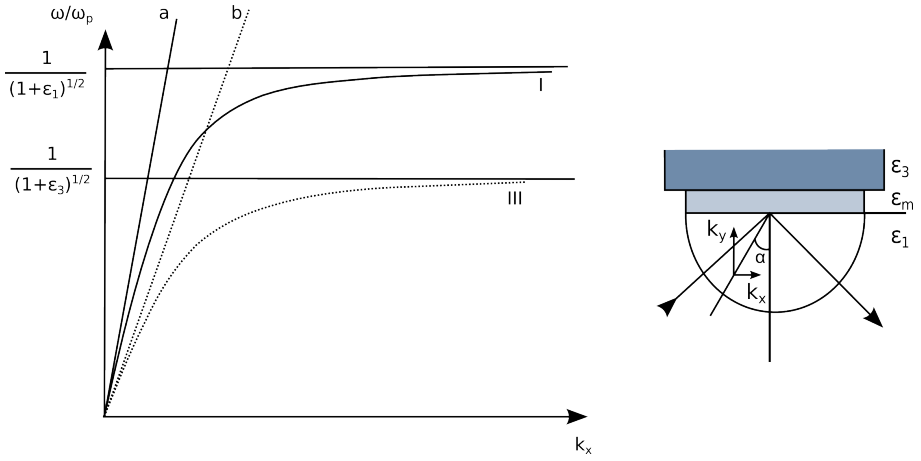

Figure 2.14: On the left, surface plasmon dispersion curves for the interface $\varepsilon_1/\varepsilon_m$, curve I, and $\varepsilon_3/\varepsilon_m$, curve III, and their respective dispersion relations for normal light in the medium: line a for ε_1 and line b for ε_3. On the right, a sketch of a typical SPR setup geometry (dielectric/metal/dielectric) necessary for the excitation of the surface plasmon. Re-drawn from RPH Kooyman.[136]

2.3.2 Excitation of surface plasmons

In an SPR system there are normally three materials, namely a thin layer of metal between two dielectrics (see figure 2.14). This three layer system is more complex than the one discussed above, however the general concepts remain unchanged.

Without rewriting the equations for the three layer systems, the surface plasmon dispersion equations for k_x at each interface between the two dielectrics and the metal are shown in figure 2.14.

The curves I and III represent the plasmon dispersion for the interfaces $\varepsilon_1/\varepsilon_m$ and $\varepsilon_3/\varepsilon_m$, respectively. Lines a and b indicate the dispersion relations between the normal[d] light in the medium ε_1 and ε_3, respectively.

Line a and curve I intersect only at the origin, thus in this configuration ($\varepsilon_1/\varepsilon_m$ only) the normal light component cannot provide a wave vector and angular frequency that can excite a surface plasmon. Therefore, a second interface is added ($\varepsilon_3/\varepsilon_m$) such that $\varepsilon_1 < \varepsilon_m < \varepsilon_3$. Curve III represents the dispersion of the plasmon along this new interface.

Line b now intersects curve I meaning that a surface plasmon can be excited at the $\varepsilon_1/\varepsilon_m$ interface. By adjusting the incoming angle, α, it is possible to tune the incident wave vector $k_x = kn_3 \sin\alpha$ such that it excites the surface plasmon. In particular any k_x between line a and b will excite a plasmon wave in the metal layer.

[d] Perpendicular electric field component of the light.

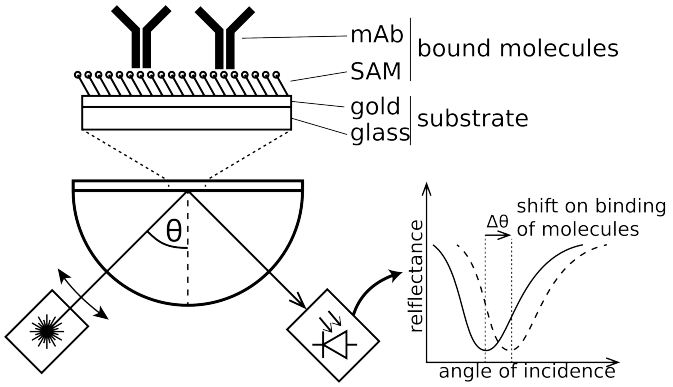

Figure 2.15: Schematic representation of the experimental setup. Light, p-polarized, is incident on the backside of a glass slide coated by thin layer of Ti/Au. The SPR instrument measures the angle at which a minimum in intensity is observed, resonance angle, θ. Changes in θ are caused by changes in the refractive index of the medium adjacent to the thin metal film that occur, for example, when a protein binds to the interface. Adapted from Lahiri at al.[137]

When SPR is used for the characterisation of biological systems or for sensor applications we can generally assume that the molecules of interest dissolved in solution adsorb to a metal/solution interface. These molecules replace the solution molecules at the interface. The molecules of interest will generally have a different refractive index in respect to the solution and thus the average refractive index changes.

Because the surface plasmon is an evanescent field in the direction normal to the surface, only the dielectric changes that occur close to the metal/solution interface are detected. The penetration depth of the plasmon field is approximately equal to half the wavelength of the incident.[136]

We have seen that a change in refractive index induces a change in the wave vector, in particular k_x can vary according to equation 2.33. This generates a change in the phase, θ, of the reflected electric field. If we plot the intensity of the reflected light against its angle of incident (equation 2.31) when resonance conditions occur, then a minimum become apparent (figure 2.15). This angle is known as the resonant angle and is the output of the instrument. When the refractive index changes (e.g. because molecules bind to the surface) then the resonant angle shifts towards higher values (figure 2.15).

A ratio of $\Delta\theta/\Delta\varepsilon \approx 250$ was estimated.[136] A $\Delta\theta \approx 1$ m$^\circ$ can detect, a variation of $\Delta\varepsilon \approx 4 \times 10^{-5}$, making SPR a very sensitive technique. In fact taking into account the refractive index of water and the average refractive index of proteins, $\Delta\theta = 1$ m$^\circ$ corresponds to approximately 10 pg/mm^2 of bound proteins.[136] In particular for

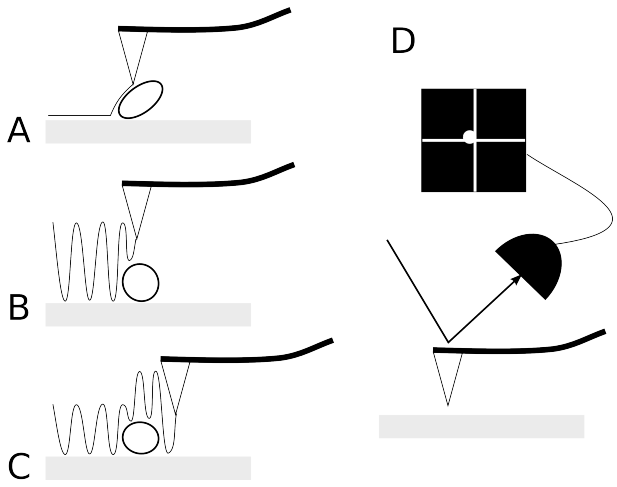

Figure 2.16: A schematic diagram of the AFM operational mode, A, contact mode, B, non-contact mode, C, tapping mode. D, displacement detection system based on laser beam deflection by means of a photodiode. Adapted from Alessandrini et al.[138] and Meyer et al.[138]

our instrumentation (AutoLab ESPRIT) a conversion factor of a 122 m°mm^2/ng is recommended by the manufacturer of the instrument.

2.4 Atomic force microscopy

Atomic force microscopy (AFM) is an imaging technique used for the topographic characterisation of materials, low dimensional systems and biological molecules. Both the very high spatial resolution and the ability to operate in air, liquid and vacuum makes it ideal for the study of both surfaces and biomolecules.

An AFM image is created by monitoring the delfections of a cantilever with a very sharp tip at the end while it moves across a surface following the features of the surface. The movements of the tip necessary to follow the surface features are recorded and constitute the AFM image.

The first AFM was based on the deflection of a cantilever kept in contact with the surface of the sample. The contact of the tip with the surface is maintained at all times by maintaining a constant force between tip and sample, with the resulting deformations in the cantilever, caused by the features on the surface, recorded. Whilst the cantilever moves on the surface it imposes a vertical and lateral force upon the features themselvs, therefore if the features are softer than the cantilever they will be deformed by it.

An approach to overcome this limitation and open AFM imaging to biological molecules was to operate the AFM cantilever in a *non-contact* mode.[139] The cantilever

is maintained at a fixed distance from the surface (between 1 and 10 nm) and is oscillated at its resonant frequency. The amplitude of the oscillations vary accordingly to the strength of long-range attractive and repulsive forces between the cantilever and the surface which are strongly disturb dependant. The *non-contact* method has the advantage of applying minimal vertical and lateral forces directly to the sample, allowing imaging of delicate biological samples.

A different method consist of maintaining an intermittent contact with the surface by oscillating the cantilever at a frequency close to its resonant frequency. Here the amplitude of the oscillation is kept constant rather than the distance from the surface. Because of the intermittent contact between the cantilever tip and the surface this method is commonly referred to as *tapping mode.*[140]

In this mode, when the oscillating cantilever approaches the surface the amplitude of the oscillation is damped by the contact and the topography of the surface is obtained by recording the feedback signal required to maintain the oscillation constant.[138]

Different strategies can be used to detect the variation happening in the cantilever upon interaction with the topography of the surface. Currently the most widely adopted strategy measures the deflection of the cantilever indirectly by illuminating the cantilever with a laser beam and measuring its reflection across a photodiode.[141] The beam reflection generates an amplification effect. In fact, the change in amplitude of the impinging laser beam on the photodetector, ΔA, can be used to measure the deflection of the cantilever, Δz according to:

$$\Delta A \approx 2\frac{D}{L}\Delta z, \tag{2.36}$$

where D is the distance between the cantilever and the photodetector and L is the length of the cantilever.

For example during acquisition in *tapping mode* the height of the cantilever is detected with this method and the information is given to a feedback circuit that maintains the amplitude of the oscillation of the cantilever constant at each scanning point. The position of the scanning point is recorded in a 2D matrix, then by adding the information coming from the feedback circuit a 3D image of the topography of the sample is generated.[138]

2.4.1 Interactions of the AFM tip with the surface

Although a complete understanding of the tip-sample interaction has not been achieved to date, models have been proposed to describe these complex interactions. Although these models remain conflicting and incomplete.

The interaction between the sample and the tip of the cantilever is the result of the cumulative effect of multiple forces that are difficult to discern making the full understanding of each interaction with the tip difficult.[142,143]

In order to describe the tip-sample interaction in tapping mode AFM, one must take into account the long-range attractive forces between the tip and the sample, the mechanical compliance of the contact region and the contact area. The contact area is a function of the surface forces that act during contact, as well as by the externally applied load and by the elasticity and geometry of the materials.

The long-range intermolecular interactions such as van der Waals forces act between the atoms of the tip and the surface. Van der Waals forces are the collections of dipole-dipole interactions occurring between two permanent or induced dipoles. The dipoles present in the tip will interact with the dipoles present on the sample surface when the two come in proximity with each other.

These forces act radially in space in every direction where both the tip and surface are non-flat at the nanometer scale. Therefore for simplicity, the tip and surface geometries can be approximated by hemispherical surfaces. In particular, the tip is modelled by a hemisphere and the surface roughness by a succession of spheres. For this geometry, the van der Waals force, F_{vdW}, resulting from the summation of all the van der Waals forces acting between two hemispherical volumes, can be described by:[144]

$$F_{vdW}(d) = -\frac{h}{6d^2}\frac{R_t R_s}{R_t + R_s}, \tag{2.37}$$

where h is the Hamaker coefficient ($\approx 10^{-19} - 10^{-20}$ J), R_t and R_s are the radius of the tip and the effective radius of the surface roughness, and d is the distance between the tip and the surface.

The van der Waals forces are in equilibrium with short range forces which are mainly repulsive due to the electrostatic repulsion between the electron clouds surrounding each collections of atoms. This repulsive force acts only for very short distances and it weakens when the atoms of the tip and the atoms of the surface are further away. The interaction force becomes zero when the distance between the atoms reaches a few of Angstroms and becomes fully repulsive when the atoms are in contact.[145]

A separate adhesion force is induced by capillary condensation of vapour in ambient conditions. Vapour, on hydrophilic surfaces, condenses between the pores of the surface. The condensed vapour induces the formation of a water meniscus between the tip and

the surface. This phenomenon is described by the Kelvin equation:[146]

$$R_{gas}T\log\frac{P}{P_0} = \frac{\gamma_L V_m}{r_k}, \tag{2.38}$$

where γ_L is the surface tension of the liquid, R_{gas} is the gas constant, P is the vapour pressure, P_0 is the vapour pressure at saturation, V_m is the molar volume of the liquid and r_k is the kelvin radius given by the combination of curvature radii, r_1 and r_2, of the meniscus itself defined as:[147]

$$\frac{1}{r_k} = \frac{1}{r_1} + \frac{1}{r_2}. \tag{2.39}$$

The dimension of the capillaries for which condensation occurs depends upon the vapour pressure. Higher vapour pressure (i.e. higher humidity) will start condensation of water in wider capillaries. In particular, a capillary neck will form when the tip approaches the surface and reaches a distance equal to the Kelvin radius.

The pressure in the meniscus formed is higher than outside therefore the meniscus exerts an adhesion force between the tip and the surface that overpowers the other forces in ambient conditions. This force is determined by the pressure within the meniscus and the geometry of both the tip and the surface across the meniscus forms. The exact determination of the this force will then depend upon the contact angle that the vapour forms with the tip and surface at any given point. However a simpler approximation was proposed to describe this process:[147]

$$F_{cap} = \frac{4\pi R\gamma_L\cos\theta}{1 + d/d_0} \tag{2.40}$$

From the equation we can see that the capillary force increases with the approaching of the tip to the sample and maxima is reached when the tip is in contact with the surface. In any ambient imaging condition this force dominates the tip interaction with the surface. For the imaging of soft features this can create a problem because it deforms the features itself and can displace them on the surface.

For this circumstance the AFM imaging can be performed in liquid media eliminating the formation of the capillary.

However, in liquid other forces come into play. As seen in section 2.1.3 upon immersion of a surface in a solvent molecules dissolved in solution approach the surface/liquid interface forming an *electrochemical double layer.*[49] If the molecules in solution are polar, the surface acquires a charge by adsorption or binding of such molecules or by ionisation of the surface atoms. As a consequence more molecules are attracted from

the solution, forming a second layer of charged molecules.

Other solvated molecules that come into close proximity to the double layer will be attracted or repulsed to/from the surface depending on the distance between them and the surface. These molecules form a diffuse layer that further extends into solution to a distance varying between 1 nm and hundreds of nm. The entire system is dynamic, with different molecules in balance between the diffusion forces that "pull away" them into the bulk of the solution and the attraction that the surface exerts upon them.[143]

The interaction of the surfaces of the tip and the sample will disrupt the dynamic equilibrium originally established between each surface and the solution. If the two surfaces are similarly charged this force is repulsive and needs to be accounted for during the acquisition of images in liquid. This force can be attenuated by adjusting the concentration of charged molecules in solution, effectively screening the two surfaces from each other.

Furthermore, it must be considered that the mechanical forces and chemical interactions influence each other. In a liquid environment this is further complicated by the presence of two surface/solution interfaces.[143]

2.4.2 Modelling of the cantilever

The movement of the cantilever can be approximated by the motion of a beam where the total summation of all forces exerted are concentrated in a single point at the end of the beam through the use of a modified Euler-Bernoulli beam equation.[142]

This equation describe the deformations of a beam under a certain load applied to the cantilever by adding to this equation the forces between the tip and the sample (described above) we can model the displacement of the cantilever tip. We note that this approximation is not relevant for the description of surface/tip interaction where the geometry of the tip and surface must be accounted for.[142]

Even if the Euler-Bernoulli equation can be used to describe the movement of the cantilever, the solution of this equation is not easy to find and therefore a further approximation is made on the geometry of the cantilever. The mass of the cantilever is concentrated in a single point at the tip of the cantilever and the properties of the material, such as its stiffness, are modelled by a spring connected to this point-mass. In this case the displacement of the tip can be described by the differential equation:

$$mz'' = -kz - \frac{m\omega_0}{Q}z' + F_0\cos\omega t + F_{ts}(d), \tag{2.41}$$

where z, z' and z'' are the point displacement, its velocity and acceleration, respectively. k, m and ω are the elastic constant of the spring, effective mass of the cantilever and

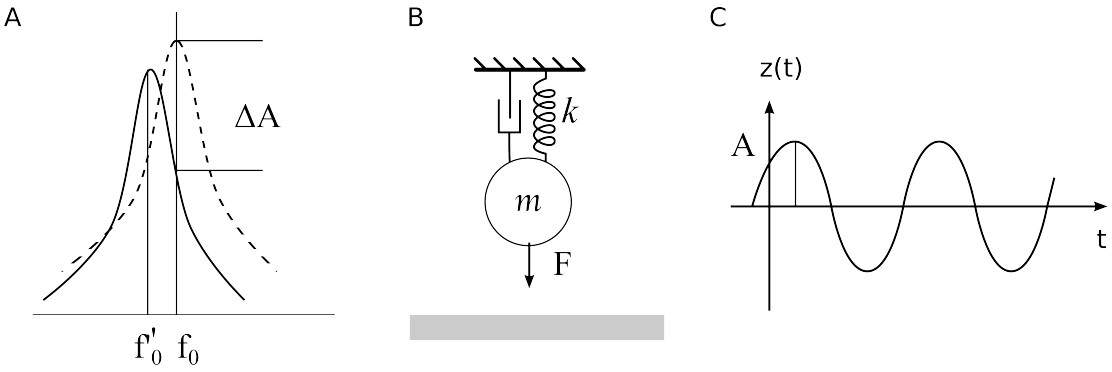

Figure 2.17: A schematic diagram of: A, cantilever resonance peak before and after contact with the surface (damped); B, point-mass model of the cantilever for damped harmonic oscillator model; C, steady state solution of cantilever displacement.

angular frequency respectively. Q is the quality factor of the cantilever $Q = f_0/\Delta f$ that describe the sharpness of the resonance peak around the resonance frequency, f_0 and $\omega_0 = 2\pi f_0$. F_0 is the amplitude of the force that drive the cantilever and F_{ts} are the summation of the tip/sample interactions.

This model is equivalent to the description of a damped harmonic oscillator where the resonance frequency is given by $\omega_0 = \sqrt{k/m}$.

The mechanical interaction between the tip and the sample can be modelled by various contact mechanics models, depending on the force applied to the tip and the properties of both the tip and the samples, such as elastic properties and stiffness. For non-compliant samples (i.e. stiff samples) and measurements in air, the interaction between tip and sample can be described by the model proposed by Derjagin, Muller and Toporov (DMT).[148] Here, we report the main equations that describe this model, without the full derivation of them. Accounting for all the forces described, the tip-sample interaction force, F_{ts}, depends on the distance between the tip and the sample surface, d. F_{ts} can be calculated by:

$$F_{ts} = -\frac{hR_t}{6d^2}, \qquad d > a_0$$
$$F_{ts} = -\frac{4}{3}E_{eff}\sqrt{R_t}(a_0 - z - z_0)\frac{3}{2} + F_a d, \qquad d \leqslant a_0$$

where E_{eff} is the effective Young's modulus, which is a measure of the stiffness of the material, a_0 and z_0 are the intermolecular distance and the instantaneous average cantilever deflection, respectively.

In a simplified model and considering the equation and conditions just described, the steady state solution of the movement of the cantilever is approximated by a sinusoidal

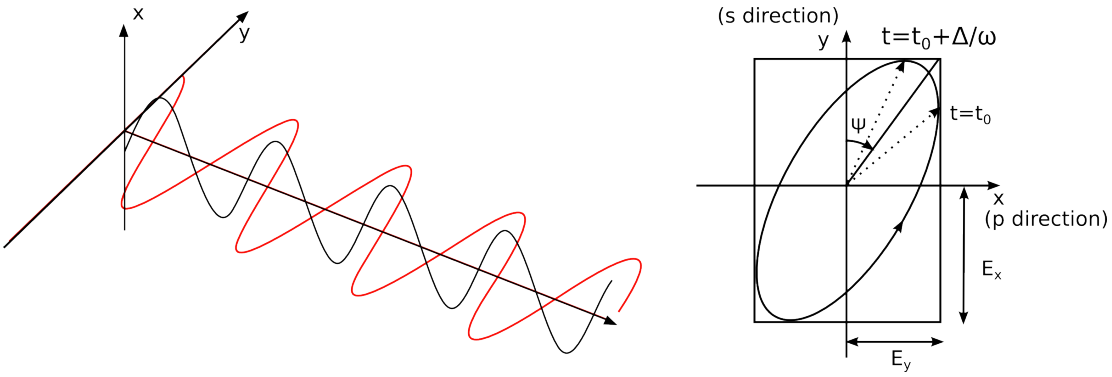

Figure 2.18: Schematic of elliptically polarised light and the parameters measured by the ellipsometer, Ψ and Δ.

wave:

$$z(t) = z_0 + A\cos(\omega_0 t - \varphi), \tag{2.42}$$

where the t is the time, φ is the phase of the cantilever, A is the amplitude of the oscillation and ω_0 is the angular resonant frequency. Note that we are only taking into account the first sinusoidal mode coincident with the resonant frequency.

2.4.3 Application in this study

In this study tapping mode AFM in ambient conditions was used to study the aggregation of molecules in mixed monolayers adsorbed on gold surfaces. The mixed monolayer was formed by two molecules of different lengths. Since the difference in thickness between the two components of the monolayer is about 2 nm, an ultra-smooth template stripped gold substrate was used to minimise the surface roughness.

AFM imaging allowed visualisation of clusters of the thicker component over a less thick layer. Moreover it allowed quantification of the number and dimension of highlands.

2.5 Ellipsometry

Ellipsometry is a surface analysis technique often used to determine thickness and the refractive index of materials and thin films. Ellipsometry is based on measuring the change in different parameters (characteristics) of the reflected light from a surface.

A beam of light can be seen as an electromagnetic wave. The propagation of this wave in a medium relies on the movement of electrons and therefore it can be described

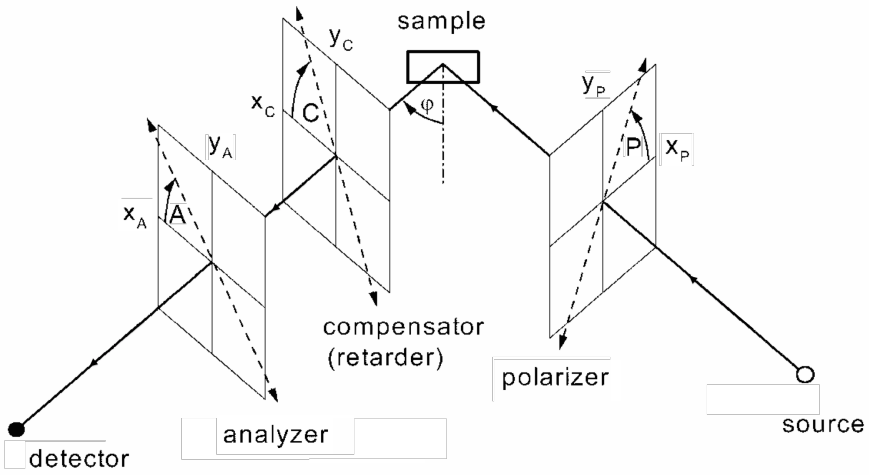

Figure 2.19: Schematic representation an ellipsometer in a ploariser-sample-compensator-analiser configuration. Adapted from J Hulmicek.[149]

as an electric field,[e] E.

As described before (section 2.3), the electric field can be described in space and time by two perpendicular components (E_x and E_y) each a sine wave laying on the $x = 0$ and $y = 0$ planes and evolving in time (figure 2.18). In general the two components will not be in phase and have different amplitudes thus generating an elliptical polarised light (figure 2.18).

The two parameters measured by ellipsometry are two angles, the first is the phase difference between the two components, Δ, and the second, Ψ, is related to the relative amplitude of the two components (E_{x0} and E_{y0}), such that $\tan\Psi = E_{x0}/E_{y0}$.

The two components of E can therefore be written as:[149]

$$E_x(t) = \mathrm{Re}(E_{x0}e^{i\Delta}e^{i\omega(t-t_0)}); \quad E_y(t) = \mathrm{Re}(E_{y0}e^{i\omega(t-t_0)}), \tag{2.43}$$

and their elliptical polarisation can be written as the Jones vector:

$$\begin{bmatrix} \sin\Psi e^{i\Delta} \\ \cos\Psi \end{bmatrix}. \tag{2.44}$$

In a typical ellipsometer the light beam coming from the light source, non-polarised, is linearly polarised by a polariser before illuminating the sample. The reflected light, which has been elliptically polarised, passes through a compensator (or retarder) and

[e]The induced magnetisation occurring in the material is negligible and it is too slow to follow the rapid propagation of light at the used wavelength.

goes through a second polariser (called analyser) in the detector where any change in polarisation happening is recorded (figure 2.19).[149]

For the investigation of alkanthiols self assembled on gold, spectroscopic measurements are taken of Δ and Ψ by varying the incident light wavelength between 300 nm and 800 nm. The self assembled monolayer (SAM) can be modelled as a transparent film (i.e. the refractive index is assumed to be a real number). The refractive index, n, can then be modelled by using a Cauchy dispersion equation, as follows:[149]

$$n(\lambda) = A + \frac{B \cdot 10^4}{\lambda^2} + \frac{C \cdot 10^9}{\lambda^4}, \tag{2.45}$$

where A, B and C are the Cauchy parameters and are specific to the material. For the purpose of this study, A, B and C are limited to vary between 1.45-1.50, 0-1 nm^2 and 0-0.2 nm^4, respectively. A clean gold sample is used as a reference surface and the air surrounding the sample is assumed to be $n = 1$.

Ellipsometry was used for the estimation of the average thickness of mixed monolayers. By changing the ratio between two SAM molecules of different lengths, the average height is expected to vary in proportion to the concentration of the adsorbed molecules on the surface. Knowing the theoretical thickness of both SAMs an estimation of the surface concentration of both molecules is possible.

2.6 X-ray photoelectron spectroscopy

X-ray photoelectron spectroscopy (XPS) is a surface analysis technique that involves the irradiation of the substrate with mono-energetic soft X-ray under a high vacuum ($\approx 10^-9$ mbar) where the energy of the emitted electrons is measured. Each element has a unique spectrum and the spectrum from a mixture of elements is approximately the sum of the peaks of each element.

The X-ray beam is emitted by a rotating anode, collected by the monochromator lens and focused on the sample; irradiating an area of 0.5 mm diameter. The photoelectrons emitted from the sample (with a take off angle of 90°) are collected by a multi-element lens and focused on the electron energy analyser. To avoid scattering of the electrons the XPS chamber is kept under ultra-high vacuum at a pressure lower than 10^{-9} mbar during acquisition (see figure 2.20).

During XPS a sample is irradiated with mono-energetic soft X-rays that penetrate the sample 1 to 10 μm below the surface. The photons interact with the atoms causing emission of electrons by means of the photoelectric effect.

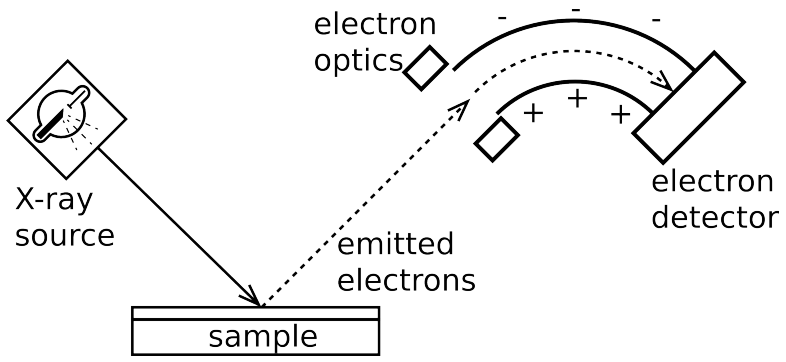

Figure 2.20: Schematic diagram of an XPS set-up. The X-ray beam is emitted by a rotating anode, collected by the monochromator lens and focused on the sample (X-ay source). The photoelectrons emitted from the sample, are collected by a multi-element lens optical element and focused on the electron energy analyser.

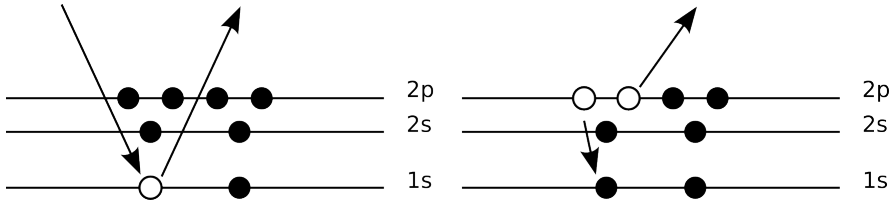

Figure 2.21: A set of schematics of the XPS emission; a photon causes the emission of an electron by means of photoelectric effect (left). The relaxation of an outer electron causes the emission of a second electron by Auger effect, (right).

However, the mean free path of the emitted electrons is shorter than that of photons. The sampling depth of XPS is defined as the depth from which 95% of all photoelectrons are scattered by the time they reach the surface. For Al k-α radiation the sampling depth is between 3 to 10 nm.

Of all the electrons that leave the sample only the electrons emitted within few nanometers below the surface leave the sample without energy loss. The energy of these electrons is distinguishable from the background, forming the peaks in the spectra. The electrons that instead enter deeper into the substrate, undergo inelastic loss before emerging from the surface form the background.

In the photoelectric effect (see figure 2.21) when a beam of photons of frequency, ν, impacts an electron, the latter is emitted only if the photon has an energy $\hbar\nu$ bigger than the energy needed to release the electron. This energy corresponds to the binding energy (BE) of the electron to the atom.

The emitted photoelectron has therefore a kinetic energy, KE $= \hbar\nu -$ BE[150]. In the

XPS the emitted electrons, as detected by the spectrometer, have energies equal to:

$$KE = \hbar\nu - BE - \phi_s; \tag{2.46}$$

where ϕ_s is the work function of the spectrometer. The binding energy can be thought of as the difference between the initial and final energy states before and after the photoelectron has left the atom. Since each element has a unique set of binding energies then XPS can be utilised to estimate the concentration of elements on the surface.

In addition to photoelectrons, electrons can be emitted by the so called Auger effect. In this case the electron is emitted after relaxation of an excited ion after photoemission. In the Auger process, an outer electron falls into the orbital vacancy caused by the photoelectron emission and a second electron is emitted to dissipate the excess energy.

The Auger electron possesses kinetic energy equal to the difference between the initial ion and the final ion state. This is found to be independent from what caused the first ionisation. Hence photoionisation usually leads to two emitted electrons: a photoelectron and an Auger electron.

By looking at the energy peaks obtained by means of XPS on mixed monolayers adsorbed on gold surfaces, it is possible to estimate the ratio of different elements on each surface and their energy status.[102,151]

In this study surface analysis by XPS is accomplished by irradiation of a sample by a monochromatic Al k-α (1486.7 eV) source. For the interest of this study, mixed SAMs adsorbed on gold surfaces have been characterised by means of XPS. The terminal group of the two SAM molecules is different, in particular one molecule terminates with a chain of 6-ethylene -glycols chain and the other with a carboxylic-acid.

Considering that only one of the two SAM molecules is terminated by a carboxylic acid, the energy peak recorded for the energy range usually associated with the C=O bond (289.3 eV) was used as estimation of the ratio between the two different SAMs on the surface.

Chapter 3

Materials and protocols

3.1 Materials

Acetone, absolute ethanol, methanol, tris, Decon 90, platinum wire and silver/ silver-chloride reference electrode (662-1795) were purchased from VWR® International Ltd (UK).

11-mercapto-1-undecanol (MUD) (figure 3.1), NaOH, glacial acetic acid, HCl, ethanol 200 proof, sodium phosphate monobasic monohydrate, sodium phosphate dibasic, sodium acetate trihydrate, tris buffer saline (TBS), SIGMAFAST™ NBT/BCIP® (nitro blue tetrazolium/5-bromo-4-chloro-3-indolyl phosphate) tablet, bovine serum albumin (BSA) and human chorionic gonadotropin (hCG) were sourced from Sigma-Aldrich® Co (USA).

Acid capped esa(ethylene glycol)undecanethiol (OEG) and acid-capped tetra(ethylene glycol)undecanethiol (4EG) were purchased from ProChimia Surfaces Sp.z o.o. (Poland) and Asemblon Inc (USA), respectively (figure 3.1).

1-Ethyl-3-[3-dimethylaminopropyl]carbodiimide hydrochloride (EDC), N-hydroxysuccinimide (NHS) and ethanolamine-HCl were purchased from GE healthcare UK Ltd (UK), diluted in deionised (DI) water (Millipore, 18.2 mΩ) upon arrival, aliquoted and stored at -20 °C.

Lighting-link alkaline phosphatase (AP) conjugation kit and anti-mouse AP-conjugated antibodies were obtained from Innova Biosciences Ltd (UK) and Bethyl Laboratories, Inc. (USA) respectively.

Dual-phase epoxy glue EPOTEK® 353-ND and square-section ethylene propylene diene monomer (EPDM) rubber rings were sourced by Epoxy Technology Inc. (USA) and Mantek Manufacturing Ltd (UK) respectively.

Standard bare gold disks, fitting AUTOLAB ESPRIT® surface plasmon resonance (SPR) system were sourced from Metrohm Autolab BV (The Netherlands).

Finally, two monoclonal anti β-hCG antibodies (mAb-A and mAb-B) were supplied

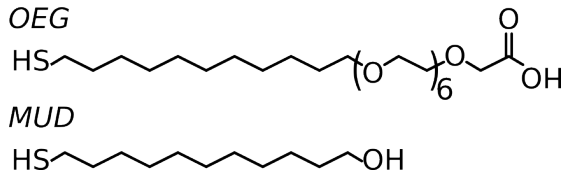

Figure 3.1: Skeletal model of the SAM molecules used for the formation of mixed monolayers in this study.

by Abbott Laboratories (USA).

3.2 Methods

3.2.1 Buffers and solutions

Acetate and phosphate buffers Acetate and phosphate buffers were prepared by mixing the respective buffer components cording to table 3.1. For buffers of different molarity the same ratio between the buffer components is maintained but the concentration is adjusted. In the same table the calculated ionic strength is reported in molar. The apparent dissociation constants were assumed to be pK_a = 4.68 for acetic acid, pK_{a1} = 2.15, pK_{a2}=6.86 and pK_{a3}=12.32 for the dissociation of phosphoric acid.

Acetate buffer 50 mM				Phosphate buffer 50 mM			
pH	Na-acetate M	Acetic acid M	Ionic strength M	pH	Na_2HPO_4 g/L	NaH_2PO_4 g/L	Ionic strength M
4.5	0.0193	0.0307	0.0193	5.5	0.294	6.614	0.054
5.0	0.0338	0.0162	0.0338	6.0	0.852	6.071	0.062
5.5	0.0436	0.0064	0.0436	6.5	2.140	4.820	0.080
6.0	0.0478	0.0022	0.0478	7.0	4.097	2.918	0.108
				7.2	4.854	2.182	0.119
				7.5	5.763	1.298	0.131
				8.0	6.613	0.471	0.143

Table 3.1: Reference table used to generate acetate buffer and phosphate buffer at different pH by mixing sodium acetate trihydrate (NaAc) and acetic acid; and sodium phosphate monobasic monohydrate ($NaH_2PO_4 \cdot H_2O$, MW = 137.99 g/mol) and sodium phosphate dibasic anhydrous (Na_2HPO_4, MW = 141.96 g/mol), respectively.

TBS. Tris buffer saline was prepared according to manufacturer instructions from a ready powder pack by adding the content of the pouch to 1 l of DI water and mixing the solution overnight. The resulting buffer yields 0.05 M tris buffered saline (NaCl - 0.138 M; KCl - 0.0027 M) pH 8.0 at 25 °C. The buffer pH was then adjusted by titration with HCl to pH 7.1, where necessary.

MES buffer. MES buffer pH 5.6 was prepared by dissolving 4.881 g of MES in 40 ml of DI water then adjusting the pH by titration with 3 M NaOH solution until pH 5.6 is reached and then topping up the solution with DI water until reached a final volume of 50 ml. The stock solution was then diluted to the appropriate molarity before use.

NHS-EDC mixture. NHS-EDC mixture was prepared freshly prior to use from NHS and EDC aliquots as recommended by the manufacturer. Aliquots of EDC (800 mM) and NHS (200 mM) were dissolved in DI water and stored at -20 °C. Each aliquot was defrosted upon use and diluted 1:1 with 100 mM MES buffer (pH 5.6), then the prepared NHS and EDC were mixed together in a 1:1 ratio as suggested in the NHS-EDC activation protocols.[152] The mixture is then used to modify the COOH groups present on the SAM of the functionalised samples as detailed below.

NBT/BCIP. SIGMAFAST™ NBT/BCIP® tablets were dissolved prior to use in 10 ml DI water as recommended by the manufacturer. The tablets were dissolved in a 15 ml tube wrapped in aluminium foil to protect the solution from light.

SAM solutions. Prior to use, an appropriate amount of MUD or OEG was dissolved in a 5% glacial acetic acid and 200 proof ethanol solution to generate 0.5 mM SAM solutions. Acetic acid was added to avoid the formation of dimers between OEG molecules due to the formation of hydrogen bonds between carboxylic acids.[153]

In the case of mixed SAMs solutions, MUD and OEG were prepared separately as described and different ratios of these solutions were mixed together to yield solutions with final molar fractions of 0.05%, 0.1%, 0.5%, 1% and 5% of MUD in OEG. At the same time 100% MUD and 100% OEG SAM solutions were prepared.

3.2.2 Sample cleaning and preparation

SPR disks. As per manufacturers instructions glass SPR disks coated with a thin Ti/Au layer were sonicated in 100mM NaOH and 0.1% Triton X100 aqueous solution, and in ethanol 200 proof for 10 minutes prior to immersion in OEG solution prepared as described in section 3.2.1. The devices were incubated for a minimum of 16 hours in the SAM solution, rinsed in acidic ethanol (0.2% HCl), as per manufacturers instructions, and DI water to promote hydration of the ethylene glycol groups that is essential for resistance to non-specific adsorption.[105] The devices are then mounted on the SPR instrument (AUTOLAB ESPRIT®, Metrohm Autolab BV, The Netherlads).

Electron-beam evaporated gold samples. Electron-beam evaporated gold (EEG) coated wafers were used as the substrate for both colorimetry and electrochemistry.

Ti/Au (15 nm/80 nm) was evaporated by electron-beam evaporation at a base pressure of 10^{-7} mbar over Si/SiO_2 wafers. Prior to evaporation the Si/SiO_2 wafers were cleaned by 5 minutes sonication in acetone, methanol and DI water. The evaporated wafers were spin-coated with 1813 photo resist to protect the surface from contamination in ambient air.

Prior to functionalisation with MUD or OEG, the wafer was cut in devices of appropriate size and cleaned by sonication in acetone, ethanol and isopropanol for 10 minutes each to remove the photo resist from the devices, clean the gold surface, and to ensure the formation of ordered SAMs.[154]

The EEG samples were then dried under N_2 stream and cleaned by freshly prepared piranha solution (70% sulphuric acid, 30% hydrogen peroxide) for 5 minutes. The samples were then sonicated in DI water for 10 minutes and in ethanol 200 to remove the residues from piranha cleaning and reduce the oxide layer formed on the gold after exposure to piranha solution.[155] After piranha cleaning, prior to incubation of the sample in the SAM solution all steps were performed taking extra care to avoid contamination of the surface, for example the ethanol used for sonication was of higher grade (200 proof ethanol) than the one used before piranha (absolute ethanol).

A further cleaning of the surface was performed in UV-Ozone for 10 minutes. To reduce the oxidised gold surface formed during the UV cleaning procedure, the devices were rinsed in ethanol 200 for 20 minutes.[156,157] The clean substrates were then transferred to 0.5 mM OEG, 5% acetic acid and ethanol 200 solution and incubated for a minimum of 16 and 40 hours for colorimetry experiments and electrochemistry respectively.

Rod electrodes. Gold rod electrodes (eDAQ, Poland), 1 mm diameter, were polished mechanically with 0.3 μm polishing alumina aqueous suspension (MetPrep Ltd, UK) and optically checked for major defects. They were then sonicated for 5 minutes in acetone, ethanol, isopropanol and deionized (DI) water (Millipore, 18.2 mΩ)

Electrochemical polishing was performed on each electrode in 100 mM H_2SO_4 solution, cycling the potential between -0.3 V and 1.5 V (vs Ag/AgCl/KCl electrode) for 25 scans[157]. The acid solution was changed after 10 sweeps.

Template stripped gold samples. Template stripped gold (TSG) samples were prepared as follows: SiO_2 capped Si wafers, used as templates, were cleaned by sonication in acetone, methanol, Decon 90 (1:20) and DI water for 5 minutes each (figure 3.2 A). Subsequently a 120 nm thick gold layer was directly deposited on the bare wafers by electron-beam evaporation at a base pressure of 10^{-7} mbar (figure 3.2 B). Microscope slides were then cut to appropriate size and glued on the gold-coated wafers with a two-

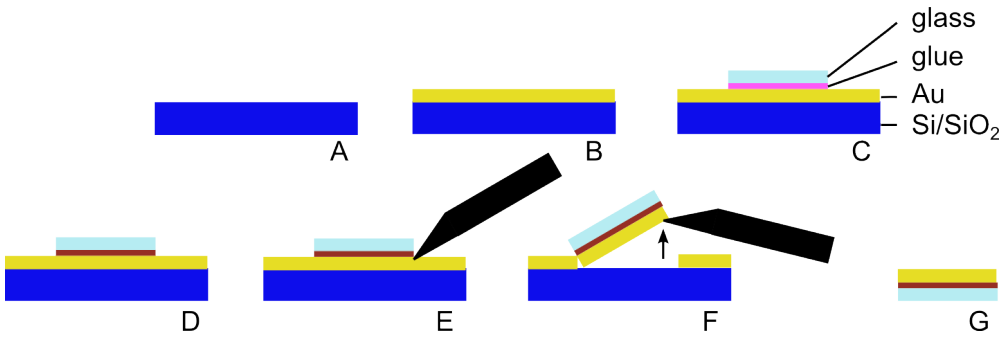

Figure 3.2: Depiction of template stripped gold sample preparation. A) Clean Si/SiO_2 template. B) Evaporation of gold. C) Adhesion of microscope slide fragments on the template by means of exopy glue. D) Epoxy glue curing 2 minutes at 180 °C. E) and F) removal of glass fragments from Si/SiO_2 template with a clean blade. G) Resulting template stripped gold sample.

component epoxy glue (EPOTEK® 353-ND – figure 3.2 C). The glue was then cured for 2 minutes on a hot plate at 180 °C (figure 3.2 D). The samples were thus kept at room temperature until used.

Immediately before use, the glass slide devices were separated from the Si/SiO_2 wafer such that the gold was stripped from the template (figure 3.2 E-F).

3.3 Surface plasmon resonance

3.3.1 Preparation of devices and instrumentation

SPR disks were prepared as described in section 3.2.2 and mounted on the instrument. The SPR instrument allows measurements in two channels simultaneously, therefore checks were carried out to confirm there was no leakage between the two channels of the SPR to avoid cross talking, prior to each experiment. As per manufacturer instructions it was checked that the minimum intensity of the reflected light was lower than 8% and happened for angles between -1600 and -1500 millidegrees (m°). This ensures good sensitivity and that the resonant angle (θ) remains in the detection range of the instrument throughout the experiment.

The surface was then stabilised in water and in the buffers used during the experiment, by exposing the surface to consecutive injections of fresh solutions every 2 minutes, for 30 minutes or until stabilisation was reached. The surface was considered stable when the SPR angle (θ) of a new injection was within 1 or 2 m° of the angle recorded for the previous injection.

3.3.2 Electrostatic interactions

Mouse monoclonal anti β-hCG antibody (mAb-B) was injected on the surface in buffers with different pH, namely 100 mM acetate buffers with pH ranging between 4.5 and 6 and 100 mM phosphate buffers with pH between 5.5 and 8 with 0.5 pH unit intervals for both buffers. The buffers were prepared as detailed in section 3.2.1.

After 30 minutes of surface stabilisation in each buffer the antibodies were diluted in the same buffer to a concentration of 50 μg ml^{-1} and were adsorbed on the surface for 45 minutes. The surface was then rinsed with the same buffer and regenerated with 50 mM NaOH solution. The procedure was repeated for a second buffer.

3.3.3 Antibodies immobilisation

With the aim of studying the influence of coupling buffers on the activity of the surface (i.e. the binding of the antigen to the immobilised antibodies) different coupling buffers were used to immobilise mAb-B antibody on the surface, namely 50 mM acetate buffers with pH 4.5, 5 and 5.5 and phosphate buffers with pH 6, 7 and 7.5.

The steps followed for the immobilisation of the antibodies on the surface are summarised by the scheme in figure 3.3. SPR disks were modified with OEG, as described in section 3.3.1 and mounted on the instrument. After stabilisation in water and the appropriate coupling buffer (figure 3.3 step A), NHS-EDC mixture was freshly prepared as explained in section 3.2.1 and injected on the surface. After 10 minutes incubation the mixture was drained and the surface was rinsed with the respective coupling buffer (figure 3.3 step B).

A solution of mAb-B (20 μg ml^{-1}) in the respective coupling buffer was injected on the surface and incubated for 1 hour, allowing the formation of covalent bonds between the NHS on the surface and the amine groups exposed on the surface of the antibodies (figure 3.3 step C). The surface was then rinsed with coupling buffer three times, for 10 minutes each. Then 1 M ethanolamine pH 8.5 was incubated on the surface for 10 minutes to deactivate any free NHS binding-sites (figure 3.3 step D).

For clarity, an example of the SPR signal acquisition during mAb-B immobilisation procedure just described can be seen in figure 3.4. The example shown was obtained for mAb-B immobilised in acetate buffer at pH 5.5.

3.3.4 Antigen binding

The sensor surface, prepared as explained in the previous section, was stabilised in 100 mM phosphate buffer (pH 7.2) for 30 minutes, changing the buffer solution every 2 minutes, and then challenged with the antigen hCG at appropriate concentrations (figure

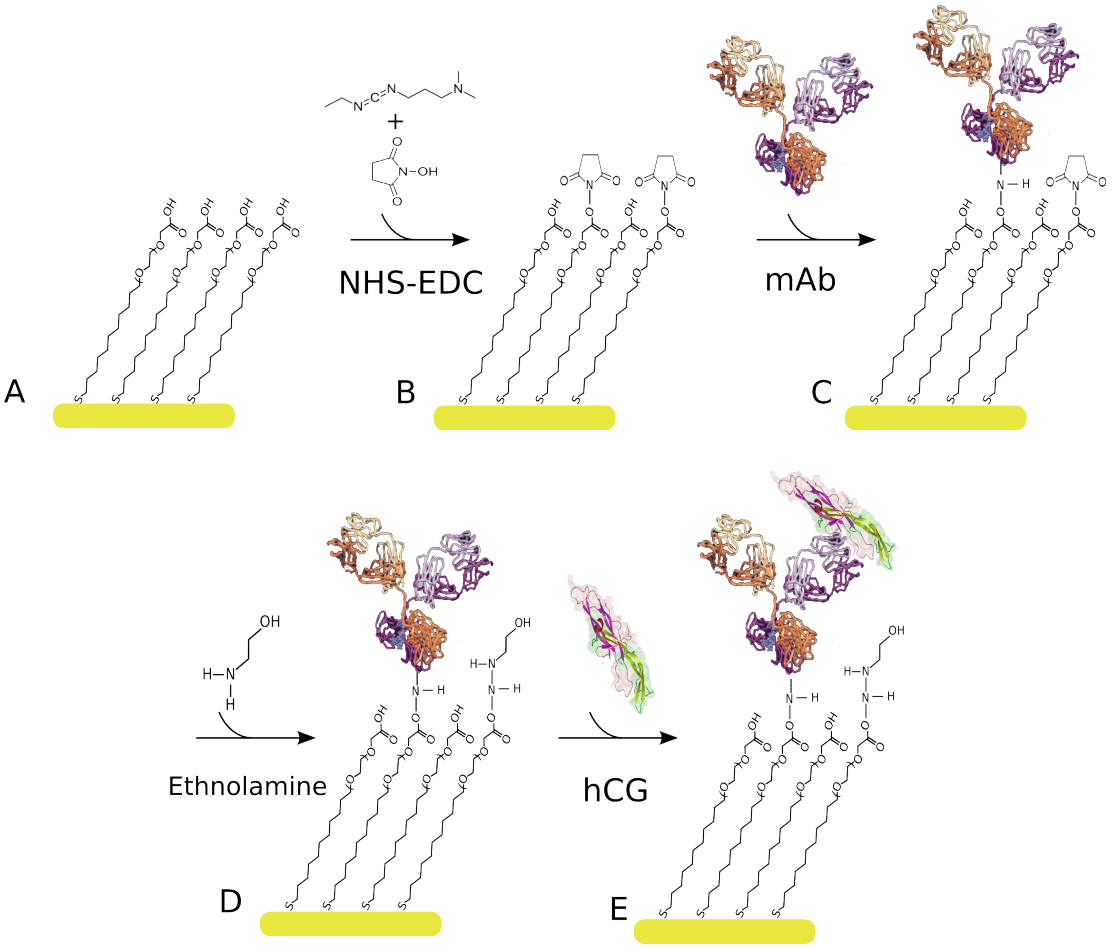

Figure 3.3: Sequence of the binding steps involved in the assembly of the SPR sensors. A) Formation of the OEG monolayer. B) Activation with NHS-EDC mixture.C) Antibody immobilisation by amine coupling. D) Blocking of the residual sites activated by NHS-EDC with ethanolamine. E) Binding of theantigen.

3.3 step E).

3.4 Electrochemical biosensor characterisation

Electrochemistry measurements were performed using a three electrode configuration. A silver/silver-chloride (3M KCl) electrode (662-1795 VWR International Ltd, UK) was used as the reference electrode, and a platinum wire as the counter electrode. The working electrode was constituted by either a gold rod electrode or the exposed area of an EEG or TSG samples. The EEG and TSG electrode area was defined by compression of a square-cut rubber gasket (3.41 ± 0.13 mm internal diameter) over the sample surface.

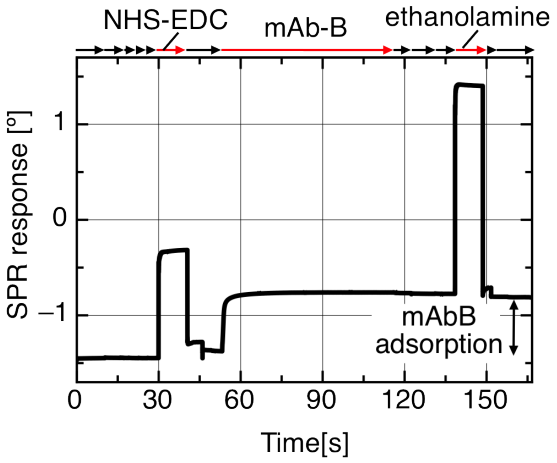

Figure 3.4: Example of SPR acquisition for mAb-B immobilisation on OEG modified gold disk by means of NHS-EDC. The black arrows represent the incubation in coupling buffer, the red arrows the incubation in NHS-EDC in MES pH 5.6, mAb-B 20μg/ml in coupling buffer (acetate buffer 50mM pH 5.5) and ethanolamine 1M pH 8.

Measurements were performed using a VSP potentiostat (Bio-Logic SAS, France), equipped with a low current option and acquisition software Ec-Lab®.

Cyclic voltammetry (CV) scans were performed between -0.5 V and 0.6 V in 100 mM phosphate buffer (pH 7.2) containing 2 mM of the redox couple $Fe(CN)_6^{3-}/Fe(CN)_6^{4-}$ at 62 mV s^{-1}, for five cycles.

EIS scans were performed in a frequency range between 100 kHz and 50 mHz, recording 7 points per decade, by applying a sinusoidal signal of 10 mV in amplitude against open circuit voltage, unless specified. For faradaic EIS 100 mM phosphate buffer (pH 7.2) containing 2 mM of the redox couple $Fe(CN)_6^{3-}/Fe(CN)_6^{4-}$ was used, while for non faradaic EIS phosphate buffer (pH 7.2) was used either 10 mM or 100 mM as detailed below.

The impedance spectra were analysed by fitting appropriate equivalent circuit models to the measured data (ProFit® QuanSoft, Switzerland).

3.4.1 Gold rod electrodes

3.4.1.1 SAM functionalisation

After electrochemical polishing of the rod electrodes (section 3.2.2), the electrodes were sonicated in water and ethanol for 5 minutes, rinsed in ethanol and dried in N_2 flow, then immersed in a 0.5 mM solution of 4EG in absolute ethanol and incubated overnight. The electrodes were rinsed in ethanol to remove any non-specifically bound 4EG and a CV scan was performed.

3.4.1.2 Antibody functionalisation

Monoclonal anti hCG antibodies were grafted on the monolayer by NHS-EDC chemistry following the procedure illustrated in figure 3.3. The SAM modifIed electrodes were

immersed in a freshly prepared NHS-EDC mixture for 15 minutes. The electrodes were then rinsed in water and immersed in a solution of antibody, 0.3 mg ml^{-1} in 10 mM acetate buffer 10 (pH 4.5) for 1 hour. The NHS activated sites were blocked by immersing the electrodes in tris solution (100 mM, pH 8) for 20 minutes.

3.4.1.3 Surface characterisation

Rod electrodes were cleaned and functionalised as described above. Faradaic EIS measurements were performed applying a DC bias of 0.215 V vs reference electrode. For cleaned bare gold rod electrodes EIS was performed between 100 kHz and 1 Hz. Scans of bare gold, SAM and SAM/antibody functionalised electrodes were taken on each electrodes after 20 minutes incubation in the measurement buffer.

Cyclic voltammetry (CV) characterisation was carried out on bare gold surface, SAM and SAM/antibody functionalised electrodes after each functionalisation step. The CV scans were performed after EIS characterisation as specified above.

Non faradaic EIS measurements were performed in 10 mM phosphate buffer (pH 7.2) applying a DC bias of 0.215 V vs reference electrode for frequencies between 100 kHz and 50 mHz. Scans of the SAM and SAM/antibody functionalised electrodes were taken on each electrodes after 20 minutes incubation in the measurement buffer.

3.4.1.4 hCG detection

Rod electrodes were polished mechanically and electrochemically (see section 3.2.2), then the SAM was assembled as described in this section. The electrodes were rinsed in ethanol and incubated 15 minutes in a weakly acidic ethanol solution, rinsed, and incubated for 1 hour in water.

mAb-B were grafted to the monolayer by means of NHS-EDC chemistry, as follows: the rod electrodes were rinsed in water and 10mM acetate buffer (pH 4.5), then immersed in 0.15 mg ml^{-1} mAbB solution in acetate buffer, for 3 hours. The electrodes were then rinsed in phosphate buffer and incubated in 100 mM tert-butylamine solution for 20 minutes. The electrodes were stored in 10 mM phosphate buffer (pH 7.2) for 2 hours before measurement.

EIS scans were performed every 20 minutes until a stable baseline was established. Where mentioned, the functionalised electrodes were exposed to 0.01 mg ml^{-1} BSA in buffer solution for 20 minutes before acquiring a new EIS spectrum.

The target, hCG, was diluted 10 times at a time, mixing accurately the tubes every time, to the desired concentration in 10 mM, pH 7.2, phosphate buffer. The electrodes were exposed to hCG solution directly in the electrochemical cell. The EIS was performed 20 minutes after the exposure. After the measurement the solution was replaced

with a solution at higher concentration and measure would be repeated.

3.4.2 E-beam evaporated gold electrodes

EEG devices were obtained and cleaned as detailed in section 3.2.2. The devices were then incubated in OEG solution for 40 hours (see section 3.2.1). Functionalised devices were thoroughly rinsed in ethanol and DI water. The devices were mounted in the electrochemical cell which defines the working electrode area by means of a rubber gasket.

3.4.2.1 Antibody immobilisation

After assembling the electrochemical cell, the mAb-B were bound to the surface by means of NHS-EDC chemistry following the procedure illustrated in figure 3.3 steps A to D. The chip was incubated in 100 mM MES buffer (pH 5.6) for 20 minutes. Then, NHS-EDC mixture (section 3.2.1) was incubated on the surface for 15 minutes. The surface was rinsed in MES buffer and 10 mM acetate buffer (pH 5.0) three times.

The mAb-B antibody was then immobilised on the surface for 1 hour in acetate buffer at a concentration of 20 μg ml^{-1}. The devices were rinsed with acetate buffer for three times and incubated for 15 minutes. Ethanolamine 100 mM in acetate buffer was injected on the surface and left for 30 minutes to quench the remaining NHS-EDC activated sites.

The surface was then rinsed with acetate buffer for 3 times and the measuring buffer. Samples were either measured in 100 mM phosphate buffer (pH 7.2) with and without redox probes (2 mM) or in horse serum. The latter was used for the calibration of the sensor. Prior to any electrochemical measurement the measuring buffer or serum was incubated for 20 minutes.

3.4.2.2 Electrochemical measurements

EEG devices were prepared as described above. Characterisation of the surface for clean gold, SAM and SAM/antibody functionalised devices was performed by means of CV and EIS.

Non faradaic EIS measurements were performed in 100 mM phosphate buffer (pH 7.2) applying a 10 mV AC voltage, with no DC bias, for frequencies between 100 kHz and 50 mHz. While faradaic EIS measurements were acquired in 100 mM phosphate buffer (pH 7.2), with 2 mM redox couple, $Fe(CN)_6^{3-/4-}$, applying a DC bias between the redox couple oxidation and reduction potentials, namely 0.215 V vs reference electrode.

Cyclic voltammetry (CV) was performed on bare gold surface, SAM and SAM/antibody functionalised electrodes at each functionalisation step. The CV scans were per-

formed after EIS characterisation, between -0.5 V and 0.6 V in phosphate buffer (100 mM) containing 2 mM of the redox couple, at 62 mV s^{-1}, for five cycles.

3.4.2.3 Sensor calibration in serum

Fresh devices were functionalised with OEG and mAb-B as described above. After immobilisation of antibodies on the surface the chip was incubated in serum for 20 minutes prior to EIS measurement. Impedance spectroscopy was performed between 100 kHz and 50 mHz by applying 10 mV AC perturbation with no DC bias. After each measurement the cell was emptied and fresh horse serum was injected. The incubation step and measurement was repeated for three more times.

Devices that were not stable in phase, i.e. the phase at 0.1 Hz, $\varphi_{0.1}$ would vary more than 0.1 degree between each measure were disregarded. After the fourth serum blank measure the first spiked serum injection was performed in the same way as the blank injections. Spiked serum with hCG concentration varying from 2.6×10^{-14} to 2.6×10^{-9} were injected in increasing order. Four injections, unevenly spaced in concentration, were sequentially measured. This ensures that the concentration and time, or number of injections, are unrelated. The phase at 0.1 Hz was extracted from the EIS scans and the average of multiple scans was used a sensor output.

3.5 Mixed self assembled monolayers for biosensors

TSG samples were prepared as detailed in section 3.2.2 and immediately immersed in freshly prepared SAM solutions (section 3.2.1). The TSG samples were incubated in the SAM solution for 40 hours.

Different samples were prepared for electrochemical and contact angle measurements, while XPS and ellipsometry were carried out on the same samples. Before measuring, each sample was rinsed with absolute ethanol, sonicated for two minutes in 0.2% HCl spiked ethanol, then rinsed and sonicated for two minutes in DI water. The samples were dried under a stream of dry N_2 and measured.

3.5.0.4 Electrochemical impedance spectroscopy

Non faradaic EIS was carried out in 100 mM sodium phosphate buffer at pH 7.2, after twenty minutes pre-incubation in the same buffer. Impedance spectra over a frequency range from 50 mHz to 100 kHz were acquired by applying of a 10 mV sinusoidal signal against open circuit voltage. Each measurement comprises three frequency scans, and three measurements were taken per sample at intervals of twenty minutes.

3.5.0.5 Contact angle

Contact angle measurements of static, advancing and receding water drops were carried out on all samples. Multiple samples, four to six spots per sample and two to four images per measurement, were acquired for each SAM. Images were recorded digitally by means of a CCD camera and analysed with ImageJ 1.46 software (National Institutes of Health, USA) equipped with the drop analysis plug-in.

The static angle was recorded by dispensing a droplet of DI water of about 1.5 μl volume from a square cut needle onto the surface. The advancing angle was measured by reintroducing the needle in the centre of the droplet and adding water until the contact line advances, while the receding angle was measured by retracting the water droplet until the contact line recedes.

3.5.0.6 Ellispometry

The thickness of the SAM for each sample has been estimated by means of null ellipsometry, using a Jobin-Yvon UVISEL, and by using a clean template stripped gold sample as reference surface. The measurements of the amplitude ratio, Ψ, and phase shift, Δ, were taken at an incident angle of 70°. The spectra were then fitted using DeltaPsi2©, assuming a simple three layer system. The SAM was modelled as a transparent thin film using a Cauchy dispersive model. The incident angle of the light was treated as a free parameter to allow for small deviations in the tilting angle, caused by the way the template stripped gold samples were fabricated.

3.5.0.7 X-ray photoelectron spectroscopy

XPS spectra were obtained using a Thermo Electron Co ESCA Lab 250 in ultra high vacuum. The chamber pressure was maintained lower than 10^{-9} mbar during data acquisition. Two sets of samples were irradiated by a monochromatic Al Kα X-ray beam (1486.7 eV) with diameter of about 0.5 mm in two different regions. Survey and detailed scans were obtained in Large Area XL magnetic lens mode with a pass energy of 150 eV and 20 eV, respectively. The spectra were obtained with an electron take off angle of 90°.

Spectra were analysed with the CasaXPS© software, all spectra were corrected by shifting the C 1s peak to 285.0 eV to compensate for residual charge on the surface. We note that the binding energies (BE) of uncorrected C 1s peaks were between 284.95 eV and 285.13 eV, except for one of the spots on the MUD:OEG 0.1% sample (BE of 285.49 eV).

For quantitative analysis of the XPS spectra a 70%-30% Gaussian-Lorentzian peak shape was used. The background was removed using a Shirley function for both Au 4f

and C 1s peaks, while a linear function was used for the S 2p and O 1s.

3.5.0.8 Atomic force microscopy

Tapping mode AFM images were acquired using a Dimension Series 3100 (Veeco Instruments, Cambridge, UK), and using a silicon tip (Veeco Instruments, Cambridge, UK) with a typical resonant frequency of 300 kHz at room temperature in air. Three to five regions of each samples were scanned.

The scanned area have been selected as follows: an initial scan of 5x5 μm has been performed and then an area of 1x1 μm has been selected in the same field of view. Afterwards the AFM tip was moved to a different region with a distance of at least a few mm and the procedure repeated.

This page would be intentionally left blank if we would not wish to inform about that.

Chapter 4

Antibody layers as recognition systems for biosensors

4.1 Introduction

The adsorption of antibodies to solid surfaces has been the subject of numerous studies[158–160] due to their possible use as recognition elements in biosensors.[46,47] Antibodies with high binding specificity and efficiency can be selected and mass produced in vitro[161] for use in biosensors[28,162–164] allowing for the detection of analytes.

The use of antibodies on the surface of biosensors enables said surface to bind specific targets, or antigens, and immobilise the target in close proximity to the surface.

The antibodies act as the recognition element of the sensor and are immobilised on, or in close proximity to, the transducer. In a biosensor the binding of the target usually leads to a change in one or more of the physical or chemical properties of the recognition element. This change is detected by the transducer and an output signal is generated; ideally the output is proportional to the concentration of the target in solution.

A variety of biosensing techniques have used antibodies as a detection element. A few examples include ELISA systems,[22] quartz crystal microbalances,[71] electrochemical immunosensors[165] and surface plasmon resonance (SPR) sensors.[166]

This chapter focuses on the formation and optimisation of gold surfaces with antibodies for biosensor applications.

Biological function of Antibodies. Antibodies are proteins responsible for the detection of foreign objects that enter the host's system and are a fundamental part of the immune response.

The first event in the immune response to a new pathogen, the object that causes

the pathology, is the non-specific recognition of the pathogen by macrophage cells. This exposes antigens, specific to the pathogen, so that the rest of the immune system is activated. This starts a chain of events that induces B-cells to produce antibodies (immunoglobulin G, in particular) specific to the pathogen antigen. The antibodies produced bind to infected cells, which also display the pathogen antigen, marking them for destruction.

Monoclonal and polyclonal antibodies. Over the years, the use of antibodies for both the diagnosis and treatment of diseases has increased the need for selection and production of antibodies on a large scale and against a multitude of targets.

A distinction in laboratory-produced antibodies can be made between polyclonal, monoclonal and recombinant antibodies according to the production method used.

Monoclonal antibodies (mAb) are produced by copies, or clones, of a single parent cell; polyclonal antibodies are produced from several different immune cells producing different antibodies to the same antigen.[161]

Monoclonal antibodies are produced by clones of one parent B-cell, producing the desired immunoglobulin G, obtained from an animal that has been exposed to the substance that is the subject of study.[161] On the other hand, polyclonal antibody production relies on the purification of immunoglobulin G from blood serum, extracted from an immunised animal. A disadvantage of this method is that for the production of new antibodies successive extractions of serum are necessary, and new, identical, polyclonal antibodies can only be produced again from the same animal.

Monoclonal antibodies might be considered preferable because, after the extraction of the B-cell producing the desired antibody from the immunised animal, the production of clone cells and of the antibody can be performed in vitro.[167]

Recombinant antibodies are antibodies produced by inserting a DNA sequence of the wanted antibody in bacterial cells and forcing these cells to produce the wanted proteins. The immunoglobulin G is then extracted from the cells. The DNA sequence can still be obtained from an immunised animal.[47]

Due to the potential for the selection of specific immunoglobulins G to virtually any analyte and the convenience of in-vitro production, antibodies are often used as the recognition element in biosensor devices.[47]

Immonoglobulin G structure. Antibodies are proteins composed of two pairs of identical peptide chains: two identical long chains, called heavy chains, and two identical short chains, called light chains. The four peptide chains are bound together so that the final structure forms three lobes arranged in a "Y" shape, see figure 4.1.

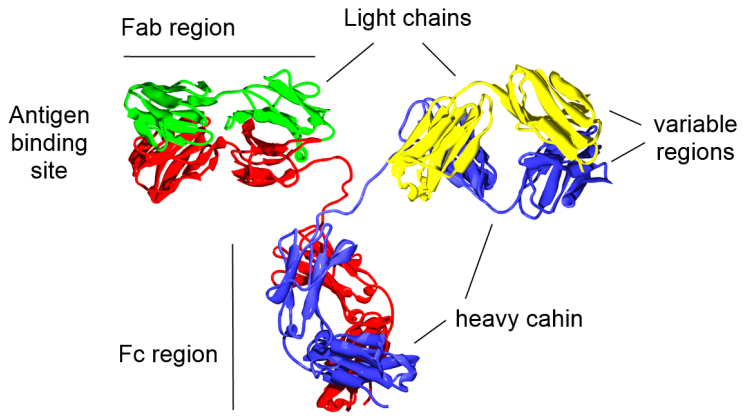

Figure 4.1: Typical structure of an immunoglobulin G antibody shown for the identification of the antibody chains and domains. The structure of antibodies is highly conserved across different species. Each antibody is formed of four chains. Two short light chains (yellow and green) and two long heavy chains (red and blue). The fragment crystallisable (Fc) region is formed of two constant domains from each heavy chain. The fragment antigen binding (Fab) regions consists of two constant domains, i.e. domains which are constant in different antibodies, one from the heavy and one from the light chain, and two variable domains, again one from each chain. The variable domains have a conserved structure between different antibodies but have variable loops that make them specific to an antigen. These variable loops constitute the antigen binding sites. Crystallographic structure adapted from Harris et al.[168]

The lower lobe of the "Y" is composed of a portion of the two heavy chains forming the so called fragment crystallisable (Fc) region (figure 4.1). Each arm of the "Y" consists of the continuation of one of the heavy chain and one light chains forming the fragment antigen binding (Fab) region.

The regions devoted to the binding of the antigen, the recognition regions, are located at the end of the Fab regions. In this region both the light and heavy chain have a variable domain, usually identical in both Fabs. This variable region determines the specificity of the antibody to a particular antigen.

4.1.1 Immobilisation of antibodies on surfaces

Non-oreiented immobilisation of antibodies. With the aim of developing a label-free biosensor platform with high sensitivity and specificity, monoclonal antibodies were immobilised on the surface of an electrochemical biosensor. In this study, the sensor surface was first functionalised with a -COOH terminated self assembled monolayer (SAM). The antibodies were then covalently bound to the surface through the use of N-

hydroxysuccinimide (NHS) and 1-Ethyl-3-[3-dimethylaminopropyl]carbodiimide (EDC) activation of the -COOH groups on the SAM.

Because of its convenience, easy preparation and execution, the NHS-EDC immobilisation procedure is very commonly used in biosensor research to immobilise proteins on SAM-modified surfaces and use them as capture molecules.[137]

The NHS-EDC immobilisation mechanism consists of promoting the formation of a covalent bond between the carboxylic acid on the SAM, and amine groups (-NH_2) present on the surface of the protein. Since amine groups are very commonly found on the surface of proteins, virtually any protein can be immobilised with this method. However, this also means that any of the amines on the protein surface can react with the -COOH, leading to randomly oriented protein layers.[137]

In the case of immobilisation of probes on the surface of biosensors, the orientation of the probe itself on the surface might be critical. The recognition and binding of the target by antibodies requires that the antigen arrives in close proximity to the recognition region present in the Fab-regions so that the two molecules can interact and bind.[47]

Antibodies are proteins that have been selected by evolution to operate in solution and have, in their natural environment, free movement in any direction. Once they are artificially immobilised on the surface, however, they lose the potential to orient themselves in the optimal way to bind the antigen. In this scenario the antigen has to approach the antibody in the correct orientation. Therefore, to facilitate the binding of the antigen, the antibody recognition regions, located at the end of the Fab regions, should be easily accessible and exposed to the measuring solution, rather than buried and facing the surface.

With the aim of optimising the sensitivity of the sensor, i.e. achieving the highest possible sensor output at any given antigen concentration, we studied the influence that different conditions for the immobilisation of antibodies on the SAM modified surface have on the sensitivity of the surface.

Considering that the orientation of the probes on the sensor surface is expected to influence its sensitivity, numerous publications dedicated to the study of protein adsorption[96,169] and orientation[97,158] are found. The parameters investigated are usually the conditions of the buffer used for the immobilisation, such as buffer pH and ionic strength,[111,170] or the characteristics of the surface itself, such as hydrophobicity, presence or spacing of functional groups, and surface charge.[111,137]

Since what is considered optimal is relative to the goals of each application, we have to define which characteristics of the sensor we aim to optimise. The sensor should

be as sensitive as possible, meaning that low concentrations of the target in solution can be detected, and the sensor output should be maximised, i.e. for the same concentration of the target in solution, a surface yielding a higher response would be preferable.

With the aim of using the sensor for investigating clinical samples, the sensor surface should be selective, i.e. it should bind the target even when present in solutions containing high salt and protein concentrations and should resist non-specific adsorption of other molecules present in complex protein solutions.

To achieve these goals, the orientation and density of the antibodies on the surface should be optimised.[158] However, maximising the number of antibodies on the surface does not necessarily maximise the number of available, easily accessible, binding sites.[55,137,158] The antibodies might be oriented upside down, with the Fab regions facing the surface, or neighbouring antibodies might be too close to each other and hinder the access of the binding region to the antigen.

Therefore, oriented antibody immobilisation methods can be used. For example, adsorption of bacterial protein G or A to the surface prior to the immobilisation of the antibodies has been showed to increase the proportion of antibodies bound to the surface with the Fab regions exposed to the solution,[158] i.e. binding the Fc region of the antibodies on the surface, thus leaving the recognition regions easily accessible.

Immobilisation techniques, such as the creation of a covalent bond between carboxylic acids (-COOH) on the surface and amine groups exposed on the protein mediated by NHS-EDC chemistry, are quicker, easier to implement, and more controllable than using protein mediators,[137,163] such as protein G. However, the immobilisation is influenced by electrostatic interactions and van der Waals forces between the antibodies and the surface during the initial adsorption which impacts on both the antibody orientation and density.[55,111]

4.1.2 Electrostatic interactions

The influence of the adsorption conditions, such as buffer pH, ionic strength and surface charge, on the adsorption of proteins to the surface have been studied.

By means of Montecarlo simulations and verified by experimental results, it was shown that electrostatic interactions (interactions between charged molecules) and van der Waals forces (i.e. weaker interactions usually occurring between dipoles or polarisable molecules) both determine the orientation of adsorbed antibodies.[159] When electrostatic interactions are weak, i.e. for low surface charge density and high ionic strength solutions, the van der Waals forces play a major role in adsorption to the sur-

face. In this case the antibodies would be attracted to the surface in a flat orientation, i.e. such that a larger portion of the surface of the antibody can interact with the surface of the sensor.[159,169]

However, if the ionic strength of the coupling buffer is low, the surface charge has a higher influence on the attraction of antibodies. When the interaction between the antibodies and the surface is dominated by electrostatic interaction, the charge of the antibody itself plays a role in its final orientation. In fact, if the antibody has a high dipole moment, i.e. opposite regions of the antibody have opposite charge, the region of the antibody that has a charge opposite to the charge of the surface will be preferentially attracted to the surface.[55,98,111]

The total net charge of a protein will vary with the pH of the buffer solution, i.e. for pH higher than the isoelectric point (pH > pI) the net charge of the protein is negative and vice versa. On hydrophilic surfaces, if the protein has a charge opposite to the surface, the electrostatic interactions will contribute to the attraction of the protein. In reverse, if the protein and the surface have the same charge the electrostatic interactions will repel the protein.[55,137]

Studies on charged polymer[55], charged OEG[137] and silica[171] coated surfaces show that the final amount of protein adsorbed is at a maximum when the protein charge has a small opposite charge with respect to the sorbent surface.[55,137]

The change in ionic strength of the buffer changes the radius at which the ionic interactions have an effect; for higher ionic strength the concentration of ions dissolved in solution is higher so the ions act as a screen between the proteins and the surface[55,137] and between the proteins themselves[171] making the electrostatic interactions less relevant.

For example, the influence of ionic strength of the buffer, on the binding of an antibody to a COOH-terminated SAM surface, was analysed by varying the concentration of NaCl in the buffer and maintaining the same pH. Upon addition of NaCl the amount of protein bound to the SAM would decrease, indicating that the increase in the ionic strength decreases the effect that the electrostatic interactions have on attracting the protein to the surface.[137]

Spacing of the antibodies. It has been shown that increasing the density of antibodies on the surface can decrease the proportion of antibodies that interact with the antigen.[137,171] For example, when monoclonal antibodies were immobilised on silica with a density of 1.4 ng/mm^2, 70% of the antibody binding sites were available for binding to antigens. When the density was equal to 2.5 ng/mm^2 only 5% of the antibodies were able to bind an antigen.[171]

A similar independent study showed the same trend in antibody activity with increasing density of antibodies, always adsorbed to silica surfaces.[170] In this study the occupied binding sites decreased from 70%, when adsorbed at 1 ng/mm^2, to 13% when adsorbed with a density of 2.7 ng/mm^2.[170]

Both these results suggest that at higher surface coverage the antibodies are hindered, making the binding of the antigen less efficient.[163,170,171]

In a separate study the spacing of immobilised proteins on -COOH terminated SAMs was studied by spacing the available binding sites (-COOH groups) on the surface. This was done by mixing said monolayer with an -OH terminated SAM.[137]

Looking at the effect that the spacing of -COOH groups has on the amount of protein adsorbed, the data showed that the amount of protein immobilised on the surface did not increase linearly with the increasing mole fraction of OEG (and -COOH groups). For example, for carbonic anhydrase II a mole fraction of 2% OEG in the monolayer leads to an adsorption that is 60% the adsorption measured for a 100% OEG SAM. For lysozyme, the amount of protein immobilised on a 2% OEG monolayer is equal to 80% the amount of lysozyme immobilised on 100% OEG.[137] This can be explained by the fact that only a small fraction of -COOH present on the surface is involved in the binding of the protein, because the protein immobilised is so much bigger than the SAM molecules. For example, the cross-section of carbonic anhydrase II is more than 60 times the cross-section of the SAM molecules.[137]

4.1.3 Aim and overview

Since most electrochemical biosensor transducers are fabricated using gold electrodes, and also a great variety of non-electrochemical biosensors use gold substrates, studies of protein adsorption to gold surfaces are very relevant in biosensor research. Finding a method that maximises the response of the surface to the target would be of great advantage, since it could lead to higher sensitivities.[172]

As discussed in the introduction SAMs can be used to make the substrate more hydrophilic and immobilise proteins without loss of functionality.

Moreover, oligo(ethylene glycol) or poly(ethylene glycol) modified SAMs are used in this study for their known non-fouling properties.[100–102]

With the aim of developing a label free impedance biosensor for the detection of hCG in both buffer and serum, the adsorption and activity of an anti-hCG monoclonal antibody (mAb B) to a hexa(ethylene glycol)carboxy-capped alkanethiol (OEG) modified gold surface is reported, see figure 3.1.

This particular SAM was chosen because the carboxylic acid group can be modified

by NHS-EDC chemistry for easy immobilisation of antibodies on the surface.

As discussed, electrostatic interactions of the antibody with the surface play an important role in the adsorption of proteins and antibodies. To test the influence of electrostatic interactions the antibodies were injected on the devices in buffers at different pHs and left to interact with the surface through only electrostatic interactions, i.e. without NHS-EDC immobilisation chemistry.

For the -COOH terminated OEG monolayer the surface is negatively charged at the tested pHs. It was found that the adsorption and the adsorption rate of antibodies on the surface decreased with increasing buffer pH up to pH 6. Very low adsorption was found for buffers with a pH higher than 6.

We can attribute the sudden decrease in adsorption rate at around pH 6 with a decrease in electrostatic interactions between the antibodies and the surface, since no other conditions were changed. We attribute this behaviour to the decreased net charge of the protein, due to the fact that the pH is close to the pI of the antibody.

Estimating the amount of antibodies bound to the surface and the amount of hCG bound to the antibodies, we observe a lower efficiency in the binding of the antigen with increasing antibody density. This can be attributed to steric hindrance between close molecules in more densely packed layers. However, the aim of immobilisation of antibodies for biosensor applications should be to maximise the final response, to achieve higher sensitivity.

Considering that we are looking at the optimisation of immobilisation protocols for antibodies on SAM coated surfaces to be used in biosensors, the optimal condition is the one that provides maximum binding of the antigen to the surface. When the surfaces were challenged with the antigen the highest response was found for pH $\approx$ pI -1, which corresponds to the pH that maximises the binding of the antibodies.

4.2 Results and discussion

4.2.1 Adsorption of monoclonal antibody to the surface

As discussed in the introduction of this chapter, the adsorption of proteins to surfaces is driven by interactions between the surface and the proteins. To find which binding conditions give a sensor surface with the highest sensitivity, the binding of mAb-B to the SAM modified surface in different buffer conditions was studied by means of SPR.

Initially, as detailed in section 3.3.2, the antibodies were adsorbed to the SAM modified gold disk at a concentration of 50 μg/ml in buffers with different pH, without activation of the SAM by means of NHS-EDC chemistry. The adsorption curves in the

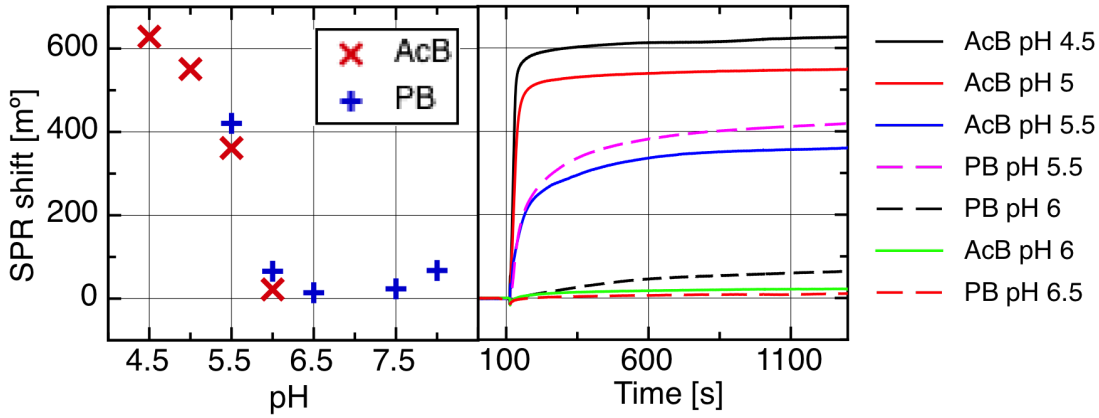

Figure 4.2: On the left, SPR response of mAb-B on OEG modified gold disk in different buffer conditions after 20 minutes of adsorption plotted against the pH of the coupling buffer, 100 mM, acetate buffer (AcB, ×), and phosphate buffer (PB, +). On the right, SPR response plotted vs time for some of the conditions plotted on the left. Acetate buffer (−) and phosphate buffer (- -) at different pH.

different buffers obtained by means of SPR are reported in figure 4.2 and the SPR shift, $\Delta\theta$, after 20 minutes, for each curve, is plotted against the buffer pH. This value was chosen as measure for comparison of the amount of adsorbed antibodies on the surface between the different buffers.

The electrostatic interactions between the antibodies and the monolayer were investigated by exposing the OEG modified surface to mAb-B at 20 μg/ml in various coupling buffers, at 100 mM, at varying pH from 4.5 to 8 with 0.5 unit intervals. The buffers used were acetate buffer for pHs from 4.5 to 6 and phosphate buffer for pHs from 5.5 to 8.5, figure 4.2.

A significant change in the amount of mAb-B adsorbed to the SAM is observed between pH 5.5 and pH 6. For pH $\leqslant$ 5.5, the SPR response, 20 minutes after injection, is higher than 350 m°. This corresponds to an adsorption of more than 2.8 ng/mm^2. The SPR response was less than 55 m° (0.44 ng/mm^2) for pH $\geqslant$ 6, see figure 4.2.

The amount of protein adsorbed to the surface is commonly attributed to the level of electrostatic interaction between the surface and the protein itself.[55,111,137,173] We expect that an opposing charge between the protein and the surface will attract the protein to the surface and that the attraction will increase with increasing charge difference. Minimum adsorption is expected when the protein and the surface have the same charge or when one of them is neutral.[55,111,137,173]

The pK_a of a surface functionalised with an acid-capped monolayer is defined as the value of the pH of the solution in contact with the SAM when half of the acid functional

groups are ionised.[174] The pK_a of -COOH terminated SAMs has been determined by various studies and is generally between 4.3[175] and 5.7.[176] Therefore, the OEG coated surface is expected to be negatively charged, or at least neutral, at the pHs investigated.

As mentioned in the introduction, the net charge of a protein in solution is dependant on the particular protein composition and on the pH of the solution. The antibody pI is indicated by the manufacturer to be between 6.4 and 6.8.

As shown in figure 4.2 a decrease in the SPR response was observed for increasing buffer pH, in particular for pHs between 4.5 and 6. Since very low adsorption is observed for pH $>$ 6, i.e. for a pH close to or higher than the antibody's pI, the electrostatic interactions between antibody and surface seem to play a major role in the adsorption of mAb-B.[163,171] With decreasing pH it is expected that the protein net charge is increasingly positive,[137,173] enhancing the attraction of the antibody to the surface.

The data in figure 4.2 show saturation of the SPR angle shift for pHs equal to 5 or lower. This is not surprising because at pH 4.5 we observed an adsorption of 5.1 ng/mm^2 which, according to the calculations of Buijs et al.,[111] is an almost completely saturated layer.

Minimal adsorbance was observed for buffers with pH $\geqslant$ 6. At these pHs the surface is expected to have a negative charge[177] so the low interaction of the protein with the surface can be attributed to either the neutrality (pH = pI) or negative net charge (pH >pI) of the antibody .

The ideal buffer ranges, corresponding to the respective $pK_a \pm 1$,[178] for the acetate and phosphate buffer are approximately 3.7 $<$ pH $<$ 5.7 and 5.8 $<$ pH $<$ 7.9, respectively. Ideally the buffers should be used only within these pH ranges. However, to demonstrate that the change in adsorption at pH = 6 was not due to the change in the buffer from acetate to phosphate, we also used acetate and phosphate buffer solutions of pH 6 and 5.5, respectively, to create an overlap in the buffer pHs.

Both acetate and phosphate buffers show a similar response at similar buffer pH. This further suggests that the amount of antibodies bound to the surface is mostly dependent on the buffer pH, and therefore on the charge of the antibody, rather than on the composition of the buffer itself. As expected, the amount of the antibody adsorbed to the surface increases with the increase in positive charge on the antibody surface.

As discussed in section 4.1.2, in addition to the protein charge, the electrostatic interactions are influenced by the ionic strength. The ionic strength, I, of an electrolyte can be determined according to:

$$I = \frac{1}{2}\sum_{i}^{n} c_i z_i^2, \tag{4.1}$$

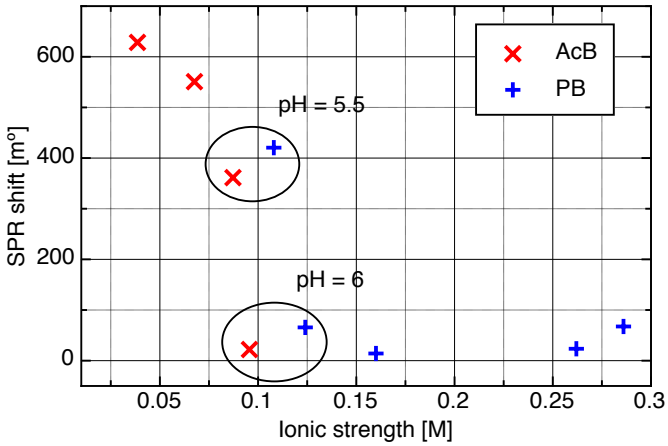

Figure 4.3: SPR response of mAb-B on OEG modified gold disk in different buffer conditions after 20 minutes of adsorption plotted against the ionic strength of the coupling buffer 100 mM, acetate buffer (AcB, ×), and phosphate buffer (PB, +). Circle indicates buffer at equal pH.

where c_i and z_i are the molar concentration and charge number of the ion i and n is the number of ionic species in solution.

Figure 4.3 shows the SPR response to the adsorption of mAb-B plotted against the ionic strength of the buffer instead of the pH. While there is a sharp decrease in SPR response due to a change in pH from 5.5 to 6, we note that the for acetate buffer pH 6 the SPR response is lower than phosphate buffer pH 5.5 although the latter has higher ionic strength. This suggests that the buffer pH, and thus the charge of the antibody, dominates the adsorption of the antibody on the surface over the ionic strength.

Furthermore, the adsorption rate also increases with decreasing pH for buffer pH lower than 6 (figure 4.4). The adsorption rate was estimated by fitting the SPR adsorption curves just after injection of the mAb-B, for a time interval of 15 seconds, by means of a linear regression fit of the SPR response curve. All the fits have a correlation coefficient equal to 0.99 or higher. The slope of the fit was then used as estimation of the initial adsorption rate of mAb-B to the surface.

We note that the adsorption rate decreases rapidly from 12.5 $\pm$ 0.4 ng/mm^2 per minute at pH 4.5 to 0.04 $\pm$ 0.001 ng/mm^2 per minute at pH 6. This further suggests that the forces involved depend on the pH and thus on the charge of the protein. At pH $>$ 6, (pH $\geqslant$ pI of protein) the electrostatic interactions seem to be minimal.

4.2.1.1 Activity of the antibody on the surface

So far the density and rate of adsorption of antibodies approaching the surface by means of electrostatic interactions was analysed; while the antibodies were not covalently bound to the surface. However, the final activity of the surface, i.e. the response to the antigen, is more important than maximising the density of the antibodies, al-

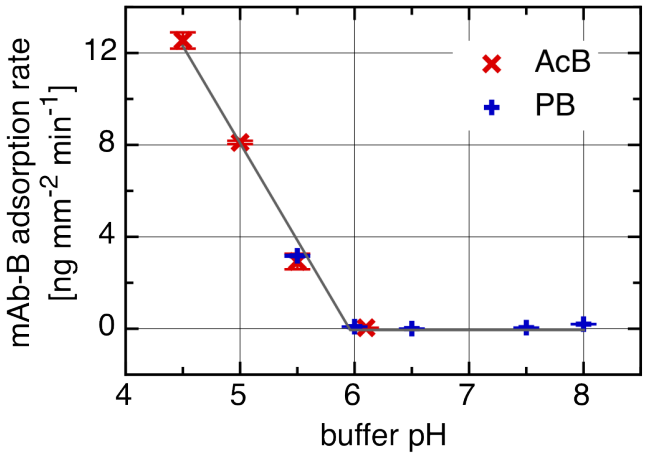

Figure 4.4: Initial adsorption rate (ng/mm^2 per minute) of mAb-B on OEG modified gold surface, measured in SPR, in both acetate buffer (AcB, ×) and phosphate buffer (PB, +) against buffer pH. The grey curve is a guide to the eye.

though the two are related. Therefore, mAb-B was bound covalently to the SAM in buffers at different pH and the activity of the surfaces was checked by challenging the surface with the antigen hCG.

As detailed in section 3.3.3, mAb-B was immobilised by creating a covalent bond between amines on the antibodies and carboxylic acids on the surface by means of NHS-EDC intermediates.

An estimation of the amount of adsorption of mAb-B to the sensor surface was performed by SPR. Gold disks coated with OEG were modified by NHS-EDC, then mAb-B was bound to the surface in buffers with a pH between 4.5 and 7.5. This allowed us to check the activity of the antibodies immobilised for pH conditions that promote mAb-B adsorption (pH < 6) and for the pHs that do not (pH > 6). The activity of these surfaces was estimated by injecting hCG at gradually higher concentrations (see section 3.3), the results are reported in figure 4.5.

To compare the binding of mAb-B to the surface by means of NHS-EDC in different buffer conditions the total shift estimated by the difference in the SPR angle before injection of mAb-B and after inactivation of NHS-EDC was taken, as suggested in established protocols.[137] An example of the mAb-B adsorption immobilisation and the respective SPR shift is shown in figure 3.4. Moreover the total shift was converted to mass density (assuming a conversion factor of 122 m°mm^2/ng), then plotted in figure 4.6 to compare the different adsorption amounts at different immobilisation buffer pHs.

For comparison the amount of mAb-B adsorbed to the SAM modified surface for other buffer conditions, tested separately, was plotted in the same graph. The immobilisation procedure for these samples was executed following the same protocol as described in section 3.3, the only variation was the molarity of the coupling buffer and the concentration of the mAb-B in the buffer solution, as labelled in the figure.

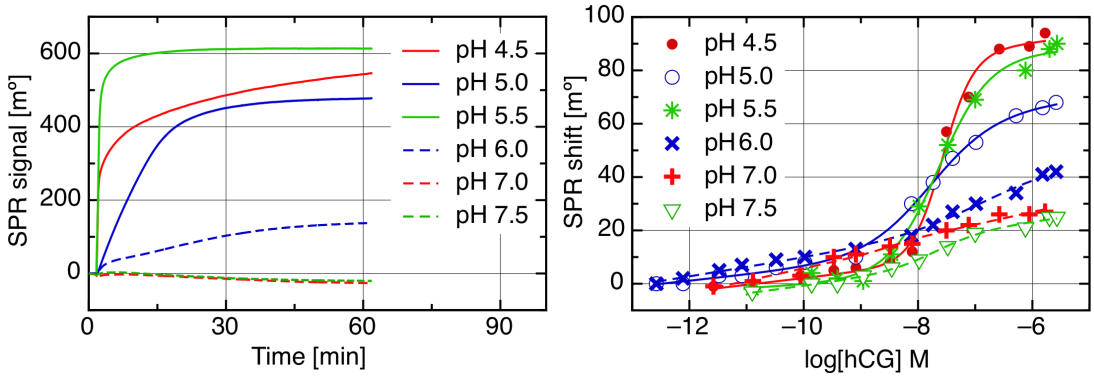

Figure 4.5: On the left, the SPR response over time for the binding of mAb-B, obtained by injecting 20 μg/ml mAb-B on the NHS-EDC modified surface under different binding conditions. Solid lines for acetate buffer pH 4.5 (red), 5 (blue), 5.5 (green) and dashed lines for phosphate buffer pH 6 (blue), 7 (red), 7.5 (green). On the right, the SPR response of the mAb-B sensor surface to hCG, plotted against logarithm of free hCG concentration in solution. This was measured in phosphate buffer pH 7.2, and fit to equation 4.5 (lines). The mAb-B was immobilised in different pH conditions as reported in the legend. Symbols and lines with the same colour correspond to data taken in the same experiment in two different channels.

We now focus on the first data set. All the data were obtained by immobilisation of mAb-B at 20 μg/ml in 50 mM acetate buffer at pH 4.5, 5 and 5.5 and 50 mM phosphate buffer at pH 6, 7 and 7.5 by means of NHS-EDC, as detailed in section 3.3. We can observe a saturated value for the amount of mAb-B immobilised on the surface from pH 4.5 to 5.5, then a rapid decrease for a pH higher than 5.5 that reaches zero at pH 7 and higher, creating a steep "step like" trend (figure 4.6).

Additionally, we note that with the activation of the carboxylic acid groups, by means of NHS-EDC, the charge of the surface changes. However, in the activation conditions used in this study (MES pH 5.6 and 10 minutes activation time) we can expect activation of no more than 25% of the carboxylic acids.[179,180] Therefore, the surface retains a considerable negative charge.

If we compare this "step" curve with the one obtained for mAb-B without immobilisation of NHS-EDC (figure 4.2) we notice that the latter shows only partial saturation at low pH. The difference can be explained by the fact that the steep "step" curve was obtained for an irreversible immobilisation, while the other was obtained by a dynamic, reversible, adsorption driven process and maintained by electrostatic interactions.

In fact, when the surface is exposed to 50 mM NaOH solution, pH 12.7, for 10 minutes the antibodies are removed, i.e. the SPR angle after the rinsing step is the same, within 10 m°, as before the injection of the mAb-B (not shown). The curve for NHS-EDC immobilised mAb-B, accounts for any reversible binding by taking the SPR

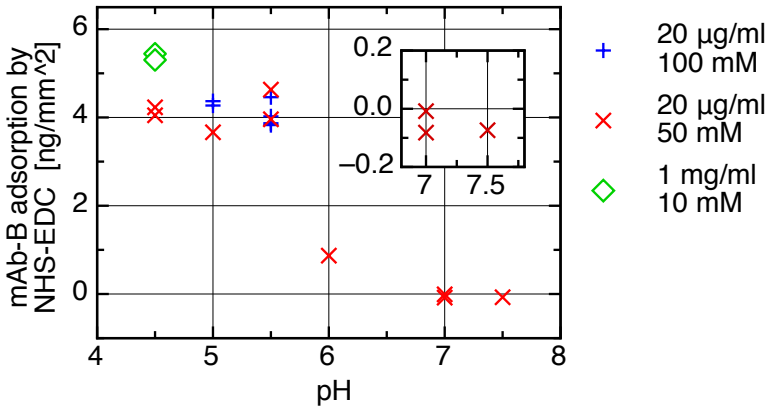

Figure 4.6: Adsorption of mAb-B, estimated as the difference between the SPR signal before mAb-B injection and after rinsing of ethanolamine, in different buffer conditions: mAb-B at 20 μg/ml in 100 mM acetate buffer ($\times$), mAb-B at 20 μg/ml in 50 mM buffer ($+$) in acetate buffer for pH 4.5 to 5.5 and phosphate buffer for pH 6 to 7.5 and mAb-B at 1 mg/ml in 10 mM acetate buffer ($\diamond$) plotted against the incubation buffer pH. The inset shows data for pH 7 and 7.5.

shift after 10 minutes exposure to 1M ethanolamine at pH 8.5.

Furthermore, we note that the second step of the NHS-EDC chemistry, i.e. binding of the primary amines (-NH_2) to NHS activated sites, is more efficient at pH 7-7.5 than pH 4.5-5.5.[181] However we observe no binding for pH 7 and 7.5. This suggests that if the antibodies are not attracted to the surface by the electrostatic interactions (pH > pI) they have very low probability of binding to the NHS activated sites, as shown in figure 4.5 (left) and figure 4.6.

The average adsorption of mAb-B immobilised by means of NHS-EDC from a solution of 20 μg/ml for all buffers with pH equal or lower than 5.5 is equal to 4.1 $\pm$ 0.4 ng/mm^2 (average $\pm$ SD). We consider this value to be the saturation value because the spread between these experiments measured as standard deviation (SD), obtained in different pH buffers, is similar to the standard deviation obtained for repeating the adsorption of mAb-B at a single pH, namely pH 5.5, in independent experiments performed over a period of several months.

We obtained an average adsorption of 4.1 $\pm$ 0.3 ng/mm^2 for mAb-B immobilised in acetate buffer pH 5.5 using a concentration of mAb-B in solution equal to 20 μg/ml. We note that the standard deviations obtained are less than 10% of the average value, which is very similar to the standard deviation found in other SPR studies.[137]

Surface activity. Finally, to test which conditions tied higher antibody activity, the mAb-B modified surfaces were exposed to the antigen in different immobilisation buffers by progressively spiking the 100 mM phosphate buffer at pH 7.2 with hCG of increasing concentrations. The experiments were performed by SPR as detailed in section 3.3. The SPR shift observed after injection of the appropriate hCG concentration, at response saturation, is plotted vs the logarithm of free hCG concentration in solution in figure 4.5 (on the right). The antibody/antigen binding kinetic follows the expected sigmoidal shape (when the concentration is on a logarithmic scale) that can be modelled using the Hill equation.

The Hill equation is a generalisation of the Langmuir isotherm for systems following a kinetic different to the single ligand/probe kinetic evaluation. The Hill equation can be derived by a binding reaction scheme in which n molecules of ligand L bind to a probe P:[182]

$$\mathrm{nL} + \mathrm{P} \overset{K_d}{\rightleftharpoons} \mathrm{PL_n}, \tag{4.2}$$

where K_d is the dissociation constant of the binding reaction of the reagents L and P giving the complex PL_n as its product.

At equilibrium the ratio between the bound probes and the total probe receptor sites is given by:

$$\frac{Bound}{Total} = \frac{[PL_n]}{[P] + [PL_n]} = \frac{[L]^n/K_d}{1 + [L]^n/K_d} = \frac{[L]^n/K_d}{1 + ([L]/K_{0.5})^n} \tag{4.3}$$

where $K_{0.5}$ is the concentration of ligand, [L], at which half of the receptors are bound and is equivalent to the n^{th} root of the dissociation constant K_d.[182]

For $n = 1$ the Hill equation describes the single probe/ligand kinetic adsorption model. The Hill equation is used to describe complex systems where not all the kinetic reactions are known, but the concentrations of a certain binder in a solution and the response of the system are known. For example, this equation might be used to describe the dose/response curve of a drug.[183]

When the concentration of the ligand is plotted on a logarithmic scale the Hill equation has a sigmoidal shape and can be rearranged in its convenient, operative formula as:[183]

$$R = B + \frac{T - B}{1 + 10^{(\log C_{50} - x)H}}, \tag{4.4}$$

where x is the logarithm of the concentration of free antigen in solution; B and T are the lower and higher asymptotes of the Hill equation; C_{50} is the concentration at which

the response is half the maximum response and H is the slope of the sigmoid in its linear section, called the Hill slope. We note that if we subtract the response baseline the lowest asymptote, B, must necessarily be zero.

In the Hill equation, for the hCG/mAb-B system under study, the concentration of the free antigen is expressed in a logarithmic scale and the slope of the linear part of the sigmoid (H) can be different from 1.

In general for a Hill slope higher than 1 the linear part will be steeper and vice versa. For $H > 1$ the binding of ligand to the probe is called cooperative, i.e. this mathematical model describes a binding model where the binding of the ligand promotes the binding of more ligand. For $H < 1$ the slope of the sigmoid would be lower than one and the binding is called non-cooperative, i.e. the binding of the ligand hinders the binding of more ligand.[183]

To account for any non-specific responses the model can be modified by adding a linear component, becoming:[183]

$$R = \frac{T}{1 + 10^{(\log C_{50} - x)H}} + (mx + q), \tag{4.5}$$

where m and q are assumed to be the slope and intercept of the non-specific response.

The SPR response to hCG (figure 4.5, right) measured as described above was fitted to equation 4.5. The successive injections of hCG on the surface introduce a non-specific response resulting in a linear increase of the SPR response with the injections. This response was considered to be non-specific because it is also observed for surfaces with no mAb-B bound. In fact, we note that the immobilisation of mAb-B at pH 7 and 7.5 yield an SPR response, after 1 hour, lower than the baseline of $\approx$ 20 m$^\circ$ (figure 4.5, left) and after inactivation of still active NHS-EDC is instead $\approx$ 10 m$^\circ$ lower than the baseline before injection of the mAb-B (not shown). This indicates that the amount of mAb-B bound to the surface for buffer pH 7 and 7.5 is negligible. However, these surfaces show a linear response to the subsequent injections of hCG.

It is unlikely that the hCG binds to the surface by covalently binding with NHS groups because the NHS on the surface was inactivated with 1M ethanolamine at pH 8.5.[137] Further investigations of non-specific binding are discussed later. The response at each injection is of only a few m$^\circ$ ($\approx$ 5 m$^\circ$) however the cumulative response is clearly noticeable (figure 4.5).

To compare the activity of antibodies immobilised under different conditions, the response of the sensors at saturation was measured for each condition. The response at saturation, or maximum response, was estimated by fitting the Hill equation of the

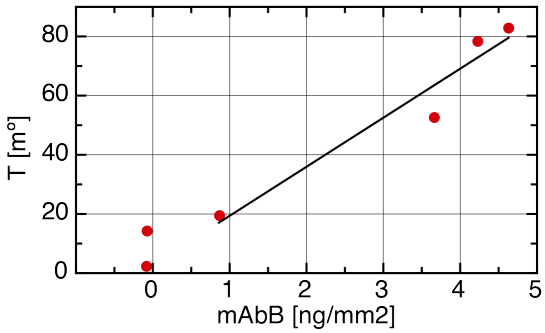

Figure 4.7: Plot of parameter T from equation 4.5 vs concentration of mAb-B on the surface estimated by SPR.

hCG/surface binding curves (figure 4.5) by evaluating the parameter T (equation 4.5) for each condition. The highest value of T was obtained for mAb-B immobilised at pH 5.5.

We note that, since the Hill equation used for fitting the sensors response accounts for non-specific binding, the parameter T corresponds to the saturation response, already subtracted from the non-specific binding. Therefore, the immobilisation condition that yields the highest T parameter can be considered the condition that maximises the specific response of the sensor surface.

The highest saturation response of the surface was obtained for the surface with the highest density of antibody bound to the surface. Therefore, we have plotted the saturation response of all the surfaces investigated against the mAb-B surface density (figure 4.7).

The maximum response of the sensor increases with the increase in the density of antibodies bound to the surface. It has been suggested that higher sensitivities are achievable for SPR sensors when a balance between number of binding sites and the steric hindrance caused by a too highly-packed layer is achieved.[137,184] However, here the highest response was obtained for the highest density of the mAb-B.

Up to 4.5 times less antibody binding is observed for coupling buffer at pH 6 (0.9 ng/mm^2) than at pH 5.5. The lower mAb-B adsorption reflects lower surface activity when the surface is challenged with hCG (Fig. 4.5).

It is useful to note that the buffer used at pH 6 is phosphate buffer while for pH 4.5 to 5.5 it is acetate buffer. However, during the investigations of adsorption of mAb-B without NHS-EDC, mAb-B adsorbed in phosphate buffer showed a very similar, if not slightly higher, adsorption than acetate buffer for the same pH (Fig. 4.2). This indicates that is unlikely that the difference in adsorption is due to the different buffer composition. In addition, NHS-EDC chemistry is not inhibited by the use of phosphate buffer as it has been used for binding proteins to SAM modified surfaces in similar protocols.[137]

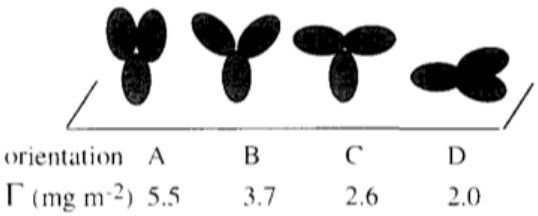

Figure 4.8: Schematic drawing and respective calculated adsorbed amounts, Γ, of some possible orientations of the adsorbed antibodies. A, B and C are antibodies oriented with Fab fragments facing the solution, often referred to as "Fab-up" orientation, with compacted, intermediate and repelling Fab fragments respectively. D, The antibody bound to the surface with both Fab and Fc regions, often referred to as "side-on" orientation. Adapted from Buijs et al.[55]

Antibody density. The efficiency of the antigen/antibody binding on the surface is here estimated as the molar ratio of the bound hCG and the immobilised antibodies. Even if the response of the sensor increases with the amount of antibodies on the surface, it has been noted that the antigen/antibodies ratio at surface saturation is at its highest for pH 6. 75% of the antibodies are bound to the antigen at 0.9 ng/mm^2, consistent with what is reported in the literature that lower densities of the antibodies on the surface lead to higher binding efficiencies.[137,170,171]

However, the difference between the maximum and minimum efficiencies reported in the literature are larger than observed here. As discussed in the introduction of this chapter, a variation in antigen/antibody binding efficiency from 70% to 5% and 70% to 13% on SiO_2 surfaces has been reported.[170,171] Instead, in this study, the lowest efficiency (47%) was observed at pH 5 (mAb-B adsorption of 3.7 ng/mm^2) rather than at pH 5.5, which has the highest density of antibodies (4.6 ng/mm^2). The latter surface yields a binding antigen/antibody efficiency of 59%.

It could be argued that the antibodies are not close enough to each other to observe the effect of steric hindrance. However, a maximum density of 5.5 ng/mm^2 for a layer of antibodies was calculated.[55] This condition can be realised in the event that the Fab regions are as close as possible to each other and the antibodies are immobilised with either the Fc or Fab fragments facing the surface (figure 4.8). These calculations assume homogeneous orientation of the antibodies.

A different value of maximum antibody density, 3.77 ng/mm^2, is obtained if the antibodies are modelled as a homogeneous sphere, i.e. a sphere with the same molecular

weight as the antibody but with an homogeneous distribution of mass, that has a radius of 3.6 nm and a molecular weight of 150 kDa[137] distributed in a regular hexagonal pattern. This model is closer to the assumption that the antibodies are randomly oriented on the surface. In this case, the theoretical value for the maximum density is lower than the observed density which indicates a preferential "Fab-up" or "Fc-up" orientation. The fact that the surface shows response to hCG shows that the antibody are not all in a "Fc-up" orientation.

As mentioned, the density of mAb-B observed at pH 5.5 was equal to 4.64 ng/mm^2, which fits well between the two theoretically calculated extreme values. Therefore, the mAb-B formed a densely packed layer at pH 5.5 and shows the highest surface activity.

We note that the optimal buffer pH for NHS-EDC immobilisation, pH 5.5, is also the highest pH value tested that shows electrostatic interactions with the non NHS-activated surface (figure 4.2). Since the surface is negatively charged, and attraction of the antibody is observed only for pH lower than 6, we assumed that at pH 5.5 the charge of the antibody is slightly positive.

Previous work showed that optimal binding conditions were obtained for proteins bound to the surface when the buffer pH was equal to pI minus 1 unit, giving a slight positive charge to the protein.[137,172] However, the higher response of the surface in these studies is not the result of higher density of the probes on the surface.

It has been suggested that, for negatively charged surfaces, the antibody will be attracted to the surface predominantly by its most positive charged region, the Fc region.[172] Therefore, the pH of the coupling buffer in relation to the pI of the antibody and the charge of the carboxyl group, influences both the amount and the orientation of the antibody binding.

In their work, Puertas et al. immobilised three antibodies with three different pIs, specific to three different antigens, on carboxy-activated magnetic nanoparticles.[172] Each antibody was covalently bound to the nanoparticles in buffer solutions with pH similar, higher and lower than the antibody's pI. The surface was then blocked with BSA for 16 hours to avoid non-specific adsorption of the antigens to the nanoparticles.[172]

The activity of the antibodies bound to the nanoparticles was estimated by challenging the antibodies with their respective antigen. Activity was measured by means of spectrophotometry. Immobilising the antibodies in buffers with pH $<$ pI increased the measured activity of the antibodies when compared to antibodies immobilised in pH $>$ pI.

However, this was not attributed to a higher density of the adsorbed antibodies; when the density of the antibodies was maximised but the antibodies were not positively charged while binding, a decrease in the antibody response was observed.

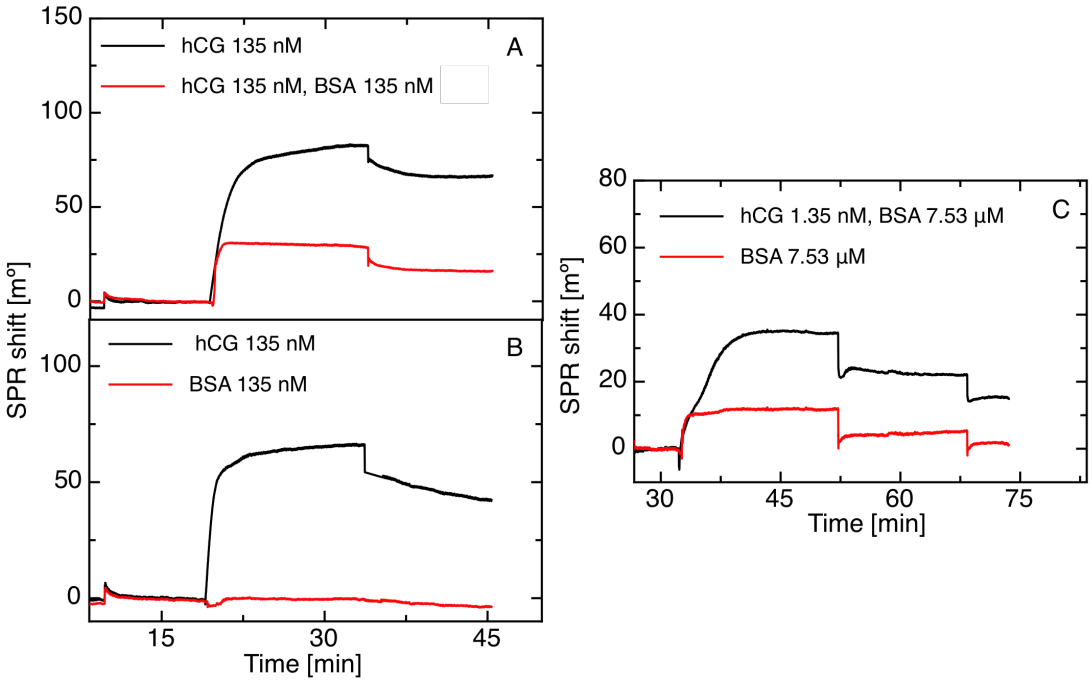

Figure 4.9: Binding curves recorded by means of SPR of hCG, BSA and hCG and BSA recorded in three separate experiment as shown in the respective plots. The legends indicate the concentrations of hCG and BSA in each experiment. Prior to injection of hCG and hCG-BSA the surface was functionalised with mAb-B in acetate buffer pH 5.5. The binding curves were recorded in PB pH 7.2 100 mM (A and B) and TBS pH 8.0 (C).

The authors concluded that the increase in the response of the antibodies to the antigen in solution was due to improved immobilisation conditions of the antibodies that would preferentially bind the nanoparticles, by leaving the antigen binding regions exposed to solution, favouring the binding of the antigen.[172]

4.2.1.2 Non-specific binding

When developing a biosensor it is important to evaluate the surface activity as well as the amount of non-specific binding. As previously discussed a non-specific response was observed for consecutive injections of hCG. Therefore further investigations of this non-specific response were performed.

The response of the surface to other proteins was tested (figure 4.9). BSA was chosen as negative control for mainly two reasons. First, BSA is thought to easily bind to surfaces non-specifically, it is in fact used in many studies to block non-specific binding of

proteins to surfaces[29,111,185] and is often used as negative control.[186,187] Second, serum albumin are present in high concentration in blood serum (41-45 mg/ml)[188] therefore checking the selectivity of the sensor to BSA is a first step to gauge how the sensor would behave when using complex protein solution, such as serum.

For each experiment an SPR disk was functionalised with OEG SAM as per the usual protocol and mAb-B was immobilised on the surface following the discussed protocol in acetate buffer pH 5.5.

The SPR instrument allows the measurement of two separate channels. To compare the size of the two molecules it can be assumed that the proteins can be represented as hard spheres of uniform density (ρ = 1.30 g/cm^3).[137] We can then calculate an equivalent radius, r, for both hCG and BSA according to:[137]

$$r = 10^8 \left(\frac{3MW}{4\pi\rho N_A} \right)^{1/3} \tag{4.6}$$

where MW is the molecular weight of the protein and the equivalent radius is expressed in Å.

Assuming a molecular weight of 37 kDa for hCG[189] and 66 kDa for BSA[190] the equivalent radii were determined to be 22 and 27 Å, respectively. Thus the linear extension of BSA is approximately 20% larger than hCG.

The surface was challenged with hCG at a a concentration of 135 nM as well as hCG and BSA both at a concentration of 135 nM and the results are shown in figure 4.9 A. We note that the response of the sensor to 135 nM hCG, over three separate experiments under the same conditions, is equal to 75 $\pm$ 8 m$^\circ$ (0.62 $\pm$ 0.06 ng/mm^2) while the response to hCG and BSA both at the same concentration is 29 m$^\circ$. This is significantly lower than the response to hCG alone. The response to hCG is 2.6 times higher than hCG and BSA, suggesting that the BSA interferes with the binding of hCG to the antibody-functionalised surface. However, when the surface is challenged with only 135 nM BSA the surface shows no response (figure 4.9 B).

The mAb-B modified surface was challenged with high concentration of BSA, 0.5% BSA (7.52 μM), on one channel and 0.5% BSA and 1.3 nM hCG on the other channel. The measurements were carried out at the same time. The response to the hCG + BSA was 4.8 times higher than the response to BSA.

This indicates that even a high concentration of BSA is only minimally adsorbed by the surface, in comparison with the antigen, and that the surface binds the hCG even when mixed with high concentrations of other proteins.

A separate negative control was carried out to check for non-specific adsorption of hCG to the surface. A new SPR disk functionalised with the OEG SAM was used. On one channel mAb-B was immobilised in phosphate buffer, pH 5.5, as described before. On the second channel a different antibody, namely a commercial anti-mouse antibody not specific to hCG, was immobilised on the surface under the same buffer conditions (an adsorption of 5.2 ng/mm^2 was observed).

In this case, no binding of hCG was detected for the anti-mouse antibody, i.e. the SPR angle measured after 10 minutes of injection of hCG was within 1 m$^\circ$ of the SPR angle before injection. A response of 42 m$^\circ$ was observed for an mAb-B modified surface, which is consistent with the previously shown hCG response.

4.3 Conclusions

Understanding the mechanism of adsorption of recognition molecules, such as antibodies, to a surface is important for the optimisation of biosensors. It was found that for antibodies immobilised in buffers with pH lower than the antibody pI the adsorption of proteins to the surface is favoured by higher electrostatic interactions.

The loss of surface activity, as high as ten fold, shown in different studies[137] induced by higher densities of the probe on the surface was not noted in this study. The surface activity, estimated by means of SPR, increases for immobilisation buffers with a pH lower than 6, which corresponds to immobilisation conditions that yield a higher density of the antibodies. In general, higher density of the antibody layer shows higher response of the surface.

With the intention of building an impedimetric electrochemical biosensor we want to maximise the responsiveness of the surface so that high sensitivity, defined as a low limit of detection and high signal response, can be achieved.

Chapter 5

Electrochemical biosensor for clinical diagnostics

5.1 Introduction

The initial goal of this study was the development of multiplexed label free electrochemical biosensors. Different types of electrochemical biosensors have been developed over the years. They are usually classified by either the electrochemical technique used or the measured quantity.[24] Voltammetric and amperometric techniques involve applying a static, DC, voltage at the electrode/solution interface, changing the electrode conditions, and measuring the current flowing through the electrode.

Impedance biosensors, instead, measure the impedance of electrode/solution interface without disruption of the initial state of the interface. This is possible by applying a small alternating current, AC, typically 10 mV amplitude, which does not perturb the state of the electrode, around a steady DC bias and measure the current perturbation. The impedance is then measured as a ratio between the applied voltage and the measured current. When this process is repeated at multiple frequencies an impedance spectrum, $Z(\omega)$ can be obtained, which is known as electrochemical impedance spectroscopy (EIS) (see section 2.1.4).

If the impedance of the electrode changes when a molecule of interest binds to a recognition element immobilised on the biosensor surface, EIS can be used as detection technique of the change of the impedance.

Impedance biosensors are label free biosensors, i.e. they do not require any labelling of the analyte, or the use of a second labelled probe for detection; this means that the same system can detect virtually any analyte just by changing the probe attached to the surface. In contrast, a sandwich-assay uses two antibodies. The first is attached to the surface; this antibody detects the antigen and binds it to the surface. In a separate

step the surface is exposed to a second, labelled, antibody, that in the presence of a substrate generates the signal.

Impedance biosensors are usually cost effective, by using inexpensive mass producible electrodes,[191] e.g. electrodes produced by means of photolithography or screen printed electrodes[192] and relatively simple instrumentation. For example, simple lock-in amplifiers have been used to measure the differential impedance between two electrodes.[66]

They can be multiplexed, i.e. multiple electrodes can be fabricated on the same device by using electrode arrays and multiple measurements can be performed at the same time.[24,191]

They are easy to use because they require minimal, or no, sample manipulation and the time involved in the measurement is much shorter than sandwich-assays, which require multiple rinsing and long incubation times.

The combination of these properties gives to impedimetric biosensors the potential to be used in point-of-care environment for screening multiple biomarkers as part of clinical check-ups from a single sample without any sample manipulation.

To reach this goal it is essential that the sensor can selectively detect low concentration of the analyte from a complex solution that contains high quantity of other proteins, typically for blood samples, a protein concentration of 70 mg/ml is expected.[31]

5.1.1 Measurement of impedance

5.1.1.1 Faradaic measurements

Different approaches to the building of impedance biosensors have been used over the years. A very common approach is to estimate the change in charge transfer resistance, R_{ct}, in a redox probes rich environment in the presence of the biomarker of interest.[92,192,193] Usually the R_{ct} is extracted from the EIS spectra according to the choice of an equivalent circuit as seen in section 2.1.4.3.

This method requires the introduction of redox probes in the system, e.g. ferri-ferrocyanide couple, and it measures a change in the R_{ct}, generally increase, due to a progressive hindering of the electron exchange between the redox probes and the sensor surface. The degree of blocking is proportional to the amount of analyte binding to the surface.

Detection limit of the order of pg/ml have been shown for this biosensors. For example a detection limit of 7 pg/ml of IgG was found for a rabbit IgG/anti-IgG system after 30 min incubation measuring in a 10 mM PBS (PB saline) buffer (0.05% Tween) in the presence of a 5 mM redox probes.[193]

Although the addition of redox probes to the system is suitable in a laboratory environment it is somewhat inconvenient for the implementation of a point-of-care device. Moreover, the value of the measured R_{ct} is proportional to the amount of electron transfer from solution to the electrode and it scales with the size of the electrode surface itself. This makes the miniaturisation of this kind of sensor electrodes intrinsically more challenging, which can be a limiting factor for multiplexed applications.

5.1.1.2 Non faradaic measurements

A second approach is to estimate the capacitance change[32,48] of the working electrode, in absence of redox probes. As detailed in section 2.1.4.4 the sensor surface can be modelled as a series of three capacitors according to equation 1.5.

In previous work, the total capacitance, C_{tot}, has been evaluated by measuring the transient current at the working electrode occurring with the application of a potentiostatic step.[32,48] With this method Bergerren et al. developed biosensors for antibodies, antigens, proteins, DNA fragments, and heavy metal ions.[21] For exampe, hCG and Interleukine-6 were detected from concentration as little as 15×10^{-15} M and 5×10^{-16} M, respectively,[32,48] in low molarity phosphate buffer. This is one of the most sensitive biosensors for hCG reported to the author's knowledge.

We remind that the total capacitance, C_{tot}, can be modelled, as a planar capacitor, by:

$$C_{tot} = \varepsilon_0 \varepsilon_r A/d, \tag{5.1}$$

where ε_0 and ε_r are the absolute and relative permittivity constants, respectively; A is the surface area of the electrode and d is the distance between the electrode and the outer Helmholtz plane of the electrochemical double layer.

Impedance contributions. As discussed in section 2.1.4, the change in capacitance was attributed[32,48] to an increase in the distance, d, between the surface of the electrode and the outer Helmholtz layer caused by the binding of the target to the electrode surface. The binding of the target increases the thickness of the recognition layer, in fact it displaces the molecules adsorbed to the probes and pushes them further away from the electrode, increasing the distance of the outer Helmholtz plane from the electrode (figure 1.5).

The understanding of the mechanisms that allow the detection of molecules as change in impedance can help to improve the design of a biosensor by enhancing the characteristics of the surface or of the measurement method so to achieve higher sensitivity.

Models of the electrode/solution interface should predict these changes. Other than an increase in thickness other factors can contribute to the change in capacitance, and impedance, of the electrode.

First, the binding of the target can change the permittivity of the recognition layer. If the target has a very different permittivity, ε_r, than the probe, its binding will affect the average permittivity. Moreover the binding of the target displaces water molecules associated with the surface and since water and proteins have very different permittivity (ε_r is between 2 to 5 for biomolecules and 80 for water)[24] the displacement of water decrease the permittivity of the layer. The total capacitance of the electrode will vary with the change in permittivity according to equation 5.1, so the capacitance of the electrode decreases with the binding of analyte.

Second, the change in charge of the surface. If the probe is in a different charge state than the target, the binding of the target changes the charge of the recognition layer thus the species associated with the electrochemical double layer change to accommodate the change in charge surface.[194,195]In general, probe and target will have different isoelectric points, pI. As already mentioned the isoelectric point is the pH at which a molecule has zero net charge. If two molecules with different pIs are in the same solution they will have different charge states. Thus the pH can affect the measurement by influencing the charge of probe and target, therefore to control the charge of the proteins the pH needs to be controlled.

A change in pH can affect the electrode capacitance, by changing the charge of the surface of the electrode that will influence the electrochemical double layer. For short chain SAMs the capacitance change can be up to 40%; the effect becomes smaller with increasing SAM chain length.[196]

Furthermore, the properties of the probe molecules and its immobilisation step influence the surface activity. Some of these factors have already been discussed, including the probe density, its charge related to the pH, the loss of probe activity when immobilised on the surface and the affinity of the surface to the target. These factors have been used to explain the observed discrepancies between similar assays for different targets.

To increase the sensitivity to a change in the recognition capacitance happening upon binding of the target, a very good blocking SAM is desirable. The presence of defects makes the change in capacitance more difficult to detect. In fact, the defects in the insulation properties of the SAM can be modelled by a leakage resistor added in parallel to the capacitance. The presence of this leakage resistor can dominate the behaviour of the system thus making the change in capacitance more difficult to detect.[32,48]

Dipoles. For example, it was shown that acid capped SAMs, for pHs at which the acid is partially ionised, a negative applied voltage in EIS induces protonation and deprotonation of the acid which add a significant contribution to the electrode impedance, at frequencies near 10 Hz, depending on the kinetics of the protonation/deprotonation and is a physical explanation for a leakage resistance in non-faradaic systems. [197,198]

Moreover, dipoles in the SAM functional groups can affect the permittivity and thus the capacitance of the SAM. This phenomenon can also partially explain why otherwise similar targets give different response, such as a change in capacitance. The dipoles' response to the AC signal varies in frequency, as they can react to slow changes, low frequencies, of the electric field but not to fast changes, high frequencies, making the dielectric constant, ε_r, not constant over the frequency spectrum.

An applied voltage can induce a change in the probe/target conformation and net charge which would induce a change in impedance of the recognition layer. Moreover it can also change the impedance of both the surface capacitance and the charge transfer resistance, R_{ct}.[24]

In this study, the adsorption of an antibody layer to an acid-capped SAM coated gold electrode was studied by means of EIS and cyclic voltammetry (CV), under both faradaic and non-faradaic conditions. Moreover, the binding of the antigen and the consequent change in impedance at the working electrode was studied by means of EIS, in absence of redox probes. Different equivalent circuits were used to model the change in capacitance and resistivity of the SAM and recognition layer upon the antigen binding event. Detection of the antigen from spiked horse samples was possible and a calibration curve was obtained.

One of the challenges presented by modelling the impedance of working electrodes is that the electrode behaviour is generally non ideal. Even when models, or equivalent circuits, take into account the non idealities they represent either a simplification of the system or the equivalent circuit has a high number of free parameters, making the choice of which parameter to monitor arbitrary.

Therefore a quantity that takes into account the overall change in impedance which is at the same time easy to record and does not require post processing, fitting, of the EIS spectra is highly desirable.

In general, the phase of the impedance of the electrode solution/interface at low frequency is as close to -90° as the behaviour of the electrode is similar to an ideal planar capacitor (figure 5.1). The SAM and recognition layer impedances change upon binding of the antigen and this change can be seen as a phase shift in the low frequency range. For simplicity, instead of fitting the impedance spectrum, a single point in the

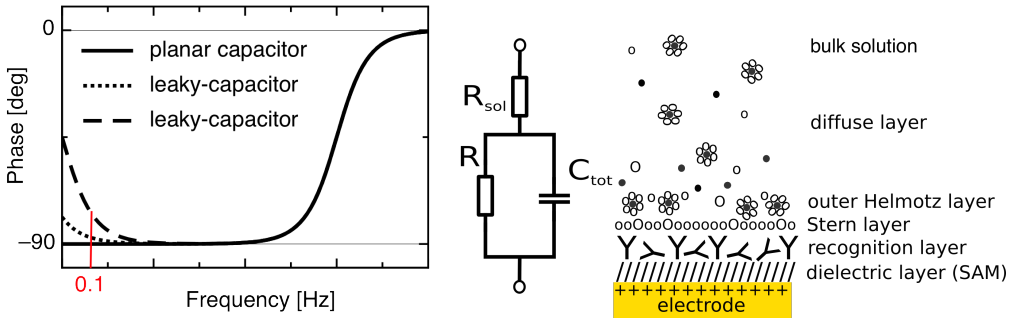

Figure 5.1: On the left, phase of the impedance for a planar capacitor (−), and leaky capacitors. The leaky-capacitor circuit model is a capacitor with a parallel resistor, the phase at low frequency for such circuit deviates from -90°. On the right, sketch of modified electrode with SAM and recognition layer and the electrical double layer.

low frequency range was chosen as the quantity to represent the phase shift at low frequency. The phase at 0.1 Hz, $\varphi_{0.1}$, was extracted from the EIS spectra and used as the sensor output. The magnitude and direction of the shift change with the initial condition of the electrode.

Rod electrodes were measured in low molarity phosphate buffer with a DC bias of 0.215 V, against Ag/AgCl reference electrode; in this case the starting phase at 0.1 Hz is $\varphi_{0.1} = -75°$, instead evaporated gold on Si/SiO_2 templates electrodes measured in serum with no DC bias showed initial phase $\varphi_{0.1} = -88°$. The different initial conditions of the SAM/antibody layer reflects the different change of phase of the impedance.

The impedance of the rod electrodes, which start from a relative high phase, can not be modelled by a single total capacitance. The initial rise of the phase towards 0° at low frequency, in the EIS spectra, can be modelled by adding a leaky path in parallel to the SAM/antibody capacitor (figure 5.1).

The initial leakiness can be attributed for the most part to the DC bias applied.[119] In fact, it has been shown by Boubour et. al that pinholes can be induced in a compact monolayer by applying DC biases during non faradaic EIS measurements; for these monolayers the phase of the impedance, at low frequency, would increase together with the DC bias applied in a comparable way with the results found in this study.[119] We think that the DC bias induces defects in the layer reflected in a rise in the phase. When the antigen binds to the antibody a shift of the phase at low frequency towards −90°, of the EIS spectra is observed. This phase shift in the equivalent circuit model can be modelled by an increase in the leakage resistor (figure 5.4). We speculate that the phase change is due to the rearrangement of the layer surrounding the antigen binding site which induce the change in impedance and phase.

By looking at the phase shift at 0.1 Hz a linear relationship between $\varphi_{0.1}$ and the logarithm of the concentration of hCG was found between 2.6×10^{-17} M and 2.6×10^{-13} M with a sensitivity of 0.4°/decade.

For the evaporated gold electrodes the initial phase of the sensors measured in full serum is on average equal to -88°, at 0.1 Hz. The difference in initial phase can be attributed to both: the absence of DC bias and the presence of high concentration of proteins in solution which can adsorb to the electrode and hinder, or slow down, the kinetic of the access of ions to the electrode surface. The average phase for this sensors in phosphate buffer at 0 V DC bias is in fact -81°, which suggest that the proteins and charge present in the horse serum influence the capacitance.

The binding of the antigen induces an increase in $\varphi_{0.1}$. We hypothesise that, prior to the exposure to the antigen, the electrode surface partially adsorbs the serum proteins impeding the access of ions to the electrode surface. When the antigen binds to the antibodies the non-specifically adsorbed proteins are displaced and the leakiness of the system increases, thus the increase in phase.

The evaporated gold sensors showed a higher detection limit, namely 2.6×10^{-14} M, which can be explained by the fact that the antigen has to compete with the serum proteins that are previously adsorbed to the surface. The sensor showed a linear range over 5 decades and the saturation limit was not yet reached. The sensitivity reported is slightly higher, namely 0.6°/decade.

5.2 Results

5.2.1 Rod electrodes, preliminary investigations

Initially, gold rod electrodes were used as test system to evaluate the possibility of fabricating label-free impedance immunosensors. The rod electrodes offer a standard well studied system that helps estimate the challenges of the task and determine preliminary conditions for the fabrication of such sensors.

Measuring the phase of the impedance, rather than a quantity that is intrinsically related to the surface area of the device such as the magnitude of the impedance, the charge transfer resistance, or the capacitance of the layer, has the advantage of not scaling with the surface area. Therefore, as long as it is possible to measure the current at the working electrode the measured signal will not decrease with the sensor surface size. Moreover, since the measured signal is independent of the size of the electrode, the signal-to-noise ratio does not scale with the size of the electrode itself. This is a highly desirable characteristic for a biosensor because it gives the sensor the potential

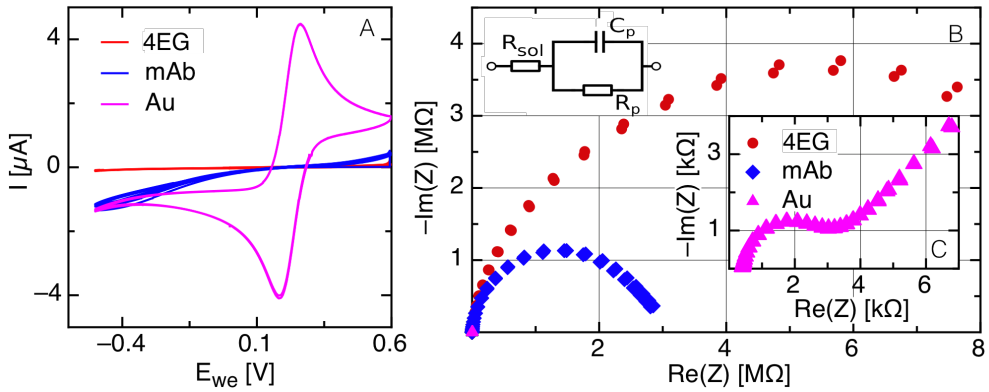

Figure 5.2: A) cyclic voltammogram after assembly of 4EG SAM (red) on a gold rod electrode (0.79 mm^2), after antibodies (mAb) immobilisation (blue) and of clean gold. B) Nyquist plot for the same electrode acquired by means of EIS for frequencies between 100 kHz and 50 mHz for SAM (•) and mAb B(◆) functionalised electrodes. Equivalent circuit valid in first approximation for coated electrodes only. C) EIS from 100 kHz to 1 Hz for clean gold (▲) electrode. All measurements were carried out in phosphate buffer 100mM and ferri-ferrocyanide redox probes 2 mM.

of miniaturisation and therefore multiplexing.

As described in section 3.4.1 mechanically and electrochemically cleaned rod electrodes were functionalised with a 4EG monolayer. EIS and CV scans were performed as described in section 3.4.1 for SAM coated electrodes before and after functionalisation with antibodies as well as after desorption of the SAM-mAb layer.

The CV and EIS scans before and after desorption of the SAM and SAM-Ab layer were compared to evaluate the quality of the blocking layer, see figure 5.2. As discussed in section 2.1.2 SAM functionalised electrodes are expected to hinder the electron current, otherwise exchanged, between the redox probes present in solution and the electrode surface. Therefore absence of redox current peaks is expected for SAM coated electrodes.

Typical CV scans for bare gold, SAM functionalised and immobilised antibodies are shown in figure 5.2. No reduction and oxidation peaks were observed for SAM coated electrodes, both before and after functionalisation with antibodies which indicates blocking of the exchange of electrons between the redox probes and the electrode surface.

To compare the bare gold surface with the SAM and SAM-mAb layer a CV scan of the clean electrode was performed. The voltammogram showed oxidation and re-

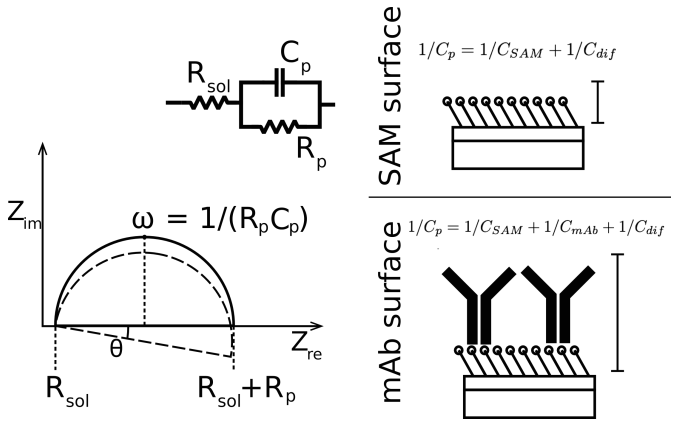

Figure 5.3: Equivalent circuit of a coated electrode and respective Nyquist plot (−) of the impedance. The capacitance C_p represents the coated electrode for either SAM coating or SAM/mAb coating. The deviation from the ideal case (dashed semicircle) is shown.

duction peaks for the redox probes $Fe(CN)_6^{3-/4-}$. The exchanged charge between the electrode and redox probes was estimated by integration of the current/potential peak for potentials between 0 and 0.4 mV, resulting in a reduction peak of -7 ± 1 μC and an oxidation peak of 9.4 ± 0.3 μC with a peak separation of 67 ± 14 mV, indicating that the redox probes were free to exchange electrons with the gold surface, while they were completely blocked from the SAM and antibody layer.

To characterise further the properties of the functionalised electrodes, EIS was performed on the electrodes in presence of redox probes, see figure 5.2. The charge transfer resistance for the bare gold was calculated to be 5 ± 2 Ω/cm^2, which is comparable with the charge transfer resistance of similar systems.[198,199]

For coated electrodes the faradaic processes should be blocked, therefore the Nyquist plot is expected to be a semicircle (figure 5.3), i.e. the linear component of the Nyquist plot at low frequency, due to the diffusion limitations of the faradaic processes, is not expected to be present because the faradaic processes are hindered by the coating layer (see section 2.1.4.3). The semicircular shape of the Nyquist plot observed for EIS measurements in the presence of redox probes (figure 5.2), together with the absence of redox peaks in the voltammogram, for both the SAM coated and mAb B functionalised electrodes, suggests that the faradaic processes, typical of redox processes at low frequencies, are blocked for frequencies down to at least 50 mHz, suggesting that the SAM is a good blocking layer to redox processes (see also section 2.1.4.3).

Keeping this in mind, in first approximation, we can model the coated electrode as a

RC circuit (see figure 5.2 and 5.3). The Nyquist plot for such a circuit is a circumference centred at $R_{sol} + R_p/2$, where R_{sol} is the solution resistance, with a radius equal to $R_p/2$ and the maximum of the circumference is reached for $\omega_{max} = 1/(R_p C_p)$. C_p is the total capacitance as in equation 2.21.

One of the electrodes was functionalised with antibodies and further characterised. As expected the capacitance becomes smaller when the antibodies are immobilised on the SAM coated electrode because the distance between the electrode surface and the Helmholtz plane increases (equation 5.1). The calculated total capacitances for the SAM ($C_{p,SAM}$) and SAM and antibodies ($C_{p,SAM/mAb}$) coated electrodes are $C_{p,SAM} = 153$ nF and $C_{p,SAM/mAb} = 85$ nF. The theoretical value of $C_{p,SAM/mAb}$ calculated assuming that the permittivity, ε_r, and surface area are constant for the SAM and the SAM and antibody layer is equal to 24 nF,[a] which is 3.5 times lower than $C_{p,SAM/mAb}$ estimated by EIS. This indicates that the antibody layer is less thick or less dense than expected.

As discussed, the difference in capacitance is mostly attributed to the difference in thickness of the layers[32,48] but also to their composition, i.e. difference in permittivity, ε_r, of the antibody layer with respect to the SAM. Even if both the SAM and the antibodies are organic molecules, the antibody layer is not as ordered as the SAM, is less dense, and each antibody has a complex solvent shell around it, different from the SAM. The SAM instead is a compact ordered layer where the alkyl chains are attracted together by strong hydrophobic interaction.

Moreover, we note that the electrochemical double layer is a complex structure of solvent and solute molecules adsorbed to the surface and its composition varies with the surface composition and charge[195,196] (see section 2.4). The binding of antibodies changes the charge of the surface. In fact, the antibodies net charge in solution at pH 7.2 is positive, the antibodies pI = 6.4 - 6.8, instead the charge of the acid-capped SAM is negative (surface $pK_a = 4.3 - 5.7$)[175,176]. We expect that the change in surface net charge increases the capacitance of the layer. As it has been shown previously that the capacitance of mercaptohexadecanoic acid changes with solution pH, and surface charge, of up to 40% in low molarity buffer.[196]

Part of the discrepancy could also be attributed to the fact that the model used to fit the Nyquist plot is only a crude approximation. In fact, a circumference fit results in a depressed circumference (figure 5.3), i.e. the diameter of the semi-circumference does not lie on the real axis but is tilted at an angle from the axes, about 16°. Even if part of the capacitance change can be attributed to a change in thickness and density of the layer, in this instance, the thickness is not the only contribution to the change.

In summary, the discrepancy can come from a change in permittivity, a change in the surface charge, and electrochemical double layer composition, and an error due to

[a] The thickness of the SAM and antibody were estimated to be 2.9 nm and 7.2 nm respectively.

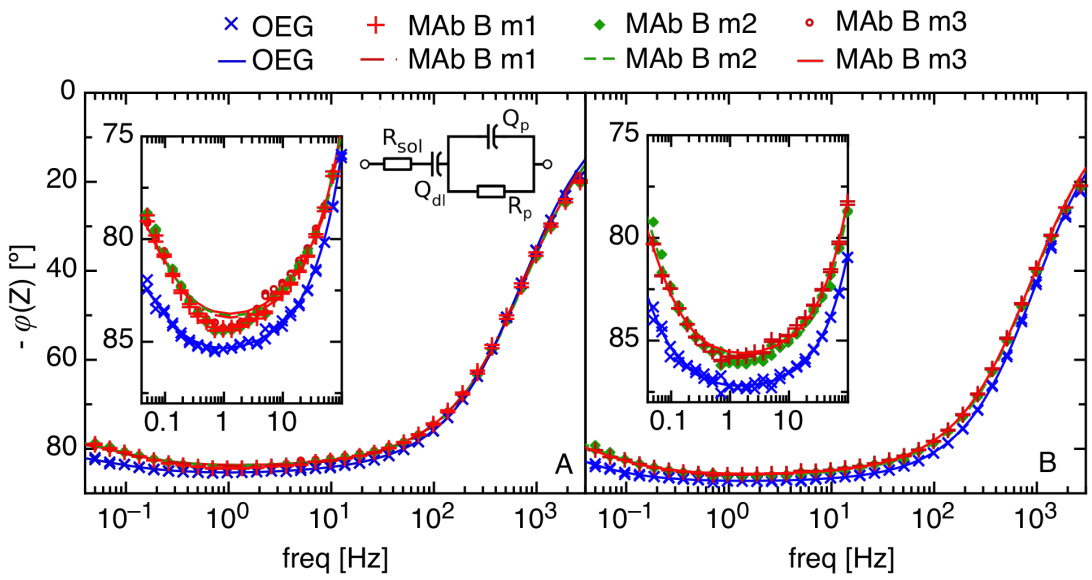

Figure 5.4: Typical phase of the impedance, φ, measured at the working electrodes by means of EIS vs frequency, for rod electrodes coated with 4EG SAM before ($\times$) and after ($+, \blacklozenge, \circ$) immobilisation of antibodies and respective fits (lines). Measurements were performed in phosphate buffer 10 mM, with an excitation amplitude $V_a = 10$ mV and DC bias of 0.215 V vs OCV. Fits are obtained form equivalent circuit shown in the figure where R_{sol} is fixed to 3.8 kΩ and $\alpha_{dl} = 1$, therefore the constant phase component Q_{dl} is equivalent to a capacitor. Q_p and R_p represent the CPE and resistor modelling the SAM or the SAM and antibody layer. Insets show the impedance phase and the fits from 100 Hz to 50 mHz.

the simplistic approximation.

5.2.1.1 Non-faradaic impedance spectroscopy

A separate batch of electrodes were prepared and measured as discussed in section 3.4.1. Measurements in absence of redox probes were carried out by means of EIS. The phase of the impedance, φ, and respective fit to the impedance are plotted in figure 5.4. The equivalent circuit used for fitting φ is shown in the inset in figure 5.4. The equivalent circuit was chosen so that it would approximate the impedance of the electrodes and would minimise the number of circuit elements and free parameters. Further details about the choice of this equivalent circuit are discussed in chapter 6. In chapter 6 it is shown that the change in impedance and phase at low frequency was related to the presence of defects in the SAM-coated electrodes and that the proposed equivalent circuit would approximate the electrode impedance in the presence of such defects.

Regarding the fitting procedure, initially all the parameters are left free to vary. Then R_{sol} was fixed to the average of all fitted values of $R_{sol} = 3.8$ kΩ. This value, as expected, is higher than the R_{sol} estimated in chapter 6, 650 Ω. The change can be attributed to two reasons: first, the molarity of the buffer is 10 times lower; second, the geometry of the system is very different and the counter electrode is about 5 times further away than in the system used in chapter 6.

When left free, α_{dl} is equal to 0.99 ± 0.01 and therefore was fixed to 1, which implies that the constant phase element (CPE), Q_{dl}, is behaving like a capacitor. Focusing on the difference between the SAM layer and the SAM/mAb layer we note that there is an increase of phase, at 0.1 Hz, for SAM/mAb of $2.9^\circ \pm 0.2^\circ$, which corresponds to a change in $\omega_p = (R_p Q_p)^{-1/\alpha}$ equal to 4 ± 1 ms^{-1}, where the impedance of the CPE is defined as in equation 2.15.

The advantage of measuring the phase of the impedance, other than being a quantity that does not depend on the surface area of the electrode, is that it is directly measurable, while parameters like C_p, R_p and ω_p require additional data analysis and rely on a model for fitting process of the EIS and hence introduce errors due to inaccuracy of the model and processing time.

For electrochemical biosensors a few equivalent circuits are used as models of the system but without an unanimous consensus. Moreover, it is important to keep in mind that these circuits are equivalent circuits of the total impedance rather than actual models of the physical properties of electrode surface, i.e. the impedance of the equivalent circuit and the system under study are similar, they have the same electrical behaviour, but they do not necessarily model the physical processes happening at the surface.

Moreover, the phase, here, is extracted from EIS scans but once chosen a fixed frequency to monitor the phase can be measured at a single frequency and monitored in real time, which makes the acquisition and processing of the signal significantly easier and faster.

hCG biosensors in buffer. As a proof of concept gold rod electrodes modified with mAb B were used as biosensors to detect hCG. EIS measurements were carried out in 10 mM phosphate buffer applying a bias of 0.215 mV against the reference electrode. After determination of a baseline the buffer was spiked with hCG at different concentrations; each measurement was taken after 20 minutes incubation in the spiked buffer.

The phase at 0.1 Hz ($\varphi_{0.1}$) was then extracted from the EIS spectra and plotted against concentration, see figure 5.5. To check for and avoid unspecific binding the

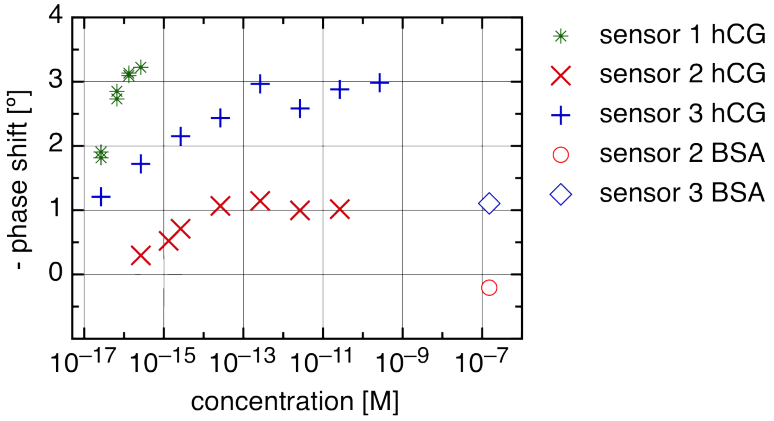

Figure 5.5: Phase shift of rod electrodes to hCG $(\times, +, \star)$ plotted against concentration. The phase shift at 0.1 Hz $\varphi_{0.1}$ was calculated using the phase of the sensor with blank buffer as baseline. The response of the sensor is measured after 20 minutes incubation in either buffer or spiked buffer.

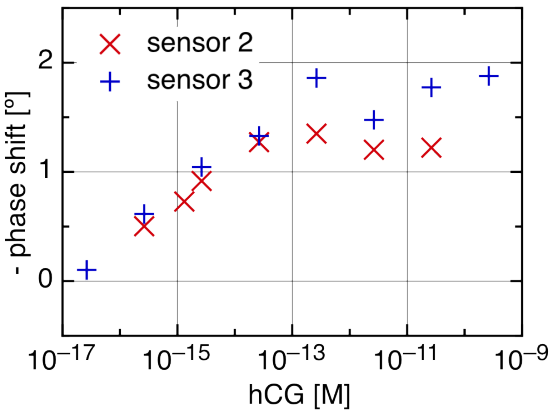

Figure 5.6: Response of rod electrodes to hCG $(\times, +)$ plotted against concentration. The response is estimated as the phase shift at 0.1 Hz from the BSA response. The BSA response is used as calibration method and is determined as the sensor response after 20 minutes of BSA blocking at 0.15 μM in buffer, measured against a baseline determined by blank injections of buffer.

response of the sensor before and after BSA blocking was also taken for two of the sensors.

The response to BSA is significantly smaller than the response to hCG, especially taking into account that the used BSA concentration is 10 orders of magnitude higher than the first measured hCG concentration.

We note that for one of the sensors, the phase shift after BSA blocking is about -1.1°, while for the other sensor is 0.2°. However for both sensors the response to hCG is very similar. Therefore we used the response of the sensor after BSA blocking as the calibration and used this as the new baseline (see figure 5.6). Sensor 1 is omitted because it was not tested for non specific binding to BSA.

We note that after BSA calibration the response of the different sensors at different concentrations is very close to each other. The sensors' response is linear between

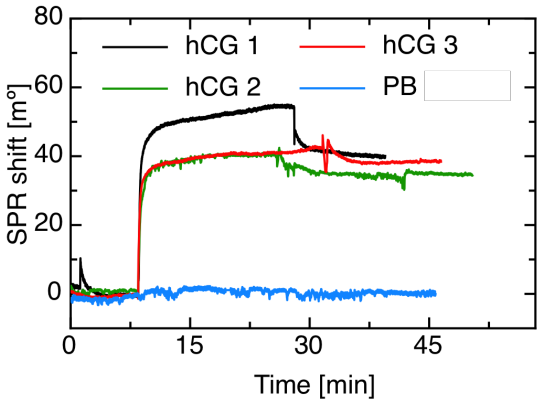

Figure 5.7: Response of mAb-B modified surface measured by means of SPR in 10 mM PB pH 7.2 to hCG 135 nM (hCG 1, 2 and 3) and to PB 10 mM (PB).

2.6×10^{-17} M and 2.6×10^{-14} M with a sensitivity of 0.4° per decade.

As discussed, the detection limit found is two order of magnitude smaller than the capacitive sensor developed by Bergerren et al[48] for hCG measured in similar conditions.

In section 2.1.5 the accuracy and precision of the instrument was discussed. Since only the variation of the system's phase is used as biosensor output, rather than its absolute value, the precision has to be taken into consideration for evaluating the reliability of the measurement. It was found that for a dummy cell with impedance comparable to the system under measurement, the standard deviation of the phase over 100 measurements at 0.1 Hz was 0.1°.

The effect of the low ionic strength buffer conditions on the binding of hCG to mAb-B was controlled by means of SPR. mAb-B were immobilised on OEG modified SPR chips using the same buffer conditions used in the electrochemical experiments. Then the mAb-B were exposed to PB 10 mM, pH 7.2, spiked with hCG 135 nM. We note that the response of the surface in 10 mM PB is comparable with the results found in chapter 4 obtained in PB pH 7.2 100 mM.

5.2.2 Sensing in serum on evaporated gold electrodes

Although rod electrodes are considered a very useful and reliable means of characterising the surface and sensor capabilities they are, however, a solution feasible only in a laboratory environment, due to the mechanical cleaning methods necessary before use and the enormous waste of material should they be used as disposable devices.

As with many other devices the more straight forward way for the fabrication of a device on a large scale is the use of photolithography. Micro-fabricated devices represent a cost effective way of obtaining gold electrodes.

Furthermore measurements in phosphate buffer are a good environment for prelimi-

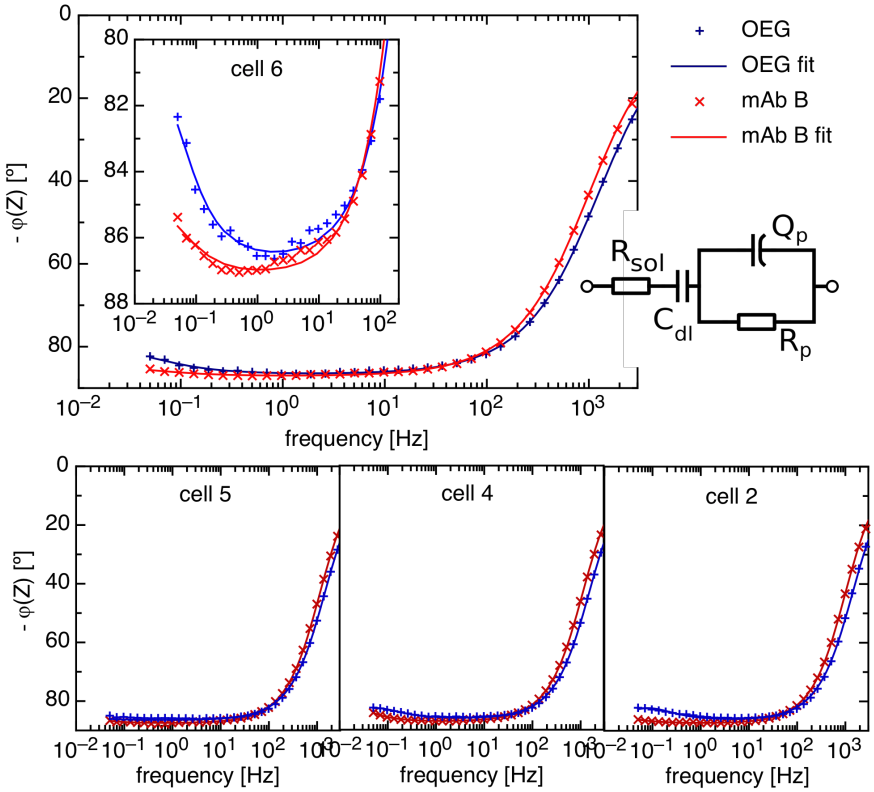

Figure 5.8: EIS spectra examples and fits for OEG monolayer and antibodies immobilised on EEG devices measured in phosphate buffer. The equivalent circuit used to fit the spectra is shown in the inset.

nary investigations. However for the development of devices that are going to be used to detect analytes from serum and blood sample the characterisation of the sensor should be performed in a similar environment, i.e. full serum.

5.2.2.1 Surface characterisation

Initially experiments were carried out on e-beam evaporated gold (EEG) samples, as described in section 3.2.2; the working electrode area (9.13 mm^2) was defined by means of a square-cut rubber gasket. The electrochemical cell was designed to ensure a good static sealing and definition of clear edges such that the whole surface of the electrode is exposed to the bulk solution.

Initially a characterisation of the blocking properties of the SAM, similar to the one carried out for rod electrodes, was performed on SiO_2 devices. Redox precesses were found to be blocked by the SAM, as evidenced by CV scans which showed absence of

redox peaks and EIS measurements performed in presence of redox probes absence of faradaic processes (not shown).

The immobilisation process of the antibodies was characterised in phosphate buffer, see figure 5.8. A decrease in the phase of the impedance at low frequencies is generally observed. On average a shift of phase at 0.1 Hz equal to $\Delta\varphi_{0.1} = 2.4^\circ \pm 0.8^\circ$ was observed across six samples. As discussed in chapter 6 the lowering of the phase is related to a decrease in current leakage of the coating layer. In this case we believe that the antibodies form a layer that further hinders the access to the gold surface from ionic current thus the decrease in phase. Together with the shift in phase, the estimated ω_p varies from 0.09 ± 0.03 s^{-1} to 4 ± 2 ms^{-1}, decreasing 22 times, after the immobilisation of the antibodies. This suggests that the SAM/antibody layer is less leaky than the SAM layer alone, in particular slowing down the kinetics of the current flow between the electrode surface and the buffer solution.

We note that this behaviour is different from the one found for the rod-electrode-based biosensors. However, the sensors are very different in nature, in particular the morphology of the gold surface between the mechanically polished rod electrodes and the thin gold film on EEG electrodes is very different. This is anticipated to lead to significantly different SAMs on the two different surfaces, with different number of defects etc. Furthermore, the measurements on the rod electrodes were carried out at a bias of 0.215 V, while the EIS measurements on the evaporated thin film electrodes were carried out at a zero DC bias. It has been reported that DC bias induces defects in the monolayer[119] further increasing the difference between the two systems. Further comments on the different behaviour of the two systems are found below.

5.2.2.2 Sensor calibration in serum

Subsequently to the characterisation of the antibodies immobilisation, new sensors were made and characterised by means of EIS in horse serum, to test both the selectivity of the sensor for hCG and the behaviour of the sensor for real samples. Measurements of the devices in serum before immobilisation of the antibodies were not taken, since part of the protein in the serum might adsorb to the surface and interfere with the immobilisation of the antibodies.

A calibration curve of the sensor, monitoring the change in phase at 0.1 Hz, $\varphi_{0.1}$, was taken for concentrations of hCG between 26 fM and 0.26 μM. The calibration curve in horse serum is reported in figure 5.9. The phase, $\varphi_{0.1}$, increases linearly with the logarithm of hCG concentration, over 5 decades showing a sensitivity of 0.6 ± 0.1 $^\circ$/decade towards hCG in horse serum. The curve shown is the average over 4 samples.

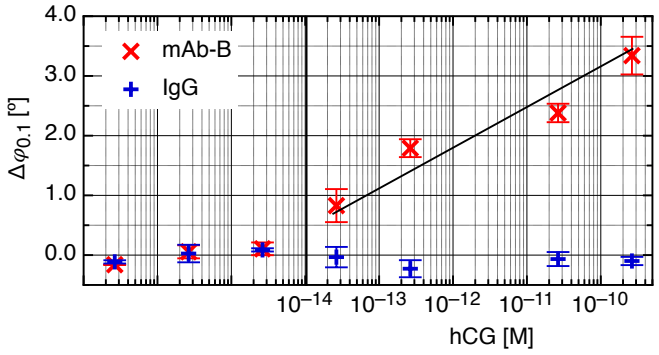

Figure 5.9: Phase shift recorded at 0.1 Hz, measured by means of EIS for EEG samples functionalised with mAb-B (×) and anti mouse IgG (+). On the left, sensor baseline determined by blank serum injections. On the right, sensor response to hCG spiked serum for flat gold sensors. Error bars represent ±SD over four samples for mAb-B and three for IgG. Linear fit (line) of the phase shift vs log[hCG] for hCG response from 26 fM to 0.26 μM $y = (0.6 \pm 0.1)x + (8.5 \pm 0.8)$, r=0.96.

The lowest concentration detected for hCG in serum was 26 fM while in buffer was 2 orders of magnitude lower. This can be explained by the fact that in healthy horse serum there is a total protein concentration estimated to be between 51 and 72 g/L [200] competing for the binding to the surface with hCG to which the surface was exposed to previously. In fact it is not uncommon to see higher detection limits for sensors in serum compared to buffer. In section 4.2.1.1 we showed that presence of BSA in the measured solution can interfere with the binding of hCG with mAb-B modified surface.

The detection limit obtained in serum is similar to the one obtained for the capacitive sensor discussed in the introduction, but the latter was obtained in 10 mM phosphate buffer. [48]

The fact that the sensor shows no response to blank injections of serum, i.e. not spiked with hCG, helps in correlating the response of the sensor to the concentration of hCG when the sensor surface is exposed to spiked buffer. Furthermore, the third concentration tested was 100 times more concentrated than the second concentration tested, instead of 10 times, to create a discontinuity between time and concentration as well as injection number and concentration. Taking these controls into account, it can be concluded that the phase shift is not related to a time drift.

Furthermore, as control, EEG samples have been modified with an antibody non-specific to hCG, namely an anti-mouse IgG, to verify that the response to the hCG spiked buffer is specific to the mAb-B to hCG interaction. The average phase shift for three samples is shown in figure 5.9.

In a purely capacitive model the binding event should lead to an increase of the

thickness of the recognition layer and hence lead to a decrease in its total capacitance, assuming the permittivity constant to remain unchanged.[21] However the k_d for the antibodies used in this study was estimated to be equal to 13 $\pm$ 2 nM by means of SPR. Assuming the Langmuir binding model to be valid for concentrations five orders of magnitude lower than k_d, at concentrations of 26 fM the fraction, ϑ, of antibodies binding sites occupied by hCG, $\vartheta = [\text{hCG}]/(k_d + [\text{hCG}])$, is equal to 2×10^{-6} of the total.

Keeping this in mind it is difficult to believe that the binding event would generate a layer with enough change in thickness to result in a measurable change in total capacitance. Therefore we analysed the impedance spectra by means of different equivalent circuits to understand how each component contribution varies and what this can possibly tell us about the binding event.

We note that factors such time drift, solution injection or solution exchange might alter the equilibrium of the sensor and hence distort the results. In order to avoid such influences, in this study only devices where a stable baseline was achieved in the first four blank measurements, over the course of two hours, were used as sensors. Unfortunately it has to be noted that only 25% of the samples prepared would reach stability in this time window. Due to the high rate of rejection other ways of fabricating the sensors are explored later in the thesis.

Equivalent circuits. First, the equivalent circuit used to model the system in buffer was used successfully to fit the impedance in serum for antibody functionalised electrodes (see figure 5.10 B). However, when the sensor is exposed to hCG spiked serum, the phase spectra show a different behaviour, i.e. a peak in the phase appears around 2 to 3 Hz. This feature can not be successfully fitted with the same circuit because this would require a further time constant. A possible explanation for the appearance of this peak is discussed later in this section.

As discussed in section 2.1.4.1, an equivalent circuit is an abstract model of the electrode/solution interface that simply has the same impedance behaviour of the interface in frequency. If a behaviour of the electrode or of any molecule bound to it becomes relevant the behaviour of the electrode/solution interface will change therefore a new representation of the system might be needed so that the newly emerged behaviour can be accounted for.

Therefore, other equivalent circuits were tested. At first the classic Randles circuit, as shown in figure 5.2, was considered. Even when a CPE was used instead of the total capacitance, the generated fits diverge from the analysed data, especially for the data collected after incubation of the antigen.

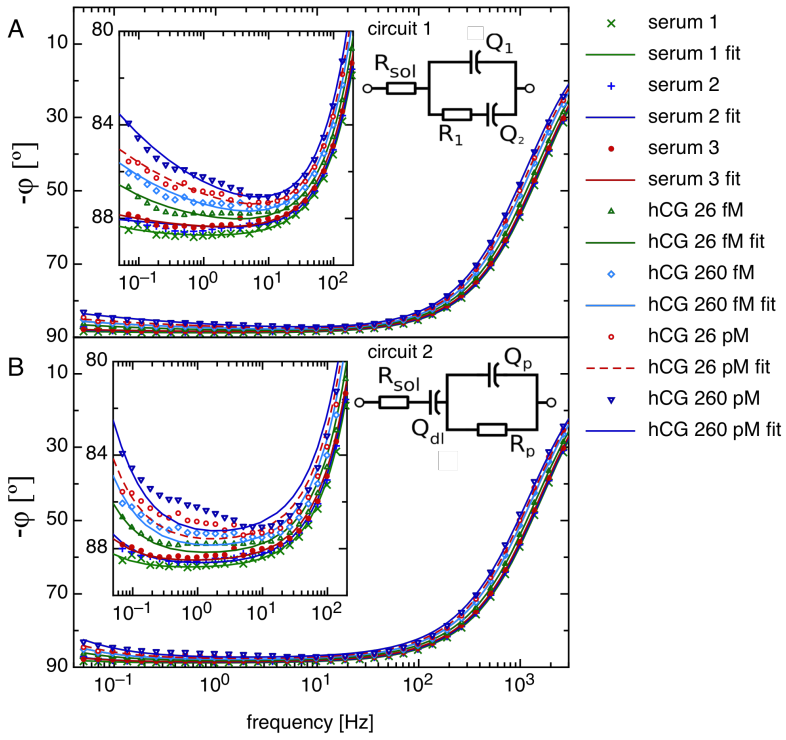

Figure 5.10: Comparison between fits using different equivalent circuits, as shown in the insets, for the same set of measurements, used as an example. The Impedance phase, φ, spectra was measured by means of EIS in serum. Blank serum measures were obtained injecting fresh serum and incubating for 20 minutes, on a modified OEG gold electrode after immobilisation of antibodies. The phase spectra for spiked serum were obtained in the same way.

Moreover the Randles equivalent circuit is introduced for the modelling of redox processes, which are absent in this case. We note that such circuits have to be used with caution, as the extracted fitted parameters might be misleading and lead to unfounded conclusions.

A second equivalent circuit, consisting of a modified Randles circuit, where the total capacitance is substituted by a CPE and in series to the resistor R_p a CPE is added (figure 5.10 A). The modified Randles circuit does provide a better fit but the value of the resistor R_1 is either a few MΩ or lower than a few nΩ, i.e. is approaching zero, de facto approximating a wire and leaving the two pseudo capacitance in parallel. Although the impedance fitted with this model is closer to the observed data the peak feature in the phase it can not be fitted by such circuit because as it only has two time constants. Moreover this model behaves very differently for different samples so it was not used.

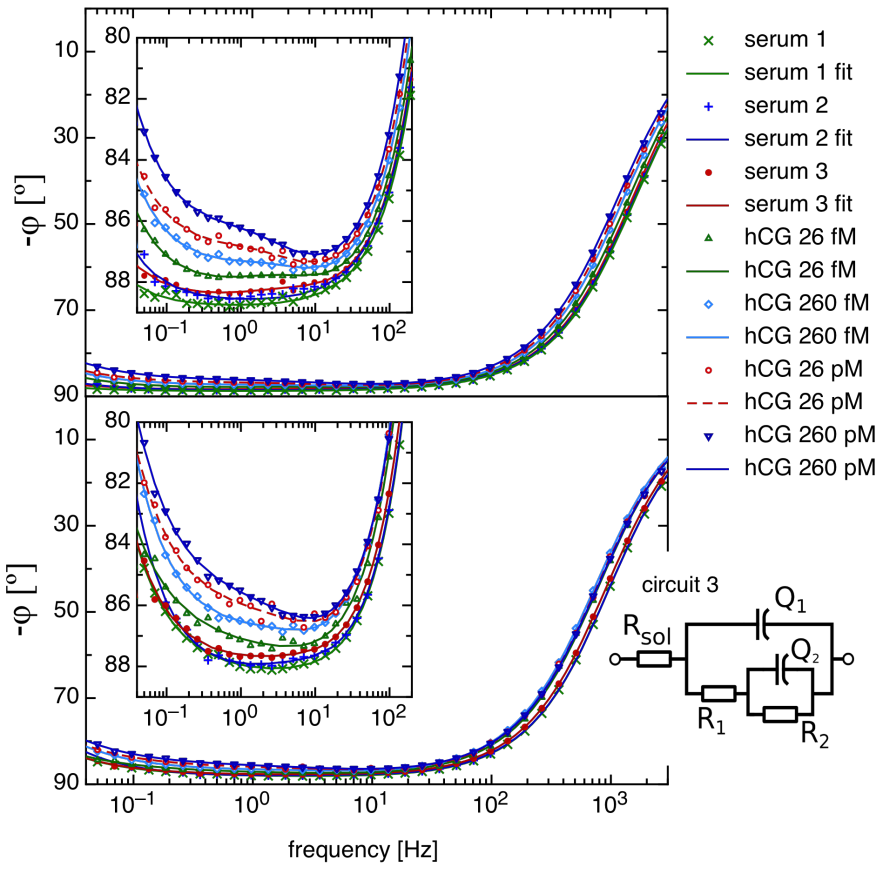

Figure 5.11: Examples of EIS spectra for two different cells and respective fits for antibody layer immobilised on EEG devices measured in blank serum (serum 1, 2 and 3) and after incubation in spiked serum at different hCG concentrations, varying between 24 fM and 240 pM. The fits were carried out using the model shown in the figure inset, where R_{sol} and α_1 are fixed to 804 Ω and 0.98 respectively.

A third equivalent circuit, introduced by others[126,201] to model potential induced pin holes in SAM coated electrodes was found to generate the best fits, i.e. the fits had lower χ^2 and follow the features of the phase spectra, see figure 5.11 (circuit 3).

There are three main differences between the circuits in figure 5.10 and 5.11. First, circuit 3 has one more circuit component, R_2, which increases the number of free parameters by one. Second, there is a direct resistive path from the surface to the solution, R_{sol}-R_1-R_2, that models pinholes through the whole layer, allowing a direct access to electrons or ions to reach the surface.[201] Last, the parallel arrangement of Q_2 and R_2 introduces a third time constant hence it can fit the bump shaped peak in the phase at $\approx$ 2 Hz.

A similar peak, centred at 8 Hz, was observed for mercapto-undecanoic acid (MUA) SAM when EIS scans were performed in 50 mM NaF, pH 8.5, with a DC bias of −0.1 to −0.3 V vs saturated calomel electrode.[197] In this study this behaviour was attributed to protonation and deprotonation of the acid of the SAM functional group when subject to the AC voltage at frequencies around 8 Hz while it was absent at pH 7.5 and or 0 V DC bias. It is emphasised in the paper that this impedance was considered due to changes in the degree of ionisation at the plane of dissociation and not due to a faradaic reactions.[197]

In a similar way we can interpret the peak at 2 Hz, increasing with the antigen concentration in solution and binding to the surface, as a change in surface charge happening around the hCG binding site where either the hCG acts as dipole or the antigen binding induce a change in the surrounding area of the surface charge that make this effect to be noticeable. Further investigations of this phenomenon are needed to either confirm it or exclude it.

The antibody layer can be modelled with all three equivalent circuits, see figures 5.10 and 5.11. This indicates that circuit 3, which has 5 components, is over defined in this case. In particular the time constant associated with the peak is redundant. In fact while fitting the data, the parameters associated with Q_2 and R_2 would randomly approach zero or infinity. The same can not be said about the spectra recorded after the binding of hCG, moreover the difference between the two equivalent circuits, and the importance of ω_2, accentuates with the increased concentration of hCG in the spiked serum.

It was found that both Q_1 and Q_2 (circuit 3) increase with the concentration of hCG, thus Z_{Q1} and Z_{Q2} decrease. However due to the redundancy of the 5 components for fitting the non-spiked serum samples, a baseline is difficult to obtain for the blank measurements which would make the use of this circuit for the calibration of a sensor difficult. Instead, since the phase is a measured quantity it does not have the same problem in the determination of its value, making this parameter more suitable for sensing purposes. However, to compare the change in phase and the equivalent circuit, the circuit components Q_1, Q_2, R_1 and R_2 were plotted vs $\varphi_{0.1}$, see figure 5.12.

We note that the phase shift with increasing hCG concentration is opposite to the phase shift observed for the rod electrode sensors in buffer. The binding of hCG induces an increase in phase. As discussed, an increase in phase is associated with a more conductive/leaky layer. From the analysis of the fitted parameters the phase change is a contribution of an increase in both CPE's pseudo capacitance and a decrease of the

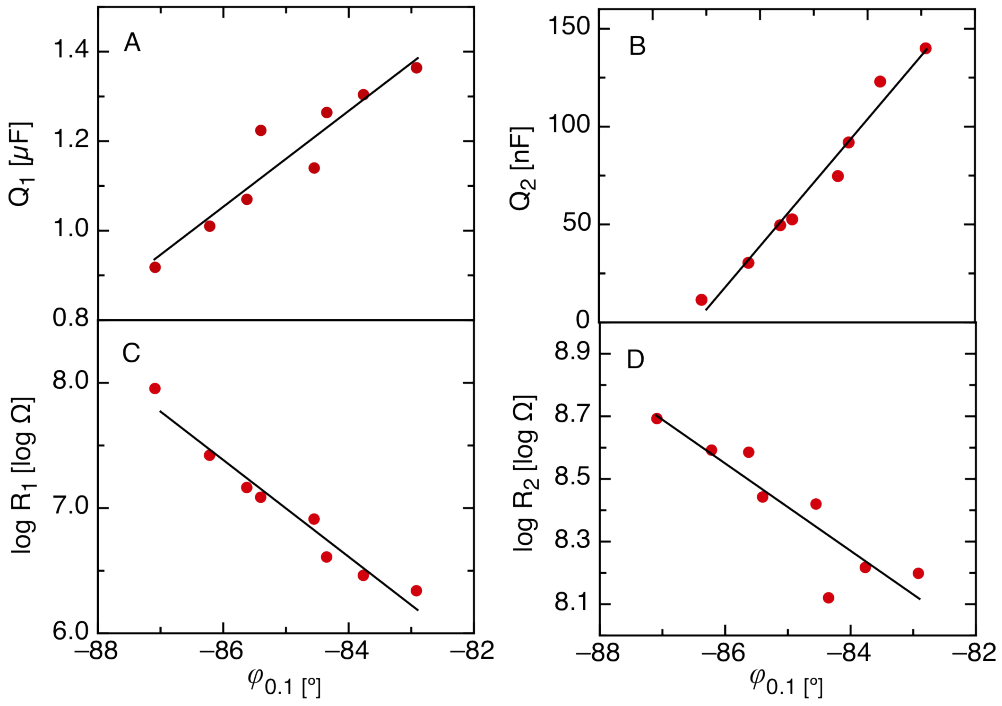

Figure 5.12: Plots of Q_1 (A) and Q_2 (B) estimated by fitting of EIS spectra for sensors in serum plotted against the phase at 0.1 Hz and respective linear fits. The fits are $Q_1 = (115 \pm 8)nF/^\circ + (10.9 \pm 0.6)\mu F$ with a correlation coefficient $r = 0.97$ and $Q_2 = 3(2 \pm 2)nF/^\circ + (2.8 \pm 0.2)\mu F$, $r = 0.98$. At the bottom, plots of $\log R_1$ (C) and $\log R_2$ (D) against $\varphi_{0.1}$ and linear fits. The fits have correlation coefficient of 0.97 and 0.89.

resistivity of the SAM/antibody/hCG layer, R_1 and R_2, see figure 5.12 C and D. We speculate that the phase change is due to the rearrangement of the layer surrounding the antigen binding site which induce a decrease in impedance.

As discussed the capacitive model in which the binding event increases the thickness of the layer, and therefore diminish the total capacitance, might not be valid at the concentration analysed, so we speculate that other factors come into play.

Two factors act at two different scales. On one side, the variation in thickness is a global change of the layer and to be relevant has to involve a big portion of the sensor surface, which is unlikely to happen at these concentrations. On the other side, the rearrangement of the recognition layer and electrochemical double layer due to the presence of the antigen and the possible introduction of dipoles effects is a local event that involves the binding site. The consequences of this modification would impact on the surrounding area due to the density of the SAM and antibody layers. This phenomena increases the conductivity of the layer, more current 'leaks' from solution

to the electrode are formed, thus they can be interpreted as introduction of defects in the SAM/antibody layer.

The opening of pinholes model is also reflected in the decreased resistivity of the system with increasing phase, $\varphi_{0.1}$, and increasing concentration of hCG. The parameters R_1 and R_2 decrease exponentially with the phase; in figure 5.12 C and D the logarithm of R_1 and R_2 vs phase, and a linear fit, are represented for clarity. The accentuation of defects can explain the decrease in resistivity of the layer, the nature of the increased capacitance, however, would remain unexplained.

In conclusion we showed that the phase at a single point in frequency, in particular at low frequencies, is related to the changes that happens to the whole system (see figure 5.12). These changes can be understood by modelling the system with multi component equivalent circuits but for the purpose of bio-sensing this would be an over complication and can lead to the introduction of errors due to inaccuracies in the model and hence large uncertainties in the fitting procedure. The monitoring of $\varphi_{0.1}$ results in a convenient way of monitoring the whole impedance change with no post processing required.

We have established a linear relationship between the phase shift, $\Delta\varphi_{0.1}$ and the logarithm of hCG concentration over five decades in serum with a lowest detected concentration of 26 fM and that the phase shift is due to an overall decrease in impedance due to local rearrangement of the recognition layer and change in surface charge.

5.2.3 Towards electrode arrays

With the aim of developing a platform for multiplexed biosensor arrays, i.e. devices containing multiple electrodes functionalised with different antibodies preliminary studies were carried out. Two aspects were investigated, the reproducibility of the response of the sensor between electrodes, and the possibility of miniaturisation of the electrodes.

At first 8-electrode arrays of gold electrodes, Ti (15 nm) / Au (80 nm), were made by means of double layer lithography on glass slides in an e-beam evaporator. The eight 0.5 mm radius electrodes are arranged, as shown in figure 5.13, in a square pattern. The electrodes were characterised by means of EIS after adsorption of the SAM, the antibody layer and exposure to hCG at 2.6 nM in phosphate buffer.

As a measure of intra-device reproducibility, the spread of values found for electrodes on the same chip, measured as standard deviation (SD), therefore undergone the same process, was used.

Within the same chip the phase spectra for different SAM coated electrodes is sim-

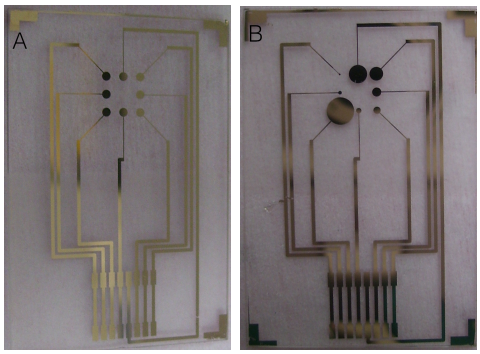

Figure 5.13: Micro fabricated electrode arrays fabricated by means of photolithography (Ti/Au). A) 1 mm electrodes, B) multi size electrode array, the radius of the smallest and largest electrodes are 0.1 and 1.5 mm respectively.

ilar, and the standard deviation on the phase at 0.1 Hz in fact is of 0.16°. This spread is comparable with noise found for measurements on the same electrode.

However, on occasions it was observed that if the electrode did not present a well blocked layer, for example $\varphi_{0.1} = -74°$ then the spread would be significantly higher, in fact the SD for a typical electrode with such characteristics was around 3.5°. It was noted later that the devices that presented higher phase at 0.1 Hz and higher spread were devices that were incubated for 16 hours instead of 40 hours.

Although many studies report SAM incubation times of 16 hours or less, we have observed higher reproducibility of the SAM phase, between different samples and for electrodes in the same sample, for SAMs incubated for 40 hours or longer.

This can be due to the fact that longer incubation times lead to better blocking of the electrode, thus the phase reaches values closer to -90°. Moreover in a direct comparison of two 8 electrodes devices, prepared at the same time, where one chip was incubated for 16 hours and the other for 40 hours in MUD, was carried out. Voltammograms between -0.2 V and 0.5 V, in phosphate buffer 100 mM and redox probes 2 mM, were performed. The 16 hour chip electrodes show a small redox activity, i.e. the CV scans are not completely flat at the redox probes potentials even if no defined redox peaks are present. On the contrary, the voltammogram of the electrodes incubated for 40 hours shows no redox activity. An example of the two voltammograms are shown in figure 5.14.

The phase of different size electrodes on the same chip was also compared. On the same chip, the phase of eight electrodes with different diameter were compared. The radius of the electrodes varied from 100 μm to 1.5 mm, however as expected the phase spectra for frequencies lower than 10 Hz were very similar. In fact the phase at 0.1 Hz in phosphate buffer was $\varphi_{0.1} = -87.5° \pm 0.5°$, except for the smallest electrode

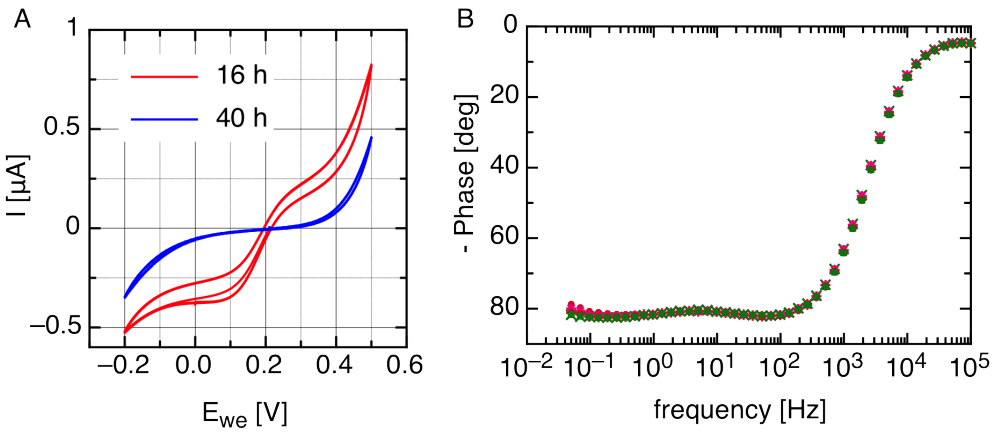

Figure 5.14: A) Voltammogram of 0.5 mm microfabricated electrodes after immobilisation of mercaptoundecanol SAM for 16 (red line) and 40 (blue line) hours measured in phosphate buffer 100 mM with 2 mM redox probes. B) Impedance phase spectra after incubation of hCG, of eight electrodes on one chip. The spectra with the highest phase correspond to the electrodes measured just after hCG injection.

which was $\varphi_{0.1} = -78.3°$. CV scans were performed in phosphate buffer 100 mM and redox probes 2 mM and no redox activity, and no peaks were observed for all electrodes.

On devices with 8 electrodes with radius equal to 0.5 mm the reproducibility of antibodies immobilisation was tested. All electrodes on the device were processed in the same way. After immobilisation of OEG SAMs the carboxylic acid was modified via NHS-EDC chemistry, as explained in section 3.4.2, and mAb B to hCG were immobilised on the electrode. The phase at 0.1 Hz for all electrodes was then analysed. A slightly higher spread of the phase is observed after immobilisation of the antibodies in respect to a spread observed for the SAM only, in fact the SD found was equal to 0.54° (figure 5.14 B).

As a preliminary test on the reproducibility of the response, the modified electrodes were challenged with hCG, due to the great number of electrodes to be analysed at the same time only one concentration of hCG, 2.6 nM, was measured. Impedance spectroscopy of the electrodes after immobilisation of hCG was carried out and the phase at 0.1 Hz was extracted from the spectra. From the measurements carried out in phosphate buffer on rod electrodes, we expect a shift of about −2°, see figure 5.6, after 20 minutes incubation.

Two electrodes were measured just after injection of hCG and do not show a significant shift in phase, i.e. $\Delta\varphi_{0.1} = 0.2 \pm 0.3$, however the electrodes measured after 20 minutes incubation in hCG spiked buffer show a phase shift of $-2.7 \pm 0.7°$. We note

that the spread in the sensor response to 2.6 nM hCG has a similar spread to the spread of the antibody modified electrodes $\varphi_{0.1}$ which was 0.5°.

In the perspective of using this method for biosensor arrays further testing is required. In fact if the same noise in the detection of hCG should be found for smaller concentrations it might interfere with an accurate reading of the sensor response.

We note however that for rod electrodes the noise of the sensor response at concentrations higher than 0.2 nM, i.e. at concentrations for which the sensor response saturates in buffer, was higher than the noise obtained in the linear range of the calibration curve (fig. 5.6). Furthermore, testing of reproducibility of the sensor response in serum on micro-fabricated electrode will be necessary in due course.

5.3 Conclusions

Electrochemical impedance spectroscopy (EIS) was used for the characterisation of label free impedance biosensors with sensitivity for the model target human chorionic gonadotropin (hCG). The assembly of ethylene-glycol terminated monolayer has been studied on gold electrodes. The monolayer has been used to immobilise a monoclonal anti-hCG antibody (mAb B) on the surface. The surface was then characterised by EIS and used for the detection of the antigen.

Two different kinds of electrodes were tested. Rod electrodes were used for the characterisation of the hCG biosensor in buffer. The phase shift at a fixed frequency of 100 mHz was employed as the measure for the amount of binding observed and the sensor was calibrated for a range of different hCG concentrations in solution. The phase shift vs the logarithm of the concentration was found to show a linear relationship between 2.6×10^{-17} M and 2.6×10^{-13} M, with a sensitivity of 0.4 degree per decade. A negative control experiment using a much higher concentration of bovine serum albumin (BSA), 1.5×10^{-7} M, led to a phase shift comparable to a hCG concentration of ten orders of magnitude lower, and it was concluded that the observed signal was due only to specific binding of the antigen to the antibody (mAb B).

Considering the sensor showed good resistance to non specific binding the same SAM and mAb B system was tested on evaporated gold electrodes for detection of hCG in serum. A linear relationship of the phase shift vs the logarithm of hCG concentration was found between 2.6×10^{-14} M and 2.6×10^{-10} M with a sensitivity of 0.6 degree per decade. The sensor did not show response to consecutive injections of serum therefore it was concluded that the phase shift was related to the concentration of hCG in the spiked serum. The sensor response shows good detection limit especially considering

that for diagnostics and therapeutic monitoring purposes the hCG levels of interest in serum are in a range from 3×10^{-12} to 3×10^{-7} M[202].

The low limits of detection found were motivation for deeper investigation of the system. Both the electrodes were characterised by EIS and equivalent circuits were used to investigate the properties of the biosensor. Linear relationships were found between the phase shift and the elements, resistors and constant phase elements, of the equivalent circuit, validating the significance of the phase shift, at a single point in frequency, as a directly measurable quantity that represents the variation of the impedance of the electrode.

Furthermore preliminary investigations were made towards micro-fabricated electrode arrays showing reproducibility of the sensor characteristics and sensor response to the target in buffer solution. Further measurements in serum will be required to investigate the sensor reproducibility in clinical samples.

This page would be intentionally left blank if we would not wish to inform about that.

Chapter 6

Mixed self assembled monolayers as coating layers for biosensors

Introduction

Self-assembled monolayers (SAMs) have been studied for many decades.[72,82] SAMs are a versatile means for the modification of physical and chemical properties of surfaces, including their hydrophobicity,[101,203] biocompatibility, non-fouling properties,[101,102,125,204] or the ability to bind covalently to biomolecules.[110,204,205] They have been employed to modify a variety of surfaces such as silicon oxide,[82] gold[151,203] and other metals.[72,106]

Thiol-gold chemistry, in particular in conjunction with alkyl chains, provides an optimal combination of ease of SAM preparation and characterisation,[72,203] structural order and versatility of modification of the functional group.[72] Therefore, they have been extensively studied in the past and used for a large variety of applications.[72,125]

The formation of SAMs has been extensively characterised and reviewed previously.[72,125,206] Chain to chain interactions such as Van Der Waals and dipole-dipole forces drive the packing of the monolayer. In the case of the formation of SAMs from alkyl chains, the longer the chain the faster the formation will be.[72]

A variety of intrinsic and extrinsic causes may generate defects in the monolayer such as defects at the SAM crystal edge, defects at gold grain boundaries or step edges, surface impurities or vacancy islands.[125]

A very common application is the use of SAMs at the interface between the solid state device and the biological molecules in biosensors, where the SAM serves as the non-fouling layer to reduce unwanted, non-specific binding of biological molecules such as proteins.[102,104] Furthermore, the SAM provides the chemical functionality to bind specific receptor molecules[204] for biological detection.[18]

Oligo- and poly-ethylene glycol chains (oligo-EG, poly-EG) have been used extensively to reduce the non-specific protein absorption[101,102] and improve biocompatibility[204] of SAM modified surfaces[104,106] and often oligoEG-terminated alkyl thiols are used to form such SAMs.[104,106,110,204] Oligo-EG alkyl thiols have been reported to form a monolayer constituted by a layer of all-trans extended alkyls tilted at a 30 degree angle. While the ethylene glycol groups form either a liquid-like amorphous phase or a semi-crystalline layer consisting of oligo-EG molecules extending perpendicular to the gold surface.[106]

As mentioned, COOH-terminated SAMs can be used to bind proteins, e.g. antibodies, on the surface of a biosensor by means of NHS-EDC chemistry. However, COOH-terminated oligo-EG groups are bulky compared to the alkyl chains and hence sterically hinder the formation of a densely-packed, well-ordered SAM,[104,106,153] leading to presence of defects such as pinholes and lower than expected thickness.[104,106] In applications such as capacitive biosensors, where the receptor molecules are usually covalently bound to the functional group of the SAM, a well-ordered and highly-packed SAM with a high dielectric constant is required. The receptors attached to the SAM and subsequently the bound ligand will change the capacitance associated with the Stern layer. It is this effect that forms the basis of the biosensor.[21]

As discussed in section 2.1.3, when a potential is applied to the electrode, a charge will accumulate at its surface and an equal and opposite charge will be induced in the solution forming an electrical double layer. The capacitance of a SAM coated electrode at the electrode/solution interface can be described by a series of three capacitors[21] according to equation 2.21.

The presence of defects in the monolayer decreases the insulation of the SAM and are often modelled by a leakage resistor, R_{leak}, in parallel with the capacitance. The presence of this resistive component in the surface impedance can reduce the sensitivity of the measured impedance to the change in capacitance.[21,24]

It has been suggested that small molecules can be added as spacers to reduce steric hindrance caused by the bulky functional groups which interfere with the formation of the SAM[102,110] whilst retaining the original properties. It has been reported that oligo-EG-terminated SAMs retain their non-fouling properties even when they are diluted up to 40% by alkanethiols.[100]

Here, we investigate the quality and dielectric properties of a range of OEG terminated SAMs with varying degrees of alkenthiols spacers, with the aim to reduce the presence of defects and therefore enhance their dielectric properties in order for such SAMs to be used in label free electrochemical biosensors.

Owing to their excellent non-fouling properties and the extensive use of oligo-EG-alkanethiols for biosensing applications, a monolayer formed by a carboxy-terminated-$(EG)_6$ alkane (OEG) chains has been chosen for this study (figure 3.1). The monolayer was characterised by means of electrochemistry, AFM, XPS, ellipsometry and contact angle measurements.

The presence of defects such as pin-holes was clearly evident throughout electrochemical impedance spectroscopy (EIS) measurements, where the phase of the impedance was found to increase considerably at low frequencies as expected for loosely-packed monolayers.[119,201]

Improved dielectric properties of the monolayers were achieved by mixing the OEG terminated monolayer with different percentages of mercapto-undecanol (MUD) molecules.

6.1 Results and discussion

All the samples were prepared as described in sections 3.2.1, 3.2.2 and 3.5.

6.1.1 Electrochemical impedance spectroscopy

EIS is a very sensitive tool for the investigation of the dielectric properties of SAMs and can hence reveal valuable information on the presence of defects such as pin holes. A range of mixed SAMs with MUD:OEG ratios of 0.05% to 5% as well as 100% MUD and OEG were investigated and the corresponding EIS measurements are shown in figure 6.1.

Various possible equivalent circuits have been discussed in section 2.1.4. From a qualitative analysis of the impedance and considerations about the formations of SAMs an appropriate equivalent circuit was chosen as follows.

First we consider that the phase spectra of the OEG and the mixed monolayers show a minimum of -89° at about 1Hz, and the phase increases for lower frequencies (figure 6.1B). Therefore, we conclude that the equivalent circuit should present two time constants and that the capacitive components are non-ideal, i.e. they should be represented by constant phase elements. Moreover we note that the increase in phase is not due to a faradaic current as the measurements were performed in absence of redox probes. Hence, only transient currents can pass across the electrode/solution interface without charge transfer. The use of a charge transfer resistance was deemed not suitable to model this particular situation (see also discussion in section 5.2.2) and the circuit shown in figure 6.2 was used instead to model the impedance data.

The impedance spectra of all SAMs were fitted using this equivalent circuit, and initially all parameters were left free to vary. The parameter α_2 of the constant phase

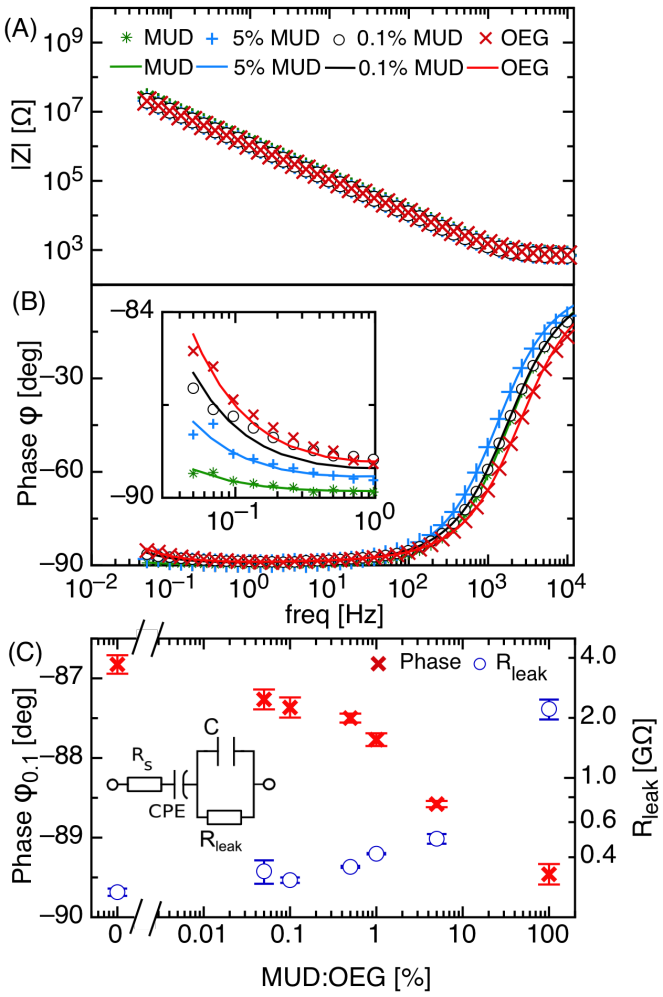

Figure 6.1: Typical magnitude, $|Z|$ (A), and phase, φ (B), of the impedance of the working electrode as a function of frequency measured by EIS and corresponding fits (lines) for MUD ($*$), OEG ($\times$) and the mixed SAMs: 0.1% ($\circ$) and 5% ($+$) MUD in OEG. The inset shows the detailed view at low frequencies. (C) Phase of the impedance at 0.1 Hz, $\varphi_{0.1}$ ($\times$), and SAM resistance, R_{leak} ($\circ$), obtained from the fit to the impedance with the equivalent circuit shown in the inset, both plotted against the molar fraction of MUD to OEG in the solution used for the formation of the SAMs. Standard deviation of the fitted parameter R_{leak} and between different measurements for the phase, are reported as error bars. The electrode area is 36.5 mm^2.

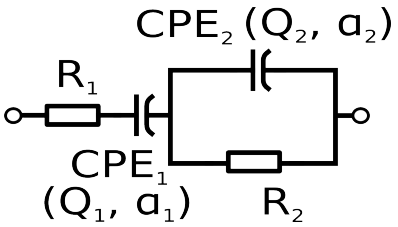

Figure 6.2: Equivalent circuit employed to fit the electrode solution interface.

element CPE_2 consistently reached the limit of 1 for all samples, and hence the CPE was replaced by an ideal capacitor (C). Furthermore, since R_1 is generally associated with the solution resistance[126,128] (R_s) which is governed by the buffer strength and the geometry of the cell, it was fixed for all samples to 647 Ω which corresponds to the average of R_1 of all investigated SAMs.

The remaining circuit elements (CPE_1, CPE_2 and R_2) can be associated with the solution/electrode interface. We note that R_2 and CPE_2 constitute a leaky capacitor, therefore we will refer to these elements as R_{leak} and C. Often leaky capacitors are used for modelling defects in monolayers or insulating coatings.[201]

The quality of the fits to the data depends only weakly on the value of α_1 within a small range and therefore α_1 was fixed to the average of all fitted α_1 ($\alpha_1 = 0.82$) to simplify data interpretation. The final circuit is shown in the inset of figure 6.1 C.

Both R_{leak} and the phase of the impedance at 0.1 Hz ($\varphi_{0.1}$) are plotted in figure 6.1 C as a function of percentage of MUD in the SAM solution used to generate the monolayers.

As discussed, both a smaller SAM resistance as well as higher than -90° phase for frequencies smaller than 1 Hz can be interpreted as an increased number of pin-holes in the SAM.[119] The increase of R_{leak} with MUD percentage indicates a reduction of leakyness in the SAMs with high MUD percentage, probably due to a better packing of the SAM molecules.[21,126]

A perfectly packed monolayer is expected to behave like an ideal capacitor.[21,126] At low frequencies the phase is expected to be equal to $-90°$ and R_{leak} to be infinite.

For the MUD monolayer a phase lower than -89.5° was found at frequencies below 10 Hz and the fitted R_{leak} for MUD is equal to 1.6 ± 0.1 GΩ, indicating that MUD forms a well packed monolayer with a negligible amount of pinholes, as expected.

The opposite is found for the 100% OEG SAM, where the phase at 0.1 Hz and R_{leak} are equal to -86.8° ± 0.1° and 315 ± 6 MΩ, respectively. This is consistent with the hypothesis that monolayers formed from 100% OEG are considerably less well packed than MUD SAMs. The addition of 5% MUD to the SAM solution leads to an increased

R_{leak} of about 30%.

Although the length of the alkane chain in the MUD and OEG SAMs is identical, the steric hindrance caused by the EG chain and the carboxylic acid present in OEG leads to a less well packed and therefore less insulating monolayer.

It has been reported that the steric hindrance caused by the ethylene glycol (EG) chains should not interfere significantly with the formation of a well packed monolayer [106] because the cross section of the coiled EG groups is compatible with the alkane chain spacing for packed SAMs. [106] However, the carboxylic acid present in OEG molecules might lead to a less well packed and therefore less insulating monolayer, as it was observed in this study. Nevertheless, by adding even a small amount of MUD, i.e. 0.1% or more, to the SAM solution, the phase decreases noticeably (figure 6.1 C). This suggests that the small number of MUD embedded into the mixed SAM can relax the stress between the OEG molecules and therefore lead to better packing, which in turn results in improved dielectric properties.

6.1.2 Contact angle

The ratio of absorbed molecules on the surface is not necessarily the same as the molar ratio in solution but it depends on the reaction kinetics of each molecule and the solvent. [102,125] However, it is possible to establish experimentally which conditions of the SAM formation (such as stoichiometry of the solution, solvent and incubation time) will give the desired stoichiometry of the SAM on the surface and therefore reliably form the required monolayer. [102,125] Depending on the intermolecular interactions, the mixed SAM will either be homogeneous or will show clusters of molecules of the same type. [125]

As a preliminary characterisation of the different monolayers, the wetting properties of the mixed SAMs have been studied by means of water contact angle. The results for static, (θ_s), and difference between advancing (θ_a) and receding (θ_r) apparent contact angles are shown in figure 6.3. The MUD monolayer showed a very low static contact angle ($\theta_s = 13^\circ \pm 3^\circ$) as expected for a well ordered hydrophilic layer. In contrast, the OEG monolayer showed a static contact angle of $37^\circ \pm 1^\circ$. Interestingly, the mixed SAMs all showed static contact angles of around 30°, independent of the MUD concentration in the SAM solution.

The hysteresis, defined as $\theta_h = \theta_a - \theta_r$, is an indication of both roughness and chemical homogeneity and thus the distribution of MUD and OEG on the surface. [132,207] The hysteresis is relatively small for the MUD SAM ($\theta_h = 9^\circ \pm 3^\circ$) and it increases for mixed MUD:OEG SAMs reaching saturation for concentration of MUD smaller than 1% (e.g. $\theta_h = 22^\circ \pm 1^\circ$ for 0.5% MUD). These results can be interpreted in the light of the

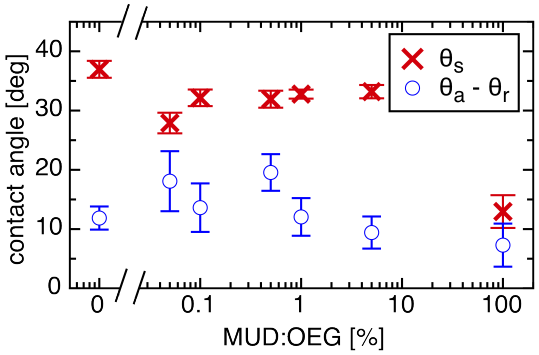

Figure 6.3: Static angle, $\theta_s(\times)$, and hysteresis, $\theta_a - \theta_r$ $(\circ)$, for all monolayers plotted against the molar fraction of MUD in OEG. The error bars represent the SD over multiple spots over at least four samples.

hypothesis that the mixed SAMs form islands or clusters of OEG and mixed SAMs, and the raised OEG islands behave like geometrical defects. The presence of islands increases the hysteresis but for increasing MUD percentage the density of OEG islands decreases, thus the decreasing hysteresis.[207]

6.1.3 Ellipsometry

The quality of a SAM in terms of packing density is reflected in its thickness. The molecules in alkane-thiol-based SAMs are generally tilted away from the surface normal by around 30°, and a reduction in packing usually results in a reduction of this tilt angle, and hence in a increase of the monolayer thickness.

The theoretical thickness of the OEG SAM is equal to 34.9 Å, taking into account the C-S bond, the 11-carbon-alkyl-chain tilted at 30° and the carboxylic acid and assuming a helical conformation of the EG groups with a length of 2.78 Å per EG.[106] The thickness of the MUD SAM, using the same assumptions, is estimated to be 14.4 Å.

We estimated the average thicknesses of all SAMs by ellipsometry on three samples for each MUD:OEG dilution. The measurements for the OEG and MUD SAM are in good agreement with the expected values: 13.6±1.3 Å for MUD, and 33±2 Å for OEG, suggesting that the monolayers have the alkyl chains tilted at about 30° angle and the EG groups are prevalently in a helical conformation.

The variation in thickness between the 100% OEG and the MUD:OEG dilutions is plotted in figure 6.4. We note that only for MUD percentages of 5%, a significant decrease in thickness is observed, while all other SAMs show thickness similar to the OEG monolayer.

The thickness variation for 5% MUD:OEG would suggest a surface concentration of MUD of about 60%. However the variation in thickness should not be attributed exclusively to the increased concentration of MUD on the surface but also to a change in the conformation of the OEG molecules in respect to 100% OEG. In fact for OEG monolayers with lower concentration of OEG molecules an amorphous configuration,

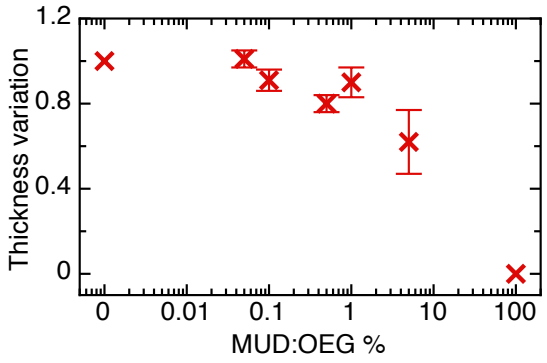

Figure 6.4: Plot of thickness variation estimated by means of ellipsometry and normalised to the measured thickness of the OEG and MUD monolayers. Error bars represents the standard deviation between three samples.

with higher degrees of freedom, of the EG chains is expected, resulting in a lower thickness.

6.1.4 X-ray photoelectron spectroscopy

The chemical composition of the assembled monolayers was studied by XPS. First, a survey scan (Fig. 6.5) was carried out and only peaks corresponding to Au, C, O and S were detected, and no additional peaks were observed. Detailed scans (figure 6.5) were then recorded for the Au 4f, C 1s, O 1s and S 2p peaks. From these, the elemental composition of the different SAMs was estimated, taking into account the relative sensitivity factor of the instrument (table 6.1).

For all SAMs the Au presents two peaks corresponding to Au $4f_{7/2}$ (BE 84.0 $\pm$ 0.1 eV, FWHM is 0.8 $\pm$ 0.0 eV) and Au $4f_{5/2}$ (BE 87.6 $\pm$ 0.1 eV, FWHM is 0.8 $\pm$ 0.0 eV), see figure 6.5.

For pure MUD monolayer the C 1s peak presents two components corresponding to the saturated carbon to carbon (C-C) and alcohol (C-OH) bonds (BE of 285.0 eV and 286.9 $\pm$ 0.1 eV respectively).

Instead, for both the pure OEG and the mixed MUD:OEG monolayers the C 1s peak presents three components (BE of 285.0 eV, 286.9 $\pm$ 0.1 eV and 289.3 $\pm$ 0.2 eV). The second component, BE equal to 286.9 eV, defines an area that is on average more than 7 times bigger than the second component for MUD because it takes into account both the ether bond (C-C-O) present in the EG groups of the OEG and, for the mixed monolayers, the alcohol bond present in the MUD. The third component corresponds to the carboxylic bond (C=O) present in OEG.

Considering that the C 1s peak has a negligible component for BE equal to 289.3 eV (C=O) for 100% MUD while it is noticeable for mixed MUD:OEG and 100% OEG monolayers and the C=O bond can only be found if the carboxylic acid group is present (figure 3.1), the C=O component can be used to estimate the percentage of OEG

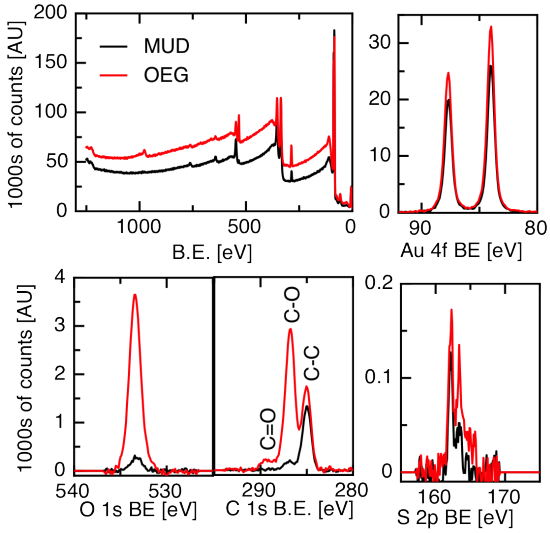

Figure 6.5: From the top left corner, XPS spectra for survey scan and C 1s, O 1s, and S 2p detailed scans for 100% MUD (black lines) and 100% OEG monolayers (red lines). The background has been removed from all spectra.

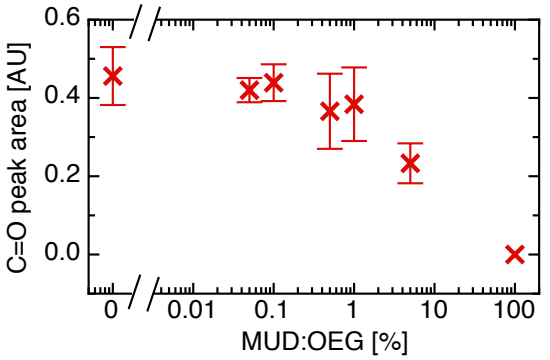

Figure 6.6: Area of the peak corresponding to carboxylic bond (B.E. 289.3 eV) estimated by means of XPS plotted against the molar fraction of MUD in OEG, error bars represents ±sd between at least four spots on two samples.

molecules on the surface.

The inclusion of MUD molecules in the monolayer can be calculated from the COOH:S ratio or from the peak intensity of the C=O component. However, the S 2p signal is consistently lower than the theoretical value as the signal is suppressed by the presence of the monolayer, thus leading to inflated element to sulphur ratios. In fact the theoretical value of COOH:S ratio for OEG is 1 but the experimentally determined value is 1.4 ± 0.3. Furthermore the S 2p signal contains a large amount of noise, as can be seen in figure 6.5 which can introduce undesirable noise in the calculated COOH:S ratio. Thus the peak intensity corresponding to C=O bond was used instead.

The peak intensity of each spot, intended as the area subtended by the peak centred at B.E. equal to 289.3 eV for all SAMs was normalised to the intensity of the Au 4f signal and then plotted against the percentage of MUD in the SAM formation solution (figure 6.6). We note that the peak intensity shows little difference for the samples with MUD concentration up to 1% while it is lower for 5% MUD:OEG monolayers.

Theoretical values										
Monolayer	C 1s %		O 1s %		S 2p %		C:S		O:S	
OEG	71.4		25.7		2.9		25.0		9.0	
MUD	84.6		7.7		7.7		11.0		1.0	
Measured values										
Monolayer	C 1s %	(SD)	O 1s %	(SD)	S 2p %	(SD)	C:S	(SD)	O:S	(SD)
100% OEG	77.6	0.9	20.0	0.9	2.4	0.2	32.0	3.6	8.2	1.1
0.05% MUD	76.6	0.9	20.7	0.6	2.7	0.4	28.9	4.6	7.8	1.0
0.1% MUD	74.7	5.6	22.7	5.2	2.6	0.4	29.4	5.9	8.7	0.9
0.5% MUD	77.2	1.1	20.2	1.3	2.6	0.2	30.1	2.3	7.9	1.2
1% MUD	77.8	1.0	19.6	1.4	2.6	0.3	30.0	3.6	7.6	1.5
5% MUD	77.1	0.7	19.8	0.5	3.1	0.2	24.7	1.5	6.3	0.3
100 % MUD	88.8	0.5	6.1	0.4	5.1	0.4	17.6	1.4	1.2	0.1

Table 6.1: Summary of quantitative analysis of XPS spectra. SD represent the standard deviation over at least fours spots on two sample.

6.1.5 Atomic force microscopy

Mixed SAMs are known to arrange in clusters of molecules of the same type if it yields a better packing of the monolayer. AFM imaging allows the observation of the distribution of molecules in the SAM. The distribution of the OEG molecules on the surface and the possible formation of islands can then be observed. Examples of typical AFM scans are reported in figure 6.7.

The template stripped gold has been found to have a rms roughness of 3.1±0.4 Å (figure 6.8). The low roughness of the gold surface allows to distinguish the formation of islands in the OEG and mixed MUD-OEG SAMs. In figure 6.8 a typical AFM image of MUD monolayer on TSG is also reported for comparison.

For OEG and 0.05% MUD:OEG SAMs it is possible to see an even distribution of the OEG molecules across the surface with formation of small and very close to each other islands (figure 6.7 C). These SAMs appear mostly homogeneous. With the increasing of the fraction of MUD in the SAM solution the islands become bigger and spaced further apart. From the analysis of the height profiles (figure 6.7 A) there is a clear difference between OEG and 0.05% MUD:OEG compared with the other mixed SAMs. For example, the peak to peak distance, measured on at least 5 profiles for each sample, for 0.05% and 5% MUD:OEG is of 29 ± 0.6 nm and 65 ± 13 nm, respectively.

To quantify the surface coverage of the islands a watershed algorithm was used on the height images of each sample which selects the highest parts of the image. This algorithm finds the local minima of the inverted surface of an AFM image and the boundaries of the grains. Once inverted, at each point of the height image a virtual droplet is applied and its potential energy is minimised so that the droplets that are not

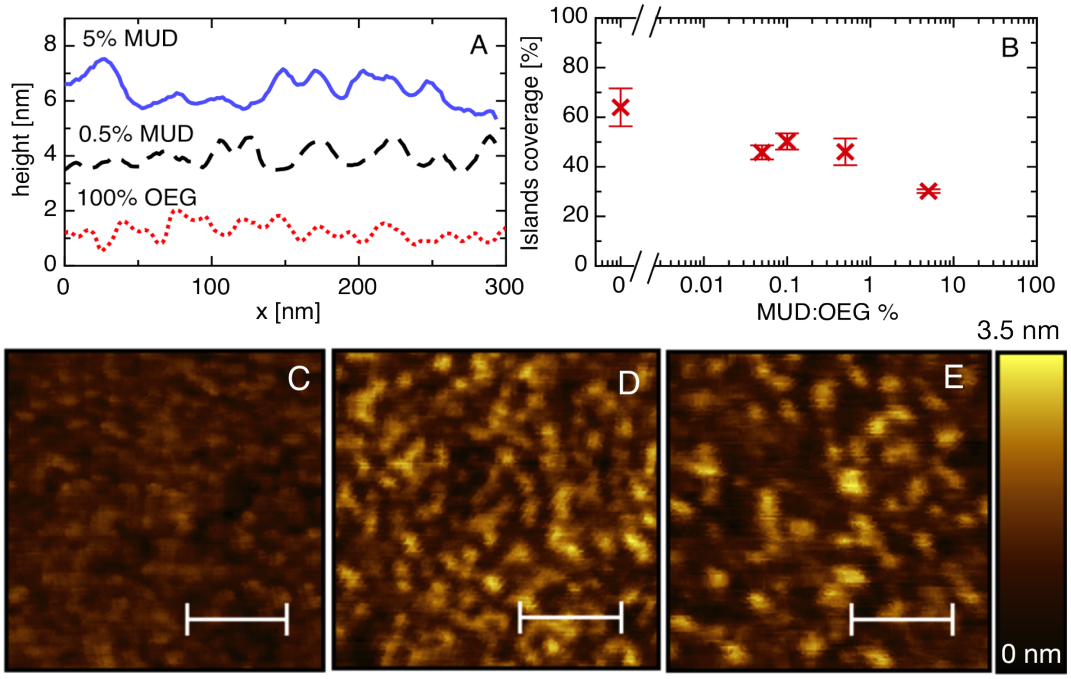

Figure 6.7: A) Profiles for mixed monolayers MUD:OEG at different concentrations, namely 0.05% (red dotted line), 0.5 % MUD in OEG(black dashed line) and 5 % (solid purple line). The profiles have been offset for clarity. B) Island coverage area estimated by means of a watershed algorithm for grain detection over at least three samples. Typical height images obtained by means of AFM of different mixed monolayers assembled from solutions with molar fractions of mixed monolayers MUD:OEG at different ratios, namely 0.05%, C, 0.5%, D, and 5 %, E. The scale bar is fixed at 100 nm.

in a local minimum will reach a minimum, following the steepest path to it, thus filling the minimum "valley" and creating a system of "lakes", each representing a grain.

The area coverage of the grains was therefore determined and plotted against MUD:-OEG % in figure 6.7 B. We note that for 100% OEG a certain granularity is detected so the islands surface coverage is equal to 64% ± 8%.

To compare the data obtained by EIS, ellipsometry, AFM and XPS we normalised all data by fixing the value for 100% MUD of each data set to zero and the one for 100% OEG to one. The resulting data, phase of the impedance at 0.1 Hz, the conductivity of the SAM, $G_{leak} = 1/R_{leak}$, the monolayer thickness, the C=O ratio and the island surface coverage, are shown in figure 6.9.

We note that all data follow a non-linear trend, with little difference between the 100% OEG SAM and the mixed SAMs with small MUD concentration (MUD < 1%) followed by a rapid decrease of the quantities towards 100% MUD.

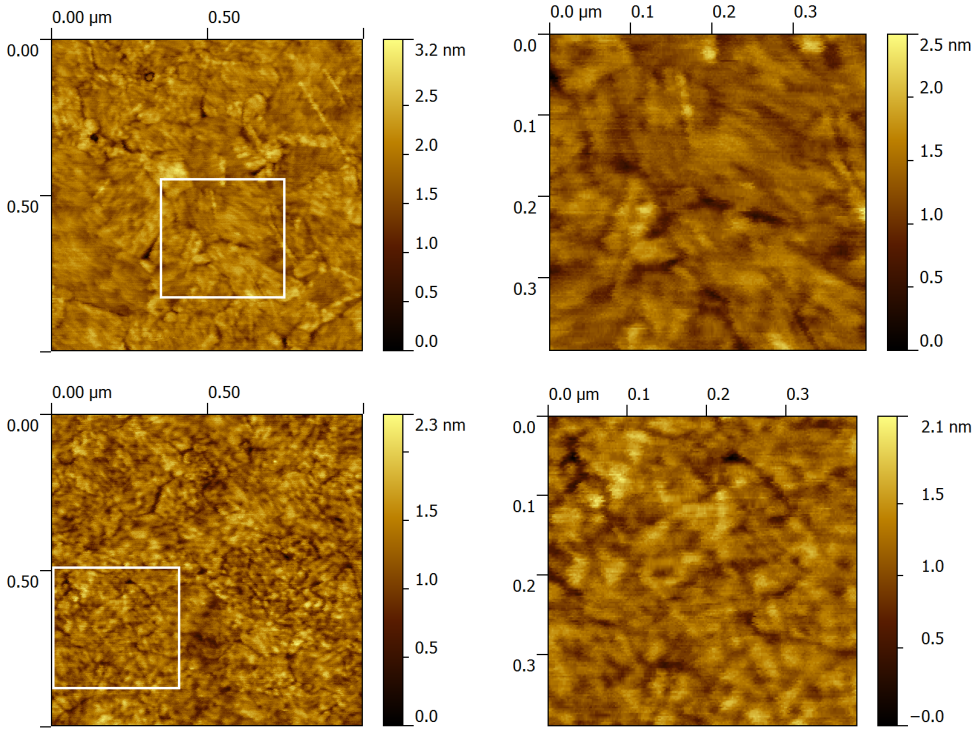

Figure 6.8: Left, example of height image of template stripped gold sample (top) and MUD SAM (bottom) obtained by means of AFM. The box outlines the area section corresponding to the zoomed image on the right.

We note that the islands coverage and the variation in C=O peak area follow the normalised phase closely, suggesting that the improved blocking properties of the electrode is due to a significant rearrangement of the monolayer and the formation of two different, highly blocking regions, both containing MUD molecules.

We concluded that the higher blocking behaviour of the monolayer has two contributions: first, MUD molecules inserted in the OEG SAM to release steric hindrance and these form a more closely packed SAM resulting in improved blocking; second, MUD clusters with properties similar to 100% MUD SAMs.

This leads to two different types of mixed monolayers. In the island domains, the concentration of MUD is very small and the EG groups of the OEG molecules are closely packed and extend perpendicular to the substrate. In contrast in the MUD clusters, OEG molecules can still be present but at low concentrations. Thus the EG groups create a disordered amorphous phase while the alkyl chains of both the MUD and OEG molecules create a highly ordered, well-blocking, SAM.

The formations of two mixed SAM phases would explain the small discrepancy be-

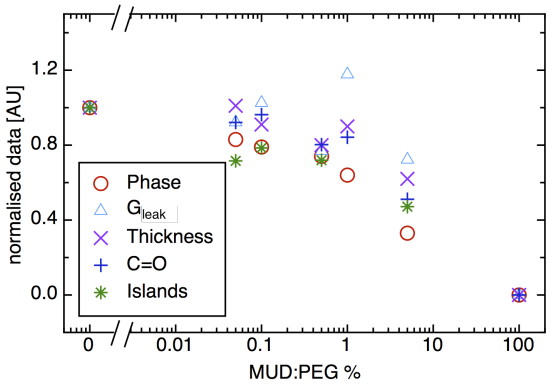

Figure 6.9: Normalised SAM conductivity, G_{leak} (○), SAM thickness (△), carboxylic acid to sulphur ratio, COOH:S (+), phase at 0.1 Hz, $\varphi_{0.1}$ (×) and islands coverage (·) by fixing the respective values for MUD to 0 and for OEG to 1. The line traced offers a guide to the eye for the overall trend.

tween the change in islands coverage obtained from the change in C=O component, estimated by XPS, and the SAM thickness, estimated by ellipsometry, with the increasing of MUD concentration in the mixed SAMs.

Conclusions

Electrochemical impedance spectroscopy was used to characterise the dielectric properties of OEG and mixed MUD:OEG SAMs. An equivalent circuit model has been proposed to model the presence of defects in the monolayers. XPS, ellipsometry and contact angle have been used to characterise the composition of the monolayers.

Electrochemical biosensors and in particular capacitive sensors, will benefit from SAMs with improved dielectric properties. This study showed that even a small amount of MUD, less than 5%, in the mixed MUD:OEG SAMs leads to a considerable rearrangement of the mixed SAM that leads to a decrease of the phase of the impedance at low frequencies as well as an increase in the resistivity of the SAM of 30%.

This page would be intentionally left blank if we would not wish to inform about that.

Chapter 7

Conclusions and future work

7.1 Conclusions

Clinical diagnostic and efficient monitoring of therapies require accurate and easy to perform detection of biomolecules from biological fluids. The aim of this study was to develop an electrochemical biosensor platform for the detection of clinically relevant analytes and biomarkers that requires minimum sample handling and hands-on procedures to address this challenge.

The simultaneous, cost effective analysis of a large variety of biomarkers from a single patient sample enables the possibility of searching for multiple risk indicators in routine check-ups, allowing early diagnosis and hence early medical intervention.

A highly sensitive, label-free electronic biosensor platform was developed, which requires no time-consuming sample handling steps. A limit of detection in spiked animal serum of better than 26 fM was demonstrated.

Since a great variety of relevant analytes can be selectively recognised by appropriate target-specific antibodies, antibodies are employed in a large range of biosensors as detection probes. A system that utilises relies on the antigen/antibody interactions for the generation of the signal can potentially detect a large variety of targets.

In this study the binding of a monoclonal antibody to its target, human chorionic gonadotropin (hCG), was used as model system for the development of a label-free immunosensor.

The enormous advances in semiconductor technology over recent decades opens up the possibility to produce inexpensive and reliable devices of varied applications and complexity, from thermometers to smart phones and laptops. The main advantage of electronic devices is the possibility of miniaturisation and integration of multiple

functions on a single device. For example the acquisition, processing and analysis of multiple sensor information could be done in just a single portable device.

However, biosensor systems generally require biological components as recognition elements, and biological systems are not ideally suited to be integrated into electronic devices. The successful development of biosensors therefore requires the development of a suitable interface between the device and the biological molecules that connects the two and take advantage of both systems so that reliable, cost effective and selective biosensors can be achieved.

Given the potential that an electronic device could perform all the analysis required for clinical diagnostic with just a single device, significant research efforts have been focused on the development of electrodes which can detect analytes. Electrochemical biosensors have emerged as a very promising option.

From the various electrochemical techniques, discussed in section 2.1, non-faradaic electrochemical impedance spectroscopy (EIS) was chosen as the analytical method for this study. In fact non-faradaic EIS is well suited for the detection of biomarkers in clinical samples without the need for time-consuming sample preparation such as pre-labelling.

The detection of the analyte by means of EIS is based on the detection of a change in impedance of the electrode solution interface upon binding of a molecule to the surface of the electrode. This method is intrinsically suited for label-free detection of biomolecules, provided the appropriate probe is attached on the surface. In fact no labelling of the sample or multiple binding sequences are required for detection.

With all these considerations in mind, this study focused on the development of a non-faradaic EIS immuno-sensor platform for the detection of analytes from full blood serum samples, including the characterisation of the sensor surface.

To achieve good sensitivity and selectivity of the sensor the immobilisation of the antibodies on the surface was performed by binding the antibodies on a self assembled monolayer (SAM). Because COOH-terminated hexa(ethylene glycol)undecanethiol (OEG) self assembled monolayers allow the immobilisation of proteins by simple chemistry and have shown good non-specific protein absorbance resistance while forming compact reliable SAMs on gold, OEG has been chosen as the interface between the sensor electrode and the immobilised antibody and sample solution.

With the aim of optimising the binding of the probe, anti-hCG monoclonal antibody (mAb-B) was immobilised on the OEG SAM in different binding conditions (see chapter 4). It was found that the antibodies were attracted to the surface by means of

electrostatic interactions with increasing adsorption for decreasing pH (section 4.2.1). However the immobilisation of the antibodies by covalent bond reached saturation at pH $\approx$ pI $-$ 1. This condition showed slightly higher binding of antibodies on the surface in respect to lower pH values.

The activity of the different surfaces was investigated to identify the surface that yields higher response to exposure to hCG. It was found that highest response was obtained for mAb-B immobilised at pH $\approx$ pI $-$ 1, which is the same pH that maximised the binding of mAb-B on the surface (section 4.2.1.1). At the same time the surfaces showed good resistance to the non-specific adsorption of proteins.

Utilising this principles, a biosensor to detect hCG in full serum was demonstrated. For diagnostics and therapeutic monitoring purposes the hCG levels of interest in serum are in the range from 3×10^{-12} to 3×10^{-7} M.[202] By using the phase of the impedance at 100 mHz as the sensor output, a linear relationship of the phase shift vs the logarithm of hCG concentration was found between 2.6 $\times10^{-14}$ M and 2.6×10^{-10} M with a sensitivity of 0.6 degree per decade.

The sensor response shows an excellent detection limit, lower than necessary for hCG as clinical biosensor, and lower or comparable with the most sensitive studies found.

All of the highly sensitive published results for the detection of hCG were reported for spiked buffer solutions which usually show lower detection limits than when used in full serum. The reported limits of detection range from 5×10^{-15} M[48] to about 10^{-12} M.[29] This has to be compared with the sensitivity of the system reported here, which in fact showed a detection limit for the sensors in buffer three order of magnitude lower than the detection limit found in serum. In phosphate buffer the sensor has linear range between 2.6×10^{-17} M and 2.6×10^{-13} M, with a sensitivity of 0.4 degree per decade.

Moreover, a negative control experiment using a much higher concentration of bovine serum albumin (BSA), 1.5×10^{-7} M, led to a phase shift comparable to a hCG concentration of ten orders of magnitude lower, and it was concluded that the observed signal was due only to specific binding of the antigen to the antibody (mAb-B).

With the aim of developing a biosensor platform for biosensor arrays for the detection of multiple targets, investigations on micro-fabricated electrodes were carried out (section 5.2.3). The repeatability of the surface characteristics for SAM modified 1 mm diameter electrodes was tested and was found to be promising, e.g. the phase of the impedance at 0.1 was $\varphi_{0.1} = -87.5^\circ \pm 0.5^\circ$. Moreover micro-fabricated electrodes modified with OEG and mAb-B were interrogated with hCG at 2.6 nM, the average response of the sensors was found to be $\varphi_{0.1} = -2.7 \pm 0.7^\circ$.

The dielectric properties of OEG, 11-mercaptoundecanol (MUD) and mixed MUD:-OEG monolayers, at different ratios, were studied by means of EIS (see section 6.1.1).

An equivalent circuit model was proposed for the characterisation of the surface and the modelling of defects in the SAMs. At the same time XPS, AFM, ellipsometry and the contact angle measurements were used to characterise the composition of the monolayer adsorbed to the surface (see sections 6.1.2 to 6.1.5).

The study showed that small amounts of MUD in the mixed MUD:OEG SAMs leads to a considerable decrease of the phase of the impedance at the low frequencies as well as a significant increase in the resistivity of the SAM, indicating significant improvement of the dielectric properties. However, a considerable change in the formations of clusters of OEG molecules was shown by AFM imaging.

We concluded that the improved blocking behaviour of the mixed monolayers resulted from the insertion of MUD molecules between defects of the OEG layer in two ways: between molecules of the clusters and in between different clusters. This led to two separate phases in the monolayer: the clusters at high concentration of OEG and the phase between clusters with lower concentration of OEG. In these regions the ethylene glycol chains of the monolayer form an amorphous, disordered, phase that has lower thickness than the clusters. The clusters are composed, instead, by ethylene glycol chains arranged in an helicoidal ordered phase. In both phases the high resistivity is provided by the undecanethiols chains that are well packed.

7.2 Future work

Although other applications are possible for biosensors, healthcare is the most cited area of applications for biosensors. Biosensors can help in diagnostic or monitoring and management of illness. However, other application areas such as the monitoring of infections and food contaminations, are equally important for the prevention of death and illness.[4]

Although sensitive detections, i.e. detection limits below ng/ml, have been reported for label-free electrochemical biosensors very few impedance biosensors have entered the market. Some of the problems are associated with immunosensors, or at least label-free immunosensors, e.g. non-specific response cause by high non-specific background, lack or difficult implementation of amplification of the response etc. Others are related to impedance biosensors, such as incomplete understanding of the change in impedance of the electrode solution interface related to the binding of the target.

Moreover, a clear connection between the binding of the analyte and response should be made experimentally[24] by showing negative controls or selectivity from complex solutions, such as serum, taking care of showing the response, or better non-response, to non-spiked solutions.

As mention, one of the great limitations is that the mechanisms by which the binding of the analyte changes the impedance is unclear, often the analysis of the impedance shift is limited to a brief discussion of how the measured parameter changes with the concentration without a suitable discussion of the fundamental underlying mechanisms. For this reason a more in-depth investigation of the system developed in this study is still necessary to achieve the ultimate goal of a point-of-care label-free biosensor platform for clinical diagnostic.

An interesting study would be to compare how differently functionalised surfaces behave when used as biosensors. We have shown that the antibodies form a densely packed layer, therefore it would be of interest to understand if the density of the antibody on the surface is critical for achieving high sensitivities in EIS. In this respect it would be useful to perform an experiment comparing different antibody dilutions on similar SAM. Two sets of dilutions have to be investigated. The first consists of varying the spacing of the antibodies by changing the functionalisation of the gold electrode surface. This can, for example, be achieved by diluting the acid-capped OEG with shorter OH-capped OEG. The second investigation consists of diluting the antibody which is specific to the target of interest with a non-specific antibody, i.e. an antibody hat has no affinity for the target while keeping the overall antibody concentration on the surface constant. If the critical factor is the high density of the antibody on the surface the sensitivity is expected to decrease with increasing dilutions.

Multiplexed biosensor can be used to bind different targets. To improve the capability as diagnostic tools it would be useful to have on the same device multiple electrodes capable of detecting different analytes that are related to the same disease.

For example it has been reported that different isoforms of hCG and different ratios between the concentration of different isoforms can be used as a specific cancer marker.[202,208] Therefore an assay to detect all the isoforms simultaneously is of clinical relevance and highly desirable.

To generate such a device an integrated array of electrodes functionalised with different mAb to the epitopes of hCG and the various hCG isoforms is required. Different hCG isoforms have some common epitopes so it is important to analyse the sample for all present epitopes at the same time with different mAb and then post-process the data to extrapolate the concentration of each isoform.

In order to realise such sensor arrays a number of requirements have to be considered. First, the characterisation of a sensor made on micro-fabricated electrodes for a single isoform has to be carried out and optimised. Obtaining good repeatability of the same sensitivity between all the electrodes at this stage is very important because errors

in the sensitivity will be amplified in the post-processing analysis. Then a process to functionalise the electrodes on the same array with different monoclonal antibodies has to be implemented and optimised and finally a study on cross-reactivity between the electrodes would also be necessary.

Arguably one of the most promising application areas for biosensors such as the one reported here is for point-of-care clinical diagnostics for such applications it would be appropriate to perform deeper investigations on micro-fabricated electrodes as sensor devices and their integration into lab-on-a-chip devices, including simple micro-fluidic devices for tasks such as sample handling

This can be achieved by integrating the electrodes in a microfluidic system that allows measurements in real time, use small samples and simplify the use of the sensor itself. Microfluidic system can be integrated with blood filters that separate the serum from the blood cells allowing the analysis of clinical sample in a point-of-care environment.

With the aim of the creation of a lab-on-a-chip device the reference and counter electrodes should be integrated on the micro-fabricated device and the measuring electronics should be miniaturised so that the device would be portable and suitable for point-of-care applications.

Althoug not commonly used in electrochemistry research set-ups, circuits for the measurement of the impedance have been proposed.[66] With the use of lock-in amplifiers sensitive and reliable measures are possible and offer a very cost effective solution.

Ideally the electronic instrument should have a way to connect to a disposable functionalised device. For example standard USB ports can be used to make electrical contact with the device and connect to the electrodes.

Always with the focus of portability and ease-of-use in mind for point-of-care the measurement should be as short as possible and the output interpretation should be easy, so that non trained users can make full use of the device. In this respect measurements that involve fitting of data and their interpretation should be avoided. Even if the fitting procedure can be automated, divergences between the device and the model used might make the results difficult to interpret.

We note that although we used EIS and fitting procedure to help the understanding of the system in this study the sensor output proposed is a direct measurable quantity that can also be measured on its own, i.e. it is possible to measure the phase of the impedance at the single frequency without measuring the entire spectrum. This can accelerate the acquisition of the signal and allow to monitor the impedance change as function of time possibly leading to even more sensitive devices.

Bibliography

[1] J. Hughes, "Thomas willis (1621–1675)," *J. Neurol.*, vol. 247, no. 2, pp. 151–152, 2000.

[2] G. Lindeboom, "Herman boerhaave," *Brit. J. Hist. Sci.*, vol. 4, no. 4, pp. b1–b4, 1968.

[3] J. Wang, "Electrochemical biosensors: towards point-of-care cancer diagnostics," *Biosens. Bioelectron.*, vol. 21, no. 10, pp. 1887–1892, 2006.

[4] A. P. F. Turner, "Biosensors: sense and sensibility," *Chem. Soc. Rev.*, vol. 42, no. 8, pp. 3184–96, 2013.

[5] J. Li, S. Li, and C. F. Yang, "Electrochemical biosensors for cancer biomarker detection," *Electroanal.*, vol. 24, no. 12, pp. 2213–2229, 2012.

[6] D. Grieshaber, R. MacKenzie, J. Vörös, and E. Reimhult, "Electrochemical biosensors-sensor principles and architectures," *Sensors*, vol. 8, no. 3, pp. 1400–1458, 2008.

[7] N. Jaffrezic-Renault, "Label-free affinity biosensors based on electrochemical impedance spectroscopy," in *Microelectrode Biosensors* (S. Marinesco and N. Dale, eds.), vol. 80 of *Neuromethods*, pp. 295–318, Humana Press, 2013.

[8] L. Clark and C. Lyons, "Electrode systems for continuous monitoring in cardiovascular surgery," *Ann. N.Y. Acad. Sci.*, vol. 102, pp. 29–45, 1962.

[9] X. Li, X. Yang, and S. Zhang, "Electrochemical enzyme immunoassay using model labels," *Trends Anal. Chem.*, vol. 27, no. 6, pp. 543–553, 2008.

[10] G. Farace, G. Lillie, T. Hianik, P. Payne, and P. Vadgama, "Reagentless biosensing using electrochemical impedance spectroscopy," *Bioelectrochemistry*, vol. 55, no. 1, pp. 1–3, 2002.

[11] P. Luppa, L. Sokoll, and D. Chan, "Immunosensors- principles and applications to clinical chemistry," *Clin. Chim. Acta*, vol. 314, no. 1-2, pp. 1–26, 2001.

[12] S. Keighley, P. Li, P. Estrela, and P. Migliorato, "Optimization of dna immobilization on gold electrodes for label-free detection by electrochemical impedance spectroscopy," *Biosens. Bioelectron.*, vol. 23, 2008.

[13] M. Mir, A. Homs, and J. Samitier, "Integrated electrochemical dna biosensors for lab-on-a-chip devices," *Electrophoresis*, vol. 30, no. 19, pp. 3386–97, 2009.

[14] L.-D. Li, H.-T. Zhao, Z.-B. Chen, X.-J. Mu, and L. Guo, "Aptamer biosensor for label-free impedance spectroscopy detection of thrombin based on gold nanoparticles," *Sens. Actuatuators B*, vol. 157, no. 1, pp. 189–194, 2011.

[15] M. Rodriguez, A.-N. Kawde, and J. Wang, "Aptamer biosensor for label-free impedance spectroscopy detection of proteins based on recognition-induced switching of the surface charge," *Chem. Commun.*, vol. 34, pp. 4267–4269, 2005.

[16] Y. Fung and Y. Wong, "Self-assembled monolayers as the coating in a quartz piezoelectric crystal immunosensor to detect salmonella in aqueous solution," *Anal. Chem.*, vol. 73, pp. 5309–5309, 2001.

[17] M. Vareiro, J. Liu, W. Knoll, K. Zak, D. Williams, and A. Jenkins, "Surface plasmon fluorescence measurements of human chorionic gonadotrophin: Role of antibody orientation in obtaining enhanced sensitivity and limit of detection," *Anal. Chem.*, vol. 77, no. 8, pp. 2426–2431, 2005.

[18] E. Katz and I. Willner, "Amperometric amplification of antigen-antibody association at monolayer interfaces: design of immunosensor electrodes," *Journal of ElectroAnal. Chem.*, vol. 418, no. 1-2, pp. 67–72, 1996.

[19] A. Sargent and O. Sadik, "Monitoring antibody–antigen reactions at conducting polymer-based immunosensors using impedance spectroscopy," *Electrochim. Acta*, vol. 44, no. 26, pp. 4667–4675, 1999.

[20] P. Estrela and P. Migliorato, "Chemical and biological sensors using polycrystalline silicon tfts," *J. Chem. Mat. Chem.*, vol. 17, no. 3, pp. 219–224, 2007.

[21] C. Berggren, B. Bjarnason, and G. Johansson, "Capacitive biosensors," *Electroanal.*, vol. 13, no. 3, pp. 173–180, 2001.

[22] A. Benkert, F. Scheller, W. Schössler, C. Hentschel, B. Micheel, O. Behrsing, G. Scharte, W. Stöcklein, and A. Warsinke, "Development of a creatinine elisa

and an amperometric antibody-based creatinine sensor with a detection limit in the nanomolar range," *Anal. Chem.*, vol. 72, no. 5, pp. 916–921, 2000.

[23] H. A. Katus, J. G. Hurrell, G. R. Matsueda, P. Ehrlich, V. R. Zurawski, B. A. Khaw, and E. Haber, "Increased specificity in human cardiac-myosin radioimmunoassay utilizing two monoclonal antibodies in a double sandwich assay," *Mol. Immunol.*, vol. 19, no. 3, pp. 451–5, 1982.

[24] J. Daniels and N. Pourmand, "Label-free impedance biosensors: Opportunities and challenges," *Electroanal.*, vol. 19, no. 12, pp. 1239–1257, 2007.

[25] P. D'Orazio, "Biosensors in clinical chemistry," *Clin. Chim. Acta*, vol. 334, no. 1-2, pp. 41–69, 2003.

[26] G. Herzog and D. Arrigan, "Electrochemical strategies for the label-free detection of amino acids, peptides and proteins," *The Analyst*, vol. 132, no. 7, pp. 615–632, 2007.

[27] D. Thévenot, K. Toth, R. Durst, and G. Wilson, "Electrochemical biosensors: recommended definitions and classification," *Anal. Lett.*, vol. 34, no. 5, pp. 635–659, 2001.

[28] N. Laboria, A. Fragoso, W. Kemmner, D. Latta, O. Nilsson, M. L. Botero, K. Drese, and C. K. O'Sullivan, "Amperometric immunosensor for carcinoembryonic antigen in colon cancer samples based on monolayers of dendritic bipodal scaffolds," *Anal. Chem.*, vol. 82, no. 5, pp. 1712–1719, 2010.

[29] R. Chai, R. Yuan, Y. Chai, C. Ou, S. Cao, and X. Li, "Amperometric immunosensors based on layer-by-layer assembly of gold nanoparticles and methylene blue on thiourea modified glassy carbon electrode for determination of human chorionic gonadotrophin," *Talanta*, vol. 74, no. 5, pp. 1330–1336, 2008.

[30] J. Tang, B. Su, D. Tang, and G. Chen, "Conductive carbon nanoparticles-based electrochemical immunosensor with enhanced sensitivity for alpha-fetoprotein using irregular-shaped gold nanoparticles-labeled enzyme-linked antibodies as signal improvement," *Biosens. Bioelectr.*, vol. 25, no. 12, pp. 2657–2662, 2010.

[31] S. Ameur, H. Maupas, C. Martelet, N. Jaffrezic-Renault, H. B. Ouada, S. Cosnier, and P. Labbe, "Impedimetric measurements on polarized functionalized platinum electrodes: application to direct immunosensing," *Mat. Sci. Eng.*, vol. 5, no. 2, pp. 111–119, 1997.

[32] C. Berggren, B. Bjarnason, and G. Johansson, "An immunological interleukine-6 capacitive biosensor using perturbation with a potentiostatic step," *Biosens. Bioelectron.*, vol. 13, no. 10, pp. 1061–1068, 1998.

[33] Y. Wang, H. Xu, J. Zhang, and G. Li, "Electrochemical sensors for clinic analysis," *Sensors*, 2008.

[34] I. Bachmatova, R. Meškys, and V. Laurinavičius, "Improvement of screen-printed carbon electrodes by modification with ferrocene derivative," *Sens. Actuatuators B*, vol. 95, no. 1, pp. 378–383, 2003.

[35] V. Laurinavicius, B. Kurtinaitien, V. Liauksminas, A. Jankauskait, R. Simkus, R. Meskys, L. Boguslavsky, T. Skotheim, and S. Tanenbaum, "Reagentless biosensor based on pqq-depended glucose dehydrogenase and partially hydrolyzed polyarbutin," *Talanta*, vol. 52, no. 3, pp. 485–93, 2000.

[36] S. Berchmans, R. Sathyajith, and V. Yegnaraman, "Layer-by-layer assembly of 1, 4-diaminoanthraquinone and glucose oxidase," *Mater. Chem. Phys.*, vol. 77, no. 2, pp. 390–396, 2003.

[37] W. Albery and P. Bartlett, "Amperometric enzyme electrodes: Part i. theory," *J. Electroanal. Chem. Interfacial Electrochem.*, vol. 194, no. 2, pp. 211–222, 1985.

[38] Y. Kajiya, H. Sugai, C. Iwakura, and H. Yoneyama, "Glucose sensitivity of polypyrrole films containing immobilized glucose oxidase and hydroquinonesulfonate ions," *Anal. Chem.*, vol. 63, no. 1, pp. 49–54, 1991.

[39] G. Du, C. Lin, and A. Bocarsly, "Electroanalytical detection of glucose using a cyanometalate-modified electrode: requirements for the oxidation of buried redox sites in glucose oxidase," *Anal. Chem.*, vol. 68, no. 5, pp. 796–806, 1996.

[40] P. Hale, T. Inagaki, H. Karan, Y. Okamoto, and T. Skotheim, "A new class of amperometric biosensor incorporating a polymeric electron-transfer mediator," *J. Am. Chem. Soc.*, vol. 111, no. 9, pp. 3482–3484, 1989.

[41] Y. Degani and A. Heller, "Direct electrical communication between chemically modified enzymes and metal electrodes. i. electron transfer from glucose oxidase to metal electrodes via electron relays, bound covalently to the enzyme," *J. Phys. Chem.*, vol. 91, no. 6, pp. 1285–1289, 1987.

[42] T. Ohara, R. Rajagopalan, and A. Heller, ""wired" enzyme electrodes for amperometric determination of glucose or lactate in the presence of interfering substances," *Anal. Chem.*, vol. 66, no. 15, pp. 2451–2457, 1994.

[43] F. Palmisano, P. Zambonin, D. Centonze, and M. Quinto, "A disposable, reagentless, third-generation glucose biosensor based on overoxidized poly (pyrrole)/tetrathiafulvalene-tetracyanoquinodimethane composite," *Anal. Chem.*, vol. 74, no. 23, pp. 5913–5918, 2002.

[44] M. Zayats, E. Katz, R. Baron, and I. Willner, "Reconstitution of apo-glucose dehydrogenase on pyrroloquinoline quinone-functionalized au nanoparticles yields an electrically contacted biocatalyst," *J. Am. Chem. Soc.*, vol. 127, pp. 12400–6, Sep 2005.

[45] C. Koopal, M. Feiters, R. Nolte, B. de Ruiter, and R. Schasfoort, "Third-generation amperometric biosensor for glucose. polypyrrole deposited within a matrix of uniform latex particles as mediator," *Bioelectroch. Bioener.*, vol. 29, no. 2, pp. 159–175, 1992.

[46] B. A. Cornell, V. L. Braach-Maksvytis, L. G. King, P. D. Osman, B. Raguse, L. Wieczorek, and R. J. Pace, "A biosensor that uses ion-channel switches," *Nature*, vol. 387, no. 6633, pp. 580–583, 1997.

[47] B. Hock, "Antibodies for immunosensors a review," *Anal. Chim. Acta*, vol. 347, no. 1-2, pp. 177–186, 1997.

[48] C. Berggren and G. Johansson, "Capacitance measurements of antibody-antigen interactions in a flow system," *Anal. Chem.*, vol. 69, no. 18, pp. 3651–7, 1997.

[49] A. Bard and L. Faulkner, *Electrochemical Methods: Fundamentals and Applications*. Wiley, 2000.

[50] D. B. Hibbert, *Introduction to electrochemistry*. Macmillan, 1993.

[51] D. R. Crow, *Principles and Applications of Electrochemistry*. Blackie Academic and Professional, 1994.

[52] M. Labib, M. Hedstroem, M. Amin, and B. Mattiasson, "A multipurpose capacitive biosensor for assay and quality control of human immunoglobulin g," *Biotechnol. Bioeng.*, vol. 104, no. 2, pp. 312–320, 2009.

[53] M. Labib, M. Hedstrom, M. Amin, and B. Mattiasson, "A capacitive immunosensor for detection of cholera toxin," *Anal. Chim. Acta*, vol. 634, no. 2, pp. 255–261, 2009.

[54] M. Labib, M. Hedstroem, M. Amin, and B. Mattiasson, "A capacitive biosensor for detection of staphylococcal enterotoxin b," *Anal. Bioanal. Chem.*, vol. 393, no. 5, pp. 1539–1544, 2009.

[55] J. Buijs, J. Lichtenbelt, W. Norde, and J. Lyklema, "Adsorption of monoclonal iggs and their f (ab)2 fragments onto polymeric surfaces," *Colloids Surf., B*, vol. 5, no. 1, pp. 11–23, 1995.

[56] A. Tlili, A. Abdelghani, S. Ameur, and N. Jaffrezic-Renault, "Impedance spectroscopy and affinity measurement of specific antibody–antigen interaction," *Mat. Sci. Eng. C*, vol. 26, no. 2-3, pp. 546–550, 2006.

[57] D. Jiang, J. Tang, B. Liu, P. Yang, X. Shen, and J. Kong, "Covalently coupling the antibody on an amine-self-assembled gold surface to probe hyaluronan-binding protein with capacitance measurement," *Biosens. Bioelectron.*, vol. 18, no. 9, pp. 1183–1191, 2003.

[58] A. Quershi, Y. Gurbuz, W. P. Kang, and J. L. Davidson, "A novel interdigitated capacitor based biosensor for detection of cardiovascular risk marker," *Biosens. Bioelectron.*, vol. 25, no. 4, pp. 877–882, 2009.

[59] E. Katz and I. Willner, "Probing biomolecular interactions at conductive and semiconductive surfaces by impedance spectroscopy: routes to impedimetric immunosensors, dnasensors, and enzyme biosensors," *Electroanal.*, vol. 15, no. 11, pp. 913–947, 2003.

[60] Y.-N. Yang, H.-I. Lin, J.-H. Wang, S.-C. Shiesh, and G.-B. Lee, "An integrated microfluidic system for c-reactive protein measurement," *Biosens. Bioelectr.*, vol. 24, no. 10, pp. 3091–6, 2009.

[61] O. Sadik, H. Xu, E. Gheorghiu, D. Andreescu, C. Balut, M. Gheorghiu, and D. Bratu, "Differential impedance spectroscopy for monitoring protein immobilization and antibody-antigen reactions," *Anal. Chem.*, vol. 74, no. 13, pp. 3142–3150, 2002.

[62] Z. Wu, J. Li, T. Deng, M. Luo, G. Shen, and R. Yu, "A sensitive immunoassay based on electropolymerized films by capacitance measurements for direct detection of immunospecies," *Anal. Biochem.*, vol. 337, no. 2, pp. 308–315, 2005.

[63] R. Pei, Z. Cheng, E. Wang, and X. Yang, "Amplification of antigen–antibody interactions based on biotin labeled protein–streptavidin network complex using impedance spectroscopy," *Biosens. Bioelectron.*, vol. 16, no. 6, pp. 355–361, 2001.

[64] Y. Yun, A. Bange, W. Heineman, H. Halsall, V. Shanov, Z. Dong, S. Pixley, M. Behbehani, A. Jazieh, and Y. Tu, "A nanotube array immunosensor for direct electrochemical detection of antigen-antibody binding," *Sens. Actuatuators B*, vol. 123, no. 1, pp. 177–182, 2007.

[65] J. Rickert, W. Göpel, W. Beck, G. Jung, and P. Heiduschka, "A 'mixed' self-assembled monolayer for an impedimetric immunosensor," *Biosens. Bioelectr.*, vol. 11, no. 8, pp. 757–68, 1996.

[66] H. Maupasa, A. Soldatkina, C. Martelet, N. Jaffrezic-Renaulta, and B. Mandrandb, "Direct immunosensing using differential electrochemical measurements of impedimetric variations," *J. ElectroAnal. Chem.*, vol. 421, no. 1-2, pp. 165–171, 1997.

[67] G. Lillie, P. Payne, and P. Vadgama, "Electrochemical impedance spectroscopy as a platform for reagentless bioaffinity sensing," *Sens. Actuatuators B*, vol. 78, no. 1-3, pp. 249–256, 2001.

[68] F. Yu, X. Dai, T. Beebe, and T. Hsiai, "Electrochemical impedance spectroscopy to characterize inflammatory atherosclerotic plaques," *Biosens. Bioelectron.*, vol. 30, pp. 165–173, 2011.

[69] H. Huang, P. Ran, and Z. Liu, "Impedance sensing of allergen-antibody interaction on glassy carbon electrode modified by gold electrodeposition," *Bioelectrochemistry*, vol. 70, no. 2, pp. 257–262, 2007.

[70] C. Vericat, M. E. Vela, G. Benitez, P. Carro, and R. C. Salvarezza, "Self-assembled monolayers of thiols and dithiols on gold: new challenges for a well-known system," *Chem. Soc. Rev.*, vol. 39, no. 5, p. 1805, 2010.

[71] C. O'sullivan and G. Guilbault, "Commercial quartz crystal microbalances–theory and applications," *Biosens. Bioelectron.*, vol. 14, no. 8-9, pp. 663–670, 1999.

[72] A. Ulman, "Formation and structure of self-assembled monolayers," *Chem. Rev.*, vol. 96, no. 4, p. 1533, 1996.

[73] S. Zhang, N. Wang, H. Yu, Y. Niu, and C. Sun, "Covalent attachment of glucose oxidase to an au electrode modified with gold nanoparticles for use as glucose biosensor," *Bioelectrochemistry*, vol. 67, no. 1, pp. 15–22, 2005.

[74] D. Allara and R. Nuzzo, "Spontaneously organized molecular assemblies. 2. quantitative infrared spectroscopic determination of equilibrium structures of solution-adsorbedn -alkanoic acids on an oxidized aluminum surface," *Langmuir*, vol. 1, no. 1, pp. 52–66, 1985.

[75] L. Dubois, B. Zegarski, and R. Nuzzo, "Molecular ordering of organosulfur compounds on au(111) and au(100): Adsorption from solution and in ultrahigh vacuum," *J. Chem. Phys.*, vol. 98, p. 678, 1993.

[76] L. Strong and G. Whitesides, "Structures of self-assembled monolayer films of organosulfur compounds adsorbed on gold single crystals: electron diffraction studies," *Langmuir*, vol. 4, no. 3, pp. 546–558, 1988.

[77] X. Torrelles, C. Vericat, M. Vela, M. Fonticelli, M. Millone, R. Felici, T. Lee, J. Zegenhagen, G. Muñoz, and J. Martín-Gago, "Two-site adsorption model for the $(\sqrt{3} \times \sqrt{3})$-r30° dodecanethiolate lattice on au(111) surfaces," *J. Phys. Chem. B*, vol. 110, no. 11, pp. 5586–5594, 2006.

[78] G. Poirier and M. Tarlov, "The c(4x2) superlattice of n-alkanethiol monolayers self-assembled on au(111)," *Langmuir*, vol. 10, no. 9, pp. 2853–2856, 1994.

[79] G. Poirier, "Characterization of organosulfur molecular monolayers on au(111) using scanning tunneling microscopy," *Chem. Rev.*, vol. 97, no. 4, pp. 1117–1128, 1997.

[80] A. Ulman, J. Eilers, and N. Tillman, "Packing and molecular orientation of alkanethiol monolayers on gold surfaces," *Langmuir*, vol. 5, no. 5, pp. 1147–1152, 1989.

[81] S. Mendoza, I. Arfaoui, S. Zanarini, F. Paolucci, and P. Rudolf, "Improvements in the characterization of the crystalline structure of acid-terminated alkanethiol self-assembled monolayers on au(111)," *Langmuir*, vol. 23, no. 2, pp. 582–588, 2007.

[82] W. Bigelow, D. Pickett, and W. Zisman, "Oleophobic monolayers: I. films adsorbed from solution in non-polar liquids," *J. Colloid Interface Sci.*, vol. 1, no. 6, pp. 513–538, 1946.

[83] J. Sagiv, "Organized monolayers by adsorption. 1. formation and structure of oleophobic mixed monolayers on solid surfaces," *J. Am. Chem. Soc.*, vol. 102, no. 1, pp. 92–98, 1980.

[84] D. Allara and G. Nuzzo, "Spontaneously organized molecular assemblies. 1. formation, dynamics, and physical properties of n -alkanoic acids adsorbed from solution on an oxidized aluminum surface," *Langmuir*, vol. 1, no. 1, pp. 45–52, 1985.

[85] F. Davis and S. Higson, "Structured thin films as functional components within biosensors," *Biosens. Bioelectron.*, vol. 21, no. 1, pp. 1–20, 2005.

[86] S. Darling, A. Rosenbaum, Y. Wang, and S. Sibener, "Coexistence of the $(23\times\sqrt{3})$ au(111) reconstruction and a striped phase self-assembled monolayer," *Langmuir*, vol. 18, no. 20, pp. 7462–7468, 2002.

[87] P. Maksymovych, D. Sorescu, and J. Y. Jr, "Methanethiolate adsorption site on au(111): A combined stm/dft study at the single-molecule level," *J. Phys. Chem. B*, vol. 110, no. 42, pp. 21161–21167, 2006.

[88] G. Heimel, L. Romaner, E. Zojer, and J. Bredas, "The interface energetics of self-assembled monolayers on metals," *Acc. Chem. Res.*, vol. 41, no. 6, pp. 721–729, 2008.

[89] M. Porter, T. Bright, D. Allara, and C. Chidsey, "Spontaneously organized molecular assemblies. 4. structural characterization of n-alkyl thiol monolayers on gold by optical ellipsometry, infrared spectroscopy, and electrochemistry," *J. Am. Chem. Soc.*, vol. 109, no. 12, pp. 3559–3568, 1987.

[90] T. Li and M. Weaver, "Intramolecular electron transfer at metal surfaces. 4. dependence of tunneling probability upon donor-acceptor separation distance," *J. Am. Chem. Soc.*, vol. 106, no. 20, pp. 6107–6108, 1984.

[91] K. A. Lee, "Electron transfer into self-assembling monolayers on gold electrodes," *Langmuir*, vol. 6, no. 3, pp. 709–712, 1990.

[92] A. Fragoso, N. Laboria, D. Latta, and C. O'Sullivan, "Electron permeable self-assembled monolayers of dithiolated aromatic scaffolds on gold for biosensor applications," *Anal. Chem.*, vol. 80, no. 7, pp. 2556–2563, 2008.

[93] Y. Arima and H. Iwata, "Effect of wettability and surface functional groups on protein adsorption and cell adhesion using well-defined mixed self-assembled monolayers," *Biomaterials*, vol. 28, no. 20, pp. 3074–3082, 2007.

[94] E. Ostuni, R. Chapman, R. Holmlin, S. Takayama, and G. Whitesides, "A survey of structure-property relationships of surfaces that resist the adsorption of protein," *Langmuir*, vol. 17, no. 18, pp. 5605–5620, 2001.

[95] J. Davis, J. Tkac, R. Humphreys, A. Buxton, T. Lee, and P. Ferrigno, "Peptide aptamers in label-free protein detection: 2. chemical optimization and detection of distinct protein isoforms," *Anal. Chem.*, vol. 81, no. 9, pp. 3314–3320, 2009.

[96] E. Ostuni, B. Grzybowski, M. Mrksich, C. Roberts, and G. Whitesides, "Adsorption of proteins to hydrophobic sites on mixed self-assembled monolayers," *Langmuir*, vol. 19, no. 5, pp. 1861–1872, 2003.

[97] H. Song, X. Zhou, J. Hobley, and X. Su, "Comparative study of random and oriented antibody immobilization as measured by dual polarization interferometry and surface plasmon resonance spectroscopy," *Langmuir*, vol. 28, no. 1, pp. 997–1004, 2012.

[98] S. Chen, L. Liu, J. Zhou, and S. Jiang, "Controlling antibody orientation on charged self-assembled monolayers," *Langmuir*, vol. 19, no. 7, pp. 2859–2864, 2003.

[99] J. N. Adkins, "Toward a human blood serum proteome: Analysis by multidimensional separation coupled with mass spectrometry," *Mol. Cell. Biochem.*, vol. 1, no. 12, pp. 947–955, 2002.

[100] K. Prime and G. Whitesides, "Adsorption of proteins onto surfaces containing end-attached oligo (ethylene oxide): a model system using self-assembled monolayers," *J. Am. Chem. Soc.*, vol. 115, no. 23, pp. 10714–10721, 1993.

[101] Z. Yang, J. Galloway, and H. Yu, "Protein interactions with poly (ethylene glycol) self-assembled monolayers on glass substrates: diffusion and adsorption," *Langmuir*, vol. 15, no. 24, pp. 8405–8411, 1999.

[102] R. Chapman, E. Ostuni, L. Yan, and G. Whitesides, "Preparation of mixed self-assembled monolayers (sams) that resist adsorption of proteins using the reaction of amines with a sam that presents interchain carboxylic anhydride groups," *Langmuir*, vol. 16, no. 17, pp. 6927–6936, 2000.

[103] S. K. Arya, P. R. Solanki, M. Datta, and B. D. Malhotra, "Recent advances in self-assembled monolayers based biomolecular electronic devices," *Biosens. Bioelectron.*, vol. 24, no. 9, pp. 2810–2817, 2009.

[104] R. Wang, H. Kreuzer, and M. Grunze, "Molecular conformation and solvation of oligo (ethylene glycol)-terminated self-assembled monolayers and their resistance to protein adsorption," *J. Phys. Chem. B*, vol. 101, no. 47, pp. 9767–9773, 1997.

[105] L. Li, S. Chen, J. Zheng, B. Ratner, and S. Jiang, "Protein adsorption on oligo (ethylene glycol)-terminated alkanethiolate self-assembled monolayers: The molecular basis for nonfouling behavior," *J. Phys. Chem. B*, vol. 109, no. 7, pp. 2934–2941, 2005.

[106] P. Harder, M. Grunze, R. Dahint, G. Whitesides, and P. Laibinis, "Molecular conformation in oligo (ethylene glycol)-terminated self-assembled monolayers on gold and silver surfaces determines their ability to resist protein adsorption," *J. Phys. Chem. B*, vol. 102, no. 2, pp. 426–436, 1998.

[107] O. Pierrat, N. Lechat, C. Bourdillon, and J. Laval, "Electrochemical and surface plasmon resonance characterization of the step-by-step self-assembly of a biomimetic structure onto an electrode surface," *Langmuir*, vol. 13, no. 14, pp. 4112–4118, 1997.

[108] J. Gooding, F. Mearns, W. Yang, and J. Liu, "Self-assembled monolayers into the 21(st) century: Recent advances and applications," *Electroanal.*, vol. 15, no. 2, pp. 81–96, 2003.

[109] A. Subramanian, J. Irudayaraj, and T. Ryan, "A mixed self-assembled monolayer-based surface plasmon immunosensor for detection of e. coli o157: H7," *Biosens. Bioelectron.*, vol. 21, no. 7, pp. 998–1006, 2006.

[110] A. Anderson, A. Dattelbaum, G. Montaño, D. Price, J. Schmidt, J. Martinez, W. Grace, K. Grace, and B. Swanson, "Functional peg-modified thin films for biological detection," *Langmuir*, vol. 24, no. 5, pp. 2240–2247, 2008.

[111] J. Buijs, D. White, and W. Norde, "The effect of adsorption on the antigen binding by igg and its f(ab)$_2$ fragments," *Colloids Surf., B*, vol. 8, no. 4, pp. 239–249, 1997.

[112] D. Graesslin, H. C. Weise, and P. J. Czygan, "Isolation and partial characterization of several different chorionic gonadotropin (hcg) components," *FEBS Lett.*, vol. 20, no. 1, pp. 87–89, 1972.

[113] A. Bristow, P. Berger, J. Bidart, S. Birken, R. Norman, U. Stenman, and C. Sturgeon, "Establishment, value assignment, and characterization of new who reference reagents for six molecular forms of human chorionic gonadotropin," *Clin. Chem.*, vol. 51, no. 1, p. 177, 2005.

[114] U. Stenman, A. Tiitinen, H. Alfthan, and L. Valmu, "The classification, functions and clinical use of different isoforms of hcg," *Hum. Reprod. Update*, vol. 12, no. 6, p. 769, 2006.

[115] M. Santandreu, S. Alegret, and E. Fabregas, "Determination of -hcg using amperometric immunosensors based on a conducting immunocomposite," *Anal. Chim. Acta*, vol. 396, no. 2-3, pp. 181–188, 1999.

[116] B. Zhang, Q. Mao, X. Zhang, T. Jiang, M. Chen, F. Yu, and W. Fu, "A novel piezoelectric quartz micro-array immunosensor based on self-assembled monolayer for determination of human chorionic gonadotropin," *Biosens. Bioelectron.*, vol. 19, no. 7, pp. 711–720, 2004.

[117] A. Becka and C. Miller, "Electrochemistry at. omega.-hydroxy thiol coated electrodes. 3. voltage independence of the electron tunneling barrier and measurements of redox kinetics at large overpotentials," *J. Phys. Chem.*, vol. 96, no. 6, pp. 2657–2668, 1992.

[118] L. Zhang and X. Zhao, "Carbon-based materials as supercapacitor electrodes," *Chem. Soc. Rev.*, vol. 38, no. 9, pp. 2520–2531, 2009.

[119] E. Boubour and R. Lennox, "Potential-induced defects in n-alkanethiol self-assembled monolayers monitored by impedance spectroscopy," *J. Phys. Chem. B*, vol. 104, no. 38, pp. 9004–9010, 2000.

[120] G. Brug, A. V. D. Eeden, M. Sluyters-Rehbach, and J. Sluyters, "The analysis of electrode impedances complicated by the presence of a constant phase element," *J. Electroanal. Chem*, vol. 176, no. 1-2, pp. 275–295, 1984.

[121] M. R. S. Abouzari, F. Berkemeier, G. Schmitz, and D. Wilmer, "On the physical interpretation of constant phase elements," *Solid State Ionics*, vol. 180, no. 14-16, pp. 922–927, 2009.

[122] S. Liu, "Fractal model for the ac response of a rough interface," *Phys. Rev. Lett.*, vol. 55, no. 5, pp. 529–532, 1985.

[123] T. Pajkossy, "Impedance of rough capacitive electrodes," *J. ElectroAnal. Chem.*, vol. 364, no. 1, pp. 111–125, 1994.

[124] R. D. Levie, "On impedance measurements: The determination of the double layer capacitance in the presence of an electrode reaction," *Electrochim. Acta*, vol. 10, no. 4, pp. 395–402, 1965.

[125] J. Love, L. Estroff, J. Kriebel, and R. Nuzzo, "Self-assembled monolayers of thiolates on metals as a form of nanotechnology," *Chem. Rev.*, vol. 105, no. 4, pp. 1103–1169, 2005.

[126] E. Boubour and R. Lennox, "Insulating properties of self-assembled monolayers monitored by impedance spectroscopy," *Langmuir*, vol. 16, no. 9, pp. 4222–4228, 2000.

[127] S. Campuzano, M. Pedrero, and C. Montemayor, "Characterization of alkanethiol-self-assembled monolayers-modified gold electrodes by electrochemical impedance spectroscopy," *Journal of ElectroAnal. Chem.*, vol. 586, no. 1, pp. 112–121, 2006.

[128] J. E. B. Randles, "Kinetics of rapid electrode reactions," *Discuss. Faraday Soc.*, vol. 1, p. 11, 1947.

[129] Y.-T. Long, C.-Z. Li, H.-B. Kraatz, and J. S. Lee, "Ac impedance spectroscopy of native dna and m-dna," *Biophys. J.*, vol. 84, no. 5, pp. 3218–25, 2003.

[130] C.-Z. Li, Y. Liu, and J. H. T. Luong, "Impedance sensing of dna binding drugs using gold substrates modified with gold nanoparticles," *Anal. Chem.*, vol. 77, no. 2, pp. 478–85, 2005.

[131] A. Marmur and K. Mittal, "A guide to the equilibrium contact angles maze," *Contact Angle Wettability and Adhesion*, vol. 6, pp. 3–18, 2009.

[132] E. Decker, B. Frank, Y. Suo, and S. Garoff, "Physics of contact angle measurement," *Colloids Surf., A*, vol. 156, no. 1, pp. 177–189, 1999.

[133] C. Extrand and Y. Kumagai, "An experimental study of contact angle hysteresis," *J. Colloid Interface Sci.*, vol. 191, no. 2, pp. 378–383, 1997.

[134] L. Gao and T. McCarthy, "Contact angle hysteresis explained," *Langmuir*, vol. 22, no. 14, pp. 6234–6237, 2006.

[135] T. Young, "An essay on the cohesion of fluids," *Philos. Trans. R. Soc. Lond.*, vol. 95, pp. 65–87, 1805.

[136] R. Kooyman, "Physics of surface plasmon resonance," *Handbook of Surface Plasmon Resonance*, pp. 15–34, 2008.

[137] J. Lahiri, L. Isaacs, J. Tien, and G. M. Whitesides, "A strategy for the generation of surfaces presenting ligands for studies of binding based on an active ester as a common reactive intermediate: A surface plasmon resonance study," *Anal. Chem.*, vol. 71, no. 4, pp. 777–790, 1999.

[138] A. Alessandrini and P. Facci, "Afm: a versatile tool in biophysics," *Meas. Sci. Tech.*, vol. 16, no. 6, p. R65, 2005.

[139] Y. Martin, C. Williams, and H. Wickramasinghe, "Atomic force microscope–force mapping and profiling on a sub 100å scale," *J. Appl. Phys.*, vol. 61, no. 10, pp. 4723–4729, 1987.

[140] Q. Zhong, D. Inniss, K. Kjoller, and V. Elings, "Fractured polymer/silica fiber surface studied by tapping mode atomic force microscopy," *Surf. Sci. Lett.*, vol. 290, pp. L688–L692, 1993.

[141] G. Meyer and N. Amer, "Novel optical approach to atomic force microscopy," *Appl. Phys. Lett.*, vol. 53, no. 12, pp. 1045–1047, 1988.

[142] R. Garcia, *Tip-Surface Interaction Forces*, pp. 25–39. Wiley-VCH Verlag GmbH Co. KGaA, 2010.

[143] V. Morris, A. Kirby, and A. Gunning, *Atomic force microscopy for biologists*. World Scientific Publishing Company, 1 ed., 2010.

[144] C. Argento and R. French, "Parametric tip model and force–distance relation for hamaker constant determination from atomic force microscopy," *J. Appl. Phys.*, vol. 80, no. 11, pp. 6081–6090, 1996.

[145] N. Jalili and K. Laxminarayana, "A review of atomic force microscopy imaging systems: application to molecular metrology and biological sciences," *Mechatronics*, vol. 14, no. 8, pp. 907–945, 2004.

[146] L. Fisher and J. Israelachvili, "Experimental studies on the applicability of the kelvin equation to highly curved concave menisci," *J. Colloid Interface Sci.*, vol. 80, no. 2, pp. 528–541, 1981.

[147] J. Israelachvili, *Intermolecular and Surface Forces*. London: Elsevier Academic Press Inc., 3rd ed., 2011.

[148] B. Derjaguin, V. Muller, and Y. Toporov, "Effect of contact deformations on the adhesion of particles," *J. Colloid Interface Sci.*, vol. 53, no. 2, pp. 314–326, 1975.

[149] J. Humlek, *Polarized light and ellipsometry*, pp. 3–91. New York: William Andrew Publishing, 2005.

[150] J.-M. Levy-Leblond and F. Balibar, *Quantics: rudiments of quantum physics*. Elsevier Science Ltd, 1990.

[151] C. Pale-Grosdemange, E. Simon, K. Prime, and G. Whitesides, "Formation of self-assembled monolayers by chemisorption of derivatives of oligo (ethylene glycol) of structure HS (CH2) 11 (OCH2CH2) mOH on gold," *J. Am. Chem. Soc*, vol. 113, no. 1, pp. 12–20, 1991.

[152] Z. Grabarek and J. Gergely, "Zero-length crosslinking procedure with the use of active esters," *Anal. Biochem.*, vol. 185, no. 1, pp. 131–135, 1990.

[153] H. Wang, S. Chen, L. Li, and S. Jiang, "Improved method for the preparation of carboxylic acid and amine terminated self-assembled monolayers of alkanethiolates," *Langmuir*, vol. 21, no. 7, pp. 2633–2636, 2005.

[154] V. Bhalla, S. Carrara, C. Stagni, and B. Samorì, "Chip cleaning and regeneration for electrochemical sensor arrays," *Thin Solid Films*, vol. 518, no. 12, pp. 3360–3366, 2010.

[155] J. Hoare, "A cyclic voltammetric study of the goldoxygen system," *J. Electrochem. Soc.*, vol. 131, no. 8, pp. 1808–1815, 1984.

[156] R. Carvalhal, R. SanchesFreire, and L. Kubota, "Polycrystalline gold electrodes: A comparative study of pretreatment procedures used for cleaning and thiol self-assembly monolayer formation," *Electroanal.*, vol. 17, no. 14, pp. 1251–1259, 2005.

[157] J. Tkac and J. Davis, "An optimised electrode pre-treatment for sam formation on polycrystalline gold," *J ElectroAnal. Chem.*, vol. 621, no. 1, pp. 117–120, 2008.

[158] Y. Bae, B.-K. Oh, W. Lee, W. Lee, and J.-W. Choi, "Study on orientation of immunoglobulin g on protein g layer," *Biosens. Bioelectron.*, vol. 21, no. 1, pp. 103–110, 2005.

[159] J. Zhou, S. Chen, and S. Jiang, "Orientation of adsorbed antibodies on charged surfaces by computer simulation based on a united-residue model," *Langmuir*, vol. 19, no. 8, pp. 3472–3478, 2003.

[160] H. Xu, X. Zhao, C. Grant, J. Lu, D. Williams, and J. Penfold, "Orientation of a monoclonal antibody adsorbed at the solid/solution interface: a combined study using atomic force microscopy and neutron reflectivity," *Langmuir*, vol. 22, no. 14, pp. 6313–6320, 2006.

[161] P. A. Ward, "Monoclonal antibodies production," *National Academy Press*, pp. 1–57, 2010.

[162] A. L. Brun, S. Holt, D. Shah, C. Majkrzak, and J. Lakey, "The structural orientation of antibody layers bound to engineered biosensor surfaces," *Biomaterials*, vol. 32, no. 12, pp. 3303–3311, 2011.

[163] M. Wiseman and C. Frank, "Antibody adsorption and orientation on hydrophobic surfaces," *Langmuir*, vol. 28, pp. 1765–1774, 2012.

[164] R. Green, R. Frazier, K. Shakesheff, M. Davies, C. Roberts, and S. Tendler, "Surface plasmon resonance analysis of dynamic biological interactions with biomaterials," *Biomaterials*, vol. 21, no. 18, pp. 1823–1835, 2000.

[165] F. Lisdat and D. Schäfer, "The use of electrochemical impedance spectroscopy for biosensing," *Anal. Bioanal. Chem.*, vol. 391, pp. 1555–1567, 2008.

[166] W. Lukosz, "Principles and sensitivities of integrated optical and surface plasmon sensors for direct affinity sensing and immunosensing," *Biosens. Bioelectron.*, vol. 6, pp. 215–225, 1991.

[167] G. Köhler and C. Milstein, "Continuous cultures of fused cells secreting antibody of predefined specificity," *Nature*, vol. 256, no. 5517, pp. 495–497, 1975.

[168] L. Harris, S. Larson, K. Hasel, and A. McPherson, "Refined structure of an intact igg2a monoclonal antibody," *Biochemistry*, vol. 36, no. 7, pp. 1581–1597, 1997.

[169] C. Zhou, J.-M. Friedt, A. Angelova, K.-H. Choi, W. Laureyn, F. Frederix, L. A. Francis, A. Campitelli, Y. Engelborghs, and G. Borghs, "Human immunoglobulin adsorption investigated by means of quartz crystal microbalance dissipation, atomic force microscopy, surface acoustic wave, and surface plasmon resonance techniques.," *Langmuir*, vol. 20, no. 14, pp. 5827–5878, 2004.

[170] X. Wang, Y. Wang, H. Xu, H. Shan, and J. Lu, "Dynamic adsorption of monoclonal antibody layers on hydrophilic silica surface: a combined study by spectroscopic ellipsometry and afm," *J. Colloid Interface Sci.*, vol. 323, no. 1, pp. 18–15, 2008.

[171] H. Xu, J. Lu, and D. Williams, "Effect of surface packing density of interfacially adsorbed monoclonal antibody on the binding of hormonal antigen human chorionic gonadotrophin," *J. Phys. Chem. B*, vol. 110, no. 4, pp. 1907–1914, 2006.

[172] S. Puertas, P. Batalla, M. Moros, E. Polo, P. D. Pino, J. G. n, V. Grazú, and J. D. L. Fuente, "Taking advantage of unspecific interactions to produce highly active magnetic nanoparticle-antibody conjugates," *ACS nano*, vol. 5, no. 6, pp. 4521–4528, 2011.

[173] A. Kausaite-Minkstimiene, A. Ramanaviciene, J. Kirlyte, and A. Ramanavicius, "Comparative study of random and oriented antibody immobilization techniques on the binding capacity of immunosensor," *Anal. Chem.*, vol. 82, no. 15, pp. 6401–8, 2010.

[174] T. Lee, R. Carey, H. Biebuyck, and G. Whitesides, "The wetting of monolayer films exposing ionizable acids and bases," *Langmuir*, vol. 10, no. 3, pp. 741–749, 1994.

[175] M. Cefola, A. Tompa, A. Celiano, and P. Gentile, "Coördination compounds. ii. trends in the stability of some rare earth chelates," *Inorg. Chem.*, vol. 1, no. 2, pp. 290–293, 1962.

[176] J. Smalley, K. Chalfant, S. Feldberg, T. Nahir, and E. Bowden, "An indirect laser-induced temperature jump determination of the surface p k a of 11-mercaptoundecanoic acid monolayers self-assembled on gold," *J. Phys. Chem. B*, vol. 103, no. 10, pp. 1676–1685, 1999.

[177] S. Holmes-Farley, R. Reamey, T. McCarthy, J. Deutch, and G. Whitesides, "Acid-base behavior of carboxylic acid groups covalently attached at the surface of polyethylene: The usefulness of contact angle in following the ionization of surface functionality," *Langmuir*, vol. 1, no. 6, pp. 725–740, 1985.

[178] P. Elving, J. Markowitz, and I. Rosenthal, "Preparation of buffer systems of constant ionic strength," *Anal. Chem.*, vol. 28, no. 7, pp. 1179–1180, 1956.

[179] J. Staros, R. Wright, and D. Swingle, "Enhancement by n-hydroxysulfosuccinimide of water-soluble carbodiimide-mediated coupling reactions," *Anal. Biochem.*, vol. 156, no. 1, pp. 220–222, 1986.

[180] D. Sehgal and I. Vijay, "A method for the high efficiency of water-soluble carbodiimide-mediated amidation," *Anal. Biochem.*, vol. 218, no. 1, pp. 87–91, 1994.

[181] M. J. E. Fischer, "Amine coupling through edc/nhs: a practical approach," *Methods Mol Biol*, vol. 627, pp. 55–73, Jan 2010.

[182] J. Weiss, "The hill equation revisited: uses and misuses.," *The FASEB Journal*, vol. 11, no. 11, pp. 835–841, 1997.

[183] H. Motulsky and A. Christopoulos, *Fitting Models to Biological Data Using Linear and Non Linear Regression: A Practical Guide to Curve Fitting.* GraphPad Software Inc, 2004.

[184] J. Lee, S. Sim, S. Cho, and J. Lee, "Characterization of a self-assembled monolayer of thiol on a gold surface and the fabrication of a biosensor chip based on surface plasmon resonance for detecting anti-gad antibody," *Biosens. Bioelectron.*, vol. 20, no. 7, pp. 1422–1427, 2005.

[185] N. Faucheux, R. Schweiss, K. Lützow, C. Werner, and T. Groth, "Self-assembled monolayers with different terminating groups as model substrates for cell adhesion studies," *Biomaterials*, 2004.

[186] I. Bontidean, C. Berggren, G. Johansson, E. Csöregi, B. Mattiasson, J. R. Lloyd, K. J. Jakeman, and N. L. Brown, "Detection of heavy metal ions at femtomolar

levels using protein-based biosensors," *Anal. Chem.*, vol. 70, no. 19, pp. 4162–9, 1998.

[187] H. M. Nassef, M. C. B. Redondo, P. J. Ciclitira, H. J. Ellis, A. Fragoso, and C. K. O'Sullivan, "Electrochemical immunosensor for detection of celiac disease toxic gliadin in foodstuff," *Anal. Chem.*, vol. 80, no. 23, pp. 9265–9271, 2008.

[188] P. Goldwasser and J. Feldman, "Association of serum albumin and mortality risk," *J. Clin. Epidemiol.*, vol. 50, no. 6, pp. 693–703, 1997.

[189] L. A. Cole, "Hyperglycosylated hcg, a review," *Placenta*, vol. 31, no. 8, pp. 653–664, 2010.

[190] K. Hirayama, S. Akashi, M. Furuya, and K. Fukuhara, "Rapid confirmation and revision of the primary structure of bovine serum albumin by esims and frit-fab lc/ms," *Biochem. Biophys. Res. Commun.*, vol. 173, no. 2, pp. 639–46, 1990.

[191] A. L. Hook, N. H. Voelcker, and H. Thissen, "Patterned and switchable surfaces for biomolecular manipulation," *Acta Biomaterialia*, vol. 5, no. 7, pp. 2350–2370, 2009.

[192] I. Ciani, H. Schulze, D. K. Corrigan, G. Henihan, G. Giraud, J. G. Terry, A. J. Walton, R. Pethig, P. Ghazal, J. Crain, C. J. Campbell, T. T. Bachmann, and A. R. Mount, "Development of immunosensors for direct detection of three wound infection biomarkers at point of care using electrochemical impedance spectroscopy," *Biosens. Bioelectron.*, vol. 31, no. 1, pp. 413–418, 2012.

[193] S. Ameur, C. Martelet, and N. Jaffrezic-Renault, "Sensitive immunodetection through impedance measurements onto gold functionalized electrodes," *Appl. Biochem. Biotechnol.*, vol. 89, no. 2-3, pp. 161–170, 2000.

[194] C. Smith and H. White, "Theory of the voltammetric response of electrodes of submicron dimensions. violation of electroneutrality in the presence of excess supporting electrolyte," *Anal. Chem.*, vol. 65, no. 23, pp. 3343–3353, 1993.

[195] W. Fawcett, M. Fedurco, and Z. Kovacova, "Double layer effects at molecular films containing acid/base groups," *Langmuir*, vol. 10, no. 7, pp. 2403–2408, 1994.

[196] R. Schweiss, C. Werner, and W. Knoll, "Impedance spectroscopy studies of interfacial acid–base reactions of self-assembled monolayers," *J. ElectroAnal. Chem.*, vol. 540, pp. 145–151, 2003.

[197] I. Burgess, B. Seivewright, and R. B. Lennox, "Electric field driven protonation/deprotonation of self-assembled monolayers of acid-terminated thiols," *Langmuir*, vol. 22, no. 9, pp. 4420–8, 2006.

[198] R. Janek, W. Fawcett, and A. Ulman, "Impedance spectroscopy of self-assembled monolayers on au(111): sodium ferrocyanide charge transfer at modified electrodes," *Langmuir*, vol. 14, no. 11, pp. 3011–3018, 1998.

[199] R. Mendes, R. Freire, and C. Fonseca, "Characterization of self-assembled thiols monolayers on gold surface by electrochemical impedance spectroscopy," *J. Braz. Chem. Soc.*, 2004.

[200] B. Riond, B. Wenger-Riggenbach, R. Hofmann-Lehmann, and H. Lutz, "Serum protein concentrations from clinically healthy horses determined by agarose gel electrophoresis," *Vet. Clin. Path.*, vol. 38, no. 1, pp. 73–77, 2009.

[201] E. Boubour and R. Lennox, "Stability of omega-functionalized self-assembled monolayers as a function of applied potential," *Langmuir*, vol. 16, no. 19, pp. 7464–7470, 2000.

[202] U. Stenman, H. Alfthan, and K. Hotakainen, "Human chorionic gonadotropin in cancer," *Clin. Biochem.*, vol. 37, no. 7, pp. 549–561, 2004.

[203] C. Bain, E. Troughton, Y. Tao, J. Evall, G. Whitesides, and R. Nuzzo, "Formation of monolayer films by the spontaneous assembly of organic thiols from solution onto gold," *J. Am. Chem. Soc.*, vol. 111, no. 1, pp. 321–335, 1989.

[204] S. Herrwerth, T. Rosendahl, C. Feng, J. Fick, W. Eck, M. Himmelhaus, R. Dahint, and M. Grunze, "Covalent coupling of antibodies to self-assembled monolayers of carboxy-functionalized poly (ethylene glycol): Protein resistance and specific binding of biomolecules," *Langmuir*, vol. 19, no. 5, pp. 1880–1887, 2003.

[205] D. Samanta and A. Sarkar, "Immobilization of bio-macromolecules on self-assembled monolayers: methods and sensor applications," *Chem. Soc. Rev.*, vol. 40, no. 5, p. 2567, 2011.

[206] F. Schreiber, "Structure and growth of self-assembling monolayers," *Prog. Surf. Sci.*, vol. 65, no. 5, pp. 151–257, 2000.

[207] M. Reyssat and D. Quéré, "Contact angle hysteresis generated by strong dilute defects," *J. Phys. Chem. B*, vol. 113, no. 12, pp. 3906–3909, 2009.

[208] P. Berger, C. Sturgeon, J. M. Bidart, E. Paus, R. Gerth, M. Niang, A. Bristow, S. Birken, and U. H. Stenman, "The isobm td-7 workshop on hcg and related molecules. towards user-oriented standardization of pregnancy and tumor diagnosis: assignment of epitopes to the three-dimensional structure of diagnostically and commercially relevant monoclonal antibodies directed against human chorionic gonadotropin and derivatives," *Tumour Biol*, vol. 23, no. 1, pp. 1–38, 2002.